FLORIDA INTERNATIONAL UNIVERSITY

Miami, Florida

ROLE OF NOVEL IMMUNOREGULATORY LONG NONCODING RNAs IN AIRWAY EPITHELIAL PATHOPHYSIOLOGY AND CHRONIC PULMONARY DISEASE

A dissertation submitted in partial fulfillment of

the requirements for the degree of

DOCTOR OF PHILOSOPHY

in

BIOMEDICAL SCIENCES

by

Marko Manevski

2022

To: Dean Juan C. Cendan
Herbert Wertheim College of Medicine

This dissertation, written by Marko Manevski, and entitled Role of Novel Immunoregulatory Long Noncoding RNAs in Airway Epithelial Pathophysiology and Chronic Pulmonary Disease, having been approved in respect to style and intellectual content, is referred to you for judgment.

We have read this dissertation and recommend that it be approved.

_____
Alexander Agoulnik

_____
Madhavan P. Nair

_____
Irfan Rahman

_____
Hoshang J. Unwalla

_____
Hitendra S. Chand, Major Professor

Date of Defense: June 28, 2022

The dissertation of Marko Manevski is approved.

_____
Dean Juan C. Cendan
Herbert Wertheim College of Medicine

_____
Andrés G. Gil
Vice President for Research and Economic Development
and Dean of the University Graduate School

Florida International University, 2022

DEDICATION

This dissertation is dedicated to all my mentors, family, and loved ones who has been there for me and made this possible.

ACKNOWLEDGMENTS

This dissertation is a result of the efforts of numerous individuals and scientists that include but are by no means limited to Dr. Hitendra S. Chand, my major professor, Dr. Dinesh Devadoss, an exceptional post-doctoral fellow, other current and past laboratory members including Dr. Christopher Long, Ms. Arianne Chung, Ms. Juliet Akkaoui, Mr. Alejandro Perez, Ms. Xin Rui Yang, and more. Few words can express my gratitude to my major professor Dr. Hitendra Chand and my colleague and friend Dr. Dinesh Devadoss, as without their guidance, encouragement, tutelage, patience and support throughout, this would not have been possible. They have enabled me to complete this dissertation and taught me more than I imagined. They have opened the doors for me and allowed me to gain the skills to contribute to the scientific forefront of medical research. I would specifically like to acknowledge Dr. Devadoss as he was the project leader for the work performed under Chapter 2 and Chapter 4 of this dissertation and was the main contributor of the figures presented under these chapters.

I would also like to extend my deepest gratitude the to my dissertation committee members Dr. Alexander Agoulnik, Dr. Madhavan Nair, Dr. Irfan Rahman, and Dr. Hoshang Unwalla for agreeing to be in my committee and making all of this possible. Their patience, guidance, and help throughout the years have made me into a more capable and dedicated scientist, and their advice, feedback, and support has been quintessential for this dissertation. They have always kept an open door and showed me the value of a highly collaborative scientific environment and how it could help us all succeed.

We were lucky to be part of the Department of Immunology and Nano-Medicine at HWCOM. I am extremely grateful to our department head, Dr. Madhavan Nair for all his support and guidance over the years, as well as Dr. Madepalli Lakshmana, Dr. Hoshang Unwalla, Dr. Nagesh Kolishetti, Mrs. Adriana Yndart, and Dr. Arti Vashist for all their guidance in laboratory experiments and direct support that have made everything possible.

Of course, I am grateful to be a part of this amazing PhD program as part of HWCOM, and I would also like to mention the administrative support and encouragement from our PhD Program Director Dr. Alexander Agoulnik and Ms. Odalys De La Rosa have helped me the necessary requirements.

Furthermore, being in a small group has also taught me the value of collaborations and close relationships with other research groups. I would like to extend our highest gratitude to the group of Dr. Irfan Rahman for their support and expertise in smoke-induced lung inflammation and ROS-mediated mitochondrial dynamics and dysfunction, and particularly so as Dr. Rahman's vision and guidance helped shape our manuscripts. The guidance and help from Dr. Rahman's group with individual experiments are highly appreciated. I would also like to extend my gratitude to the group of Dr. Prem Chapagain and his student Mr. Michael Cioffi, specialists in biological physics and computational investigations of biomolecules. Through their guidance and help creating the 3D model simulations of binding between lncRNA *LASI* and SARS-CoV-2 RNA, they helped make one of the most important publications of our lab successful. Furthermore, both the labs of Dr. Chapagain as well as the lab of Dr. Glen Borchert, experts on investigating

regulation of gene expression by long noncoding RNA, for their help analyzing RNA sequencing data and guiding essential steps for multiple publications from our lab. And of particular note, I would like to extend exceptional gratitude to the group of Dr. Siddappa Byrareddy and the post-doctoral fellow Dr. Arpan Acharya, who are specialists in understanding host-viral dynamics and whose Biosafety Level 3 (BSL3) research facility was essential for our publication analyzing the SARS-CoV-2-mediated long noncoding RNA changes and interactions. I would also like to extend my gratitude to the groups of Dr. Mohan Sopori, Dr. Mehdi Mirsaeidi and Dr. Il-Man Kim as well as the NIH Lung Tissue Research Consortium, the Veterans' Administration, and the Lovelace Respiratory Research Institute for providing us with research samples that were essential for completion of our studies. BioRender.com was utilized to create the descriptive study outline figures.

I would further like to acknowledge and extend my deepest gratitude to Dr. Dinesh Devadoss, who was the primary contributor to the following figures: Figure 7, 27, 28, 29, 30, 31, 33, 34, 35, 36, and 37 (1, 2); to Dr. Glen Borchert and his group, who were the primary contributors to Figure 26 (1); to Drs. Raymond Langley and Glen Borchert who were primary contributors to Figure 6 (2); to Dr. Prem Chapagain and Mr. Michael Cioffi, who were the primary contributors to Figure 32 (1); and lastly to Dr. Christopher Long, who was the primary contributor to the imaging process in Figure 3. (3) The contributions of all of my colleagues are highly appreciated.

Of course, I would also like to extend my immense gratitude to my family in my home country of Macedonia. Without their unconditional love and support, I

would not have been able to achieve this. I thank my parents, Mrs. Evgenija Naumovska Manevska and Mr. Toni Manevski as well as my sister Ms. Ksenija Manevska for their encouragement and support throughout the years. It is for them that I have done my best every day and come this far. I would also like to thank my partner, Ms. Michelle Deville who has provided incredible support to me through the PhD progression.

I also would like to acknowledge the Frontiers publishing group as the original publisher of “Increased Expression of LASI LncRNA Regulates the Cigarette Smoke and COPD Associated Airway Inflammation and Mucous Cell Hyperplasia”, 2022, DOI: 10.3389/fimmu.2022.803362, the Elsevier publishing group as the original publisher of “Cellular stress responses and dysfunctional Mitochondrial-cellular senescence, and therapeutics in chronic respiratory diseases”, 2020, DOI: 10.1016/j.redox.2020.101443, the Cell Press publishing group as the original publisher of “Immunomodulatory LncRNA on Antisense Strand of ICAM-1 Augments the SARS-CoV-2 Infection Associated Airway Mucoinflammatory Phenotype”, 2022, DOI: 10.1016/j.isci.2022.104685 and the Nature publishing group as the original publisher of “A long noncoding RNA antisense to ICAM-1 is involved in allergic asthma associated hyperreactive response of airway epithelial cells”, 2021, DOI: 10.1038/s41385-020-00352-9, and thank them for allowing me to use the articles in my thesis. Lastly, I would like to thank the NIH (NIH AI152937) and the FIU Graduate Research Assistantship for funding my research and time at Florida International University.

ABSTRACT OF THE DISSERTATION

ROLE OF NOVEL IMMUNOREGULATORY LONG NONCODING RNAS IN AIRWAY EPITHELIAL PATHOPHYSIOLOGY AND CHRONIC PULMONARY DISEASE

by

Marko Manevski

Florida International University, 2022

Miami, Florida

Professor Hitendra S. Chand, Major Professor

COPD is currently the third leading cause of death globally, accounting for approximately 6% of all deaths in 2019, and cigarette smoke (CS) is the primary risk factor for disease development.

Transcriptomic analysis of a 3D in vitro model using differentiated human airway epithelial cells (AECs) identified a novel lncRNA on the antisense strand of ICAM-1 or *LASI* that showed increased expression upon CS exposure. The lncRNA was significantly upregulated in CS-induced Rhesus macaque airways and in human COPD airways that exhibited higher mucus expression and goblet cell hyperplasia, which was recapitulated in vitro. Blocking lncRNA expression in cell culture setting suppressed the smoke-induced and COPD-associated dysregulated mucoinflammatory response suggesting that this airway specific immunomodulatory lncRNA may represent a novel target to mitigate the smoke-mediated inflammation and mucus hyperexpression.

Additionally, not much is known about contribution of airway lncRNAs in COVID-19. RNA-sequencing analysis of nasal samples from COVID-19 patients showed significantly higher expression of secretory mucin and inflammatory gene signatures compared to the uninfected controls. COVID-19 patients showed elevated expression of inflammatory factors, airway mucins and associated transcription factors. *LASI* was induced in COVID-19 patients with high viral-load. A SARS-CoV-2 infected 3D-airway model largely recapitulated these clinical findings. Molecular dynamic modeling further suggested a stable interaction between viral RNA and *LASI* lncRNA. Notably, blocking *LASI* lncRNA reduced SARS-CoV-2 viral load and suppressed MUC5AC mucin levels. *LASI* lncRNA represents an essential facilitator of SARS-CoV-2 infection and associated airway mucoinflammatory response.

Altogether, *LASI* lncRNA may represent a novel target to control the smoke-mediated dysregulation in airway responses and COPD exacerbations, as well as in viral infection-related inflammatory responses.

TABLE OF CONTENTS

CHAPTER PAGE

LIST OF TABLES

TABLE PAGE

LIST OF FIGURES

FIGURE PAGE

ABBREVIATIONS AND ACRONYMS

ABBREVIATION	FULL NAME
AB	Alcian blue
AB-H&E	Alcian blue and hematoxylin and eosin
AB-PAS	Alcian blue and periodic acid Schiff's reagent
ACE2	Angiotensin-converting enzyme 2
AEC	Airway epithelial cells
ALI	Air-liquid interface
ATF4	Activating transcription factor 4
ARDS	Acute respiratory distress syndrome
BAL	Bronchoalveolar lavage
BALF	Bronchoalveolar lavage fluid
CB	Chronic bronchitis
CDE	Cat dander extract
cDNA	Complementary DNA
CHBEs	COPD human bronchial epithelial cells
CHOP	C/EBP homologous protein
COPD	Chronic obstructive pulmonary disease
CS	Cigarette smoke
CSE	Cigarette smoke extract
CXCL-8	Chemokine C-X-C motif ligand 8
DDX58	DExD/H-Box Helicase 58
eIF2a	Eukaryotic translation initiation factor 2A
EGFR	Epithelial growth factor receptor
ELISA	Enzyme linked immunosorbent assays
ENDS	Electronic nicotine delivery systems
EVALI	E-cigarette, or vaping, product use associated lung injury

FEV_1	Forced expiratory volume in 1 second
FISH	Fluorescent in situ hybridization
FOXJ1	Forkhead box protein J1
FOXA2	Forkhead box protein A2
FOXA3	Forkhead box protein A3
FVC	Forced vital capacity
GAPDH	Glyceraldehyde-3-phosphate dehydrogenase
GOLD	Global initiative for chronic obstructive lung disease
GRP78	Glucose-regulated protein of 78 kDa
HBECs	Human bronchial epithelial cells
HPI	Hours post infection
ICAM-1	Intercellular adhesion molecule-1
ICC	Immunocytochemistry
ICR	ICAM-1-related long noncoding RNA
IF	Immunofluorescence
IFIH1	Interferon induced with helicase C domain 1
IFN-γ	Interferon gamma
IHC	Immunohistochemistry
IgE	Immonoglobulin E
IL-1	Interleukin 1
IL-6	Interleukin 6
IL-13	Interleukin 13
IRE1	Inositol requiring enzyme 1
IRF3	Interferon regulatory factor 3
LASI	Long noncoding RNA antisense to ICAM-1
lncRNA	Long noncoding RNA

LPS	Lipopolysaccharide
MALAT1	Metastasis-associated lung adenocarcinoma transcript 1
MCh	Methacholine
MFI	Mean fluorescence intensity
miRNA	Micro RNA
MOI	Multiplicity of infection
mtDAMPs	Mitochondrial damage associated molecular patterns
MUC5AC	Mucin 5AC
MUC5B	Mucin 5B
NEAT1	Nuclear enriched assembly transcript 1
NF-κB	Nuclear factor kappa-light-chain-enhancer of activated B cells
NHBEs	Normal human bronchial epithelial cells
PERK	Protein kinase R-like ER kinase
PG	Propylene glycol
PPRs	Pattern recognition receptors
qRT-PCR	Quantitative real-time PCR
RNA-seq	RNA sequencing
ROS	Reactive oxygen species
SARS-CoV-2	Severe acute respiratory syndrome coronavirus 2
SCGB1A1	Secretoglobin family 1A member 1
siCTRL	Control small interfering RNA
SPDEF	Sam-pointed domain containing ETS transcription factor
TGF-β	Transforming growth factor beta
TMPRSS2	Transmembrane protease, serine 2
UPR	Unfolded protein response

VG	Vegetable glyceryn
WAKMAR2	Would and keratinocyte migration associated long noncoding RNA
WS-23	2-isopropyl-N,2,3-trimethylbutyramide

Chapter 1: Establishing a COPD Model

Data included in this chapter has been originally published by Elsevier Publishing Group, “Cellular stress responses and dysfunctional Mitochondrial-cellular senescence, and therapeutics in chronic respiratory diseases”, 2020, DOI: 10.1016/j.redox.2020.101443 and Frontiers Publishing Group, “Increased Expression of LASI LncRNA Regulates the Cigarette Smoke and COPD Associated Airway Inflammation and Mucous Cell Hyperplasia”, 2022, DOI: 10.3389/fimmu.2022.803362.

Chapter 1: Introduction

I. The global burden of COPD

Chronic obstructive pulmonary disease (COPD) is defined as a common, preventable, and treatable disease characterized by persistent respiratory symptoms and airflow limitation due to airway and/or alveolar abnormalities usually caused by significant exposure to noxious gases or particles and influenced by host factors including abnormal lung development. (4) COPD is currently the third leading cause of death globally, accounting for approximately 6% of all deaths in 2019. Data analysis, stratified by population income status has shown that COPD is consistently among the top five causes of death in the U.S. (5) There is extensive variability among reported studies on COPD prevalence, largely due to reliance on different methodologies of COPD diagnosis and evaluation. The gold standard for COPD diagnosis is by spirometry, according to the National Heart Lung and Blood Institute (NHLBI)/World Health Organization (WHO) Global initiative for chronic

obstructive Disease (GOLD) guidelines, which are intended to promote a concentrated effort among healthcare providers globally to address this highly prevalent disease. (6) COPD severity is classified by GOLD-stages which range from GOLD 0: at risk, to GOLD IV: severe COPD. Specifically, a post-bronchodilator forced expiratory volume in 1 second (FEV_1) < 80% of predicted value and an FEV_1/forced vital capacity (FVC) < 70% confirms a COPD diagnosis. Current estimates of the COPD prevalence range from 300 to 370 million global cases, with the highest prevalence being reported in the American continent whereas the lowest prevalence is reported in Southeast Asia. (7, 8) Among the population over 30 years of age, COPD is estimated to have a prevalence of 11.4%, with a higher prevalence in men (14.2%), as compared to women (7.6%). (9) Adeloye and colleagues (2015) further report that COPD prevalence studies in African, East Mediterranean and Southeast Asian regions are sparse. (9) The American region had the highest prevalence of 14.1%, followed by the Eastern Mediterranean region with a prevalence of 13.2%, the African region with a prevalence of 10.6%, the Western Pacific region with 10.0% prevalence and lastly the South-East Asia region with 7.6% prevalence. (9) A large-scale longitudinal population study in a Canadian population reported that the lifetime risk of physician-diagnosed COPD in a large, multicultural North American population is 27.6%. (10) They additionally report that the risk was further higher for men, for individuals from lower socioeconomic status and individuals from rural settings. However, Lamprecht and colleagues (2015), however, estimated that as many as 80% of COPD cases may be undiagnosed, and that the problem of underdiagnosis

particularly persists in low-income regions. (8, 11) They found very high variability by region in terms of underdiagnosis, with certain regions showing >90% underdiagnosis and the lowest underdiagnosis being approximately 50%. (11) Many COPD diagnoses are made upon instances of exacerbation, or upon at least some loss of lung function, which in most cases would imply a certain level of irreversible lung damage prior to diagnosis and/or potential treatment. (12) With a globally aging population, coupled with continuous exposure to COPD-augmenting respiratory insults such as cigarette smoke (CS), air pollutants, biomass fuel smoke, and occupational chemicals, the global incidence of COPD is only expected to increase, across developed and developing regions alike. (13-15) Environmental exposure to toxins or allergens exacerbates the disease and is associated with a very high 5-year mortality rate (55%) among COPD patients (16). In 2017, the estimated annual health care cost associated with tobacco use was around $157.7 billion. In the past decade only, several studies demonstrated a variety of adverse health effects associated with CS exposure. The results of these studies, although dependent on multiple factors, strongly indicate that CS detrimentally impacts human health. (17) With over 7,000 toxicants rolled together to compile a cigarette, most have been deemed as etiologic factors in the development of inflammatory diseases including nicotine, tar, benzene, carbon monoxide and more. Chronic CS exposure is known to contribute to the development of atherosclerotic processes independently and synergistically with other etiological factors, and ultimately leads to coronary artery disease (CAD). In addition, the role of CS exposure in both lung and bladder carcinogenesis has

been well-established alongside its role in a multitude of other cancers. COPD is clinically characterized primarily by chronic bronchitis and emphysema.

COPD patients often suffer from daily symptomatic presentations, but exposure to certain irritants like CS, viral infections, or even exercise can result in periods of severe disease manifestations or exacerbations. (18) These exacerbations are the major contributor of burden on the global healthcare system, and although there is significant variation between global regions, there have been approximately 3 million global COPD-related fatalities annually, with exacerbations being the primary contributing factor. (7, 14, 19) The economic healthcare burden is also steep, and in the United States, the exacerbation-related hospitalizations alone account for over 49 billion USD in annual healthcare costs. (16) Furthermore, evidence suggests that the mortality due to COPD is largely underreported. In fact, even in the most severe cases, Lindberg and colleagues (2021) estimated that less than 60% of COPD-related deaths were accurately reported. (20) COPD is often excluded or underreported as a contributing or underlying cause of death. Even severe cases of COPD were found to be underreported, and COPD underreporting was found to be largely associated with male sex and patient obesity. (20) Interestingly, studies have shown that females are more likely to develop COPD as compared to males with similar smoking history. (21) These data show that COPD is a highly prevalent, underreported, and underdiagnosed disease that imposes a heavy burden on global healthcare and is a major cause of death worldwide. Most importantly, the impact of COPD and related healthcare costs will only continue to increase and therefore, studies are needed to improve

the current understanding of underlying disease mechanisms and to develop better treatment or disease management regiments for patients.

II. COPD pathogenesis

COPD is characterized as a pathological change in the normal lung function, resulting in a progressive and an irreversible airflow limitation. The development of COPD is associated with the long-term exposure to environmental insults that lead to chronic airway inflammation and epithelial remodeling. The major observable phenotypes in COPD patients include small airway obstruction (obstructive bronchiolitis) and lung parenchyma destruction (emphysema). It is an aging-associated condition characterized by progressive and irreversible airway obstruction and tissue remodeling which causes chronic, recurring bronchitis and alveolar tissue destruction. (22) The definition of chronic bronchitis (CB) is chronic sputum production and cough for three months per year for at least two years. Most commonly, symptoms include dyspnea, cough and sputum production leading to increased rates of exacerbation, accelerated, age-associated decline in lung function, reduced quality of life and increased mortality. (14, 22) CB is present in the general population; however, it is more prevalent in COPD patients, with up to 74% patients suffering from CB. (14) CS exposure directly insults the epithelial cells lining the conducting airways of the respiratory system from the nasopharyngeal region to the alveolar region, and induces inflammatory response pathways, immune cell infiltration of the airway epithelium, and extensive epithelial remodeling.

Mucus hypersecretion is the major phenotype for CB, which is a result of airway epithelial remodeling with an increase in the percentage of mucus secretory cells, coupled with a reduced proportion of ciliated cell population. (22) Several noncoding RNAs (ncRNAs) generated from intergenic and intronic regions have now been shown to regulate all stages of gene expression and several cellular functions including the lung innate immune responses. Mucociliary clearance mechanisms are one of the primary innate defense mechanisms that physically clear the airways via mucociliary excretion. (23, 24) In the respiratory tract, 9 genes have been found to encode for mucins, of which MUC2, MUC5AC, and MUC5B are primarily found in airway secretions (25, 26). The heterogeneity in airway mucins allows entrapment of many inhaled pathogens and toxicants to help clear the airways by mucociliary clearance mechanisms, therefore, a lot of attention has been geared towards understanding the expression and the regulation of these mucins in the context of lung pathologies. Bacterial pathogens can be entrapped on mucus adherent to epithelial cells, mucus plugs favor pathogens that thrive in anaerobic conditions and many infections are polymicrobial, with the mucus mesh shielding pathogens from the immune response. (27)

There are several stages of COPD severity, as defined by the GOLD standard, ranging from GOLD 0 to GOLD IV. (6) GOLD 0 includes patients that are at risk for COPD development, show symptoms such as cough and sputum production, however, have normal spirometry results. GOLD stage I (mild COPD) includes patients with a $FEV_1/FVC < 70\%$, and a $FEV_1 > 80\%$, with or without chronic symptoms. GOLD stage II (moderate COPD) includes patients with a

$FEV_1/FVC < 70\%$, and a $30\% < FEV_1 < 80\%$ and GOLD stage III (severe COPD) includes patients with a $FEV_1/FVC < 70\%$, and $FEV_1 < 30\%$. (6) Typically, GOLD stage II presents with dyspnea upon exertion and is typically when patients seek medical help due to disease exacerbation. Exacerbations are especially frequent in patients with $FEV_1 < 50\%$.

III. Airway epithelium

Inhaled air inadvertently carries countless benign and some potentially harmful particles into our body that are subsequently deposited throughout the airways onto a protective film that is the airway mucus layer. Airway mucus is crucial as a first line of defense against harmful inhaled particles by trapping and directing them back towards the oropharynx via ciliary beating in a process called mucociliary clearance. (28) Airway epithelial cells (AECs) that lie just beneath this layer are responsible for the coordination and initiation of this process. AECs are the primary cells that line the lumen of airways and are paramount in preserving the normal airway function. They are amongst the first cells to come in contact with environmental stimuli and serve as a crucial barrier against harmful inhaled substances including CS. (24, 29) AECs are largely comprised of 3 major cell types: ciliated cells, basal cells and mucous/goblet cells, although there are other cell types recently reported such as neuroendocrine cells, deuterosomal cells, tuft cells, suprabasal cells and ionocytes. (30) Each cell type serves a specific role in maintaining proper structure and function of the airways. Basal cells, the predominant cell type in small airways (can account for approximately 30% of all cells), play a crucial role in cell adhesion, produce important bioactive molecules,

and have the ability to self-renew and differentiate in response to injury. Ciliated cells, the major cell type throughout the conducting airways move the mucus from distal airways to the oropharynx via directional ciliary beating. Mucous cells, also known as goblet cells, are vital to secreting the proper amount of mucus to trap foreign inhaled particles in the airway lumen. (26, 31, 32) Certain cell types are more rare. Suprabasal cells are a subtype of basal cells with increased expression of *KRT19* and *NOTCH3*. (30, 33) Hillock cells represent groups of cells that do not contain ciliary cells and represent a metaplastic zone of high proliferation usually found upon epithelial injury. (30) Tuft cells are chemosensory epithelial cells similar to the neuroendocrine cells with a highly distinct morphology, however their specific roles have not been identified. (34) Ionocytes account for a very small proportion of cells but are highly enriched in CFTR and likely arise from tuft cells. (35, 36) A recent study further showed that respiratory bronchioles contain a distinct cell type referred to as respiratory airway secretory (RAS) cells, which act as progenitor cells for alveolar type II (AT2) cells, thereby regenerating the alveolar tissue. (37) This regeneration is mediated by Notch and Wnt signaling, and cigarette smoke is known to disrupt the Notch signaling and induce pathological changes in COPD patients. (38)

The complex interplay amongst these cell types is therefore crucial to maintaining airways and providing proper lung function. Therefore, dysregulation of these protective processes can be seen to cause harm and contribute to the development of various respiratory diseases. In fact, numerous changes have been reported in airway epithelium that has been chronically exposed to CS.

Cellular plasticity is altered by CS. AEC are linked by intercellular tight junctions and adherens junctions. A recent study has shown that airway epithelium derived from COPD patients exhibited partial epithelial to mesenchymal transition features, such as cellular unjamming and an increase in polymerized actin. (39) Chronic CS exposure is known to result in reduced e-cadherin and β-catenin, and it has been shown to directly affect the epithelial integrity upon chronic exposure. (40, 41) The reduction of cell-to-cell contact strength induces tissue degradation with progressive exposures to CS. Interestingly, treatments targeting TGF-β may have been unsuccessful due to the fact that they do not address this loss of intercellular junctions. (39) Furthermore, mucus secretion is a hallmark of COPD progression. In a pathological state, airway mucous obstruction can be a product of multiple complex processes that involve mucin gene expression, mucin hypersecretion, and goblet cell hyperplasia. Ultimately, these processes can lead to the decline in lung function and cause significant increase in associated morbidity and even mortality. (31, 42) Airway epithelium secretes mucins MUC5AC and MUC5B, which form the first line of defense against extracorporeal pathogens. (31) Furthermore, secretory immunoglobulin (Ig)A comprised of polymeric IgA (pIgA) is produced by plasma cells and transported to the apical side of the epithelial layer where it forms a protective layer that agglutinates pathogens in a process referred to as immune exclusion. (43) In a pIg receptor (R)-deficient murine model, a COPD-like phenotype was observed, as well as airway remodeling resembling a COPD phenotype. (43)

IV. Airway mucus secretion

Airway mucus is a complex solution that is comprised of water, ions, lung secretions, serum protein transudates and mucin glycoproteins or mucins (44). Mucins are comprised of 97% water and 3% solids, with mucin glycoprotein accounting for 30% of the solid composition. (31) It is thought that airway mucous is bi-layered, with an upper viscoelastic gel layer above and a watery, periciliary layer. The function of the periciliary layer is thought to be the process of lubricating the beating cilia, while the gel layer is responsible for the actual trapping of inhaled particles, microbes or microbial byproducts. After trapping particles, the gel layer rolls onto the tips of beating cilia so that it may be cleared from the airways towards the oropharynx. Once there, the mucus is either swallowed and degraded via the gastrointestinal tract or coughed out as sputum or phlegm. (42)

Secretory mucins MUC5AC and MUC5B and strongly expressed in the airways and mucin MUC5AC expression strongly correlates to pathogen presence. (44) Both MUC5AC and MUC5B form a gel as a mesh and both form chain structures rather than branch structures. (31, 44) The primary function of the mucin layers is interacting with pathogens or microbial proteins and sequestering said pathogens, in addition to acting a solid physical barrier. (45)

Mucins are stored in the cytoplasmic granules of mucous secreting cells until exocytosis pathways are engaged that propel the mucin granules to the apical surface of the secretory AEC. A group of important chaperone proteins, known as MARCKS or myristoylated alanine-rich C kinase substrate, are critical in helping transport mucin vesicles to the plasma membrane. Once on the plasma

membrane, the mucin-containing granule forms a secretagogue complex that irreversibly docks to the membrane. Once this process takes place, mucin exocytosis is rapidly initiated, occurring in tens of milliseconds. After its release, mucin is capable of vastly expanding more than a hundred-fold in volume. This expansion process is dependent on the dilution of calcium from the granules, which allows for electrostatic expulsion and is accelerated by water, that ultimately results in a large expanded mucinous network in the airways. Of note, exaggerated and excessive exocytosis has been implicated in the mucous hypersecretion associated with COPD exacerbations (23, 42).

V. Cigarette smoke and its components

Exposure to cigarette smoke (CS) in vapor form, or in vitro exposure of cell cultures to CS extract induces numerous changes in the cells, however of primary interest for development of COPD is the aggregation of reactive oxygen species (ROS) as well as the ROS-mediated misfolding of proteins in the lung epithelium that may lead to activation of the unfolded protein response (UPR). (46).

The effect of CS exposure also varies based on complexity and chemical composition, which itself is dependent on heating conditions, including temperature and oxygen flow. The burning zone of cigarettes during the combustion process can reach as high as 900°C while the areas behind marginal oxygen levels reach approximately 700°C in the distillation zone, where pyrolytic reactions occur. Inhaled smoke drawn through the cigarette is named mainstream smoke. (47). Mainstream smoke consists of particle and gas phases, including volatile organic compounds (VOCs), and semi-volatile organic compounds

(SVOCs). Chemical classes that constitute tobacco smoke include aldehydes, ketones, carboxylic acids, phenols, nitriles, alkaloids, and various saturated and unsaturated hydrocarbons. Smoke constituents can act as electrophiles, free radicals, and reactive anions. For example, benzo[a]pyrene converts to quinone, which then produces ROS as byproducts. Hydroxyl ions, which are another crucial ROS, are formed by hydrogen peroxide via Fenton's reaction in the tar phase or by its compounds such as catechol. Redox cycling mechanisms also form semiquinones and superoxide ions, which are highly reactive. Gas-phase components such as nitric dioxide can form carbon-centered radicals by reacting with other smoke constituents. Superoxide ions react with nitric oxide to form peroxynitrite with high oxidizing capacity. Peroxynitrite can also deplete intracellular antioxidants such as glutathione. Reactive oxygen and nitrogen species (ROS and RNS, respectively) generated in mainstream smoke perpetually form reactive intermediates such as acrolein, which are cytotoxic. (48) Vastly produced polycyclic aromatic hydrocarbon (PAH) components in tobacco smoke, such as 1-Nitropyrene, was shown to augment mitochondrial genes and induce deregulation of mitochondrial genes via C/EBPα. (49) Copious amounts of exogenous reactive oxygen and nitrogen species produced in tobacco smoke offset the redox homeostasis in cells inducing oxidative stress.

VI. Genetic regulation of mucins

Mucins, produced by goblet cells of the epithelium and seromucous glands of the subepithelial mucosa, comprise 2% of the total weight of airway mucous. Mucins are noted to be long, thread-like molecules with linear peptide backbones

that undergo a complex glycosylation pattern. It has been shown that this pattern is what allows these products many broad bacterial attachments for entrapment and clearance. Specifically, in the respiratory tract, 9 genes have been found to encode for mucins: MUC1, MUC2, MUC4, MUC5AC, MUC5B, MUC7, MUC8, MUC11 and MUC13. However, only MUC2, MUC5AC and MUC5B have been found in airway secretions. Specifically, MUC5AC and MUC5B have been demonstrated as the dominant gel-forming mucins in the normal respiratory tract. (26, 50) The former is known to be a goblet cell mucin while the latter a mucin that predominates in the glands. Additionally, a lot of attention has been geared towards demonstrating the expression and role of MUC5AC and MUC5B in disease models. MUC5AC is heavily regulated at the transcriptional level. (31) Studies have therefore found an increase in MUC5AC mRNA levels in the bronchial tissue of patients with chronic bronchitis. In addition, MUC5B has been shown to be a major component of bronchial mucus from patients with obstructive pulmonary disease. (44, 51) The epithelial growth factor receptor (EGFR) is crucial for COPD-related induction of mucus secretion, via upregulation of transforming growth factor (TGF)-α. (38, 52, 53) Further, blocking EGFR phosphorylation inhibits MUC5AC secretion, however, ROS generation can account for only a part of the CS-induced EGFR activation and mucin synthesis. A large proportion of EGFR activation can be attributed to the acrolein effects, which produce cyclooxygenase products as well as increased expression of EGFR ligands that further contribute to EGFR activation. (31, 54, 55) Additional regulatory elements such as the neuregulin (NRG) 1β1 have also been identified and are believed to

play a role in COPD progression. (56) The IL-13-mediated may not play a significant role in COPD mucus dysregulation, however the recently identified SMAD signaling-mediated mucus hypersecretion may play a more significant role. (38, 54) Mucus plugging has further been reported to induce inflammatory responses even in the absence of pathogens. (27) Mucus plugs are associated with cellular hypoxia and cell death, which induces the inflammatory response via IL-1 secreted from necrotic cells. (27, 57) Numbers of necrotic AEC have been found to be elevated in COPD, and reduction of IL-1-receptor has been found to alleviate the neutrophilic inflammation. (27, 58)

VII. Dysregulation in cell energetics

Mitochondria are the major cellular oxidative stress sensors that regulate metabolism, signaling, and energetics to maintain cellular and tissue homeostasis. In addition, mitochondria are reportedly critical in regulating cellular inflammatory responses, innate immunity, and aging. (59-62) Mitochondrial dysfunction and dysregulated ROS production following lung inflammation contribute to various lung diseases and impaired lung functions. Protein folding in the ER is susceptible to extracellular stimuli and insults. The ER is a highly organized luminal network that plays an important role in protein synthesis, maturation, folding and transport. (63-67)

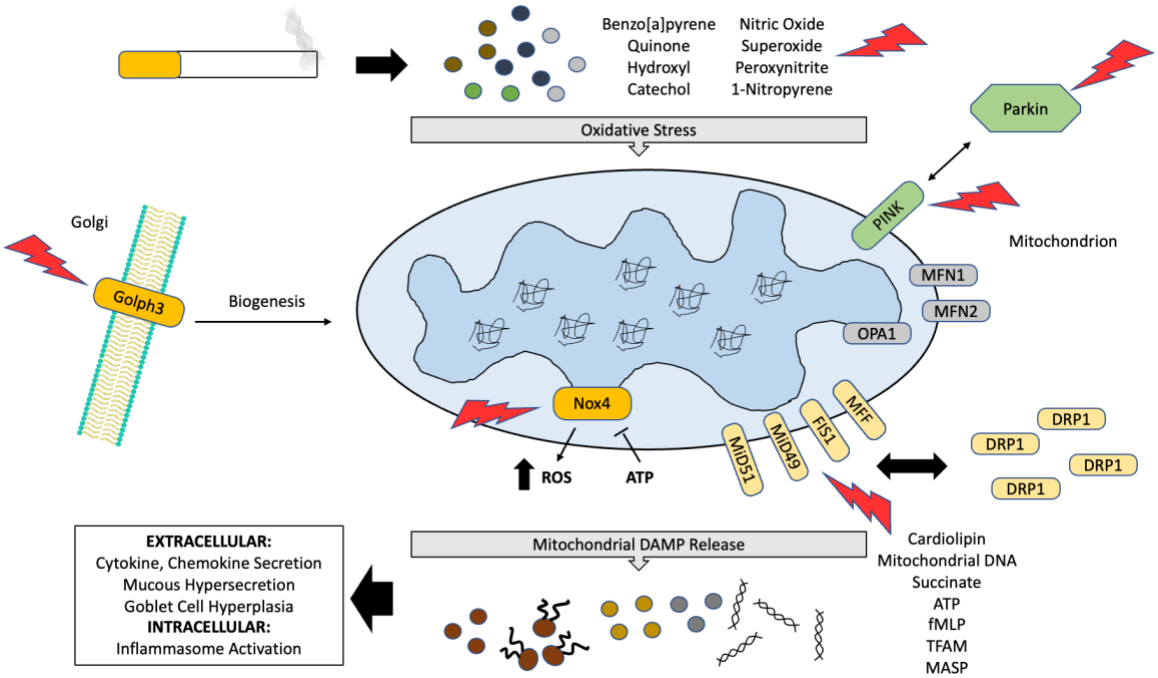

Figure 1. Potential therapeutic targets within the mitochondrial oxidative stress response pathways of the airway epithelium. Original source (68).

When ER homeostasis is disrupted by inhaled toxicants, the ER develops an unfolded protein response (UPR) in order to maintain cellular homeostasis. (65-67) Notably, dysregulated homeostasis following the unresolved stress in mitochondria and ER can initiate cell death pathways. Studies have shown that various signaling pathways, triggered by the UPR and ROS presence, are crucial to trigger cell death/apoptosis when they fail to restore protein homeostasis. (64) Previous studies have shown that CS-induced ER stress is increased in the lungs of smokers and patients with COPD and have reported oxidant-induced irreversible damage of lung proteins and induction of the ubiquitin-proteasome system or autophagic vacuoles. (69, 70) CS-induced increase in polyubiquitination of proteins in different lung cell types, in vitro in alveolar and airway epithelial cells, lung fibroblasts and alveolar macrophages, and in vivo in mouse lungs has been

reported. (69-73) Numerous pathways are involved in chronic CS-induced UPR and oxidative changes. For example, chronic CS exposure induces upregulated expression of the chaperones glucose-regulated protein of 78 kDa (GRP78), calnexin and calreticulin, protein disulfide isomerase (PDI) and other signaling molecules that play a vital role in the PERK pathway (phosphorylated-eIF2a, ATF4, and CHOP) in the human lung. (46, 73-75) Additional evidence from a mouse model of CS exposure demonstrates increased expression of phospho-eIF2α, CHOP, and p50 ATF6N protein and mRNA levels in mouse lung. (69) Acute versus chronic CS exposure in mouse showed differences in mRNA levels of ATF4 and CHOP in mouse lungs and alveolar macrophages, suggesting that UPR target genes and proteins are dynamic and cell type-dependent in vivo, at the transcriptional and translational levels. (72, 76, 77) GRP78 is an ER chaperone known to be involved in alveolar epithelial cell survival and gene expression during lung development via modulation of ER stress. (78-80) Previous reports have shown increased GRP78 protein levels in the lungs of smokers and patients with COPD. Furthermore, GRP78 serum levels were significantly increased in COPD, correlating with decline in lung function and severity of disease. (81) In another report, BALF levels of GRP78 were significantly greater in smokers compared to non-smokers and human AEC treated with CS extract showed augmented secretion of GRP78. (74) Overall, these findings on elevated ER stress protein GRP78 levels suggest that it could be used as a potential biomarker for CS-induced lung injury and chronic lung diseases. Furthermore, although the UPR seems to induce various pathologic changes in chronic pulmonary disease, it also

induces increased antioxidant expression. Specifically, the PERK/eIF2α/CHOP branch of the UPR has been shown to drive the expression of nuclear factor (erythroid 2)-related factor 2 or Nrf2. (46, 82)

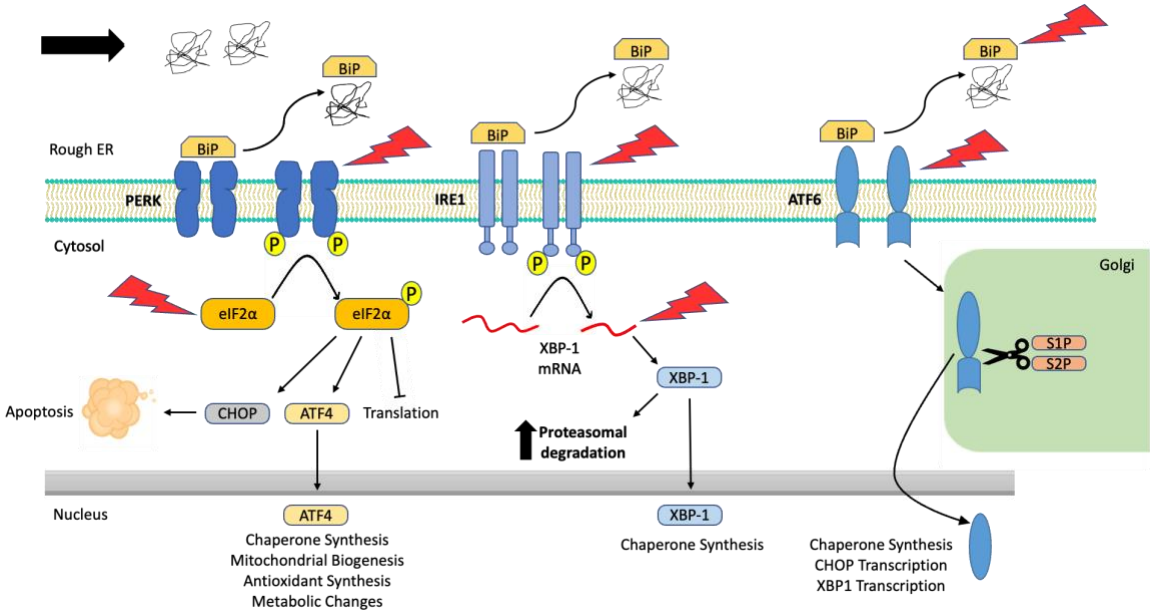

Figure 2. Molecular changes and potential therapeutic targets within the unfolded protein response pathways that are involved in chronic airway diseases. Original source (68).

In turn, Nrf2 interacts with ATF4 and together they drive the expression of genes involved in glutathione synthesis, hydrogen peroxide scavenging and more. (83) However, Nrf2 plays a critical role in CS-mediated ROS generation. ROS increase allows for nuclear translocation of Nrf2 where it affects the transcription of over 500 genes, including the NF-κB inflammatory pathway. (84) Furthermore, the PERK/eIF2α branch is significantly involved in cell fate decisions by inducing, or preventing apoptosis, particularly upon chronic ER stress. Specifically, Kasai et al. (2019) have shown that when Nrf2 interacts with ATF4, they repress the expression of CHOP, a proapoptotic gene. (85, 86) The Ire1 branch has also been

implicated in proapoptotic induction via the highly regulated Ire1-dependent decay pathway (RIDD) and all three branches (ATF6, ATF4 and XBP1) can potentially bind CHOP. (87, 88) As such, excessive inhibition of the UPR, specifically of the PERK branch may have deleterious effects, and as such, further research is required. (89) Cigarette smoke also disrupts the trans-Golgi network, where Golgi phosphoprotein 3 (GOLPH3) plays a vital role in protein trafficking and glycosylation. GOLPH3 has been linked with the ER in relation to phosphotidylinositol-4-phosphate signal termination mediated membrane docking mechanism. (90) Multiple elements have been suggested as potential therapeutic targets to alleviate the CS-induced UPR/ER dysregulation (**Figure 1-2, Table 1**).

Cigarette smoke, including secondhand, thirdhand, and modified tobacco products release chemical compounds that form ROS and RNS species. These products adversely affect cellular organelles, including the mitochondria, ER, and Golgi. Exposure to cigarette smoke compounds alters mitochondrial oxidative phosphorylation and metabolic activity, which are symptoms of debilitating diseases such as COPD and asthma. Overall, these findings on elevated mitochondrial dynamics and the quality control, essential for normal physiological functions are disrupted by the CS-induced oxidative stress and these pathways could be potential therapeutic targets against smoking-related chronic lung diseases.

Table 1. ER and mitochondrial therapeutic targets in chronic pulmonary diseases associated with CS exposure (79, 80, 86, 91-93). Original source (68).

Target	Function	Pathologic Response	Treatment
	ER		
GRP78 or BiP (Binding Immunoglobulin Protein)	UPR master regulator: binds unfolded proteins, releases downstream effectors	Binds unfolded proteins, UPR effectors dimerization and activation	Upregulate
PERK (Protein Kinase R-like ER Kinase)	UPR effector, Inactivates eIF2	Activated	De-dimerize
eIF2α	Translation initiation factor. Activates ATF4 & CHOP, Attenuates translation	Activated	/
ATF4 (Activating Transcription Factor 4)	Transcription factor, Cytoprotective	Activated	Degrade
CHOP (C/EBP homologous protein)	Apoptosis initiator	Activated	Degrade
IRE1 (Inositol-Requiring Enzyme 1)	UPR effector. Splices XBP-1, allowing translation and activation	Activated	De-dimerize
XBP-1	Transcription factor, Stimulates ER chaperone production and protein degradation	Activated	Degrade (siRNA)
ATF6	UPR effector. Activated by BiP, stimulates ER chaperone production	Activated	Degrade
Calnexin	Crucial ER chaperone	/	Upregulate
Calreticulin	Crucial ER chaperone	/	Upregulate
PDI (Protein Disulfide Isomerase)	Crucial ER chaperone	/	Upregulate
Golph3	Golgi-mitochondria transport during biogenesis	Upregulated	Downregulate/degrade
	Antioxidant Regulators		
Nrf2 (Nuclear factor erythroid 2-related factor 2)	Transcription factor, Stimulates antioxidant production	/	Upregulate
Nrf3 (Nuclear factor (erythroid 2)-like factor 3)	Transcription factor, Reduces antioxidants	Upregulated	Downregulate/degrade
	Mitochondria		
PINK (PTEN-Induced Kinase 1)	Mitochondrial kinase. Recruits Parkin to depolarized mitochondria	/	Upregulates mitophagy, diminish mtDAMPs
Parkin	E3 ubiquitin ligase, mediates mitophagy	/	Upregulates mitophagy, diminish mtDAMPs
Drp1	Cytosolic, mitochondrial fission effector	/	/
Fis1/Mff/MiD49/MiD51	Mitochondrial fission proteins involved in Drp-1 recruitment	/	/
Mfn1/Mfn2/Opa1	Mitochondrial fusion proteins	Opa1 upregulated with CS exposure	/
Nox4	Inner mitochondrial membrane enzyme. ROS sensor, immune activator	Upregulated	Downregulate/degrade

VIII. COPD therapeutic approach & perspective

Despite our understanding of COPD pathogenesis, therapy currently remains palliative. Therapy is focused on alleviating symptoms and reduction of airway inflammation. (94) Further, patients with mild COPD may frequently be overtreated and, although less frequently, patients with more severe COPD may be undertreated. (95) Further, no treatment prevents the progression of COPD. (96) Glucocorticosteroids are often ineffective at improving lung function, in fact, they are effective for 3 to 6 months, and short-term treatment does not significantly reduce lung inflammation. (94) Corticosteroids may also induce adverse effects such as impaired wound healing, increased bruising and more. (94) Treatment ultimately escalates to triple therapy (TT) with two bronchodilators and one antimuscarinic agent, and 16.5% of newly diagnosed patients initiate TT within 5 years of diagnosis. (95) Certain alternative therapies have been suggested, including the use of mesenchymal stem cells, however there is no experimental support of efficacy and standards of care have not been established. (97) Targeting cytokines using novel molecules such as AntagomiRs have been suggested as potential therapeutic avenues, (98) however, current anti-inflammatory therapeutic attempts have had very limited success. (99) There is a dire need for further investigation into novel pathways and targets for future therapy in chronic conditions such as COPD. We hypothesized that as AEC are quintessential mediators of the respiratory responses driving disease progression, novel elements such as lncRNAs serve as sensors and effectors of AEC responses and wanted to investigate their importance.

Chapter 1: Methods

I. Human lung tissue samples

Lung tissue samples were obtained from the Lung Tissue Research Consortium (LTRC) from the National Institutes of Health (NIH). The COPD patient cohorts are defined as patients with a post-bronchodilator FEV1/FVC <0.7, currently the most widely accepted and robust test for COPD. Although reports have shown that early-stage COPD may present with emphysematous or other pathologic changes prior to a presentation of an FEV1/FVC <0.7, this test remains the standard confirmation of COPD diagnosis. COPD patient samples were compared to samples from GOLD stage 0 patients, which are defined as having normal spirometry results, however, may have chronic symptoms such as cough and sputum product, and may present with risk factors for COPD such as CS usage. (6) GOLD 0 individuals may or may not progress to active COPD status and are classified as pre-COPD. (100) Both genders in each GOLD stage were grouped together and all groups include both active and former smokers. GOLD stage determination was made by spirometry testing and assigned to the appropriate GOLD stage group, per the protocols described by the National Heart, Lung, and Blood Institute and World Health Organization. (6) In this report, GOLD stages I and II were defined as patients with mild COPD status and GOLD stages III and IV were defined as patients with severe COPD status. Each group had a minimum n=6 with a mean age between 59.7 and 65.2 years old. All COPD patients had a smoking history with mean packs per year (PY) ranging between 22.4 and 41.5 and former smokers had not been smoking of a mean of 13.2 and

22.9 years. Smoking history was self-reported for all patients. Lung tissue homogenates include epithelial tissue as well as other tissues and cell types. Samples were obtained from varying anatomical regions of the lungs, however all samples contained bronchial epithelial cells as confirmed by expression of pan-cytokeratin (pan-CK) from epithelial cells and MUC5AC mucin from secretory goblet cells.

II. Real-time quantitative PCR (RT-qPCR)

For all RT-qPCR analysis, total RNA extraction was performed using the RNeasy Mini kit (Qiagen) according to manufacturer's instructions. Briefly, tissues were resected and collected tissue was weighed to be under 30 mg. Tissue lysis was performed using TissueLyser® LT (Qiagen) at 50 Hz for 3 minutes. RNA concentration was quantified using the Synergy HTX reader (BioTek, VT). Complementary (c)DNA was synthesized using the iScript Advanced cDNA synthesis kit (Bio-Rad), per manufacturer's instructions or by using the Applied Biosystems™ High-Capacity RNA-to-cDNA™ Kit per the manufacturer's instructions. For qRT-PCR, FAM-based and SYBR Green primers were used. The *LASI, ICR, WAKMAR-2, NEAT1, MALAT1* lncRNAs and *MUC5AC* and *SPDEF* mRNA levels were quantified using FAM-based primer/probe sets and TaqMan gene expression kit or the SsoFast qPCR master mix (Applied Biosystems, Thermo Fisher). *ICAM-1*, *IL6*, and *CXCL8* mRNA levels were quantified using SYBR Green-based primers and the iTaq master mix (Bio-Rad). qRT-PCR was conducted using the Bio-Rad CFX Real-Time PCR detection system.

Quantification and analysis of the results was performed using the delta-delta (ΔΔ)Ct method and U6 noncoding small nuclear RNA (snRNA), glyceraldehyde-3-phosphate dehydrogenase (GAPDH) or beta actin were used as reference genes for lncRNA expression levels expression levels as described recently. (101)

III. Immunohistochemistry and immunocytochemistry

Tissue sections or fixed cells were washed in 0.05% V Brij-35 in PBS+. Antigen retrieval was performed using 10 mM citrate buffer (pH 6.0). Blocking solution (1% NDS, 3% BSA, 1% gel, 0.2% TX-1000 and 0.2% saponin in PBS+) incubation was conducted for 1 hour at room temperature followed by incubation at 4°C overnight with primary antibodies against mucin MUC5AC (Millipore Sigma) and pan-cytokeratin (pan-CK, Santa Cruz Biotechnology). Appropriate DyLight® fluorescently-conjugated secondary antibodies (Abcam) were used, and sections were incubated for 1 hour at room temperature. Sections were mounted with DAPI-containing Fluormount-G. Immunofluorescent images were captured using the Keyence BZ-X700 microscope and image analysis was conducted using the ImageJ software (NIH). Mean fluorescence intensity per number of epithelial cells was used to compare mucin MUC5AC expression levels. Pan-CK was used as a confirmation of epithelial cell identity. Tissue sections were deparaffinized and hydrated in graded ethanol and deionized water. Histochemical staining was conducted with Alcian blue-period acid Schiff (AB-PAS) or AB followed by hematoxylin and eosin (H&E) or AB-H&E staining as described. (102) The mucus secretory cells (goblet/mucous cells) were quantified as a total number of AB-

PAS+ or just AB+ cells per millimeter (mm) basal lamina for each image. For immunostaining analyses, cell cultures grown in Nunc™ Lab-Tek™ II 8-chamber slide system were washed using 0.05% v Brij-35 in PBS(+) and immunostained as described previously (2). Cells were stained with antibodies to mucin MUC5AC (Millipore, Inc.), ICAM-1 (Cell Signaling Technology, Inc.) and pan cytokeratin (Cell Signaling Technology, Inc.). Immunostained cells were detected using respective secondary fluor-conjugated antibodies (Thermo Fisher Scientific, Inc) and mounted with DAPI-containing mounting media. Immunofluorescent images were captured using a Keyence BZ-X710 all-in-one fluorescence microscopy system and were analyzed using Keyence analysis software and Image J software (National Institutes of Health).

IV. Statistical analyses

Grouped results were expressed as mean±SEM and $p<0.05$ was considered significant. Data were analyzed using GraphPad Prism Software (GraphPad Software Inc.) using one-way analysis of variance (ANOVA) with and Tukey's multiple comparison test or using a two-tailed t test for comparison between two groups. When significant main effects were detected ($p<0.05$), student's t test was used to determine differences between the groups.

Chapter 1: Results

I. Disease severity-associated increased mucin expression, inflammation, and mucous cell hyperplasia in COPD airways

We analyzed the archived lung tissue samples obtained from 14 COPD patients and 6 control donors with no-COPD (**Table 2**).

Table 2. COPD patient cohort demographics. Original source (3).

	No COPD	Mild COPD	Severe COPD
Age*	54.2±3.2	69.2±3.9	65.1±2.7
Gender, M/F	3M/3F	4M/2F	3M/5F
Smoking in PY*	54.0±12.6 (2)	29.9±10.7 (3)	35.0±2.8 (3)
Stop Smoking (Y)*	6.6±1.6	21.4±12.8	11.9±2.5

* Mean ± SD; M = Male; F = Female; PY = Packs per Year; Y = Years

All the samples were from former smokers with or without COPD were stratified based on the on the NIH and WHO GOLD criteria (103). According to these criteria, six donor patients had mild (GOLD stage 1 or 2) COPD, and eight donor patients had severe (GOLD stage 3 or 4) COPD. To evaluate airway mucoglycoproteins (mucins) and mucous/goblet cells, tissue sections were stained with Alcian blue-hematoxylin and eosin (AB-H&E) as described recently. (2) Among the severe COPD patients, the small airways had disproportionately prominent mucus masses or plugs (**Figure 3A**). Based on the number of AB+ mucous cells in each group, there was a significant increase in mucous cell hyperplasia mucus expressing cells in severe COPD tissue samples (**Figure 3B**). Specifically, there were 31.6, 82.9, and 113.4 mucous cells per mm BL in no-

COPD, mild-COPD, and severe-COPD samples, respectively. Mucus hypersecretion is a driving factor of COPD pathology and CS exposure induces the of secretory mucin MUC5AC levels. (104-108) We also found that *MUC5AC* mRNA levels were significantly upregulated in mild and severe COPD tissue samples, with 44- and 30-fold higher expression, respectively, compared to no-COPD control tissues (**Figure 3C**).

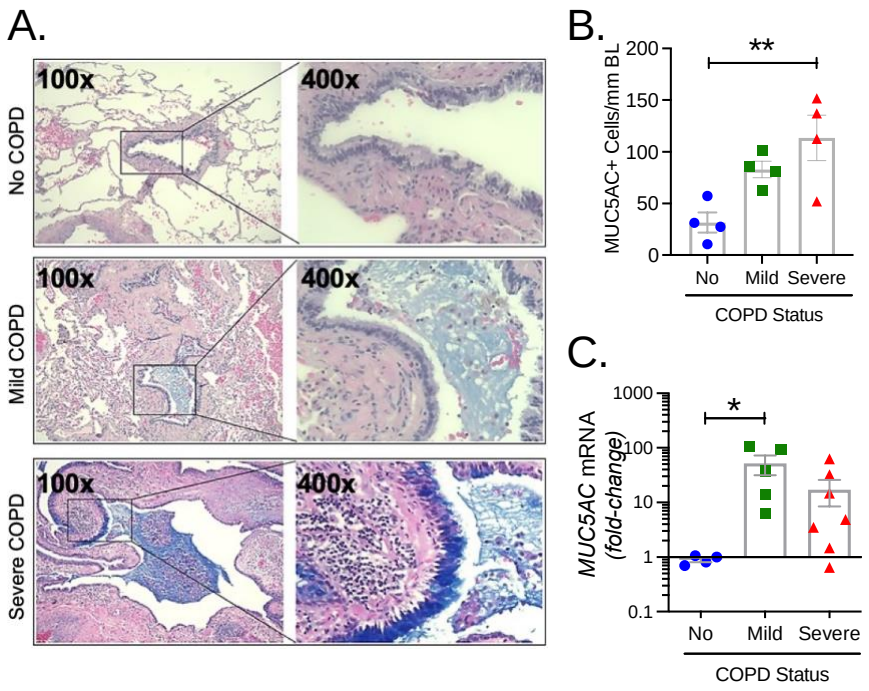

Figure 3. Archived airway sections of COPD patients show increased mucus hyperexpression and goblet cell hyperplasia. **(A.)** Representative histomicrographs of airway tissue sections from subjects with No, Mild, or Severe COPD stained with alcian blue (AB). Images are shown at 100x magnification and inset images are magnified 400x in the right panels. **(B.)** Quantification of AB+ mucous/goblet cells per mm of basal lamina (BL). **(C.)** Relative quantities of MUC5AC mRNA levels in tissues from mild and severe COPD subjects compared to control subjects with no COPD, analyzed by qRT-PCR. Data shown as mean ± SEM; n=6-8/gp; data analyzed by ANOVA with multiple comparisons; *p<0.05; **p<0.01; ***p<0.001. Dr. C. Long was the major contributor to this data. Original source (3).

In addition, we immunoprobed the tissue samples for MUC5AC protein expression and both mild and severe COPD samples showed higher MUC5AC immunopositivity (**Figure 4A**). Compared to no-COPD controls, there was a 4.2-fold and 6.8-fold increase in the percentage of MUC5AC+ cells in mild and severe COPD samples, respectively (**Figure 4B**). However, there was no significant change in the expression levels of a master transcriptional regulator of mucus response, *SPDEF* (**Figure 4C**).

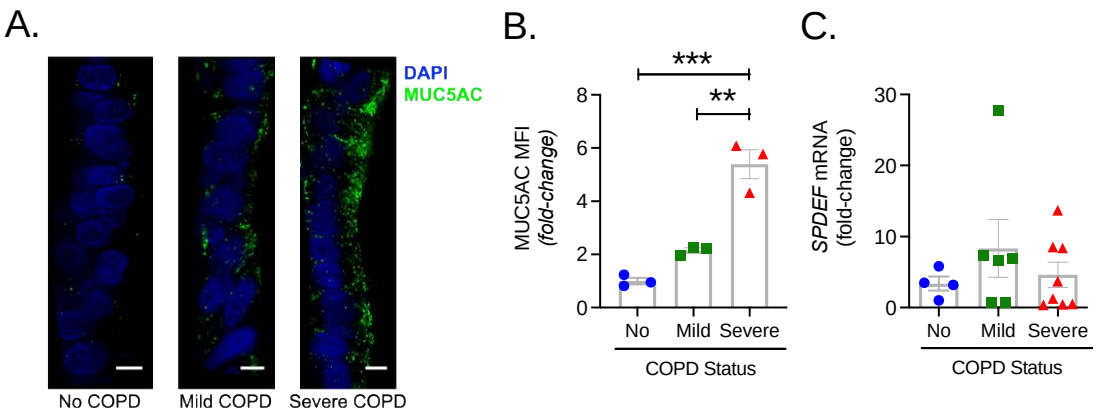

Figure 4. Archived airway sections of COPD patients show increased mucus hyperexpression and MUC5AC expression. **(A.)** Micrographs showing MUC5AC mucin immunopositivity (green) in tissue sections and counterstained with DAPI (shown in blue) to identify nuclei, scale – 10 µm. **(B.)** Quantification of MUC5AC+ cells per mm BL in each group. **(C.)** Expression levels of mucin expression-regulating transcription factor SPDEF. Data shown as mean ± SEM; n=3-8/gp; data analyzed by ANOVA with multiple comparisons; *p<0.05; **p<0.01; ***p<0.001. Original source (3).

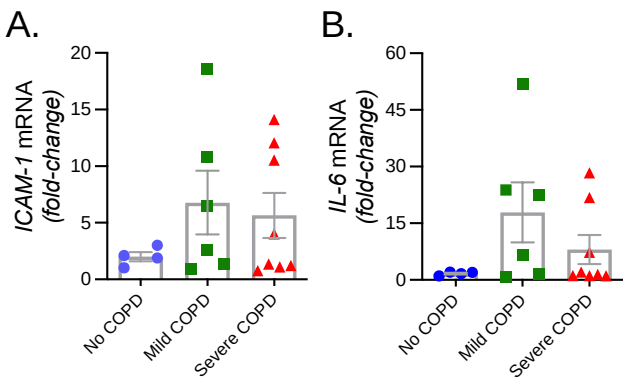

Figure 5. Expression of inflammatory factors in a COPD patient cohort. **(A.)** ICAM-1 and (**B.)** IL-6 levels in archived airway sections of COPD patients. N=4-8/gp, data analyzed by ANOVA with multiple comparisons. Original source (3).

Among inflammatory factors, mRNA levels of *IL-6* were upregulated in mild COPD samples only (**Figure 5B**) and *ICAM-1* mRNAs showed a trend towards upregulated expression in mild and severe COPD tissue samples, as compared to no-COPD controls (**Figure 5A**). These data corroborate the association of small airway tissue pathology with clinically defined COPD disease status with increased mucoinflammatory responses among COPD subjects.

Chapter 1: Discussion

Our data suggest that we have an adequate COPD model to investigate the CS-mediated airway epithelial responses. There is a clear disease progression observed in mild and severe COPD patient samples, as demonstrated by an increase in the total number of mucus secretory cells, an increase in the amount of mucus secreted from individual cells, as well as a pronounced thickening of the alveolar and parenchymal tissues. We further noticed that the mucus secretion was correlated to disease severity, however noted that there was significant variation in the expression levels of inflammatory mediators IL-6 and ICAM-1. This

observation can likely be attributed to several reasons. Firstly, when dealing with ex vivo samples, a certain level of variability is expected, second, when measuring the RNA levels in total tissue homogenate, the cell proportions may vary by sample, and the number of epithelial cells may not be the same across the different samples, and lastly, we observed that in many of the severe COPD samples, the airway epithelium was largely degraded. In fact, multiple samples were screened prior to selection of the samples used in Table 2, and many were found to have little or no viable epithelial layer to be included in the study cohorts. To summarize, using immunoprobing, as well as a histological approach and by measuring the mRNA levels of mucin MUC5AC, and inflammatory mediators such as IL-6 and ICAM-1, we have established a cohort of COPD patients that would allow for detailed investigation of the lncRNA-mediated airway epithelial responses.

Chapter 2: COPD transcriptome and a novel lncRNA

Data presented in this chapter has been originally published by Nature Portfolio publishing group (Springer Nature), “A long noncoding RNA antisense to ICAM-1 is involved in allergic asthma associated hyperreactive response of airway epithelial cells”, 2021, DOI: 10.1038/s41385-020-00352-9.

Chapter 2: Introduction

I. Epigenetic changes induced by CS exposure

With the advent of modern sequencing techniques, it became evident that less than 2% of the total human genome encodes for proteins while rest is transcribed into noncoding RNAs. The specific roles of all individual noncoding RNAs are still unclear but it is becoming increasingly evident that noncoding RNAs are key players in regulating protein expression at both the transcriptional and post-transcriptional levels. Consequentially, aberrant noncoding RNA levels can lead to dysfunctional regulation and ultimately contributing to the pathogenesis of various diseases. (109) A plethora of evidence exists that shows CS can induce many epigenetic changes, including DNA methylation, histone modification, and changes in expression of noncoding (nc)RNAs. (110) It has already been reported that CS exposure affects the expression of numerous miRNAs such as miR-21, miR-34a, miR-34c, miR-223, miR-375, miR-210, and more however recent reports have also shown that CS affects lncRNAs such as *MALAT1* and *HOTAIR* and that it takes place via IL-6/STAT3 pathways. (111) LncRNAs can interact with and bind to other lncRNAs, miRNAs, chromatin, DNA or proteins. *MALAT1* is known to bind to lncRNA *SIRT1* and they are involved in immune regulation. (112) LncRNAs

HOTAIR and *MALAT1* are vigorously studied with regards to the effect of cigarette smoke, however many lncRNAs have been identified as differentially expressed upon cigarette smoke exposure, and experimental evidence for their therapeutic potential or potential as biomarkers for disease progression is lacking.

II. LncRNAs and their potential

Advances in technology and extensive research into the realm of functional genomics has allowed researchers to discover the new class of noncoding RNA species. The ncRNA species has mostly been classified based on size into short and long noncoding RNA, with an additional class known as housekeeping RNA. Both the short noncoding and housekeeping RNA classes include some well-studied candidates. The former encompasses micro (mi)RNAs, PIWI-interacting RNAs (piRNAs), endogenous small interfering RNAs (endo-siRNAs) and promotor associated RNA (pRNA). The latter encompasses ribosomal RNAs (rRNAs), transfer RNAs (tRNAs), small nuclear RNAs (snRNAs) and small nucleolar RNAs (snoRNAs). This review will focus on the enigmatic group known as long noncoding RNA or lncRNAs. LncRNAs include a functionally diverse set of transcripts with a size greater than 200 nucleotides and are unable to encode functional proteins. The classes that have been annotated as lncRNAs so far include long intergenic non-coding RNAs (lincRNAs), natural antisense transcripts (NATs), intronic lncRNA, pseudogenic transcripts, circular RNAs (circRNAs), long enhancer noncoding RNAs (eRNAs), and transcribed ultra-conserved regions (T-UCRs) (113).

The newly identified ncRNAs along with the well-characterized proteins mediate an intricate crosstalk between mitochondria and the nucleus to maintain the airway epithelial homeostasis. Among ncRNAs, the small microRNAs (miRNAs or miRs) are implicated mainly in post- transcriptional gene regulation and a variety of innate immune processes but how these miRNAs are associated with the mitochondrial homeostasis and mitochondrial damage associated molecular patterns (mtDAMPs) is still unknown. For example, in lung tissues, mtDAMPs induce the miR-223 expression that inhibits NLRP3 inflammasome and IL-1β release and suppressing miR-223 leads to the activation of NLRP3-IL-1β and acute lung injury. (114) NLRP3 activators induce the release of the mitochondrial membrane lipid cardiolipin, another mtDAMP. (115) The miR-30a inhibited type II alveolar AEC apoptosis by repressing the mitochondrial fission dependent on Drp-1 leading to lung fibrosis. (116) miR-34/449 deficiency in ciliated cells results in reduced cilia length and numbers, which is mediated, at least in part, by the post-transcriptional repression of Cp110, a centriolar protein suppressing cilia assembly, making these miRs indispensable for mucociliary differentiation. (117) Similarly, miR-183 was shown to be essential for hypercapnia responses by regulating isocitrate dehydrogenase 2 (IDH2) that impairs mitochondrial function and cell as observed in patients with chronic lung diseases. (118) Strikingly, miR-449a is upregulated by more than 1000-fold when epithelial cells from human airways are lifted from a liquid environment to air, allowing them to undergo mucociliary differentiation. (119) Among the mucin expression regulation, miR-134-5p, miR-146a-5p, and let-7 family of miRs have been shown to regulate

chronic mucus hypersecretion as- sociated with COPD. (120) It has been reported that the let-7d miR was associated with IPF, suggesting a potential therapeutic target for controlling IPF associated pathologies. (121) Similarly, miR-21 levels had also been found significantly upregulated in IPF and increased miR-21 levels promoted the TGF-β1 activity. (122) Furthermore, miR-145-5p was recently implicated in modulating TGF- β1 levels and could be useful therapeutic target in restoring the airway epithelial homeostasis. (123)

Some lncRNAs that are transcribed in the nucleus also reside in mitochondria and play a key role in regulating mitochondrial responses. For example, lncRNA RMRP or mitochondrial RNA-processing endoribonuclease is required for mitochondrial DNA replication and RNA processing, and the lncRNA SRA or steroid receptor RNA activator is a key modulator of hormone signaling found in both mitochondria and nucleus. The mitochondrial DNA also encodes for a set of lncRNAs like lncND5, lncND6, and lncCyt b RNA encoded on the complementary strands of ND5, ND6 and Cytovhrome b genes as reviewed recently. (124) These mitochondrial DNA-encoded lncRNAs also appear to function in the nucleus and the molecular mechanisms underlying trafficking of the mitochondrial-encoded lncRNAs to the nucleus are now beginning to emerge. (124) There is also growing evidence towards mitochondria importing the cytosolic ncRNAs via yet-to-be discovered mechanisms. (125)

There is ample evidence suggesting miRNAs, an extensively studied class of short noncoding RNA, may be at the center of aberrant immune mediated inflammatory responses and oncogenesis. Particularly, overexpression or

underexpression of miRNAs has been implicated in lung cancer and various other respiratory diseases. For example, the let-7 family of miRNAs and its expression levels are implicated in both the lung cancer and COPD pathogenesis. (126) Recent seminal studies have investigated lncRNAs that are important in maintaining cellular and tissue homeostasis and preventing autoimmune responses. While most studies have looked at the changes in lncRNA expression in response to various physiological processes, some studies have also identified specific lncRNAs and their role as either inducers or restrictors of inflammatory processes. However, there is extremely limited data and further elucidation on the roles of lncRNA is necessary.

More lncRNA species have been further identified in last few years and various biological functions have been attributed to these lncRNAs. These functions primarily include alteration of protein localization, mRNA decay, chromatin modification, alternative splicing, modulation of protein activity and transcription initiation/repression. Studies have demonstrated different types of lncRNAs involved in the immune system both as inducers and restrictors of inflammation. Differing lncRNAs have even been shown to take part in multiple levels in immune cell development and processes responding to pathogens. (113) However, a large knowledge-gap remains as the role of only a small portion of lncRNAs has been illustrated.

III. COPD phenotyping and biomarkers

The pathophysiology of COPD in susceptible populations is initiated following chronic exposure to various toxic stimuli, leading key players of the innate

immune system such as alveolar macrophages and AECs to be activated by various pattern recognition receptors (PRRs). This results in the release of pro-inflammatory mediators including cytokines and chemokines, which recruit protective inflammatory cells such as neutrophils, lymphocytes, monocytes and other immune cells to the site of insult. Subsequent communication through antigen presenting cells activates the adaptive immune system to induce helper T cell differentiation (T_H1 and T_H17) and $CD8^+$ cytotoxic T cell recruitment. The bronchiolitis aspect of the disease is a result of structural changes that occur from small airway remodeling due to extensive airway inflammation. The emphysematous phenotype is a result of alveolar damage from the production of reactive oxygen radicals and the release of proteolytic enzymes by neutrophils and macrophages. (127) Both these processes illustrate pulmonary damages as a result of exaggerated and uncontrolled inflammation.

Recently, new attempts have been made to classify COPD into distinct subgroups based on the pathophysiologic derangements, response to treatment and disease progression. As a result, a movement away from a baseline FEV_1 value towards a more multidimensional approach (i.e. novel endotyping methods combined with the small-airway physiologic evaluation and imaging) is being followed to better classify the COPD phenotypes. Existing examples of COPD subgroups include 1) small airway-predominant disease, 2) alpha-1 antitrypsin deficiency, 3) emphysema, 4) chronic bronchitis, 5) frequent exacerbators, 6) asthma-COPD overlap and 7) eosinophilic versus 8) non-eosinophilic disease. By creating these distinct groups, the hope is to subsequently identify and provide

therapeutic treatment that is specifically tailored to each individual group. However, a better understanding of the epigenetic and genetic underpinnings that lead to specific phenotype remains a vital aspect if we are to successfully provide pharmacological therapy when treating the disease. (128)

IV. Long noncoding transcriptome in COPD

Certain newly discovered lncRNAs are reportedly associated with ageing in various disease models and have recently been reviewed. (67, 68) They include TERRA and TERC that control telomere function; Xist, H19, ANRASSF1 and PINT that are involved in epigenetic changes; MEG3, 7SL, GAS5, LincRNA-p21 and HOTAIR associated with loss of proteostasis; ANRIL, MALAT1, SRA, HEIH, HULC, UCA1 and Gadd7, which regulate immunosenescence; 17A, Lnc-IL7R, THRIL and Lethe involved in inflammaging; AK028326, AK141205, ES-1,-2,-3, involved in stem cell function regulation; and finally, TUC339 and Tie-1AS that are implicated in various intercellular communication mechanisms.

Li et al., (129) performed microarray analysis to identify the abnormally expressed lncRNAs in human bronchial epithelial cells induced by different concentrations of wood smoke particulate matter$_{2.5}$ (WSPM$_{2.5}$) and arterial traffic ambient particulate matter$_{2.5}$ (TAPM$_{2.5}$). Compared to control, 94 lncRNAs were upregulated and 203 were downregulated in WSPM$_{2.5}$ treated cells whereas 1292 lncRNAs were upregulated and 1362 were down- regulated in TAPM$_{2.5}$ treated cells. Based on the differential expression, GO and KEGG analysis they selected lncRNA maternally expressed gene 3 (lncRNA MEG3) for further validation and

demonstrated that lncRNA MEG3 mediates $PM_{2.5}$-induced cell apoptosis and autophagy through regulating the expression of p53.

Other than COPD, increased MUC5B expression was also associated with lung adenocarcinoma. Specifically, lncRNA MUC5B-AS1 (ENST00000532061.2) was significantly upregulated in lung adenocarcinoma tissues. (130) Further validation of regulatory mechanisms showed that lncRNA MUC5B-AS1 promoted cell migration and invasion by the formation of protective RNA-RNA duplex with MUC5B resulting in an increased expression of MUC5B in these cancer cells.

One pioneering study analyzed genome-wide lncRNA expression in COPD lung by performing a comparative microarray analysis of non-smokers and smokers with or without COPD. (131) In this study, RNA of non-smokers without COPD, smokers without COPD and smokers with COPD was extracted from human lung tissue. Participants included 3 non-smokers without COPD, 5 smokers without COPD and five smokers with COPD, however, all patients had lung cancer. Microarray analysis of 39,253 distinct lncRNAs showed differential expression of a large number of lncRNAs in COPD patients independent of smoking status. Compared to smokers without COPD, 120 lncRNAs were over-expressed and 43 underexpressed in COPD patients, indicating that smoking alters the expression of lncRNAs and that these lncRNAs may be associated with the changes in key pathogenic processes of COPD caused by tobacco smoke exposure. These lncRNAs could be involved in modulating the metabolism of several cellular mediators and in signaling pathways linked to the altered immune system in COPD

patients. Additionally, these lncRNAs may be involved in regulating the expression of coding genes in COPD patients, however, further study is required.

In another study, lncRNA and mRNA expression profiles were analyzed by microarray of peripheral blood mononuclear cells (PBMCs) from 20 healthy nonsmokers, 17 smokers without airflow limitation, and 14 COPD patients. (132) Here, they identified 158 differentially expressed lncRNAs and selected 5 lncRNAs (NR_026891.1, ENST00000502883.1, HIT000648516, XR_429541.1, and ENST00000597550.1) for further validation based on the dysregulated expression associated with COPD. The regulatory role of ENST00000502883.1 on CXCL16 expression was confirmed and consequently the role in PBMC recruitment. They also predicted the regulatory role of other lncRNAs on chemotaxis associated genes such as CXCL16, HMOX1, SLA2, and SIGLEC14. In addition, GO enrichment analysis showed that leukocyte migration, immune response, and apoptosis are the main enriched processes that are previously reported to be involved in the pathogenesis of COPD.

A whole-blood RNA sequencing analysis of 229 current and 286 former smokers reported that 171 genes including 7 lncRNAs (LINC00599, LINC01362, LINC00824, LINC01624, RP11-563D10.1, RP11-98G13.1 and AC004791.2) that were differentially expressed between current and former smokers. (133) In addition, there were significant differential usage of 9 exons from 8 genes by exon level analysis, in which 8 genes of these 9 exons were unique to one transcript, suggesting these results may indicate the presence of differentially processed variants among current and former smokers.

Another seminal study analyzed the overlapping or diverging dysregulated genes, lncRNAs, miRNAs and signaling pathways in smoking and non-smoking COPD patients. (134) The blood samples were collected from five healthy, non-smoker patients with COPD and five smoker patients with COPD. With the help of high-throughput sequencing analysis they identified that compared to the normal control, there were 96 differentially expressed lncRNAs in non-smoker and 44 differentially expressed lncRNAs in smoker COPD patients and 15 lncRNAs overlapped between non-smoker and smoker COPD patients. Based on the interaction network analysis, they found that let-7-ADRB1-HLA-DQB1-AS1 might play a key role in the pathogenesis of smoking-associated COPD while miR-218-5p/miR15a-RORA-LOC101928100/LINC00861 and miR-218-5p/miR15a-TGFβ3-RORA-AS1 interactions might involve with the pathogenesis of non-smoking COPD. Interestingly, there data suggest that miR-122-5p-A2M-LINC00987/A2M-AS1/linc0061 interactions might play key roles in COPD irrespective of the smoking status.

LncRNA ANRIL (antisense noncoding RNA in the INK4 locus) is one of the widely known functional lncRNAs that is associated with the development and prognosis of chronic inflammatory diseases. It represses the NF-κB pathway by inducing CARD-8 and downregulates the TGF-β1 expression. (135, 136) Recently, Ge et al., (137) studied lncRNA ANRIL expression and associated inflammatory cytokines from the plasma of 136 acute exacerbations of COPD (AECOPD) patients, 138 stable COPD patients, and 140 healthy controls. They observed lower expression level of lncRNA ANRIL in AE-COPD patients compared to both

stable COPD patients and the healthy individuals. Furthermore, this expression was negatively correlated with proinflammatory cytokines in AE-COPD and stable COPD patients, and with GOLD stage in AE-COPD patients, but not in stable COPD patients.

Roles of lncRNA have also been studied in animal models of COPD. In a chronic CS-induced COPD mouse model, lung tissue RNA-seq analysis was performed to investigate transcriptome profiles. (138) A total of 37,072 lncRNAs were detected, in which 109 lncRNAs and 260 mRNAs were significantly differentially expressed in CS-exposed mice compared with control animals. Based on the high-throughput data analysis, among 109 lncRNAs, 3 significantly altered lncRNAs (NR_102714, fantom3_D330021G15 and fantom3_D830009E10) are associated with protein-coding genes (UCHL1, IL1RL1and GGT5, respectively). In addition, they performed qRT-PCR analysis of 16HBE cells treated with or without CSE and also analyzed the PBMCs from 6 healthy individuals and 7 COPD patients. The lncRNA NR_102714 and the associated protein-coding gene, UCHL1 presented the same expressional tendencies in all these experimental models. UCHL1, ubiquitin C-terminal hydrolase L1, one of known ageing hallmark biomarkers associated with COPD. (139)

In an another mouse model study, Wang et al. conducted a microarray analysis to identify the CS-induced lncRNAs and mRNAs. (140) In this experiment they found total of 108 lncRNAs and 119 mRNAs that were differentially expressed in CS-exposed animals compared to controls. Based on the coding-non-coding

gene co-expression network analysis, lncRNAs AK076311 and uc007coi.2 were reportedly negatively associated with chemokine receptor 10 (CCR10), and also the lncRNA ENSMUST00000181247 was positively co-expressed with CD177. (141) The CCR10 and CD177 are inflammation-associated biomarkers in lung diseases. (142)

Similarly, type II alveolar AEC were also investigated to understand the role of lncRNAs in the lung tissue repair and maintenance of the alveolar homeostasis. (143) Lung parenchymal tissues obtained from 22 patients without COPD and 12 with COPD were examined. Significantly higher levels of cellular senescence and apoptosis of COPD alveolar epithelial cells was demonstrated through measuring senescence-associated β-galactosidase (SA-β-Gal) levels. Expanding on the previous research, the levels of a senescence-associated lncRNA or SAL-RNA, which has been demonstrated to mediate the SIRT1/FoxO3a and SIRT1/p53 pathways were evaluated. LncRNA expression of SAL-RNAs was significantly increased in the COPD group, however, a differentially processed variant, SAL-RNA1 was significantly suppressed. These studies illustrate that faulty regulation of lncRNAs in the type II airway epithelial cell senescence can contribute to the pathogenesis of COPD.

In order to help discover potential biomarkers for the diagnosis and treatment of COPD, Tang et al., (144) investigated the possible functions and mechanisms of the lncRNA, TUG1, in COPD patients compared to the non-COPD lungs (n=3). The microarray analysis showed that among the differentially expressed lncRNAs, 15% were upregulated while 17% were downregulated.

Subsequent genomic locus analysis and the correlation analysis with the protein-coding genes among the differentially expressed lncRNAs suggested that most of the differentially expressed lncRNAs in COPD lung tissue were intergenic lncRNAs (non-overlapping or bidirectional coding transcripts nearby the lncRNA), which included TUG1. These results suggest that TUG1 could potentially serve as a COPD biomarker. Recently, a broad and systematic approach was also employed to develop a genome wide screening platform that identified the functional lncRNAs. (145) Using a CRISPRi gene editing technology, the screening approach was employed to identify lncRNAs that modify robust cell growth in seven different human cell lines. The results were significant as they substantially increased the number of known functional lncRNA loci. They further demonstrated that lncRNA function in a highly cell type-specific manner and directly regulate important cellular processes.

Chapter 2: Methods

I. Airway epithelial tissues and cells

Airway tissue specimens and primary human AEC from subjects with and without asthma were obtained from deidentified organ donors through the Life Alliance Organ Recovery Agency of the University of Miami, according to protocols approved by the local Institutional Review Board. Tissue specimens were fixed in 10% neutral buffered formalin and conventionally processed for paraffin embedding and sectioning. Airway epithelial cells were isolated and cultured on air-liquid interface (ALI) as previously described. (146, 147) Normal human primary AECs were also kindly provided by Dr. Scott Randell at the Marsico Lung

Institute/Cystic Fibrosis Research Center at the University of North Carolina, Chapel Hill, USA. Lung tissues were procured under protocol #03–1396 approved by the University of North Carolina at Chapel Hill Biomedical Institutional Review Board. AECs were maintained in bronchial epithelial growth medium (BEGM, Lonza, Walkersville, MD). For ALI culture, cells were plated onto collagen IV–coated 24mm Transwell-clear culture inserts (Corning Costar Corporation, Cambridge, MA) at a density of 5 × 105 cells/cm2 in ALI media. The apical surface of the cells was exposed to air and cells were cultured for another 21 days until they were fully differentiated. (146, 147) AECs were treated with LPS (Pseudomonas aeruginosa serotype 10, Sigma-Aldrich, St. Louis, MO) or with recombinant human IL-13 (Peprotech Ltd.). Following treatments, the membrane quarters were used for RNA and protein isolation or were fixed in 4% paraformaldehyde for immunostaining.

II. Transcriptomic analysis

Illumina TruSeq Stranded Total RNAseq libraries with ribosomal depletion were prepared per manufacturer's instructions (Illumina, Inc, San Diego, CA). Libraries were sequenced on a HiSeq2500 (2 × 100 PE reads; 50 million reads/sample) at HudsonAlpha Institute for Biotechnology, Huntsville, AL. RNA-Seq data was analyzed as described previously. (148, 149) Briefly, reads were aligned to the GRCh38.P10 reference genome with Hisat2 and assembled into transcripts with Cufflinks2. CuffDiff was utilized to determine differential expression. Raw sequencing data have been deposited into the Sequence Reads Archive, and the experimental data files placed in Gene Expression Omnibus

(GEO). Long noncoding genes were identified by their accession numbers. The RNA-seq data have been deposited in NCBI's GEO47 and are accessible at GEO accession number GSE139370.

III. Pathway analysis

ToppFun (https://toppgene.cchmc.org/) was utilized for pathway analysis as previously described. (150) Briefly, significantly different gene names (HUGO Gene Nomenclature Committee names) were entered into the ToppGene Suite. Duplicate and unknown genes were removed. Gene Ontology biological process and pathway analysis were utilized to determine significantly different functional genomic changes. Fast Ward Hierarchical Clustering was performed using the Log2x + 1 transformation of the data in the JMP genomics 8.0 (SAS Institute, Cary, NC). A p value (<0.05 with FDR correction) of each annotation of a test gene is derived by random sampling from the whole genome.

IV. Real-time quantitative RT-PCR

Total RNA was isolated using RNAeasy kit (Qiagen, MD) as per manufacturer's instructions, quantified using Synergy HTX reader (BioTek, VT) and cDNA were synthesized using iScript kit (BioRad, CA). MUC5AC, SPDEF, and LASI transcripts were quantified using FAM-based primer/probe sets (Applied Biosystems, ThermoFisher) using the TaqMan Gene expression kit (ThermoFisher), whereas, ICAM-1, IL-6, and CXCL-8 mRNA were quantified using SYBR green- based primers or iTaq Master Mix (BioRad, CA) in the Agilent Stratagene Mx3000P Real-Time PCR System (ThermoFisher). Relative quantities were calculated by normalizing averaged CT values to CDKN1B or β-Actin to

obtain ΔCT, and the fold-change (ΔΔCT) over the controls were determined as described previously. (151)

V. RNA fluorescence in situ hybridization (RNA-FISH)

The RNAScope® 2.5 HD duplex assay and reagent kit (Advanced Cell Diagnostics, Biotechne) was used for RNA FISH as per the manufacturer's instructions. A double-Z probe set against *LASI* was designed containing 20 dual probes targeting various segments across the *LASI* lncRNA. RNA FISH was conducted on paraffin-embedded 5 µm tissue sections obtained from the LTRC of the NIH. Deparaffinization was conducted in consecutive xylene, graded ethanol, and deionized water. Pretreatment was conducted with hydrogen peroxide solution and the RNAScope® target retrieval buffer and protease plus solutions were used to exposure the antigen. Probe hybridization was conducted for 2 hours at 40°C in the HybEZ® II oven. The signal was amplified using the Amp1, Amp2, Amp3 and the HRP probe at 40°C in the HybEZ® II oven. The signal was detected using the tyramide signal amplification (TSA) reaction with an Alexa fluor labeled TSA kit (Perkin Elmer). Sections were then processed for immunohistochemistry or directly mounted with the 4',6-diamidino-2-phenylindole (DAPI)-containing Fluormount-G (Southern Biotechnology). Images were captured using the Keyence BZ-X700 structured illumination fluorescent microscope. Analysis was conducted with the Keyence BZ-X analysis software and using the ImageJ software (NIH). RNA FISH quantification was conducted according the RNAScope® histo (H)-score methodology. In each image, probe signals were counted for each cell, both in the nuclear and cytosolic region and assigned to appropriate bins: bin 0 (no signals),

bin 1 (1-3 signals/cell), bin 2 (4-9 signals/cell), bin 3 (10-15 signals/cell) and bin 4 (>15 signals/cell). The H-score was calculated as follows: H-score was the sum of each bin multiplied by the percentage of cells that fall into that bin. H-score = (0 x % cells in bin 0) + (1 x % cells in bin 1) + (2 x % cells in bin 2) + (3 x % cells in bin 3) + (4 x % cells in bin 4). Final H-scores ranged from 0 to 400 per group.

VI. Statistical analyses

Grouped results were expressed as mean±SEM and $p<0.05$ was considered significant. Data were analyzed using GraphPad Prism Software (GraphPad Software Inc.) using one-way analysis of variance (ANOVA) with and Tukey's multiple comparison test or using a two-tailed t test for comparison between two groups. When significant main effects were detected ($p<0.05$), student's t test was used to determine differences between the groups.

Chapter 2: Results

I. Identification of a novel long noncoding RNA in AECs

We performed a high-throughput RNA sequencing analysis to identify the novel lncRNAs that might be primary immediate-early responders regulating the inflammatory and mucus responses of HAECs. The role of identified lncRNA was validated and interrogated in airway tissues and AECs of asthmatic and control subjects.

To determine the molecular mechanism involved in this memory-based hyperreactive or 'trained' mucous response, the well-differentiated primary AECs were treated with LPS (100 ng/ml) for 2 hours to analyze the immediate early

responses. The total RNA was isolated, and the transcriptomic analysis was performed by a high-throughput RNA-sequencing as described under methods section. The rigorous *in-silico* analysis of the RNA-seq data helped identify 725 differentially expressed transcripts that were statistically significant, 65 of which were duplicates. Among these differentially expressed transcripts, we selected lncRNA AC011511.2, a lncRNA on the antisense strand of ICAM-1 or *LASI* for further analysis because ICAM-1 plays a critical role in airway inflammation and remodeling. (152) In addition, ICAM-1 expression itself is associated with LPS exposure, airway inflammation and asthma. (153) Sequencing and annotation analysis revealed that this *LASI* transcript is a 32.4 Kb long with 3 exons and 2 introns, and several putative splicing sites. This novel lncRNA showed a negligible protein coding potential with a Fickett Testcode score of 0.27327 and coding probability of 0.197913 (http://cpc2.cbi.pku.edu.cn). Next, to validate the RNA-Seq results and to interrogate the expression of *LASI* transcripts in the *in-vitro* model of trained mucous response, using a custom-made FAM-based primer-probe set specific for LASI, we analyzed the expression levels by a qPCR. The secondary LPS challenge augmented more than six-fold increase in the *LASI* transcript levels in L/10 cells compared to controls (**Figure 6D**). The RNA-seq data have been deposited in NCBI's Gene Expression Omnibus(154) and are accessible using the GEO accession number GSE139370 (and the following NCBI accession link: https://www.ncbi.nlm.nih.gov/geo/query/acc.cgi?acc=GSE139370).

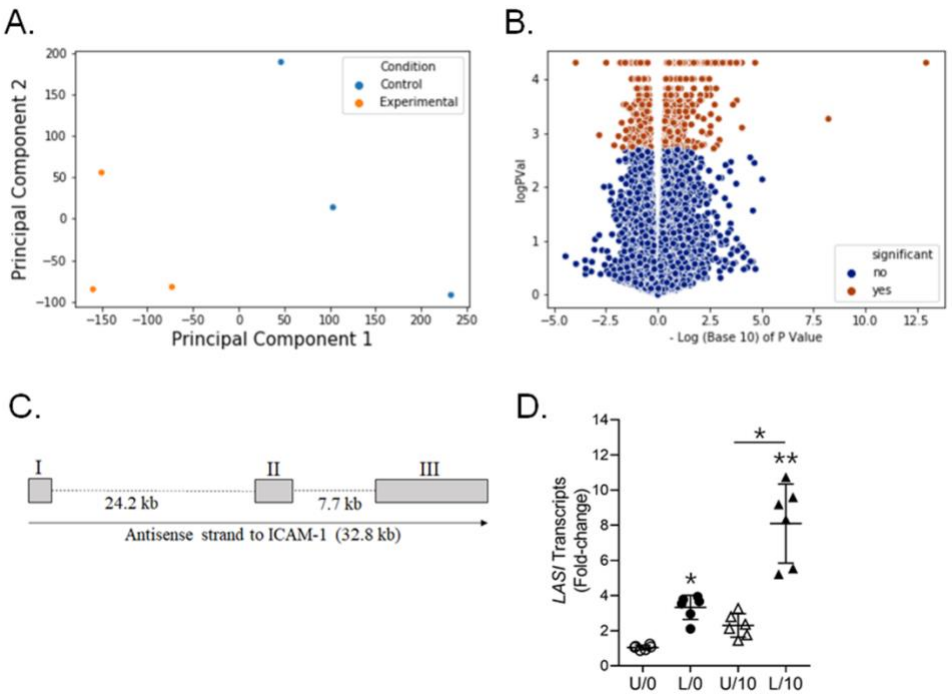

Figure 6. Transcriptomic analysis of the immediate early innate responses of HAECs and an associated increase in LASI transcript levels following LPS challenge. Primary HAECs were differentiated at the air-liquid interface and were treated with LPS (100 ng/ml) for 2h. Total RNA was isolated from cells and RNA-Seq analysis was performed. **(A.)** PCA analysis of the RNA seq data showing the distinct grouping of control and LPS-treated (experimental) samples. **(B.)** Volcano plot analysis of RNA seq data showing the distribution of transcripts that were upregulated or downregulated following LPS treatment. **(C.)** Genetic map of lncRNA LASI encoded on the antisense strand of ICAM1 within chromosome 19. **(D.)** Relative quantities of LASI transcript levels in U/0, L/0, U/10, and L/10 HAECs as determined by qRT-PCR. Data shown as mean ± SEM with n=3–6/group; *p<0.05; **p<0.01 as analyzed by the one-way ANOVA and Tukey's multiple comparison test. Drs. G. Borchert and R. Langley were the major contributors for this data. Reproduced with permission from Springer Nature (2).

A similar trend was observed in the cells treated with IL-13 (**Figure 7**) with an increased aggregation of *LASI* transcripts in the perinuclear region (**Figure 7A**) and there was 2-fold or more *LASI* transcripts per cell in IL-13-treated than non-treated condition (**Figure 7B**). In addition, IL-13 treatment induced the *ICAM-1* (**Figure 7C**) and *CXCL-8* (**Figure 7D**) with no change in *IL-6* (**Figure 7E**)

expression. Thus, the early induction of *LASI* transcripts and the observed enrichment in the nuclear/perinuclear region may be one of the the initial responses in the onset of airway mucus and inflammatory responses.

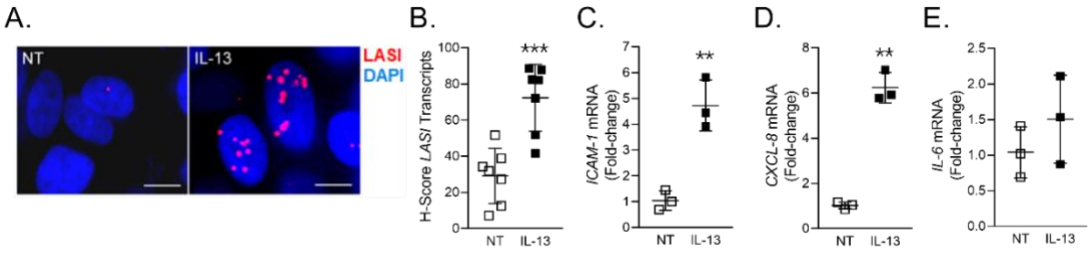

Figure 7. Nuclear/perinuclear enrichment of LASI transcripts in 3D-cultured human AECs following IL-13 treatment with increased expression of inflammatory factors. **(A.)** Micrographs of AECs showing RNA FISH stained individual LASI transcripts (red) using RNAscope® technology (ACD Inc) and DAPI-stained nuclei (blue) in IL-13-treated and non-treated AECs, scale – 5μ. **(B.)** Quantification of the number of LASI transcripts per cell in IL-13-treated and non-treated AECs. Relative quantities of ICAM-1 **(C.)**, CXCL-8 **(D.)** and IL-6 **(E.)** mRNA levels AECs as determined by qRT-PCR at 24h post-treatment. Data shown as mean±SEM; n=3-4/gp; **p<0.01; ***p<0.001 based on student's t-test. Dr. D. Devadoss was the major contributor for this data. Reproduced with permission from Springer Nature (2).

Chapter 2: Discussion

In line with our previous in-vivo observation in animal models of trained immunity of the airway epithelium, (155) this data corroborates that results that In AECs, the IL-13-mediated induction in the LASI transcript levels elevated rapidly in the nuclear/perinuclear region and possibly regulates the SPDEF translocation to augment AEC inflammatory and mucous responses.

Several cutting-edge mechanistic and population studies have now widely established the innate memory-based responses or 'trained immunity' of innate immune cells, which primarily involves epigenetic reprogramming via DNA

methylation, microRNAs and/or long noncoding RNAs. For example, studies investigating the European and U.S. farm and non-farm children pulmonary health show that early life exposure to airborne immunomodulators protects individuals against allergic asthma by activating a form of trained immunity in the lung mucosa and/or innate immune cells. (156-158) Although this trained immunity primarily shows beneficial effects, the pan-protection and the enhanced immune responses could also lead to the development of chronic disorders. (159) In parallel, this phenomenon offers a way to identify a potential target during pathophysiological conditions of these chronic inflammatory disorder either by inducing or inhibiting the targeted molecules. We have also showed that differentiated AECs also preserve a memory-dependent rapid recall response following the LPS challenge. (2) The RNA-Seq analysis of LPS-treated AECs showed that among 660 significantly differentially expressed immediate-early transcripts is a novel lncRNA *LASI* that could be responsible for this trained response. The expression pattern of *LASI* transcripts in the in-vitro airway model of trained immune response supported their significant role in the aggravated inflammation and mucus expression.

Although many AEC-associated lncRNAs were identified so far, (160, 161) there are no such reports on asthma-associated lncRNAs in AECs. Most of the identified asthma-associated lncRNAs are either specific to peripheral blood mononuclear cells (162, 163) or the airway smooth muscle cells (164, 165) which may be targeted to reduce asthma symptoms. This is the first observation of an AEC-specific lncRNA that is associated with asthma which showed immediate-

early and robust expression. The impact of lncRNAs on cell functions are primarily dictated by their subcellular localization where they can alter chromatin modification, mRNA decay, alternative splicing and regulation of transcription by *cis* or *trans* mechanisms. (166, 167) Some lncRNAs accumulate in *cis* (in nucleus) and act as *cis* or *trans* in the nucleus, some others accumulate in *trans* (in cytoplasm) and act as *trans* in the nucleus, and very few lncRNAs are synthesized in the nucleus and translocate into the cytosol. (168) During pathological conditions, lncRNAs expression and localization could be altered in a way that could affect their normal modulation of pre-transcription, transcription, and post-transcription processes by affecting their interactions with genomic DNA, mRNA, miRNA and various proteins. (169, 170)

AECs synthesize and secreted various inflammatory factors following an injury or insult, that lead to the recruitment and retention of various immune cells, which further increase the inflammatory condition of the lung. (171) Among AEC-derived inflammatory factors, IL-6 and CXCL-8 had been predominantly observed in many chronic lung diseases including allergic asthma. These are multifunctional immunomodulators, which regulate the expression of adhesion molecules like ICAM-1 and act as chemoattractants to recruit effector immune cells like monocytes and lymphocytes. (172, 173) Therefore, controlling the expression or function of these inflammatory mediators could also help in reducing the severity of a disease condition. The identification of cytokine regulating lncRNAs associated with airway inflammation and allergic asthma is gaining more attention. Recent seminal studies revealed that lncRNAs, IL17AS and MIR3142HG regulate

IL-6 and CXCL-8 expression via NF-κB pathways in IPF tissues; (174) lncRNA PVT1 regulates IL-6 and CXCL-8 release in ASMCs; (175, 176) and lncRNA ANRIL regulates IL-6, IL-13, IL-4 and IL-17 in allergic rhinitis condition. (177) AECs treated with IL13 resulted in increased IL-6, CXCL-8 and ICAM-1 expression and blocking the *LASI* expression via siRNA attenuated the mRNA expression of IL-6 and ICAM-1 but not CXCL-8. These studies thus indicate that *LASI* transcripts regulate the expression of AEC inflammatory mediators.

Conceptually, the form of 'pathogenic trained response' of asthmatic AECs observed by our group (2) is in total contrast to the development of 'host-beneficial trained response' to LPS/endotoxins or farm dust as reported in the developing lungs, where the early life exposure to immunomodulators protects against allergic asthma. (156-158) This disparity could be due the use of adult AECs in this study, and a longitudinal analysis of the pediatric AECs is needed to understand this dichotomy. In addition, the reported hyperreactive response of AECs observed here should not be compared with the low dose allergen or LPS models that involves lymphocytes which augment a tolerogenic response and are the basis for the allergen immunotherapies.

Chapter 3: *LASI* lncRNA in a COPD model

Data presented in this chapter has been originally published by Frontiers publishing group, “Increased Expression of LASI LncRNA Regulates the Cigarette Smoke and COPD Associated Airway Inflammation and Mucous Cell Hyperplasia”, 2022, DOI: 10.3389/fimmu.2022.803362.

Chapter 3: Introduction

I. *LASI* lncRNA and COPD

CS exposure has been demonstrated to induce epigenetic events such as DNA methylation, histone modifications and notably, changes in expression of noncoding transcripts such as microRNAs (miRNAs) and long noncoding RNAs (lncRNAs). (167, 178) LncRNAs may interact with various proteins, DNA, chromatin and other RNAs to induce epigenetic and transcriptomic changes affecting cell and tissue functions. (179) A growing number of lncRNAs have been implicated for a role in chronic pulmonary conditions, including CS-related immune responses, and inflammatory dysregulation. (167, 180, 181) We identified a specific immunomodulatory lncRNA referred to as *LASI*, a lncRNA antisense to ICAM-1, and confirmed its direct involvement in modulating airway inflammatory and mucus hyperexpression responses. (2)

Furthermore, we have recently observed that long-term mainstream CS exposure results in airway remodeling in cynomologus macaques (*Macaca fascicularis*) with augmented chronic bronchitis and reduction in lung functions similar to those observed in smoke-associated COPD. (182) Based on the important role of lncRNAs in COPD (167) and specifically *LASI* lncRNA in airway

epithelial cells (2), we hypothesized that *LASI* lncRNA affected the CS-induced airway inflammation and mucus hypersecretion in COPD. Herein, using the structured-illumination imaging and RNA fluorescence in-situ hybridization (FISH), we found that *LASI* lncRNA was upregulated in the small airway epithelium of animal model of chronic CS exposure as well as in former smokers with COPD, and its expression correlates with aggravated inflammatory and mucus secretory responses. In addition, unstimulated airway cells from COPD subjects showed strong association of higher *LASI* expression with upregulated expression of mucin and other inflammatory factors. Most importantly, we find blocking *LASI* expression rescues impaired airway responses due to CS-mediated dysregulations in COPD bronchial epithelial cells.

Chapter 3: Methods

I. *M. fascicularis* cigarette smoke exposure

An animal model of female cynomolgus macaques (*M. fascicularis*) was used. Experiments were performed by the Lovelace Respiratory Research Institute in Albuquerque, NM, as described before. (182) The animals were maintained at 12-hour light/dark cycle and received, unless exposed to cigarette smoke (CS), filtered fresh air (FA) with 10 to 15 air changes per hour. Female *C. macaques* were exposed to CS in H2000 whole body exposure chambers at 250 mg/m^3 total suspended particulate matter (TPM) for 6 hours per day, 5 days per week, corresponding to 4 packs of cigarettes per day as described previously. (182) At these concentrations C. macaques develop observable changes in lung

physiology within three months of exposure. Lung resections and tissue sections were obtained as described previously. (182)

II. Human lung tissue samples

Lung tissue samples were obtained from the Lung Tissue Research Consortium (LTRC) from the National Institutes of Health (NIH). The COPD patient cohorts are defined as patients with a post-bronchodilator FEV1/FVC <0.7, currently the most widely accepted and robust test for COPD. Although reports have shown that early-stage COPD may present with emphysematous or other pathologic changes prior to a presentation of an FEV1/FVC <0.7, this test remains the standard confirmation of COPD diagnosis. COPD patient samples were compared to samples from GOLD stage 0 patients, which are defined as having normal spirometry results, however, may have chronic symptoms such as cough and sputum product, and may present with risk factors for COPD such as TS usage (6). GOLD 0 individuals may or may not progress to active COPD status and are classified as pre-COPD (100). Both genders in each GOLD stage were grouped together and all groups include both active and former smokers. GOLD stage determination was made by spirometry testing and assigned to the appropriate GOLD stage group, per the protocols described by the National Heart, Lung, and Blood Institute and World Health Organization. (6) In this report, GOLD stages I and II were defined as patients with mild COPD status and GOLD stages III and IV were defined as patients with severe COPD status. Each group had a minimum n=6 with a mean age between 59.7 and 65.2 years old. All COPD patients had a

smoking history with mean packs per year (PY) ranging between 22.4 and 41.5 and former smokers had not been smoking of a mean of 13.2 and 22.9 years. Smoking history was self-reported for all patients. Lung tissue homogenates include epithelial tissue as well as other tissues and cell types. Samples were obtained from varying anatomical regions of the lungs, however all samples contained bronchial epithelial cells as confirmed by expression of pan-cytokeratin (pan-CK) from epithelial cells and MUC5AC mucin from secretory goblet cells.

III. Real-time quantitative PCR (RT-qPCR)

For all RT-qPCR analysis, total RNA extraction was performed using the RNeasy Mini kit (Qiagen) according to manufacturer's instructions. Briefly, tissues were resected and collected tissue was measured to be under 30 mg. Tissue lysis was performed using TissueLyser® LT (Qiagen) at 50 Hz for 3 minutes. RNA concentration was quantified using the Synergy HTX reader (BioTek, VT). Complementary (c)DNA was synthesized using the iScript Advanced cDNA synthesis kit (Bio-Rad), per manufacturer's instructions or by using the Applied Biosystems™ High-Capacity RNA-to-cDNA™ Kit per the manufacturer's instructions. For qRT-PCR, FAM-based and SYBR Green primers were used. The *LASI, ICR, WAKMAR-2, NEAT1, MALAT1* lncRNAs and *MUC5AC* and *SPDEF* mRNA levels were quantified using FAM-based primer/probe sets and TaqMan gene expression kit or the SsoFast qPCR master mix (Applied Biosystems, Thermo Fisher). *ICAM-1* and *IL6* mRNA levels were quantified using SYBR Green-based primers and the iTaq master mix (Bio-Rad). qRT-PCR was conducted using

the Bio-Rad CFX Real-Time PCR detection system. Quantification and analysis of the results was performed using the delta-delta (ΔΔ)Ct method and U6 noncoding small nuclear RNA (snRNA), glyceraldehyde-3-phosphate dehydrogenase (GAPDH) or beta actin were used as reference genes for lncRNA expression levels expression levels as described recently. (101)

IV. Human bronchial epithelial cell culture and CSE treatment

The primary human bronchial epithelial cells (HBECs) from COPD (CHBEs) and non-COPD (NHBEs) donors were obtained from the commercial suppliers (Lonza Inc. or MatTek Corp). All primary cell lines were grown and treated in bronchial epithelial cell growth media (BEGM from Lonza or UNC MLI Tissue Procurement and Cell Culture Core). To investigate the baseline differences between NHBEs and CHBEs, Air-liquid interface (ALI) cultures of primary cells were grown in BEGM and differentiated in bronchial ALI (B-ALI) differentiation media (Lonza or UNC MLI Tissue Procurement and Cell Culture Core), as described previously (2). ALI cultures were seeded at a density of 5×10^5 cells/cm^2 on collagen IV-coated Costar® 6.5 mm Transwells with 0.4 µm pore polyester membranes (Corning Costar Corporation). Cells were differentiated for a minimum of 21 days before treatments. Epithelial differentiation was confirmed by live cell imaging of ciliary beatings and mucus glycoproteins. Submerged cultures of primary cell lines were utilized to investigate the effect of CS treatment and *LASI* knockdown. For CS extract preparation, CS particulate matter collected on the filter membranes from mainstream smoke of 3RF4 research cigarettes (courtesy Philip

Kuehl, Lovelace Biomedical) were used for extracting CSE and final treatments of 20 µg/ml were applied. In addition, paraffin-embedded tissue sections human COPD and healthy control lungs were obtained from the LTRC.

V. Immunohistochemistry and immunocytochemistry

Tissue sections or fixed cells were washed in 0.05% V Brij-35 in PBS+. Antigen retrieval was performed using 10 mM citrate buffer (pH 6.0). Blocking solution (1% NDS, 3% BSA, 1% gel, 0.2% TX-1000 and 0.2% saponin in PBS+) incubation was conducted for 1 hour at room temperature followed by incubation at 4°C overnight with primary antibodies against mucin MUC5AC (Millipore Sigma) and pan-cytokeratin (pan-CK, Santa Cruz Biotechnology). Appropriate DyLight® fluorescently-conjugated secondary antibodies (Abcam) were used, and sections were incubated for 1 hour at room temperature. Sections were mounted with DAPI-containing Fluormount-G. Immunofluorescent images were captured using the Keyence BZ-X700 microscope and image analysis was conducted using the ImageJ software (NIH). Mean fluorescence intensity per number of epithelial cells was used to compare mucin MUC5AC expression levels. Pan-CK was used as a confirmation of epithelial cell identity. Tissue sections were deparaffinized and hydrated in graded ethanol and deionized water. Histochemical staining was conducted with Alcian blue-period acid Schiff (AB-PAS) or AB followed by hematoxylin and eosin (H&E) or AB-H&E staining as described. (102) The mucus secretory cells (goblet/mucous cells) were quantified as a total number of AB-PAS+ or just AB+ cells per mm basal lamina for each image. For immunostaining

analyses, cell cultures grown in Nunc™ Lab-Tek™ II 8-chamber slide system were washed using 0.05% v Brij-35 in PBS(+) and immunostained as described previously. (2) Cells were stained with antibodies to mucin MUC5AC (Millipore, Inc.), ICAM-1 (Cell Signaling Technology, Inc.) and pan cytokeratin (Cell Signaling Technology, Inc.). Immunostained cells were detected using respective secondary fluor-conjugated antibodies (Thermo Fisher Scientific, Inc) and mounted with DAPI-containing mounting media. Immunofluorescent images were captured using a Keyence BZ-X710 all-in-one fluorescence microscopy system and were analyzed using Keyence analysis software and Image J software (National Institutes of Health). Groups of NHBEs and CHBEs stained with MUC5AC, or ICAM-1 were analyzed separately, with exposure adjusted for each treatment. Once exposure was adjusted for MUC5AC and ICAM-1 groups, positive cells were counted as a percentage of the total cell number. The raw percentages were calculated as the fold-change compared to non-treated (NT) NHBE group.

VI. RNA fluorescence in-situ hybridization (FISH)

The RNAScope® 2.5 HD duplex assay and reagent kit (Advanced Cell Diagnostics, Biotechne) was used for RNA FISH as per the manufacturer's instructions. A double-Z probe set against *LASI* was designed containing 20 dual probes targeting various segments across the *LASI* lncRNA. RNA FISH was conducted on paraffin-embedded 5 µm tissue sections obtained from the LTRC of the NIH. Deparaffinization was conducted in consecutive xylene, graded ethanol, and deionized water. Pretreatment was conducted with hydrogen peroxide solution

and the RNAScope® target retrieval buffer and protease plus solutions were used to exposure the antigen. Probe hybridization was conducted for 2 hours at 40°C in the HybEZ® II oven. The signal was amplified using the Amp1, Amp2, Amp3 and the HRP probe at 40°C in the HybEZ® II oven. The signal was detected using the tyramide signal amplification (TSA) reaction with an Alexa fluor labeled TSA kit (Perkin Elmer). Sections were then processed for immunohistochemistry or directly mounted with the 4',6-diamidino-2-phenylindole (DAPI)-containing Fluormount-G (Southern Biotechnology). Images were captured using the Keyence BZ-X700 structured illumination fluorescent microscope. Analysis was conducted with the Keyence BZ-X analysis software and using the ImageJ software (NIH). RNA FISH quantification was conducted according the RNAScope® histo (H)-score methodology. In each image, probe signals were counted for each cell, both in the nuclear and cytosolic region and assigned to appropriate bins: bin 0 (no signals), bin 1 (1-3 signals/cell), bin 2 (4-9 signals/cell), bin 3 (10-15 signals/cell) and bin 4 (>15 signals/cell). The H-score was calculated as follows: H-score was the sum of each bin multiplied by the percentage of cells that fall into that bin. H-score = (0 x % cells in bin 0) + (1 x % cells in bin 1) + (2 x % cells in bin 2) + (3 x % cells in bin 3) + (4 x % cells in bin 4). Final H-scores ranged from 0 to 400 per group.

VII. Enzyme-linked immunosorbent assays (ELISAs)

Culture media and apical cell culture washes from NHBEs and CHBEs differentiated in 3D ALI culture for 28 days was collected prior to CSE treatment and every two days after treatment. Final apical washes and culture media

supernatant were collected prior to the termination of the experiment and was either stored at -80°C or processed for analysis. The protein levels of MUC5AC, ICAM-1, and IL-6 were determined using human ELISA kits against MUC5AC (MyBioSource Inc., San Diego, CA), ICAM-1 (LifeSpan Biosciences Inc., Seattle, WA), and IL-6 (BioLegend Inc., San Diego, CA), respectively, as per manufacturers' instructions.

VIII. LncRNA *LASI* overexpression

A full-length *LASI* lncRNA sequence utilizing all three exons was cloned into a pLenti-GIII-CMV-GFP-2A-Puro vector and a high titer lentivirus preparation was obtained from Applied Biological Materials Inc. (Richmond, Canada). Primary HBECs cultured overnight in 12-well plates were transduced with LASI-overexpression (*LASI*-OE) lentiviral preparation at 0.5 and 2 MOIs (multiplicity of infection) using a culture media containing 8 µg/ml of polybrene transfection reagent (Sigma). The GFP-tag fluorescence was followed to assess the transduction efficiency. Forty-eight-hour post-transfection, cells were harvested, and qPCR was performed for expression analysis of LASI lncRNA and other transcripts. Mock-transduced cells (or cells with 0 MOI) were used as controls to analyze the expression levels.

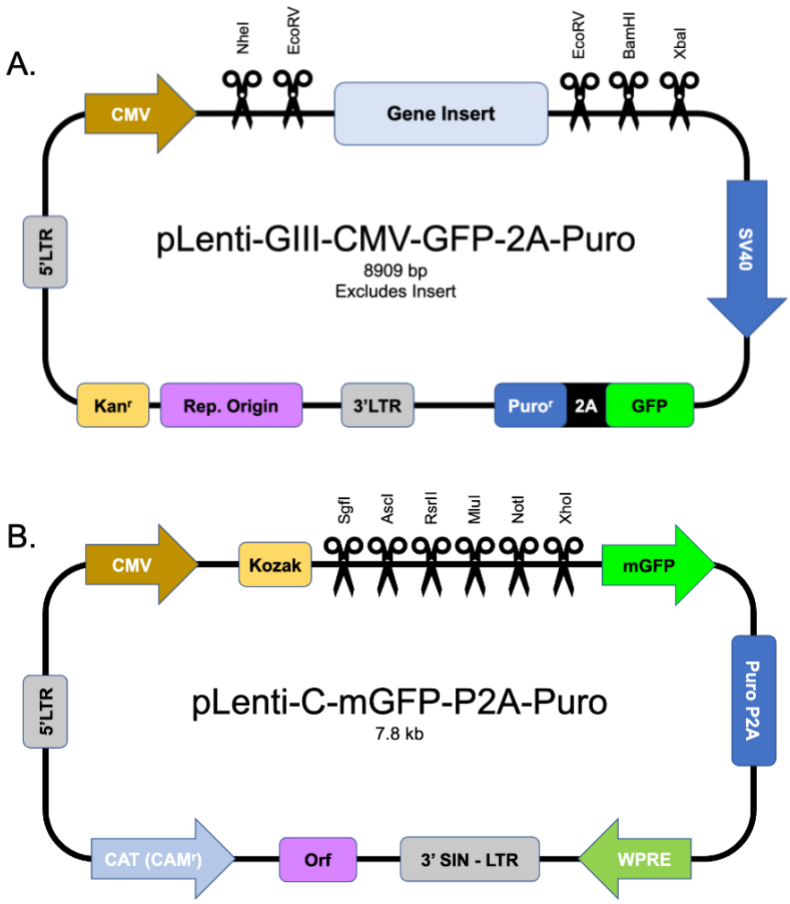

Figure 8. Lentiviral overexpression **(A.)** and control vector **(B.)** used for transduction.

IX. Statistical analyses

Grouped results were expressed as mean±SEM and $p<0.05$ was considered significant. Data were analyzed using GraphPad Prism Software (GraphPad Software Inc.) using one-way analysis of variance (ANOVA) with and Tukey's multiple comparison test or using a two-tailed t test for comparison between two groups. When significant main effects were detected ($p<0.05$), student's t test was used to determine differences between the groups.

Chapter 3: Results

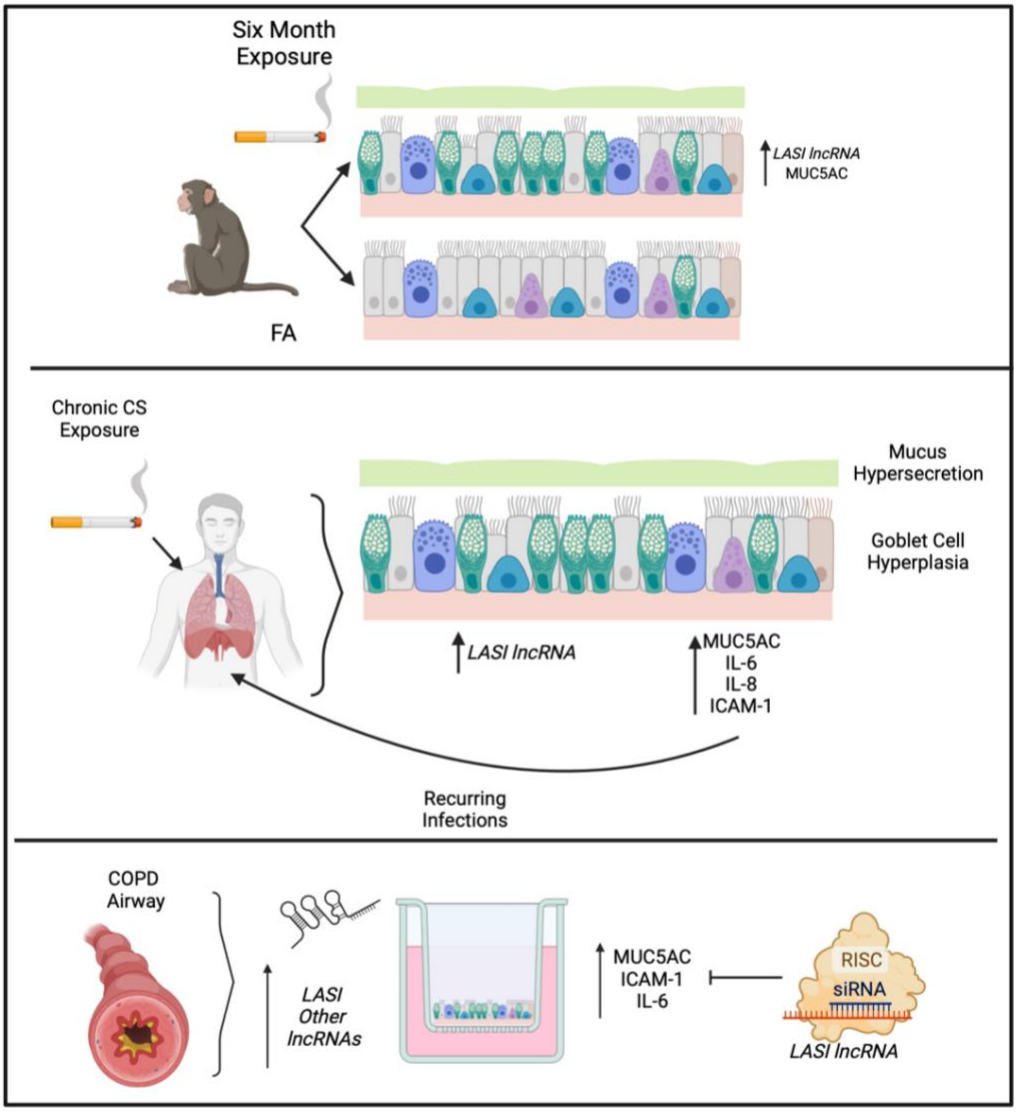

Figure 9. Experimental study design - *LASI* lncRNA in a COPD model. Created with BioRender.com. Original source (3).

I. Chronic CS exposure results in goblet/mucous cell hyperplasia and increased *LASI* lncRNA expression in bronchial airway epithelium

We recently analyzed the effects of long-term CS exposure in a large animal model where cynomologus macaques (*M. fascicularis*) were exposed to mainstream CS for twenty-seven weeks, where CS-exposed macaques showed

COPD-like respiratory phenotypes. (182) Here, we specifically analyzed the bronchial epithelial responses in archived lung tissues of CS-exposed macaques and filtered room-air (FA) exposed control macaques (n=4 each). Compared to FA group, CS-exposed macaque lungs showed significant bronchial airway epithelial remodeling with augmented goblet/mucous cell hyperplasia (**Figure 10A**) as analyzed by histochemical staining using Alcian blue and Periodic acid Schiff's (AB-PAS) reagent. There were 2.6-fold higher number of AB-PAS+ goblet/mucous cells per mm basal lamina (BL) in CS-exposed macaques compared to FA group (**Figure 10B**).

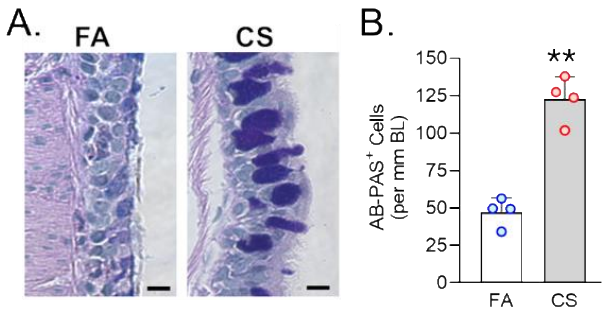

Figure 10. Chronic cigarette smoke (CS) exposure model of Cynomolgus macaques results in goblet/mucous cell hyperplasia. Bronchial airway tissues were analyzed from C. macaques exposed to mainstream CS or control filtered-air (FA) for 27 weeks as reported recently. (182*)* **(A.)** Representative histomicrographs of bronchial tissue sections showing AB-PAS-stained goblet/mucous cells in CS- and FA-exposed macaques. **(B.)** Number of AB-PAS+ cells quantified per mm of basal lamina (BL) in each group. Data shown as mean ± SEM; n=4/group; data analyzed by t-test, ** $p < 0.01$. Original source (3).

The expression levels of secretory mucin *MUC5AC* mRNA were 3-fold higher in CS group compared to FA macaques (**Figure 11A**) as determined by qRT-PCR. CS-induced MUC5AC expression was also corroborated by immunostaining of bronchial tissue sections (**Figure 11B**) with 7.9-fold higher percentage of MUC5AC-positive ($MUC5AC^+$) cells observed in CS macaques over

FA group (**Figure 11C**). Thus, chronic CS exposure results in goblet cell hyperplasia with increased expression of MUC5AC mucin.

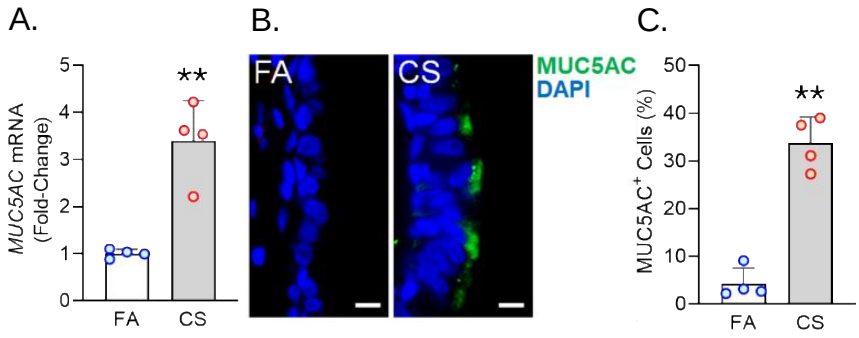

Figure 11. Chronic CS exposure model of Cynomolgus macaques results in goblet/mucous cell hyperplasia. **(A.)** Relative quantity of secretory mucin MUC5AC mRNA in CS-exposed macaques compared to FA-controls as determined by qPCR. **(B.)** Representative micrographs of bronchial tissue sections showing MUC5AC immunopositivity in CS- and FA-exposed macaques. **(C.)** Percentage of MUC5AC+ cells over the total epithelial cells quantified for each group. Data shown as mean ± SEM; n=4/group; data analyzed by t-test, ** $p < 0.01$. Original source (3).

LncRNAs are essential regulators of smoke mediated inflammatory responses (167, 178) and based on the critical role of *LASI* lncRNA in airway inflammatory and mucus hyperexpression (2), we analyzed the effects of CS on bronchial epithelial *LASI* lncRNA expression. Compared to the FA group, we observed a 2.4-fold increase in *LASI* transcript levels in CS-exposed macaques (**Figure 12A**). Cellular *LASI* expression levels were further analyzed by performing RNA-FISH as described previously (2), which allowed for single RNA molecule-level resolution and subcellular localization evaluation (**Figure 12B**). We found that *LASI* lncRNA was significantly upregulated and the number of *LASI* lncRNA transcripts per cell was significantly upregulated upon CS treatment (**Figure 12C**). Overall, in a large animal model of chronic CS exposure, bronchial epithelial cells

show a strong correlative increase in *LASI* lncRNA levels and MUC5AC mucin expression.

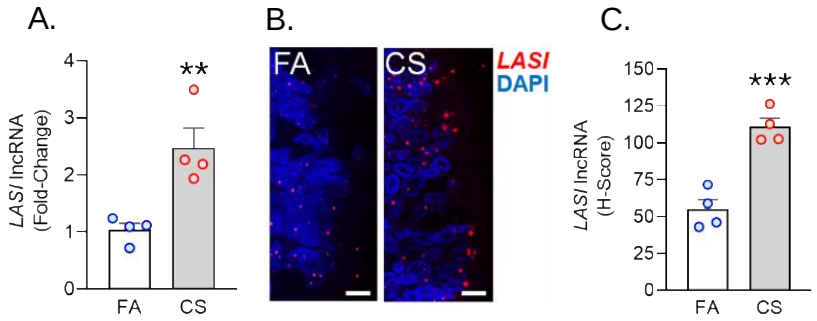

Figure 12. Chronic CS exposure model of Cynomolgus macaques results in increased LASI lncRNA expression in bronchial airways. **(A.)** Relative quantity of LASI lncRNA in CS-exposed macaques versus FA-controls as determined by qPCR. **(B.)** Representative micrographs showing LASI lncRNA expression in FA and CS macaques as determined by FISH. **(C.)** Quantification of LASI lncRNA expression in bronchial epithelial cells of each group as determined by H-score analysis described earlier. (2) Data shown as mean ± SEM; n=4/gp and analyzed by Student's T-test; **p<0.01; ***p<0.001. Original source (3).

II. LASI lncRNA levels are upregulated in COPD airway epithelium

We next investigated the correlation between the airway epithelial *LASI* lncRNA expression and the mucoinflammatory phenotype of COPD tissue samples. The transcript expression levels in lung tissue homogenates of COPD and no COPD control samples were evaluated by qRT-PCR. *LASI* transcript levels were 4-fold and 6-fold higher in the mild COPD (n=6) and severe COPD tissue samples, (n=8), respectively, compared to no-COPD control tissues (n=6) (**Figure 13A**). We also investigated of the expression of other lncRNAs such as, ICAM-1-related lncRNA (*ICR*), which regulates ICAM-1 expression by mRNA stabilization via direct interaction and duplex formation, (183) but there was no significant change in ICR levels among COPD tissue samples (**Figure 14A**).

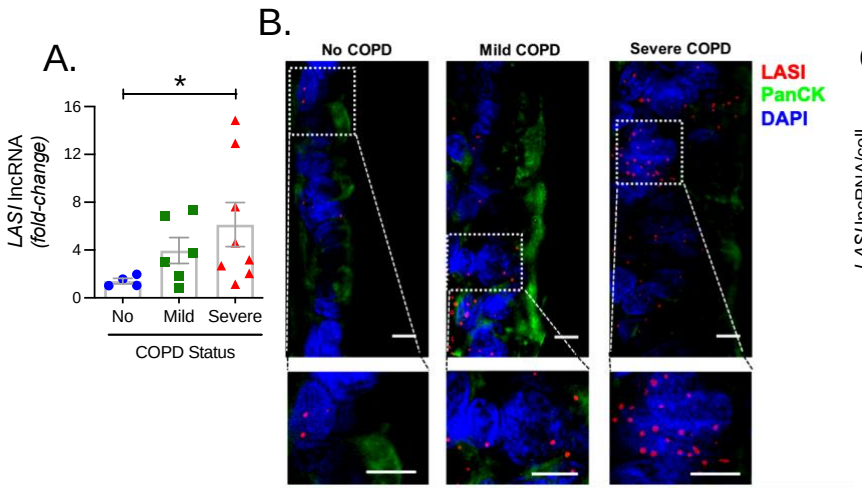

Figure 13. Archived airway sections of COPD patients show increased LASI lncRNA expression in epithelial cells. **(A.)** Quantitation of LASI lncRNA levels in mild and severe COPD subjects compared to control subjects with No COPD. **(B.)** Micrographs showing LASI lncRNA levels in airway epithelial cells of patient bronchial tissues. LASI lncRNAs were detected by RNA-FISH (shown in red) and epithelial cells were immunostained by pan-cytokeratin (panCK, shown in green) antibody, and nuclei (shown in blue) were stained by DAPI. Lower panels show magnified images of the insets drawn in upper panels (scale – 5µm). **(C.)** Quantitation for LASI lncRNAs per epithelial cell as measured by H-score analysis. Data shown as mean ± SEM; n=6-8/gp; data analyzed by ANOVA with multiple comparisons; *p<0.05; **p<0.01; ***p<0.001. Original source (3).

Similarly, there was no change in the expression levels of highly prevalent lncRNA *NEAT1* or nuclear enriched assembly transcript 1 (**Figure 14B**) and *MALAT1* or metastasis associated lung adenocarcinoma transcript 1 (**Figure 14C**). Although *NEAT1* lncRNA has been implicated as a potential prognostic marker of COPD exacerbations where its expression level correlated with disease severity. (184) Similarly, *MALAT1* lncRNA has been proposed as potential therapeutic target because silencing its expression blocked the COPD-associated lung remodeling. (185) We also analyzed the expression levels of lncRNA called *WAKMAR2* or a wound and keratinocyte migration-associated lncRNA, which

regulates the proinflammatory responses in keratinocytes (186) and there were no significant changes among COPD subjects (**Figure 14D**).

To further corroborate the COPD-associated *LASI* lncRNA expression levels and to evaluate airway epithelium specific expression, we conducted RNA-FISH to examine *LASI* expression at a single RNA molecule resolution and evaluate the *LASI* subcellular localization (**Figure 13B**). We found that in small airways, both mild and severe COPD tissue samples present with significantly upregulated *LASI* expression as compared to non-COPD controls. There was 1.4- and 1.6-fold higher *LASI* expression in pan-cytokeratin+ epithelial cells of mild and severe COPD tissues, respectively (**Figure 13C**). *LASI* transcripts were found both in the perinuclear and the cytosolic regions of bronchial epithelial cells. Collectively, these data suggest a strong correlation between *LASI* lncRNA expression and mucus hypersecretion, mucous cell hyperplasia, and COPD pathogenesis.

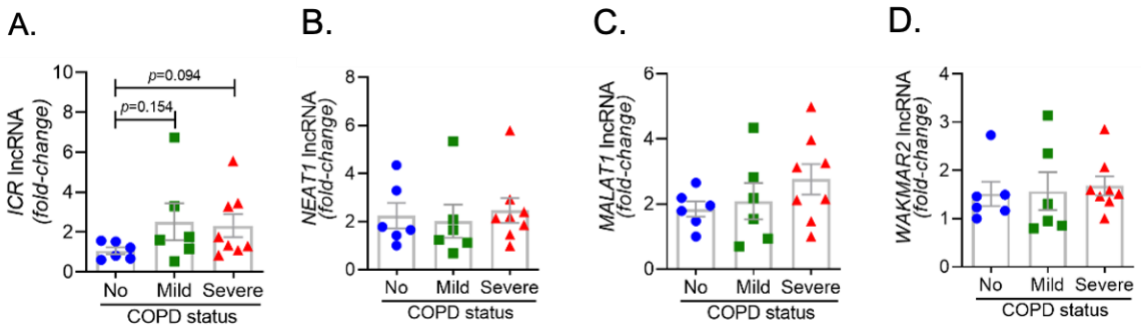

Figure 14. Expression levels of select inflammatory factors and lncRNAs in the lung tissue samples of mild and severe COPD donors versus the controls with no COPD. Relative quantities of lncRNA levels of ICR **(A.)**, NEAT1 **(B.)**, MALAT1 **(C.)**, and WAKMAR2 **(D.)**. Data shown as mean ± SEM (n=6-8/gp); data analysed by ANOVA, *p<0.05. Original source (3).

III. Primary HBECs from COPD patients show higher transcript levels of *LASI* lncRNA and the mucoinflammatory factors

To assess epithelial cell-specific responses, we next cultured primary differentiated human bronchial epithelial cells (HBECs) obtained from COPD donors (CHBEs) and compared with HBECs from control donors with no-COPD (NHBEs). Primary CHBEs are a highly representative model of COPD progression, as studies have shown that they undergo dysregulation in numerous pathways. (39) A recent study showed that CHBEs have significantly dysregulated calcium (Ca2+) signaling, a crucial messenger for various cellular processes, including ciliary beating. (187) CHBEs are also known to have dysregulated cell proportions, with higher numbers of goblet cells and reduced number of ciliary cells, as well as a notable decrease in β-tubulin and an increase in mucin MUC5AC. (188) Primary NHBEs and CHBEs were differentiated on an air-liquid interface (ALI), on transwells, as 3D airway cultures. We first compared the baseline differences between differentiated NHBEs and CHBEs, without any treatment or stimulation. Among the lncRNAs analyzed, expression levels of ICAM-1 loci associated lncRNAs, *LASI* (**Figure 15A**) and *ICR* (**Figure 15B**) were 6.2- and 8.0-fold higher in unstimulated CHBEs compared to NHBEs, respectively. Expression levels of other lncRNAs were also higher in CHBEs with *NEAT1*, *MALAT1*, and *WAKMAR-2* lncRNAs expressed at 3.3-, 1.6-, and 3.2-fold higher in CHBEs compared to NHBEs, respectively (**Figure 16A-C**).

Next, we examined the baseline expression of epithelial inflammatory factors and secretory mucins in NHBEs and CHBEs. Compared to NHBEs, the

MUC5AC mucin (**Figure 15C**), *ICAM-1* (**Figure 15D**), and *IL-6* (**Figure 15E**) mRNA levels were 3.0-, 4.6-, and 6.0-fold higher in CHBEs. In order to determine whether the changes in transcript levels recapitulate the secretory protein levels, we analyzed the MUC5AC protein levels in apical wash samples and found that MUC5AC levels were approximately 39.1 ng/ml and 152.2 ng/ml in NHBEs and CHBEs, respectively (**Figure 15F**). Protein levels of ICAM-1 and IL-6 were analyzed in NHBE and CHBE basal culture media supernatants. Secreted ICAM-1 levels were approximately 29.9 pg/ml and 200.8 pg/ml in NHBE and CHBE culture media, respectively (**Figure 15G**), with a 6.7-fold increase in CHBEs. Similarly, average secreted IL-6 level in NHBE culture media was 60.6 pg/ml whereas in CHBE culture media was 399.8 pg/ml (**Figure 15H**). Collectively, these data suggest a strong dysregulation of inflammatory responses in the bronchial epithelial cells in COPD with coordinated changes in lncRNA, mRNA, and protein expression.

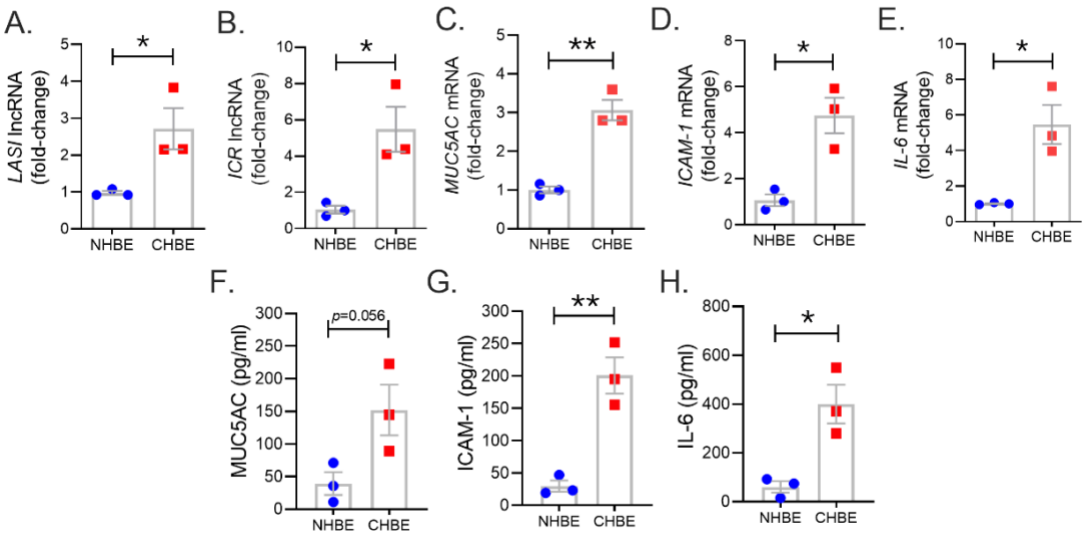

Figure 15. Differentiated bronchial epithelial cells from COPD subjects show increased expression of immunomodulatory lncRNAs, MUC5AC mucin, and IL-6 and ICAM-1 compared to control cells from non-COPD donors. Relative transcript levels for lncRNA LASI **(A.)**, and ICR **(B.)** in 3D cultured and unstimulated NHBE and CHBE cells as determined by qRT-PCR. Relative mRNA levels of MUC5AC **(C.),** ICAM-1 **(D.)**, and IL-6 **(D.)** inflammatory factors. Quantification of secretory MUC5AC mucin levels **(G.)** in the apical washes, and the IL-6 **(H.)**, and ICAM-1 **(I.)** levels in basal media supernatant as analyzed by specific sandwich ELISA assays. Data shown as mean ± SEM as fold-change over NHBEs; n = 3/gp; data analyzed by student's t-test; *p<0.05; **p<0.01. Original source (3).

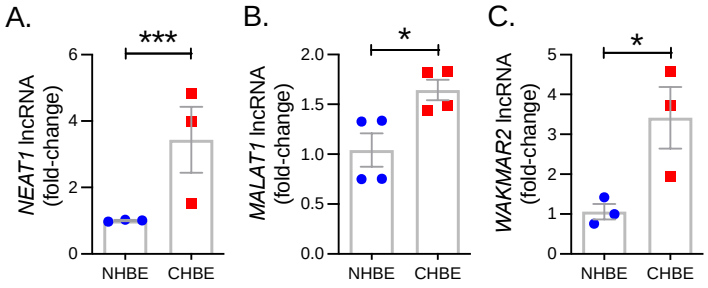

Figure 16. Differentiated bronchial epithelial cells from COPD subjects show increased expression of lncRNA NEAT1, MALAT1 and WAKMAR2. Relative transcript levels for lncRNA NEAT1 **(A.)**, MALAT1 **(B.)** and WAKMAR2 **(C.)** in CHBEs compared to NHBEs. Data shown as mean ± SEM as fold-change over NHBEs; n = 3/gp; data analyzed by student's t-test; *p<0.05; ***p<0.001. Original source (3).

IV. CS exposure results in an augmented inflammatory response in COPD HBECs

To evaluate the CS-induced response, CHBEs and NHBEs were treated with 10 μg/ml CSE for 48h as described previously (189), and total cell RNA was evaluated for changes in lncRNAs and inflammatory factors' expression. Interestingly, both ICAM-loci associated lncRNAs, *LASI* (**Figure 17A**) and *ICR* (**Figure 17B**) were significantly upregulated with 3.3-fold and 1.9-fold upregulation in CSE-treated CHBEs, respectively, as compared to CSE-treated NHBEs. However, expression levels of *NEAT1* and *MALAT1* lncRNAs failed to show any significant change following CSE treatment (**Figure 17A-17B**). But the *WAKMAR-2* lncRNA levels were 2.8-fold higher following CSE-treatment of CHBEs over NHBEs (**Figure 17C**). This change in CSE-induced lncRNAs directly correlated with expression of *ICAM-1* mRNA, which was 2.0-fold upregulated in CSE-treated CHBEs than NHBEs (**Figure 17D**). No significant changes were observed in CSE-induced *IL-6* and *CXCL-8* mRNA expression between CHBEs and NHBEs (**Figure 17E-17F**). These data suggest that the CSE induces a dysregulated response in NHBEs, and the responses are further potentiated in CHBEs; and that there is a potential direct regulatory relationship between *LASI* and *ICR* lncRNAs and ICAM-1 expression.

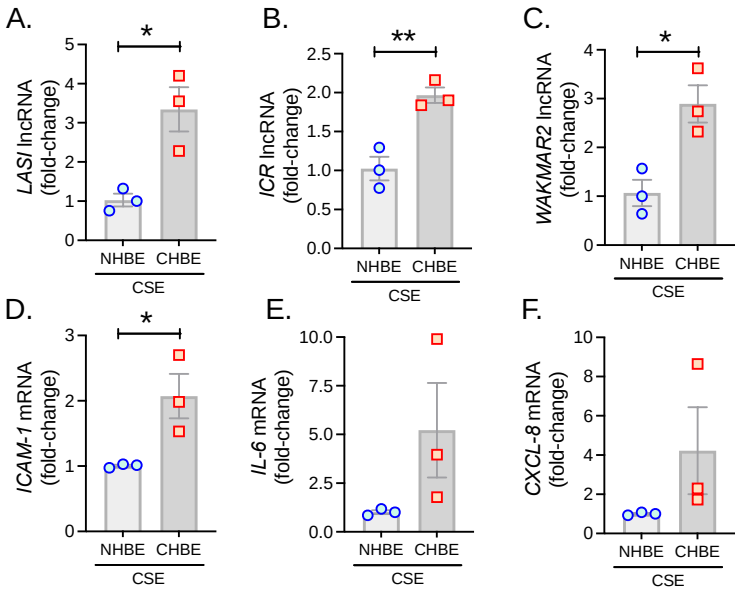

Figure 17. Cigarette smoke exposure of COPD bronchial epithelial cells induce higher levels of immunomodulatory lncRNAs, and inflammatory factor mRNAs compared to non-COPD control cells. Primary NHBEs and CHBEs grown in submerged culture setting were treated with a 20 µg/ml cigarette smoke extract (CSE) and forty-eight hours after treatment cells were harvested and qRT-PCR was performed. Relative transcript levels for lncRNA LASI **(A.)**, and ICR **(B.)** in CSE-treated NHBE and CHBE cells as determined by qRT-PCR. Relative mRNA levels of ICAM-1 **(C.)**, IL-6 **(D.)**, and CXCL-8 **(E.)** inflammatory factors. Data shown as mean ± SEM as fold-change over NHBEs; n = 3/gp; data analyzed by student's t-test; *p<0.05; **p<0.01. Original source (3).

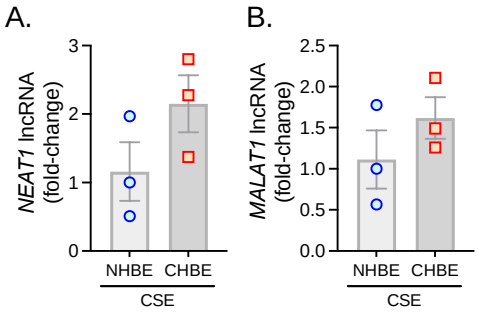

Figure 18. Cigarette smoke exposure of COPD bronchial epithelial cells induce increased trends of expression of lncRNAs. Primary NHBEs and CHBEs grown in submerged culture setting were treated with a 20 µg/ml cigarette smoke extract (CSE) and forty-eight hours after treatment cells were harvested and qRT-PCR was performed. Relative transcript levels for lncRNA NEAT1 **(A.)** and MALAT1 **(B.)**. Data shown as mean ± SEM as fold-change over NHBEs; n = 3/gp; data analyzed by student's t-test. Original source (3).

To further substantiate these findings, we additionally performed the cytometric analysis of MUC5AC and ICAM-1 protein expression in NHBEs and CHBEs grown on Labtech® slides and treated with 10 µg/ml CSE for 48h. Based on immunostaining analyses, we observed a 2.3-fold increase in the percentage of MUC5AC+ cells in CSE-treated NHBEs, and a 15.4-fold increase in CSE-treated CHBEs (**Figure 19A-19B**). Similarly, NHBEs showed a 2.3-fold increase in the percentage of ICAM-1+ cells, while CHBEs showed a 2.9-fold increase in ICAM-1+ cells upon CSE treatment (**Figure 19C-19D**). These data further suggest that CS insult causes CHBEs to respond with a significantly more severe, dysregulated mucus secretory and inflammatory response.

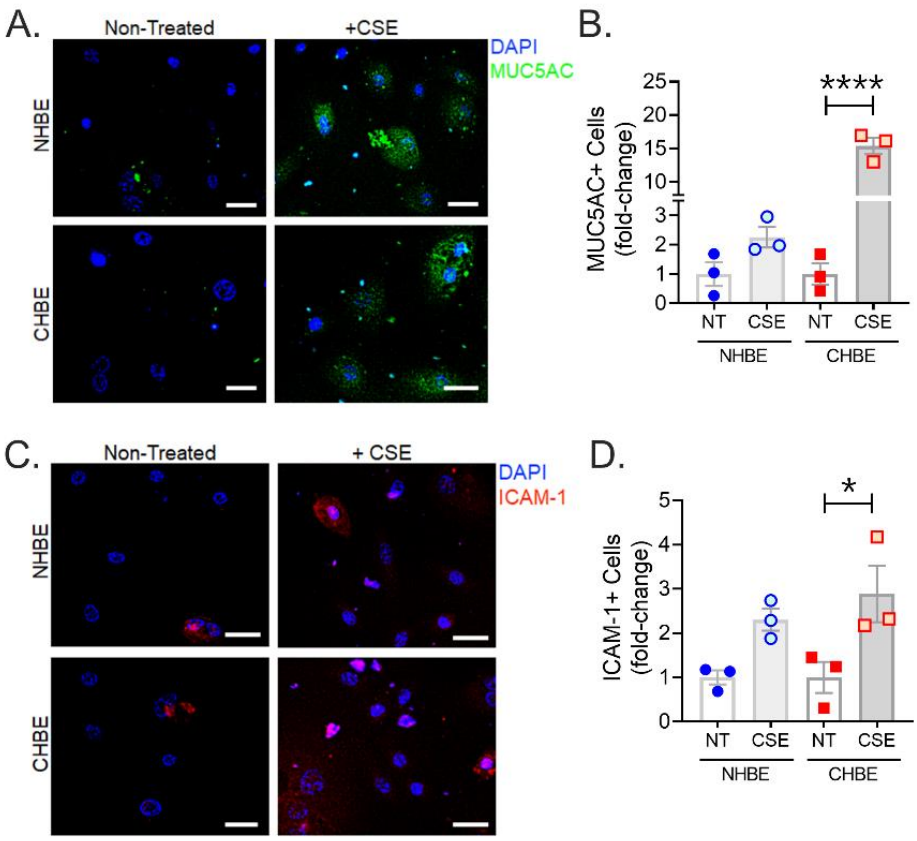

Figure 19. Cigarette smoke treatment augments mucous cell hyperplasia in CHBEs with higher ICAM-1 protein expression compared to non-COPD control cells. Primary NHBEs and CHBEs grown in LabTek-II® slides were treated with a 20 µg/ml CSE and forty-eight hours after treatment cells were fixed with 4% paraformaldehyde (PFA) and processed for staining with antibodies against MUC5AC and ICAM-1. **(A.)** Representative micrographs showing MUC5AC immunopositivity (shown in green) in NHBEs and CHBEs treated with CSE or left non-treated (NT), and nuclei were stained by DAPI (shown in blue), scale – 2µm. **(B.)** Quantification of MUC5AC-positive (+) cells in NHBEs and CHBEs treated with CSE compared to NT cells. **(C.)** Representative micrographs showing ICAM-1 immunopositivity (shown in red) in NHBEs and CHBEs treated with or without CSE. **(D.)** Quantification of ICAM-1-positive (+) cells in NHBEs and CHBEs treated with CSE compared to NT controls. Data shown as mean ± SEM as fold-change compared to NT cells; n=3/gp; data analyzed by ANOVA; *p<0.05; ****p<0.0001. Original source (3).

V. Modifying *LASI* expression suppresses the smoke-induced inflammation, mucin expression, and mucus cell hyperplasia

In order to determine whether the correlation between *LASI* lncRNA with *MUC5AC* and *ICAM-1* expression is functionally significant, we genetically silenced *LASI* lncRNA expression using siRNAs targeting *LASI* (siLASI) in differentiated CHBEs then challenged with 10 μg/ml CSE for 48h. CHBEs transfected with scrambled control siRNA (siCTRL) followed by 48 h 10 μg/ml CSE treatment served as controls. Compared to siCTRL, the siLASI-transfected CHBEs showed a 37.5% reduction in *LASI* lncRNA expression (**Figure 20A**). Interestingly, even with this moderate reduction in *LASI* expression, there was a 63.9% reduction in CSE-induced *MUC5AC* mRNA levels in siLASI-transfected CHBEs (**Figure 20B**), suggesting that functional availability of *LASI* lncRNA is necessary for CSE-mediated induction of *MUC5AC* expression in CHBEs. Notably, we found no change in *SPDEF* transcription factor levels (**Figure 21A**), suggesting that a CSE-induced and *LASI*-mediated MUC5AC expression may not be dependent on SPDEF-mediated transcriptional upregulation. Expression levels of another airway secretory mucin, *MUC5B* mRNA were not changed in siLASI-transfected CHBEs (**Figure 21B**). We also evaluated the changes in the CSE-mediated inflammatory responses in siLASI-transfected CHBEs. Notably, we found that siLASI induced a significant 36.2% reduction in *ICAM-1* mRNA levels (**Figure 20C**) and a 66% reduction in *IL-6* mRNA levels (**Figure 20D**), suggesting that *LASI* lncRNA may contribute to the expression of these inflammatory factors. However, expression

levels of inflammatory factor CXCL-8 mRNAs were not changed in siLASI-transfected CHBEs (**Figure 21C**).

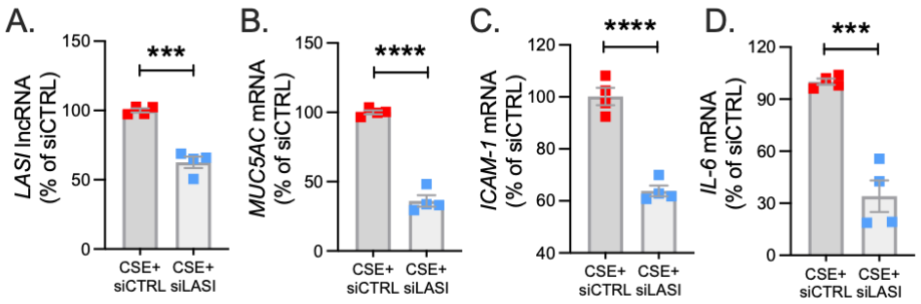

Figure 20. RNA silencing-mediated knockdown of LASI lncRNA suppresses the CSE-induced mucus secretory and inflammatory response at the mRNA level. CHBEs grown in 3D ALI tissue culture conditions were transfected with either siRNA targeting LASI (siLASI) or scrambled control siRNA (siCTRL), and cells were treated with 20 µg/ml CSE to obtain CSE+siLASI and CSE+siCTRL cells, respectively. Cells harvested forty-eight hours post CSE-treatment were analyzed for the expression levels of **(A.)** LASI lncRNA, and mRNA levels of **(B.)** MUC5AC, **(C.)** ICAM-1, and **(D.)** IL-6 by qRT-PCR. Data shown as mean ± SEM compared to CSE+siCTRL cells; n=4/gp; data analyzed by student's t-test; ***p<0.001; ****p<0.0001. Original source (3).

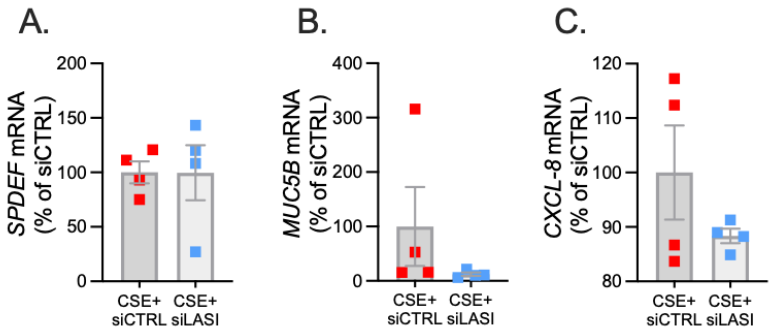

Figure 21. RNA silencing-mediated knockdown of LASI lncRNA does not induce changes in several mucus secretory and inflammatory elements. CHBEs grown in 3D ALI tissue culture conditions were transfected with either siRNA targeting LASI (siLASI) or scrambled control siRNA (siCTRL), and cells were treated with 20 µg/ml CSE to obtain CSE+siLASI and CSE+siCTRL cells, respectively. Cells harvested forty-eight hours post CSE-treatment were analyzed for the mRNA levels of **(A.)** SPDEF, **(B.)** mucin MUC5B, and **(C.)** CXCL-8 by qRT-PCR. Data shown as mean ± SEM compared to CSE+siCTRL cells; n=4/gp; data analyzed by student's t-test. Original source (3).

Next, we used sandwich ELISA to measure the secreted protein levels of mucin MUC5AC, and cytokines ICAM-1 and IL-6 in siLASI-transfected CHBEs followed by 48h CSE treatment. Interestingly, apical wash from siCTRL-transfected CHBEs had 236.6 ng/ml of mucin MUC5AC while the siLASI-transfected CHBEs had 73.9 ng/ml (**Figure 22A**). Furthermore, the culture media supernatants from the siLASI-transfected CHBEs had 298.2 pg/ml IL-6 levels compared to the 765.8 pg/ml in siCTRL-transfected CHBEs (**Figure 22B**), Similarly, siLASI-transfected CHBEs secreted 105.3 pg/ml ICAM-1 levels whereas the siCTRL-treated CHBEs secreted 138.3 pg/ml (**Figure 22C**). Overall, siLASI-transfected CHBEs showed a 2.6-fold reduction in IL-6 and a 1.3-fold reduction in ICAM-1 secretory levels following CSE treatment over siCTRL-transfected CHBEs. Notably, CSE-induced MUC5AC mucin secretion was reduced by 3.2-fold in siLASI-transfected CHBEs compared to the siCTRL-transfected CHBEs.

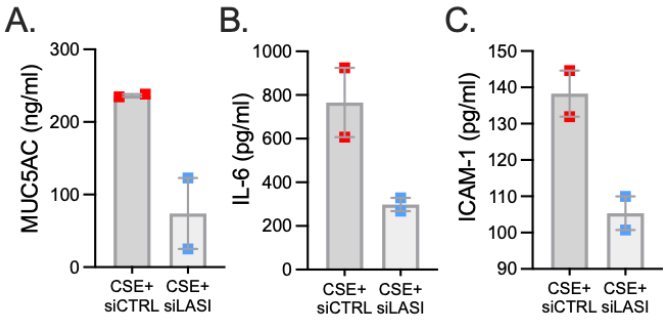

Figure 22. RNA silencing-mediated knockdown of LASI lncRNA suppresses the CSE-induced mucus secretory and inflammatory response in COPD bronchial epithelial cells at the protein level. CHBEs grown in 3D ALI tissue culture conditions were transfected with either siRNA targeting LASI (siLASI) or scrambled control siRNA (siCTRL), and cells were treated with 20 µg/ml CSE to obtain CSE+siLASI and CSE+siCTRL cells, respectively. Apical washes from 3D tissue cultures were analyzed for **(A.)** MUC5AC mucin by ELISA, and the basal media supernatants were analyzed for **(B.)** IL-6, and **(C.)** ICAM-1 protein levels by specific ELISA

assays. Data shown as mean ± SEM compared to CSE+siCTRL cells; n=4/gp; data analyzed by student's t-test. Original source (3).

We further corroborated the data by immunoprobing the siCTRL- and siLASI-transfected CHBEs for MUC5AC and ICAM-1 protein expression following 48 h CSE treatment (**Figure 23A-23B**). We found that silencing LASI expression by siLASI resulted in a 3.1-reduction in MUC5AC-expressing (MUC5AC+) cells (**Figure 23C**) and a 2.5-fold reduction in cell expressing ICAM-1 protein (**Figure 23D**). These data strongly suggest lncRNA *LASI* represents an important regulatory mediator in the CS-induced pathophysiological changes observed in COPD airways, including dysregulated immune response and chronic mucus hypersecretion.

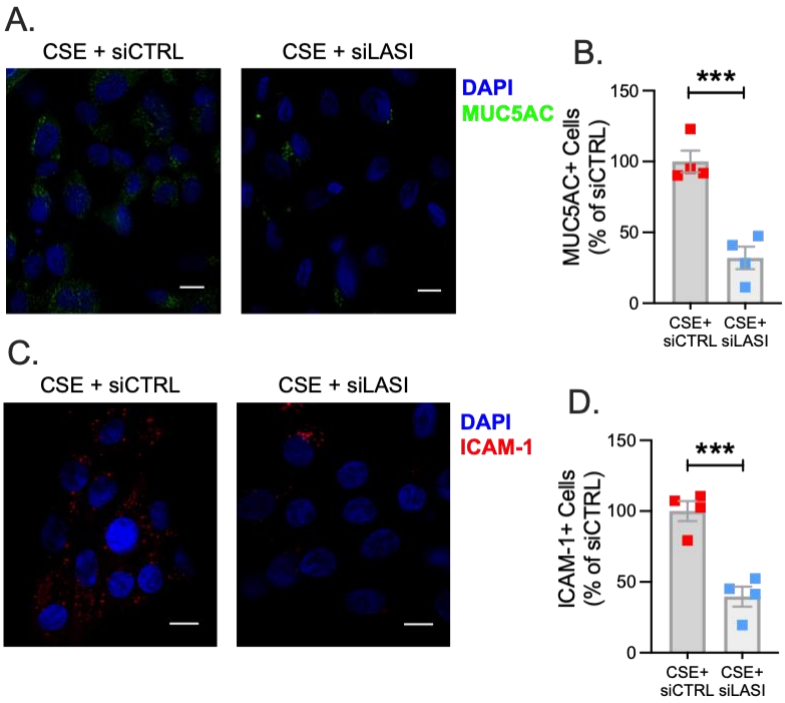

Figure 23. RNA silencing-mediated knockdown of LASI lncRNA suppresses the CSE-induced mucus secretory and inflammatory response in submerged cell culture. CHBEs grown in submerged tissue culture conditions were transfected with either siRNA targeting LASI (siLASI) or scrambled control siRNA (siCTRL),

and cells were treated with 20 µg/ml CSE to obtain CSE+siLASI and CSE+siCTRL cells, respectively. **(A.)** Representative micrographs of CHBEs transfected with siCTRL or siLASI and treated with CSE showing MUC5AC mucin immunopositivity (shown in green) and nuclei were stained by DAPI (shown in blue), scale – 5µm. **(B.)** Quantification of MUC5AC+ cells among CSE+siLASI CHBEs, shown as percentage of CSE+siCTRL cells. **(C.)** Micrographs of CHBEs showing ICAM-1 immunopositivity (shown in red). **(D.)** Quantification of ICAM-1+ CHBEs. Data shown as mean ± SEM compared to CSE+siCTRL cells; n=4/gp; data analyzed by student's t-test; ***p<0.001. Original source (3).

Furthermore, we explored whether ectopic *LASI* lncRNA expression results in increased expression of inflammatory factors. To determine whether LASI lncRNA directly mediates the expression of inflammatory factors, a lentiviral preparation encoding LASI lncRNA was used to transduce airway epithelial cells, and the ectopic LASI overexpression (LASI-OE) was followed by assessing GFP-tag fluorescence. We transduced airway epithelial cells with both 0.5 and 2.0 MOI of lentiviral vector. We found that cells transduced with 0.5 and 2.0 MOI of lentivirus-LASI resulted in 1.7- and 4.0-fold increased expression of LASI lncRNA, respectively, compared to mock-transduced (0 MOI) controls (**Figure 24A**). Interestingly, LASI-OE cells showed two-fold or higher levels of ICAM-1 mRNAs (**Figure 24B**). Expression levels of IL-6 (**Figure 24C**) and CXCL-8 (**Figure 24D**) mRNAs were also increased by as much as eight- and four-fold, respectively. Thus, ectopic overexpression of LASI lncRNA directly upregulates the airway epithelial inflammatory factor mRNA levels.

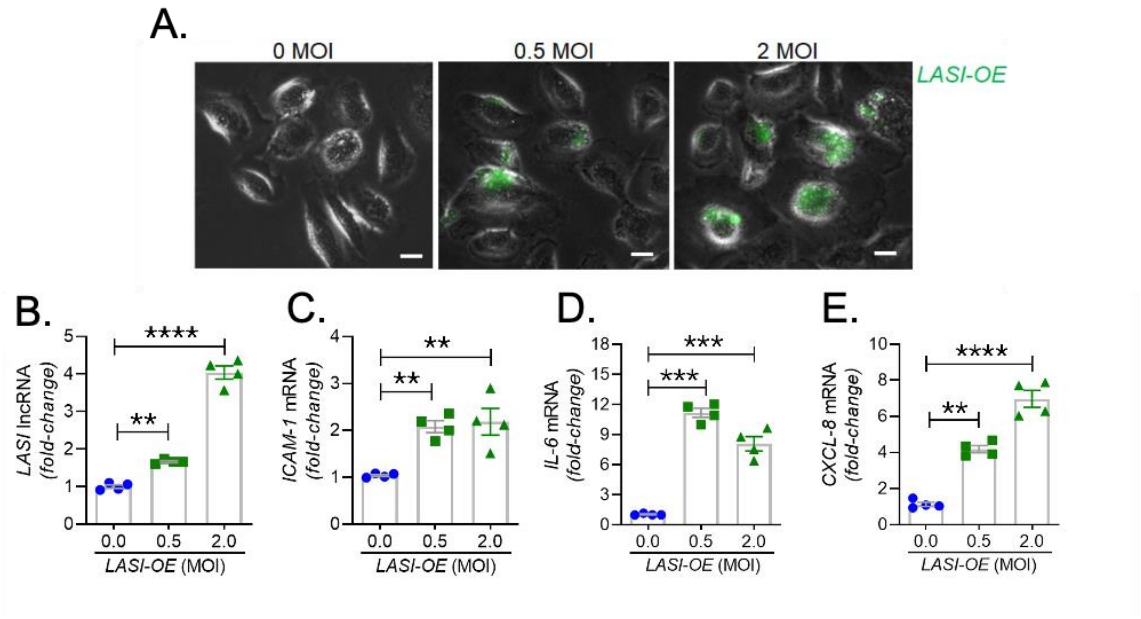

Figure 24. LASI overexpression augments the expression of inflammatory factors in NHBE cells. **(A.)** Representative micrographs of cells transduced with 0, 0.5, and 2 MOI of LASI-OE lentiviral preparation showing GFP reporter fluorescence (shown in green) and phase contrast images of cells, scale – 25μm. Cells harvested forty-eight hours post-transduction were analyzed for expression levels of LASI lncRNA **(B.)**, and mRNA levels of IL-6 **(C.)**, ICAM-1 **(D.)** and CXCL-8 **(E.)** by qRT-PCR. Data shown as mean ± SEM compared to 0.0 MOI cells; n=2/gp; data analyzed by student's t-test; ** p<0.01, *** p<0.001, **** p<0.0001. Original source (3).

Chapter 3: Discussion

Although there are numerous risk factors for developing COPD, CS exposure is the best-studied and most prevalent. Studies investigating the non-canonical inflammatory and mucus-secretory pathways underlying CS-mediated airway epithelial cells pathology and COPD-related comorbidity are needed, to unravel molecular pathways and provide novel avenues for diagnostic and therapeutic intervention. The newly discovered lncRNA molecular species are proposed as novel cellular entities that play an important role in physiology and pathophysiology, and there are studies exemplifying the extent of their potential

roles. (167, 190) In this study, we found a strong association of immunomodulatory *LASI* lncRNA expression with CS-induced airway mucus hyperexpression and inflammatory responses. The correlation was observed both in a large animal model of CS-induced COPD, and in lung tissue samples from former smokers with COPD in comparison with tissues from former smokers with no COPD. We found that lung tissue samples of CS-exposed macaques and those of COPD patients (with mild and severe COPD) presented with an increased *LASI* lncRNA expression in bronchial airway epithelial cells. *LASI* lncRNA expression correlated to the increased expression of secretory mucin MUC5AC, and innate airway inflammatory factors, IL-6, and ICAM-1, which were all upregulated in COPD tissue samples and in macaques exposed to mainstream CS. These data suggested that *LASI* lncRNA may play a role in smoke-associated bronchial epithelial remodeling and COPD. To validate the airway epithelial specific significance of *LASI* lncRNA in CS-induced responses, we utilized a 3D airway tissue culture model of primary HBECs from COPD and compared the baseline and CSE-induced responses to that of control cells from donors with no COPD. We found that unstimulated CHBEs, show a baseline upregulation of *LASI* lncRNA, along with other immunomodulatory lncRNAs such as *ICR*, *NEAT1*, *MALAT1,* and *WAKMAR2*. However, none of these lncRNAs were responsive to CSE-treatment except for *LASI* and *ICR* lncRNAs. This led us to explore the responses to CS exposure and *LASI* was the only lncRNA explored in this report which showed a potentiated dysregulated response to CSE treatment in CHBEs as compared to NHBEs. *LASI* lncRNA further showed a strong correlation with expression levels of ICAM-1, as

well as IL-6 and CXCL-8, suggesting a functional importance in COPD pathogenesis. Accordingly, we knocked down *LASI* lncRNA expression in CHBEs and discovered that a reduction in *LASI* lncRNA expression resulted in a significant reduction in CSE-induced mucoinflammatory response by reducing the expression of MUC5AC, IL-6, and ICAM-1 levels both at mRNA and protein levels. These data thus collectively implicate *LASI* lncRNA as a novel mediator of CS-induced and COPD-associated airway pathophysiology.

Cigarette smoking is strongly associated with COPD where more than 50% of COPD patients are active smokers and over 70% have a history of smoking. Notably, over 50% of COPD mortality is attributable to active smoking. (191) Patients who are exposed to CS present with exacerbated mucus secretory and airway inflammatory conditions. As such, the dysregulated response to smoke exposure may provide the most useful insight into the severe COPD pathology and potentially fatal exacerbations. (192, 193) Human COPD samples allow only for longitudinal sampling and present with extensive variability and heterogeneity, both based on environmental and genetic factors, leading to a need for animal-based models to further understand COPD progression induced by chronic CS exposure. These models do exist and are widely studied to understand the CS-mediated disease pathogenesis. However, further complications arise, as animal models such as rodent or small animal models of CS exposure do not recapitulate all aspects of human COPD progression, specifically in bronchial airway remodeling and therefore, we recently performed a study using the cynomologus macaque model of chronic CS exposure. This study allowed for very valuable data

and recapitulation of the human COPD progression and symptoms, as they were exposed for 27-weeks to mainstream CS. These animals were found to show reduced lung functions and chronic bronchitis similar to that observed in COPD smokers compared to control macaques kept in room air. Thus, we were able to employ the archived lung tissues from these well-characterized macaques to establish the correlation of CS-induced airway inflammatory responses with airway lncRNA expression. Due to the labor- and time-intensive nature of these large animal model studies, we are currently analyzing whether there is a murine homolog of *LASI* lncRNA or there is any other airway-specific lncRNA of rodent airways involved in CS-mediated inflammation. Accordingly, future studies will be planned to test the in vivo efficacy of targeting lncRNAs in suppressing CS-mediated airway remodeling and mucoinflammatory responses.

Airway mucus hypersecretion is the hallmark of COPD pathogenesis, enabling the compounding cascade of inflammation, ROS generation, and airborne pathogen retention in airways due to compromised mucociliary clearance, distal airway occlusion and inability to effectively clear the airways (22). Airway mucins MUC5AC and MUC5B are the predominant gel-forming mucins in COPD, and CS exposure and frequent bacterial or viral infection synergistically amplify MUC5AC levels. (104-108) Several other inflammatory biomarkers have been implicated with COPD and smoke-associated exacerbations. (194) Among the most prominent factors are the ICAM-family proteins, specifically ICAM-1, and an innate inflammatory cytokine, IL-6 which have shown strong association to decreased lung function in COPD, both in active and former smokers with varying

degree of severity. (195) Airway epithelial cells play a vital role in the secretion of ICAM-1 and IL-6, and could serve as drivers of the chronic changes observed in COPD. (68)

Till date, thousands of lncRNAs have been discovered, however, studies on the functional significance of the changes in lncRNA expression are lacking. The structural flexibility and 3D-conformation enables lncRNAs to interact with large number of cellular macromolecules including proteins, DNA, RNA, and chromatin to modulate epigenetic and transcriptomic changes and associated cellular responses. (179) Large number of lncRNAs have been implicated in pathology, including chronic pulmonary conditions, CS-related immune responses, and inflammatory regulation. (167, 180, 181) LncRNA-mediated regulation of innate immune responses is potentially central for the establishment of host-beneficial trained immunity (196), but these responses could be dysregulated in case of chronic pulmonary disease resulting in hyperactive inflammatory responses. Microarray analysis has shown over 39,000 lncRNAs are differentially expressed in COPD patients, stratified by smoking status. (140) Numerous lncRNAs have been experimentally characterized and shown to affect the inflammatory responses of airway epithelium via epigenetic and/or transcriptomic mechanisms and induce an accelerated aging of lung epithelium associated with COPD. (167)

Goblet cell hyperplasia is predominant in COPD progression, in fact 33% of distal conducting airway epithelium is comprised of goblet cells in severe COPD lungs, versus less than 5% observed in the distal airways of non-COPD lungs. (197) In this report, we have also reported a disease severity associated increase

in goblet cell hyperplasia in COPD tissue samples, with a 2.1- to 3.0-fold increase in goblet cell numbers per mm BL in mild and severe COPD tissues, respectively. This suggests accurate modeling of molecular level changes in COPD epithelium. We found that the lncRNA *LASI* correlates with disease severity, while other lncRNAs do not, suggesting a potential regulatory role which we further explored using an in vitro COPD model. Our panel of lncRNAs showed the *NEAT1*, *MALAT1* and *WAKMAR2* were not upregulated following CSE- treatments. Interestingly, Hu and colleagues (2020) reported increase expression of MALAT1 in COPD lung tissue specimens, however we found that there was no change in MALAT1 expression in correlation with disease severity. (181) However, to evaluate whether the effects observed were specifically driven by CS exposure, we relied on the archived tissue samples from C. macaques that were exposed to CS chronically and the data strongly suggests that long-term CS exposure is a driving factor behind the airway pathology observed. Importantly, we used primary HBECs from controls with no COPD and with COPD i.e., NHBEs and CHBEs for in-vitro validation of our ex-vivo findings. Recent reports have shown that the pathologic changes in epithelial histology, goblet cell numbers, and mucus hypersecretion are preserved in differentiated COPD subject-derived lung epithelial cells in ALI culture settings, and transcriptomic analysis showed over 200 differentially expressed transcripts. (198) The ciliary beating impairment has also been found to be reflected in differentiated CHBEs versus NHBEs. Here, we report a significant higher baseline expression, of MUC5AC, ICAM-1, and IL-6 in CHBEs, as compared to NHBEs without any treatment or stimulation. Thus, the in-vitro model

does recapitulate the differences observed in COPD subjects thus suggesting of epigenetic and transcriptomic transformations that are preserved in bronchial epithelial cells. Further, CHBEs also showed a significantly increased baseline levels of *LASI* lncRNA as compared to NHBEs. In addition, there was an increased expression of *ICR*, *NEAT1*, *MALAT1*, and *WAKMAR2* lncRNAs in cultured CHBEs, however, we did not observe any significant change in these lncRNAs in lung tissue homogenates of COPD subjects. This suggests that these lncRNAs may respond in cell/tissue-context manner, and the epithelial expression of these lncRNA may not play a direct role in COPD pathogenesis.

Also of note, we found blocking *LASI* lncRNA expression in CHBEs led to a suppressed induction of MUC5AC mucin expression with no change in transcription factor SPDEF expression, suggesting that CSE-mediated mucin expression may not directly involve the previously observed *LASI* lncRNA-and SPDEF-mediated mucin upregulation observed in allergic asthma studies. (2)

Interestingly, this implies that NOTCH3 may not be involved in CS-mediated changes in airway epithelial cells. CSE exposure induces SPDEF via NOTCH3 signaling, suggesting that *LASI*-mediated dysregulation is not dependent on NOTCH3, and further suggests a need to evaluate the role of *LASI* lncRNA on other signaling pathways involved in CS-mediated mucoinflammatory responses such as EGFR-mediated inflammation. (199) EGFR activation is observed both upon cigarette smoke exposure as well as exposure to increased levels of ROS, and EGFR-mediated pathways can have extensive downstream effects. EGFR-mediated signaling is likely to be the predominant driver of airway remodeling and

mucus cell hyperplasia in CS-induced COPD pathogenesis, and this pathway may not involve SPDEF-mediated mucous responses. (2, 38) Recently, the role of TGF-β-mediated regulation of the SMAD signaling pathway has been elucidated as a potential crucial pathway of mucus cell hyperplasia regulation as well as suggested to be a valuable potential therapeutic avenue for COPD. (54)

In terms of molecular regulation of other inflammatory factor expression, lncRNAs are shown to act as molecular sponges/scaffolds for miRNAs as reported recently in COPD. (200-202) For example, lncRNA TUG1 promotes airway remodeling via suppressing the miR-145-5p in CS-induced COPD models. The lncRNA NNT-AS1 was shown to regulate COPD associated airway cell proliferation/cell death, inflammation, and remodeling via the miR-582-5p and FBXO11 pathways. Interestingly, high levels of IL-6 and lncRNA IL6-AS1 were reported in COPD subjects with concurrent upregulation of miR-149-5p and early B-cell factor 1. Similar studies are underway to determine possible *LASI* lncRNA binding partners that contribute to airway inflammation and mucin expression.

LncRNAs modulate gene expression at multiple levels to alter the cell functions/responses. They are known to modulate chromatin structure or bind to directly to DNA. They can also bind to and suppress the expression of miRNAs or pre-miRNAs. (179, 203) LncRNAs can directly enhance or suppress the expression of many mRNAs or functional transcripts. In our studies, knockdown of *LASI* lncRNA led to a suppressed expression of CSE-induced *ICAM-1* and *IL-6* mRNAs suggesting that there is no direct interaction between *LASI* lncRNA and *ICAM-1* or *IL-6* mRNAs. Instead, *LASI* lncRNA may be indirectly affecting the

transcription of ICAM-1 and IL-6, whereby *LASI* lncRNA may be regulating the other intermediary immunoregulatory elements such as miRNAs or promoters upstream of ICAM-1 and IL-6. Accordingly, our data posit that *LASI* lncRNA may not be directly interacting with ICAM-1 protein, mRNA, or pre-mRNA, but experimental validation are needed. In a separate study we have observed that silencing ICAM-1 expression does not affect the *LASI* lncRNA levels (data not shown), thus implicating that the expression levels of these transcripts are driven independently via possible mutually exclusive transcriptional regulation of the opposite strands. The data further suggests that at the transcription level, a direct induction of *LASI* lncRNA by CSE treatment may be one of the drivers for the COPD associated mucoinflammatory responses. Furthermore, we observed that *LASI* lncRNA was expressed in perinuclear region and cytosolic regions of bronchial airway epithelial cells of both macaques and human tissues. RNA-interference based silencing works primarily in the cytosolic region and even with only 37.5% suppression of *LASI* lncRNA levels, we observed a highly significant reduction in CSE- induced MUC5AC, ICAM-1, and IL-6 expression. This data does suggest that cytosolic LASI lncRNA may be important mediator of mucoinflammatory response, but further cell fractionation studies are needed to determine the subcellular location specific role of *LASI* lncRNAs in driving the CSE-treatment and COPD associated inflammatory responses.

The present study has several limitations as outlined here and should be strongly considered for drawing the inferences. Firstly, the archived lung tissues from the large animal model study are from female macaques only as human

epidemiological studies suggest that female smokers how higher prevalence of COPD than males but the data presented here should be interpreted accordingly. Secondly, human lung tissue samples provide by LTRC (NIH), but the COPD patient cohort data collection relies on self-reported smoking history and lacks accuracy. Thirdly, the in-vitro modeling studies used NHBEs and CHBEs from three separate donors only and are from a commercial supplier with no information provided on the race, age, gender, or smoking history. Moreover, the in-vitro modeling used bronchial airway epithelial cells only and responses in other epithelial and submucosal cells are not investigated that could drive smoke- and COPD-associated airway remodeling. Additionally, this study is focused on *LASI* lncRNA only, which may act synergistically with additional lncRNAs, specifically with *ICR* lncRNA. Furthermore, the studies reported here used acute model of CS exposure using CS extract instead of direct mainstream smoke exposure. However, with data presented from animal model of CS exposure, and from COPD tissue and airway epithelial cells, this study does corroborate the strong association of *LASI* lncRNA with CS-induced transcriptional modulation of airway mucoinflammatory responses.

In conclusion, this study elucidates *LASI* lncRNA as a novel regulator of CSE-induced and COPD-associated airway epithelial dysregulation and further suggests that targeting *LASI* lncRNA expression could present a novel therapeutic intervention modality to treat COPD phenotypes of upper airways. Specifically, the currently available therapies have limited success in treating COPD pathophysiologies creating an unmet need in discovery of novel therapeutic

avenues (204-206). Recent epidemiological and pathological studies have shown that mucus hypersecretion is a prime target of COPD treatment avenues. (207) Thus, airway epithelial expressed *LASI* lncRNA may provide additional novel method of controlling mucous responses specifically when noncoding RNA-based therapeutics are shown to be promising treatment modalities. (208) The present study also suggests that the lncRNA *ICR* may play a similarly important role in CHBE dysregulation and requires further investigation. Future experiments will investigate the mechanism of action of *LASI* lncRNA to identify its binding partners and potential interactions that regulate airway innate immune responses. It is also likely that the mechanisms underlying *LASI* lncRNA effects are complex and may involve numerous downstream elements. One of the primary reasons that lncRNAs such as *LASI* are valuable is the fact they are shown in literature to be able to exert their effect via multiple effector elements and mediate the general cellular response. This may provide unique opportunities to address chronic diseases such as COPD, as compared to therapies that have already been attempted, this may allow us to moderate the general cellular responses, in contrast to significantly knocking down individual inflammatory or mucus-secretory elements, thus leading to unacceptable side effects and consequences. This study is the first step in understanding the roles of lncRNA *LASI* and its potential value for treating diseases such as COPD, and further understanding its role, as well as the roles of other lncRNA molecules that may interact in conjunction with *LASI* or independently offers more pathways for future therapeutic approach.

Chapter 4: Immunomodulatory LncRNA LASI augments SARS-CoV-2 infection-associated airway mucoinflammatory phenotype

Data Included in this chapter was originally published by CellPress publishing group, “Immunomodulatory LncRNA on Antisense Strand of ICAM-1 Augments the SARS-CoV-2 Infection Associated Airway Mucoinflammatory Phenotype”, 2022, DOI: 10.1016/j.isci.2022.104685.

Chapter 4: Introduction

I. The current state of SARS-CoV-2

Vaccination efforts have helped greatly reduce the COVID-19 spread, although variants arising from genomic mutations pose a significant risk even among vaccinated people. (209-211) SARS-CoV-2 gains entry via the upper respiratory mucosa and any host factor dysregulations occurring during this interaction can result in pulmonary and/or extrapulmonary complications. (212-215) In the first week of infection viral shedding and replication are relatively predominant in upper respiratory tract. (216) During these events, the virus evades host mucosal and innate immune responses allowing it to move towards the lower respiratory tract and eventually to systemic invasion. (217) As such, limiting shedding and viral replication in the upper respiratory tract can help block disease progression and, importantly, the expression of viral receptors can be regulated by various immunomodulators. That said, besides being the protective barrier and a competent airway lumen clearance mechanism, airway mucins typically moderate the mucosal immune responses. (218) During SARS-CoV-2 infection, however, induced inflammatory factors drive airway tissue remodeling, and severe

inflammation can cause mucus hyperexpression potentially leading to acute respiratory distress syndrome (ARDS).

II. LncRNAs and SARS-CoV-2 interaction

Analyzing host-viral interactions is vital for understanding viral pathogenesis. Several notable protein interactions necessary for SARS-CoV-2 infection and/or progression are now well documented; specific roles for the host lncRNAs during SARS-CoV-2 infection remain elusive. Roles for lncRNAs in regulating virtually every cellular function have now been reported including moderating the immune response of infected host cells as well as regulating the genomic packing and replication of several viruses. (166, 167, 203) LncRNAs play a vital role in regulating the innate immune responses and recent studies have shown that specific lncRNAs are differentially expressed during host-pathogen interactions following viral infection. (219-222) Although a few reports have examined lncRNA expression profiles for stratifying the COVID-19 disease severity and associated immune dysfunction, (223-226) studies examining roles for respiratory epithelia specific lncRNAs in SARS-CoV-2 infection are far more limited. (221, 222) Our recent studies identified a novel epithelial lncRNA *LASI* that is differentially expressed during the mucus hypersecretory response. (2) Here, we have assessed the acute mucoinflammatory response, i.e., the excessive mucus expression and inflammation, and other immunomodulatory factors and lncRNAs in a 3D airway tissue model of acute SARS-CoV-2 infection and COVID-19 patient nasopharyngeal samples to gain novel insights into early innate responses of human respiratory cells.

Chapter 4: Methods

I. Datasets and bioinformatics

Raw RNA sequencing datasets were retrieved from the sequence read archive (SRA) database under accession no. PRJNA730941. Single-end FASTQ files for all COVID-19 patients and healthy controls were obtained using the SRA toolkit version 2.11.2 that was reported recently. (227) FASTQ files were converted to FASTA using seqtk (https://github.com/lh3/seqtk). Reads were aligned to a database consisting of select cDNA sequences (obtained from Ensembl Biomart) using BLAST+ (version 2.11.0). Alignments were required to uniquely map to a single cDNA and bear >94% identity over 100 base pairs. Reads aligning to individual genes were enumerated and gene expression calculated in Reads Per Million (RPM).

II. COVID-19 patient samples

COVID-19 patient nasal swab samples were either obtained from the University of Miami Biobank facility or iSpecimen Inc. (Lexington, MA). Frozen cell pellets were processed for total RNA isolation and formalin-fixed cells were spread onto the slides for downstream analysis.

III. Airway epithelial cell model of SARS-CoV-2 infection

Studies involving SARS-CoV-2 virus infection were conducted at the University of Nebraska Medical Center BSL-3 high containment core facility. SARS-CoV-2 isolate USA-WI1/2020 (BEI; cat# NR-52384, B.1.1.7) was passaged in Vero-STA-1 knockout cells and viral titer was determined using plaque assay

(228, 229). Primary human airway epithelial cells were purchased either from the Marsico Lung Institute Tissue Core (University of North Carolina) or from MatTek Incorp (EpiAirway™, MA). Airway epithelial cells were infected with 1 MOI of SARS-CoV-2 inoculum prepared in culture media. For 3D ALI cultured cells, 200 µl was added to the apical surface and 1 ml was added to the basal side. Infected transwells were incubated for 1 h at 37°C in 5% CO_2 incubator and the plates were gently mixed every 15 m. After 30 m, apical inoculum was removed and added to the basal media and after additional 30 m total virus inoculum was removed. Transwells were washed thoroughly with PBS and fresh media was added basally. Apical washes and basolateral medium culture supernatants were collected at 1, 4, 24, and 48 h post-infection (hpi) and stored at -80ºC for downstream analysis, viral titration, and cytokine analysis. Cells were either lyzed in RLT buffer (RNeasy, Qiagen Inc) with 143 mM 2-ME for total RNA isolation or were fixed with 4% PFA (paraformaldehyde).

IV. Immunohistochemistry and immunocytochemistry

Tissue sections or fixed cells were washed in 0.05% V Brij-35 in PBS+. Antigen retrieval was performed using 10 mM citrate buffer (pH 6.0). Blocking solution (1% NDS, 3% BSA, 1% gel, 0.2% TX-1000 and 0.2% saponin in PBS+) incubation was conducted for 1 hour at room temperature followed by incubation at 4°C overnight with primary antibodies against mucin MUC5AC (Millipore Sigma) and pan-cytokeratin (pan-CK, Santa Cruz Biotechnology). Appropriate DyLight® fluorescently-conjugated secondary antibodies (Abcam) were used, and sections

were incubated for 1 hour at room temperature. Sections were mounted with DAPI-containing Fluormount-G. Immunofluorescent images were captured using the Keyence BZ-X700 microscope and image analysis was conducted using the ImageJ software (NIH). Mean fluorescence intensity per number of epithelial cells was used to compare mucin MUC5AC expression levels. Pan-CK was used as a confirmation of epithelial cell identity. Tissue sections were deparaffinized and hydrated in graded ethanol and deionized water. Histochemical staining was conducted with Alcian blue-period acid Schiff (AB-PAS) or AB followed by hematoxylin and eosin (H&E) or AB-H&E staining as described (102). The mucus secretory cells (goblet/mucous cells) were quantified as a total number of AB-PAS+ or just AB+ cells per mm basal lamina for each image. For immunostaining analyses, cell cultures grown in Nunc™ Lab-Tek™ II 8-chamber slide system were washed using 0.05% v Brij-35 in PBS(+) and immunostained as described previously (2). Cells were stained with antibodies to mucin MUC5AC (Millipore, Inc.), ICAM-1 (Cell Signaling Technology, Inc.) and pan cytokeratin (Cell Signaling Technology, Inc.). Immunostained cells were detected using respective secondary fluor-conjugated antibodies (Thermo Fisher Scientific, Inc) and mounted with DAPI-containing mounting media. Immunofluorescent images were captured using a Keyence BZ-X710 all-in-one fluorescence microscopy system and were analyzed using Keyence analysis software and Image J software (National Institutes of Health). Groups of NHBEs and CHBEs stained with MUC5AC, or ICAM-1 were analyzed separately, with exposure adjusted for each treatment. Once exposure was adjusted for MUC5AC and ICAM-1 groups, positive cells were

counted as a percentage of the total cell number. The raw percentages were calculated as the fold-change compared to non-treated (NT) NHBE group.

V. Real-time quantitative PCR (RT-qPCR)

For all RT-qPCR analysis, total RNA extraction was performed using the RNeasy Mini kit (Qiagen) according to manufacturer's instructions. Briefly, tissues were resected and collected tissue was measured to be under 30 mg. Tissue lysis was performed using TissueLyser® LT (Qiagen) at 50 Hz for 3 minutes. RNA concentration was quantified using the Synergy HTX reader (BioTek, VT). Complementary (c)DNA was synthesized using the iScript Advanced cDNA synthesis kit (Bio-Rad), per manufacturer's instructions or by using the Applied Biosystems™ High-Capacity RNA-to-cDNA™ Kit per the manufacturer's instructions. For qRT-PCR, FAM-based and SYBR Green primers were used. The *LASI, ICR, WAKMAR-2, NEAT1, MALAT1* lncRNAs and *MUC5AC* and *SPDEF* mRNA levels were quantified using FAM-based primer/probe sets and TaqMan gene expression kit or the SsoFast qPCR master mix (Applied Biosystems, Thermo Fisher). *ICAM-1*, *IL6*, and *CXCL8* mRNA levels were quantified using SYBR Green-based primers and the iTaq master mix (Bio-Rad). qRT-PCR was conducted using the Bio-Rad CFX Real-Time PCR detection system. Quantification and analysis of the results was performed using the delta-delta (ΔΔ)Ct method and U6 noncoding small nuclear RNA (snRNA), glyceraldehyde-3-phosphate dehydrogenase (GAPDH) or beta actin were used as reference genes for lncRNA expression levels expression levels as described recently. (101) To

detect the miRNA levels, cDNA was synthesized from isolated total RNA with a TaqMan® Advanced miRNA cDNA Synthesis Kit (Applied Biosystems, ThermoFisher Inc.). TaqMan® Advanced miRNA assays for *let-7b-5p*, *hsa-miR-150-5p*, *hsa-miR-197-3p*, *hsa-miR-200a-5p*, *hsa-miR-125b-1-3p* and *hsa-miR-4488* were obtained from Applied Biosystems (ThermoFisher Inc.), and the expression levels were quantified by qRT-PCR using TaqMan® Fast Advanced Master Mix (ThermoFisher Inc.). Relative quantities were calculated by normalizing data to *U6 snRNA* (Applied Biosystems, ThermoFisher Inc.).

VI. RNA fluorescence in situ hybridization (RNA-FISH)

The RNAScope® 2.5 HD duplex assay and reagent kit (Advanced Cell Diagnostics, Biotechne) was used for RNA FISH as per the manufacturer's instructions. A double-Z probe set against *LASI* was designed containing 20 dual probes targeting various segments across the *LASI* lncRNA. RNA FISH was conducted on paraffin-embedded 5 µm tissue sections obtained from the LTRC of the NIH. Deparaffinization was conducted in consecutive xylene, graded ethanol, and deionized water. Pretreatment was conducted with hydrogen peroxide solution and the RNAScope® target retrieval buffer and protease plus solutions were used to exposure the antigen. Probe hybridization was conducted for 2 hours at 40°C in the HybEZ® II oven. The signal was amplified using the Amp1, Amp2, Amp3 and the HRP probe at 40°C in the HybEZ® II oven. The signal was detected using the tyramide signal amplification (TSA) reaction with an Alexa fluor labeled TSA kit (Perkin Elmer). Sections were then processed for immunohistochemistry or directly

mounted with the 4',6-diamidino-2-phenylindole (DAPI)-containing Fluormount-G (Southern Biotechnology). Images were captured using the Keyence BZ-X700 structured illumination fluorescent microscope. Analysis was conducted with the Keyence BZ-X analysis software and using the ImageJ software (NIH). RNA FISH quantification was conducted according the RNAScope® histo (H)-score methodology. In each image, probe signals were counted for each cell, both in the nuclear and cytosolic region and assigned to appropriate bins: bin 0 (no signals), bin 1 (1-3 signals/cell), bin 2 (4-9 signals/cell), bin 3 (10-15 signals/cell) and bin 4 (>15 signals/cell). The H-score was calculated as follows: H-score was the sum of each bin multiplied by the percentage of cells that fall into that bin. H-score = (0 x % cells in bin 0) + (1 x % cells in bin 1) + (2 x % cells in bin 2) + (3 x % cells in bin 3) + (4 x % cells in bin 4). Final H-scores ranged from 0 to 400 per group.

VII. Enzyme-linked immunosorbent assays (ELISAs)

Culture media and apical cell culture washes from NHBEs and CHBEs differentiated in 3D ALI culture for 28 days was collected prior to CSE treatment and every two days after treatment. Final apical washes and culture media supernatant were collected prior to the termination of the experiment and was either stored at -80°C or processed for analysis. The protein levels of MUC5AC, ICAM-1, and IL-6 were determined using human ELISA kits against MUC5AC (MyBioSource Inc., San Diego, CA), ICAM-1 (LifeSpan Biosciences Inc., Seattle, WA), and IL-6 (BioLegend Inc., San Diego, CA), respectively, as per manufacturers' instructions.

VIII. Modeling of potential interaction site prediction and system preparation

The IntaRNA 2.0 webserver (230) was used to predict potential RNA-RNA binding sites between the SARS-CoV-2 spike viral RNA and *LASI* lncRNA. The SARS-CoV-2 vRNA sequence 1227-1238 nucleotide (nt) was predicted to bind *LASI* lncRNA sequence at 635-646 nt. To generate a 3D structure of SARS-CoV-2 vRNA duplexed with the interacting sequence of *LASI* lncRNA, SARS-CoV-2 sequence from 1198-1268 nt was used. To allow *LASI* lncRNA nucleotides to base-pair with SARS-CoV-2 vRNA, we concatenated *LASI* lncRNA sequence 635-646 nt next to the SARS-CoV-2 vRNA 1227-1238. This tandem sequence was then used to predict the 3D structure using RNAComposer (231) webserver, with the secondary structure information provided by RNAfold. (232) Finally, *LASI* lncRNA segment was renamed as a different chain (chain B), with remaining SARS-CoV-2 S vRNA sequence renumbered (chain A). Resulting complex is energy minimized, equilibrated, and further relaxed with molecular dynamics (MD) simulations.

IX. System setup and molecular dynamics simulations

The CHARMM-GUI (233) Solution Builder tool was used to prepare the system for MD simulations. The solvated system with a physiological salt concentration of 0.15 M KCl contained a total of 87,000 atoms. All-atom MD simulations were performed using the CUDA version of NAMD 2.14 (234) with the Charmm36m force field (235). Briefly, the structure was minimized for 10,000 steps

with the steepest descent method and equilibrated for 125,000 steps with 2 fs timestep under NVT (constant volume and temperature) conditions. The production run was performed under NPT (constant pressure and temperature) conditions at a temperature of 303.15 K and a pressure of 1 bar. The production run consisted of 2 fs timesteps and a total of 50M steps collecting a 100-ns trajectory. Visualization and analysis of the trajectories were performed with visual molecular dynamics (VMD). (236)

X. RNA interference-based lncRNA silencing

The 3D cultured cells were transfected with siRNA specific to LASI (siLASI) or control siRNAs (siCTRL) using X2 (Mirus biotechnologies) transfection reagent (custom made by IDT technologies Inc.) as per manufacturer's instructions and as described recently. (2) After 48h, cells were infected with 1 MOI of SARS-CoV-2 clinical isolate, and cells, apical wash and the basal media supernatant were analyzed at 48 hpi.

XI. Small RNA sequencing analysis

Small RNA-seq was performed by Novogene inc. using an Illumina HiSeq v4 genome sequencer with 20M SE50 Reads. RNA was isolated from the 3D cultured airway cells infected with SARS-CoV-2 and transfected with siLASI to block LASI lncRNA expression. Briefly, Novogene employed the NEB-Next Multiplex Small RNA Library Prep Set for Illumina (NEB) coupled with automated agarose gel size selection (30 to 200 nt) using the Pipin Prep Instrument (Sage Science) for small RNA library preparation. Raw RNA sequencing datasets were

retrieved, and FASTQ files were converted to FASTA using seqtk (https://github.com/lh3/seqtk). Adapter sequences were removed with cutadapt, and reads were aligned to the GRCh38.P10 reference genome using BLAST+ (version 2.11.0). (237) Alignments were required to uniquely map to a single position and bear 100% identity over at least 17 base pairs. Reads aligning to individual microRNAs were enumerated and gene expression calculated in Reads Per Million (RPM). Heat maps and unsupervised hierarchical clustering were generated using Heatmapper. (238)

XII. Statistical analysis

Mean and standard error for replicates of the experiments were calculated, plotted, and analyzed using GraphPad Prism v9.0 (GraphPad Software Inc., San Diego, CA). Grouped results were analyzed using a one-way analysis of variance (ANOVA) with multiple comparisons, and student's t-test was used for data analysis between two groups. Data with FDR (false discovery rate) adjusted *p*-value threshold of ≤0.05 are considered as significantly relevant using Benjamini-Hochberg correction.

Chapter 4: Results

I. SARS-CoV-2 infected individuals show induced airway mucus and inflammatory responses and increased LASI lncRNA expression

The mucosal immune response of the upper respiratory tract plays a critical role in viral entry, replication and dissemination of systemic infection, and expiratory shedding. Several innate immunoregulatory transcripts of both protein-coding and non-coding RNAs are implicated in the SARS-CoV-2 infection and host antiviral response, yet very few validated roles of lncRNAs have been reported. Therefore, we performed an analysis of the airway immune response in publicly available RNA sequencing datasets obtained from SARS-CoV-2-positive (CoV-2^{+}) patients and uninfected (CoV-2^{-}) controls (Geneset Accession: PRJNA730941). (227) Our initial analysis examined RNA-seq files obtained from nasal swab samples of 26 CoV-2^{+} and 8 CoV-2^{-} controls. We specifically analyzed for the lung mucoinflammatory response genes and associated lncRNAs, and the expression levels of *IL-6*, *ICAM-1*, and *CXCL-8* mRNAs were around ten-, six-, and five-fold higher in CoV-2^{+} individuals, respectively, compared to CoV-2^{-} controls (**Figure 26A**). Although roles for airway mucins in innate antiviral immunity are well documented (25, 239), SARS-CoV-2 infection-associated mucin signatures have not been thoroughly evaluated to date. (240)

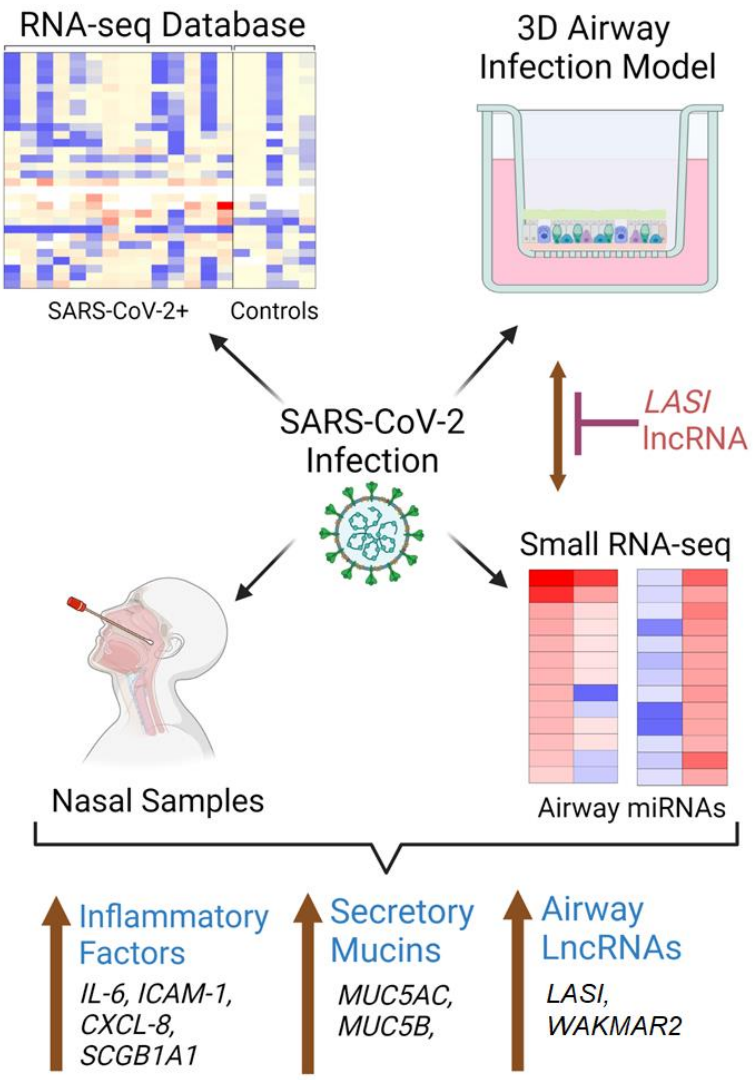

Figure 25. Experimental study design - Immunomodulatory LncRNA LASI Augments SARS-CoV-2 Infection-Associated Airway Mucoinflammatory Phenotype. Created with BioRender.com. Original source (1).

Notably, the airway secretory mucin *MUC5AC* mRNA levels in the present cohort were four-fold higher in CoV-2^{+} individuals than in CoV-2^{-} controls (**Figure 26B**). The expression levels of host factors facilitating the viral entry, such as *ACE2, NRP1, DPP4, IFITM,* and *DDX1* as well the Spike protein processing cellular proteases like *TMRPSS2, Furin, CTSB, CTSL* and *TMPRSS11D* showed

no significant change between CoV-2 positive *vs.* negative individuals (data not shown).

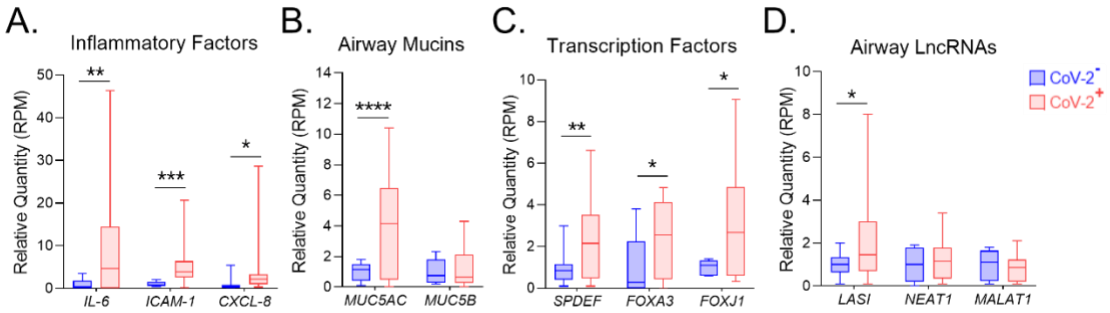

Figure 26. Expression levels of transcripts encoding inflammatory factors, airway secretory mucins, associated transcription factors, and select lncRNAs in the RNA-seq database of nasopharyngeal swabs of SARS-CoV-2 positive individuals. Relative expression of **(A.)** airway inflammatory factors IL-6, ICAM-1, and CXCL-8 mRNAs; **(B.)** airway mucins MUC5AC and MUC5B mRNAs; **(C.)** transcription factors SPDEF, FOXA3, and FOXJ1 mRNAs; and **(D.)** lncRNAs LASI, NEAT1, and MALAT1 in SARS-CoV-2 positive (CoV-2^{+}) individuals compared to SARS-CoV-2 negative (CoV-2^{-}) control individuals. The expression levels were calculated from the transcript reads per million (RPM) RNA-seq data of nasopharyngeal swabs from CoV-2^{+} subjects (n=26) compared to CoV-2^{-} control subjects (n=8) as reported recently *(227)*. (Data shown as violin plots with individual data points, medians, and quartiles; *p<0.05; **p<0.01; ***p<0.001; ****p<0.0001 by Student's t-test). Dr. G. Borchert was the major contributor for this data. Original source (1).

We have recently characterized airway lncRNAs that play essential roles in innate immune responses of respiratory mucosa (2, 167) and propose that these immunomodulatory lncRNAs may be dysregulated during SARS-CoV-2 infection and thus drive the COVID-19-associated respiratory comorbidities. Among the immunomodulatory lncRNAs analyzed (**Figure 26D**), we found that a lncRNA antisense to ICAM-1 or *LASI* (2) showed two-fold higher expression in CoV-2^{+} individuals compared to CoV-2^{-} controls. In contrast, expression levels of *NEAT1* or Nuclear Enriched Abundant Transcript-1 (222, 241, 242) and *MALAT1* or Metastasis Associated Lung Adenocarcinoma Transcript-1 (243) lncRNAs

exhibited no significant change (**Figure 26D**). Thus, our analyses indicate that compared to CoV-2$^-$ controls, the airway mucoinflammatory gene signature are strongly correlated with induced *LASI* lncRNA expression among CoV-2$^+$ individuals.

II. COVID-19 positive individuals with higher viral load show increased mucoinflammatory response

Table 3. Demographics of COVID-19 patients whose nasopharyngeal swab samples were analyzed. Medical history was available for twelve patients. Original source (1).

	Lo-VL	Hi-VL	*P-value*
Subjects	10 (7)	10 (5)	
Sex (M/F)	6M/4F	7M/3F	
Age (Y)	61.5±4.0	63.1±3.8	*0.8163*
SARS-CoV-2 N1 vRNA (C_T)	35.5±0.7	25.9±1.3	*<0.0001*
Hospitalization	7	5	
Hypertension	5	5	
Diabetes	4	0	
Infectious Disease	1	2	
Pneumonia	5	5	
Oxygen Supplementation (>6L O_2)	1	5	
ICU	3	5	
ARDS	3	5	
Obesity	5	3	

Recent epidemiological and clinical studies suggest that there is no difference in SARS-CoV-2 viral load between symptomatic and asymptomatic CoV-2^{+} individuals; however, disease severity and mortality rate among symptomatic individuals is directly correlated with airway viral load. (242, 244, 245) Therefore, to assess the correlation of viral load with mucoinflammatory responses and associated lncRNAs, we examined the nasopharyngeal swab samples procured locally from twenty CoV-2+ individuals (**Table 3**). Viral load in each subject was determined by qRT-PCR for SARS-CoV-2 N1 nucleocapsid viral RNA (vRNA) levels and were assigned as low-viral load (Lo-VL) or high-viral load (Hi-VL) CoV-2^{+} samples based on the cycle threshold (C_T) values of >30 or <30, respectively (**Figure 27A**). Applying this threshold, 10 subjects were characterized as Hi-VL (C_T =25.9±1.3; 7M/3F, 63.1±3.8 y) and 10 as Lo-VL (C_T=35.5±0.7; 6M/4F, 61.5±4.0 y) with Hi-VL subjects exhibiting 100-fold higher CoV-2 vRNA levels than Lo-VL subjects (**Figure 27A**). Hi-VL samples exhibited ~1.5-fold higher *IL-6* (**Figure 27B**) and *ICAM-1* (**Figure 27C**) mRNAs compared to Lo-VL samples. And when the expression levels were analyzed in individual samples, the expression levels of *IL-6* (**Figure 27B**) and *ICAM-1* (**Figure 27C**) mRNAs significantly correlated with CoV-2 N1 viral RNA levels, showing distinct clustering of Hi-VL and Lo-VL subjects. In agreement with RNA-seq database analyses (**Figure 26**), all of the nasal swab samples in our study cohort showed upregulated mucin expression with Hi-VL samples exhibiting robust ~10-fold higher *MUC5AC* (**Figure 27D**) and 4-fold higher *MUC5B* (**Figure 27E**) mucin mRNA levels. *SPDEF* mRNA expression

was also increased by ~5-fold in Hi-VL subjects (**Figure 27F**), and surprisingly, *SCGB1A1* expression was ~4-fold higher in Hi-VL subjects (data not shown).

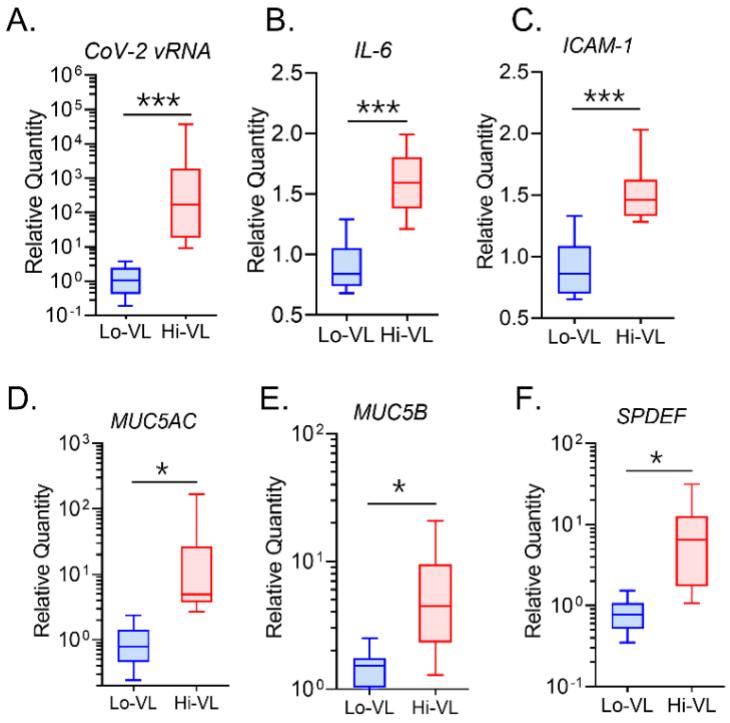

Figure 27. COVID-19 positive individuals with high nasopharyngeal viral load show increased mucoinflammatory phenotype compared to low viral load individuals. Total RNA from nasopharyngeal swab samples of COVID-19 positive individuals (n=20) were analyzed. Based on the SARS-CoV-2 nucleocapsid viral RNA expression, the individuals with high viral load (Hi-VL) had average C_T values of 25.9±1.3 (n=10), whereas those with low viral load (Lo-VL) had average C_T values of 35.5±0.7 (n=10). Relative mRNA expression of: **(A.)** SARS-CoV-2 viral RNA (CoV-2 vRNA); innate inflammatory factors, **(B.)** IL-6, and **(C.)** ICAM-1; Airway mucins **(D.)** MUC5AC, and **(E.)** MUC5B; and **(F.)** mucin regulatory transcriptional factor SPDEF in Hi-VL compared to Lo-VL patient swab samples. (Data shown as box and whisker plots with minimum to maximum range; n=10/gp; *p<0.05; **p<0.01; ***p<0.001 by Student's t-test). Dr. D. Devadoss was the major contributor for this data. Original source (1).

Taken together, these data do indicate that SARS-CoV-2 viral load dictates the extent of airway mucin and associated inflammatory factor expression among COVID-19-positive individuals.

III. Innate immunomodulatory lncRNAs are associated with SARS-CoV-2 viral load

Next, we analyzed the expression levels of select airway lncRNAs in our cohort. We found that compared to the Lo-VL samples, the expression levels of lncRNA *LASI* (**Figure 28A**), *NEAT1* (**Figure 28B**), and a wound and keratinocyte migration-associated lncRNA 2 (*WAKMAR2*) (**Figure 28D**) were all significantly upregulated in Hi-VL samples whereas lncRNA *MALAT1* levels were not significantly altered (**Figure 28C**). These data suggest that *LASI* lncRNA which plays pivotal role in airway innate responses (2), may be involved in SARS-CoV-2-associated airway inflammation. We next performed an RNA-FISH analysis to examine *LASI* lncRNA expression in airway epithelial cells of nasal swab samples and cells were also labelled for SARS-CoV-2 N1 viral RNA (vRNA). Compared to Lo-VL samples, SARS-CoV-2 N1 *vRNA* and *LASI* transcripts were enriched in perinuclear and cytosolic regions with increased expression of *LASI* in Hi-VL subjects (**Figure 29E**). In agreement with qRT-PCR analyses (**Figure 28A**), the H-score values that denote RNA expression per cell, as described recently (2), were 2.7- and 2.4-fold higher for *vRNA* and *LASI* lncRNA, respectively, in Hi-VL compared to Lo-VL samples (**Figure 29G**). The protein expression of MUC5AC mucin as determined by immunopositivity was ~16-fold higher in Hi-VL vs Lo-VL samples (**Figure 29F-29H**).

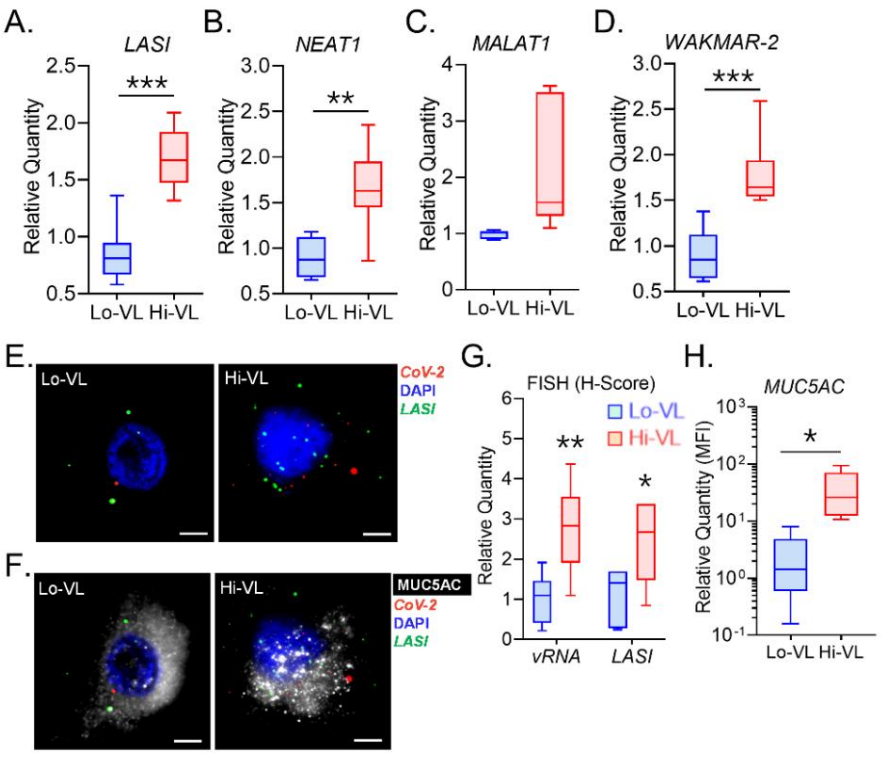

Figure 28. COVID-19 positive individuals with high viral load show increased immunomodulatory lncRNAs and the secretory mucin MUC5AC expression. Relative expression of immunomodulatory lncRNAs, **(A.)** LASI, **(B.)** NEAT1, **(C.)** MALAT1, and **(D.)** WAKMAR2 in Hi-VL compared to Lo-VL individuals' swab samples. **(E.) T**he dual-FISH analysis detected colocalization of SARS-CoV-2 viral RNA (vRNA) and LASI lncRNA in nasal swab samples. Representative micrographs from Lo-VL and Hi-VL swab samples display detection of SARS-CoV-2 nucleocapsid (CoV-2) vRNA (green) and LASI lncRNA (red) along with DAPI-stained nuclei (blue). **(F.)** Nasal swab cells showing immunoreactive MUC5AC expression (shown in white) in the dual-FISH labeled cells, scale – 2 µ. **(G.)** H-score quantitation of vRNA and LASI lncRNA in COVID-19 positive individuals. **(H.)** Relative quantitation of mean fluorescence intensity (MFI) of MUC5AC expression in Lo-VL and Hi-VL swab samples. (n=10/gp for data in A, B, C, & D; and n=4/gp for data in G & H; *p<0.05; **p<0.01; ***p<0.001 by Student's t-test) Dr. D. Devadoss was the major contributor for this data. Original source (1).

Thus, these set of data indicate that the immunomodulatory *LASI* lncRNA expression is significantly induced in Hi-VL patient cells compared to those with

Lo-VL and its expression strongly correlates with MUC5AC mucin expression in airway cells corroborating the RNA-seq data analyses (**Figure 29E**).

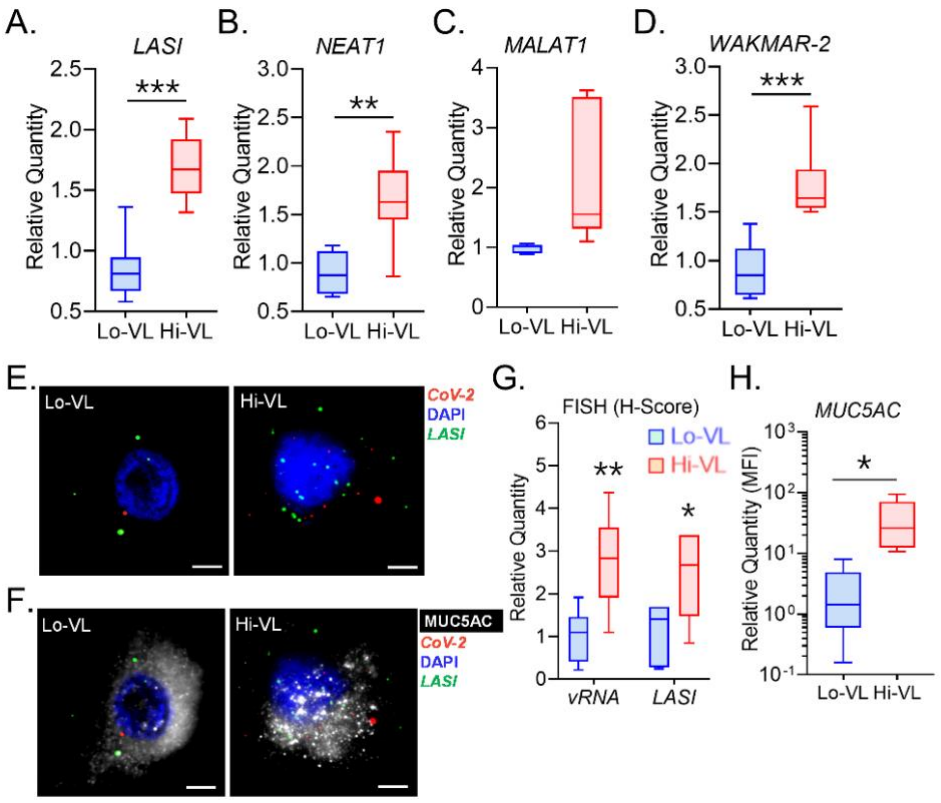

Figure 29. COVID-19 positive individuals with high viral load show increased immunomodulatory lncRNAs and the secretory mucin MUC5AC expression. Relative expression of immunomodulatory lncRNAs, **(A.)** LASI, **(B.)** NEAT1, **(C.)** MALAT1, and **(D.)** WAKMAR2 in Hi-VL compared to Lo-VL individuals' swab samples. **(E.) T**he dual-FISH analysis detected colocalization of SARS-CoV-2 viral RNA (vRNA) and LASI lncRNA in nasal swab samples. Representative micrographs from Lo-VL and Hi-VL swab samples display detection of SARS-CoV-2 nucleocapsid (CoV-2) vRNA (green) and LASI lncRNA (red) along with DAPI-stained nuclei (blue). **(F.)** Nasal swab cells showing immunoreactive MUC5AC expression (shown in white) in the dual-FISH labeled cells, scale – 2 µ. **(G.)** H-score quantitation of vRNA and LASI lncRNA in COVID-19 positive individuals. **(H.)** Relative quantitation of mean fluorescence intensity (MFI) of MUC5AC expression in Lo-VL and Hi-VL swab samples. (n=10/gp for data in A, B, C, & D; and n=4/gp for data in G & H; *p<0.05; **p<0.01; ***p<0.001 by Student's t-test) Dr. D. Devadoss was the major contributor for this data. Original source (1).

IV. 3D airway tissue model of SARS-CoV-2 infection demonstrates an immediate-early hyper-mucoinflammatory response

To better understand the association of CoV-2 induced airway inflammatory response and *LASI* lncRNA, a 3D airway tissue culture model of SARS-COV-2 infection was employed. Briefly, the primary human airway epithelial cells differentiated on air-liquid interface to mimic the conducting airway epithelium were infected with 1 MOI of SARS-CoV-2 primary clinical isolate (USA-WI1/2020). CoV-2 vRNA load was followed in apical washes, in the basal culture supernatant, and in cells at 0, 1, 4, 24, and 48 h post-infection (hpi). In apical washes, 0.89 x 10^5 viral genomic equivalents per ml were observed at 1 hpi, increasing to 20.2, 31.2, and 14.7 x 10^5 at 4, 24, and 48 hpi, respectively (**Figure 30A**). Viral load in basal media supernatant was 0.3 x 10^5 per ml at 1 hpi then increased to 3.6, 4.3, and 5.0 x 10^5 at 4, 24, and 48 hpi, respectively (**Figure 31A**). The cellular level of CoV-2 vRNA increased by 2.0-, 7.0-, and 2.6-fold at 4, 24, and 48 hpi, respectively, compared to 1 hpi (**Figure 30B**). Thus, 3D airway cells were productively infected with SARS-CoV-2 clinical isolate and the virions were shed at approximately ten-fold higher levels from the apical surface than the basal region. The expression of *ACE2* mRNA was more than 3-fold suppressed in infected at all time-points analyzed (**Figure 31B**), and *TMPRSS2* mRNA levels showed no change at 1, 4, and 24 hpi but was significantly reduced at 48 hpi (**Figure 31C**). Thus, SARS-CoV-2 infection modulates *ACE2* and *TMRPSS2* expression, as reported earlier. (246, 247) Expression of *IL-6* mRNA was 8.0-fold induced at 1 hpi with no change at 4, 24, and 48 hpi, although there was a trend towards induced expression

(**Figure 30C**). *ICAM-1* mRNA expression was 2.0-, 5.4-, and 2.4-fold higher at 1, 4, and 24 hpi, respectively, with no change at 48 hpi (**Figure 30D**). Expression of neither *NRP1* (data not shown) nor *CXCL-8* (**Figure 31D**) mRNA expression was affected following infection. However, the expression of *SCGB1A1* was induced by 4-5-fold at 1, 4, and 24 hpi (**Figure 31E**).

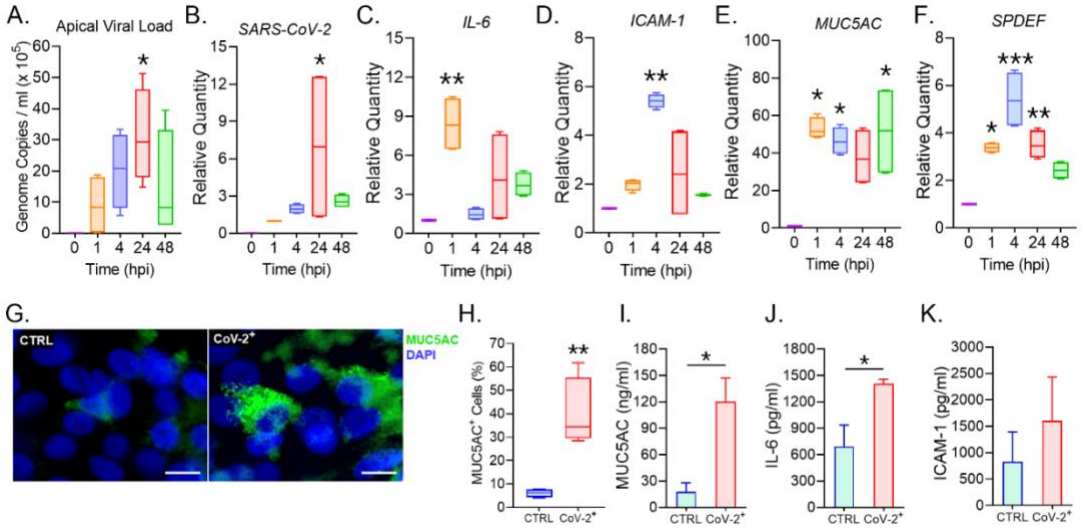

Figure 30. SARS-CoV-2 infection of human respiratory epithelial cells induces robust mucoinflammatory response in a 3D airway tissue model. Respiratory airway epithelial cells differentiated on air-liquid interface were infected with 1 MOI of SARS-CoV-2 clinical isolate (USA-WA1/2020 isolate) and analyzed at 0, 1, 4, 24, and 48 h post-infection (hpi). Viral loads were determined in **(A.)** the apical washes and **(B.)** the total cellular RNA. Relative expression levels of the inflammatory factors, **(C.)** IL-6, and **(D.)** ICAM-1 mRNA; and **(E.)** airway mucin MUC5AC; and **(F.)** SPDEF transcriptional factor in the total cellular RNA was analyzed by qRT-PCR. (n=4/gp; *p<0.05; **p<0.01; ***p<0.001 by ANOVA). **(G.)** Representative micrographs of uninfected control (CTRL) and SARS-CoV-2 infected (CoV-2+) cells showing MUC5AC (shown in green) immunoreactivity along with the DAPI stained nuclei (shown in blue), scale - 5µ. **(H.)** Percentage of MUC5AC+ cells within each treatment group. Secreted protein levels of **(I.)** MUC5AC mucin in apical washes, and **(J.)** IL-6 and **(K.)** ICAM-1 in culture media supernatants as determined by specific ELISA assays (n=4/gp; *p<0.05; **p<0.01; by Student's t-test). Dr. D. Devadoss was the major contributor for this data. Original source (1).

Interestingly, SARS-CoV-2 infection robustly upregulated *MUC5AC* mRNA expression by 53-, 46-, 37-, and 51-fold at 1, 4, 24, and 48 hpi, respectively (Figure 40E). *MUC5B* mRNA levels were also highly upregulated following infection by 13-, 11-, 16-, and 33-fold at 1, 4, 24, and 48 hpi, respectively (**Figure 31F**). Similarly, *MUC2* mRNA levels were 8-, 9-, 10-, and 13-fold at 1, 4, 24, and 48 hpi, respectively (**Figure 31G**), whereas *MUC4* mRNA levels were induced by 5-fold at 24 hpi (**Figure 31H**). In addition, there was a 3-5-fold induction in *SPDEF* mRNA levels (**Figure 30F**) and more than a 25-fold induction in *FOXA3* mRNA levels following CoV-2 infection (**Figure 31I**).

MUC5AC protein expression was assessed by immunofluorescence and quantified by ELISA to corroborate these results. In agreement with qRT-PCR analyses, CoV-2-infected (CoV-2^{+}) cells showed robust MUC5AC immunopositivity (**Figure 30G**) with as much as approximately 40% MUC5AC+ cells observed at 48 hpi compared to 6.0% in uninfected (CoV-2^{-}) controls (**Figure 30H**). In addition, apical wash MUC5AC protein levels were ~10-fold higher in CoV-2+ cells with approximately 120 ng/ml compared to 18 ng/ml observed in uninfected cells (**Figure 30I**). The secreted IL-6 levels were at 691 pg/ml in uninfected cells compared to 1400 pg/ml in the CoV-2^{+} cells at 48 hpi (**Figure 30J**), and ICAM-1 protein levels showed a trend towards increased expression from 823 pg/ml in uninfected cells to 1600 pg/ml in CoV-2^{+} cells (**Figure 30K**).

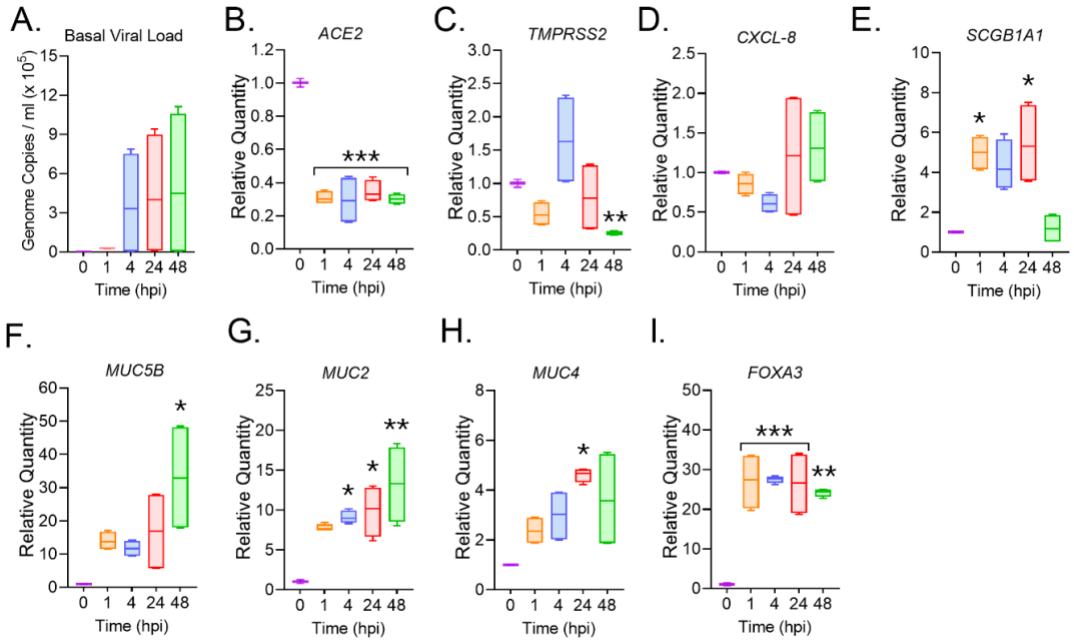

Figure 31. SARS-CoV-2 infection of human respiratory epithelial cells induces robust mucoinflammatory response. Fully differentiated RTECs were infected with 1 MOI of SARS-CoV-2 clinical isolate (USA-WA1/2020 isolate) and analyzed at 0, 1, 4, 24, and 48 h post-infection (hpi). **(A.)** Viral loads determined in the basal culture media by qRT-PCR. Relative expression levels of viral entry facilitating host factors, **(B.)** ACE2 and **(C.)** TMPRSS2 mRNA; the inflammatory factors **(D.)** CXCL-8 and **(E.)** SCGB1A1 mRNA; **(F.)** the mucin regulatory transcriptional factor FOXA3; airway mucins **(G.)** MUC5B, **(H.)** MUC2, and **(I.)** MUC4 mRNA levels as analyzed by qRT-PCR of the total cellular RNA. (n=4/gp from 2 independent experiments; *p<0.05; **p<0.01; ***p<0.001 by ANOVA). Dr. D. Devadoss was the major contributor for this data. Original source (1).

V. SARS-CoV-2 infection induces *LASI* lncRNA expression that could potentially interact with CoV-2 Spike viral RNA

In agreement with the increased *LASI* lncRNA observed in COVID-19 individuals, there was induced expression of *LASI* lncRNA at 0, 1, 4, 24, and 48 hpi in our 3D model of CoV-2 infection (**Figure 32A**). Dual-RNA FISH analyses showed CoV-2 *N1 vRNA* and *LASI* transcripts co-expression around the nuclear/perinuclear region (**Figure 32B**) with nearly 2-fold more lncRNAs in CoV-

2+ cells as assessed by H-score analysis (**Figure 32C-32D**). We also analyzed the expression of other lncRNAs and in contrast to recent reports (222, 241, 242), the expression of lncRNA *NEAT1* (**Figure 33A**) and *MALAT1* (**Figure 33B**) were significantly reduced in CoV-2-infected cells at 0,1, and 48 hpi. While *WAKMAR2* lncRNA levels were induced by more than 7-fold at 48 hpi (**Figure 33C**).

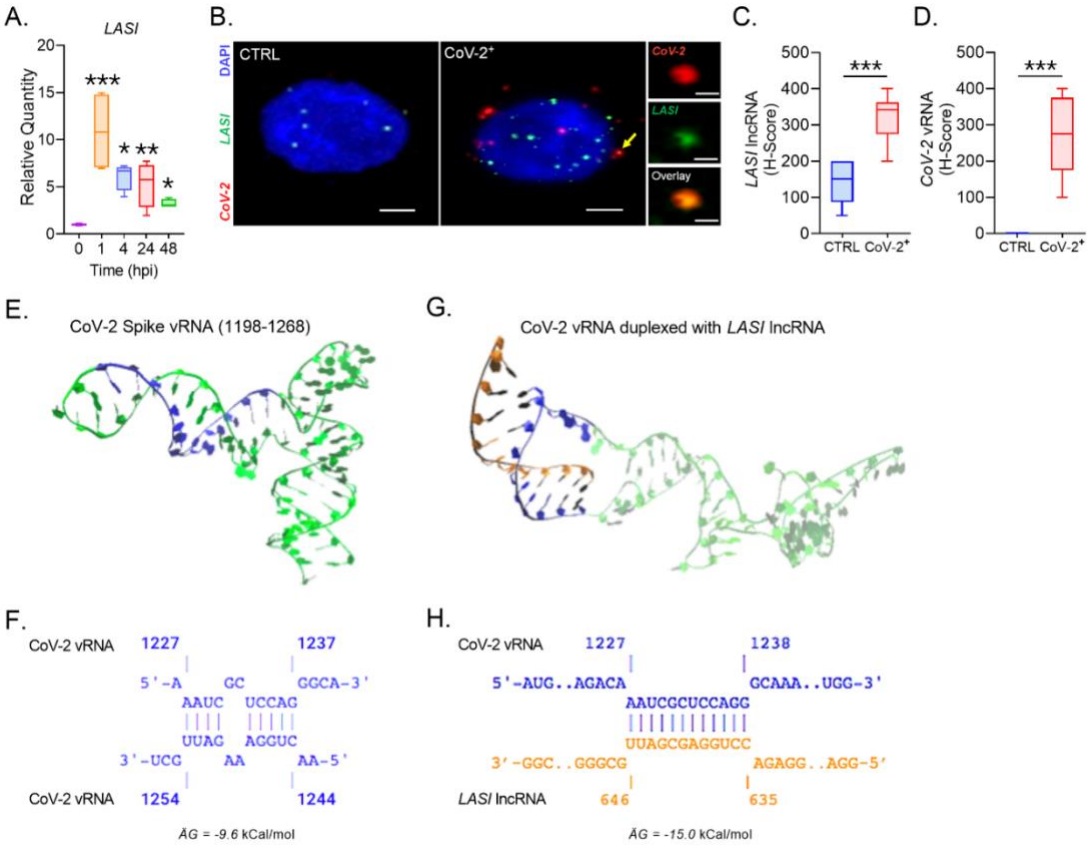

Figure 32. SARS-CoV-2 infection induces LASI lncRNA expression in human respiratory epithelial cells that potentially show direct interaction with CoV-2 spike RNA. **(A.)** Relative expression levels of LASI lncRNA in SARS-CoV-2 infected cells at 0, 1, 4, 24, and 48 hpi. (n=4/gp; *p<0.05; **p<0.01; ***p<0.001 by ANOVA). **(B.)** Colocalization of SARS-CoV-2 vRNA and LASI transcripts in CoV-2 infected (CoV-2$^+$) cells as determined by dual-FISH staining and the structured-illumination imaging analysis. Representative micrographs of dual-FISH-stained cells showing SARS-CoV-2 N1 vRNA (in red) and LASI lncRNAs (in green) along with DAPI-stained nuclei (in blue), scale – 2 µ. H-score quantitation of **(C.)** CoV-2 vRNA and **(D.)** LASI lncRNAs per cell in CoV-2+ and control cells. (n=9-10 cells/gp; **p<0.01;

***p<0.001 by Student's t-test). **(E.)** Modeled 3D structure of SARS-CoV-2 spike vRNA nucleotide sequence from 1198 to 1268, and the LASI lncRNA interacting region (1227-1237) is highlighted blue. **(F.)** The intra-sequence base-pairing of spike nucleotides forms the hairpin stem structure. **(G.)** Modeled 3D structure of the CoV-2 Spike vRNA duplexed with LASI lncRNA sequence 646-635 (highlighted in orange) at the end of 100 ns simulation (see video at online supplemental data). **(H.)** Inter-sequence base-pairing of CoV-2 vRNA with LASI lncRNA sequence (shown in orange). Dr. P. Chapagain and Mr. M. Cioffi were the major contributors for this data. Original source (1).

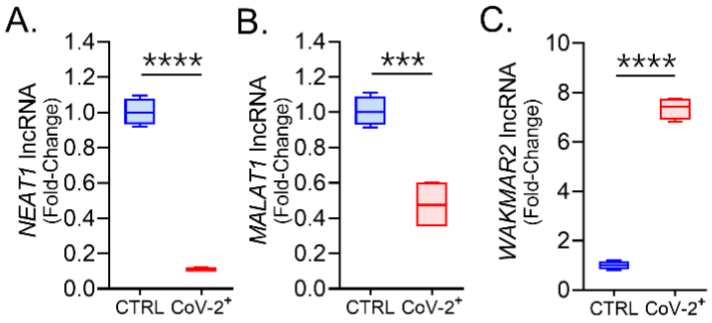

Figure 33. SARS-CoV-2 infection differentially affects the respiratory epithelial lncRNA expression. Relative expression levels of immunomodulatory lncRNA **(A.)** NEAT1, **(B.)** MALAT1, and **(C.)** WAKMAR2 levels in SARS-CoV-2 infected (CoV-2+) cells compared to uninfected controls (CTRL). (n=4/gp from 2 independent experiments; ***p<0.001; ****p<0.0001 by Student's t-test). Dr. D. Devadoss was the major contributor for this data. Original source (1).

As FISH analyses strongly suggest *LASI* lncRNA and SARS-CoV-2 vRNA may colocalize, the potential for direct interaction was assessed informatically. Notably, our sequence analyses identified a single, high-scoring potential base-pairing between SARS-CoV-2 Spike vRNA (CoV-2 vRNA) and a specific *LASI* lncRNA sequence. The segment of the modeled CoV-2 vRNA (sequence 1198-1268 nts) after minimization and equilibration is shown in **Figure 32E**. This region forms a hairpin where 1227-1237 nts are intra-sequence base-paired with 1244-1254 nts (**Figure 32F**). 3D modeling predicts a structure where this CoV-2 vRNA region can duplex with *LASI* lncRNA bases 635-646 nts with a stable base-paired

model obtained upon relaxing the structure for 100 ns of MD simulation (**Figure 32G**). This structure shows a partially unfolded CoV-2 vRNA sequence with excellent base-pairing with the *LASI* lncRNA sequence (**Figure 32H**). Compared to the intra-sequence base-pairing in CoV-2 vRNA (**Figure 32**), the inter-sequence base-pairing with *LASI* lncRNA is energetically more favorable (-9.6 kcal/mol vs. -15.0 kcal/mol) at the local interacting region. Moreover, this *LASI* lncRNA interacting region is conserved among CoV-2 variants of concern (VOCs) such as delta and omicron (**Figure 34**). Taken together, our experimental and molecular docking simulation studies suggest that *LASI* lncRNA may serve as the molecular scaffold for CoV-2 vRNA to assist in viral infection and replication.

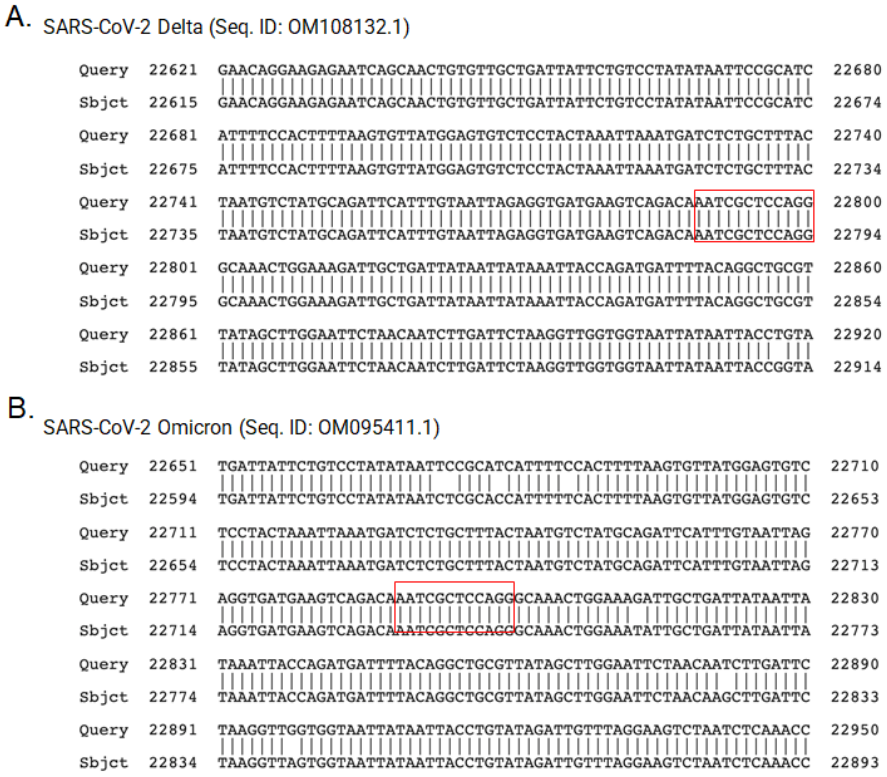

Figure 34. Putative LASI-interacting region is conserved in Spike viral RNAs of SARS-CoV-2 Delta and Omicron VOCs. Sequence alignment of spike protein encoding RNA sequences of SARS-CoV-2 alpha variant (NC_045512.2) with Delta

(A.) and with Omicron **(B.)** sequences obtained from the OM108132.1 and OM095411.1 database. The LASI-interacting region is shown in red inset. Dr. D. Devadoss was the major contributor for this data. Original source (1).

VI. Blocking LASI lncRNA expression attenuates CoV-2 altered antiviral interferon response effects and suppresses infection-dependent MUC5AC induction

To determine the role of *LASI* lncRNA in CoV-2 infection and associated mucoinflammatory response, we depleted *LASI* levels using RNA interference (siRNA) technology. Briefly, 3D cultured cells transfected with either *LASI*-targeting siRNA (siLASI) or a control siRNA (siCTRL) were infected with 1 MOI of SARS-CoV-2 clinical isolate and then analyzed at 48 hpi.

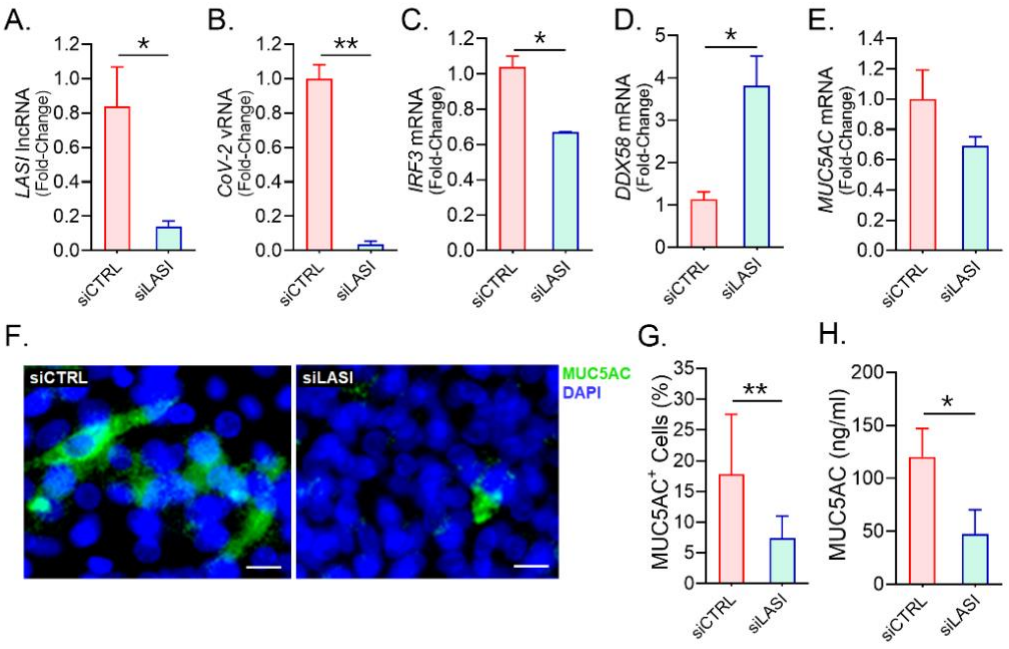

Figure 35. Blocking LASI lncRNA expression reduces the SARS-CoV-2 viral load and suppresses the MUC5AC mucin expression. Relative expression of **(A.)** LASI lncRNA and **(B.)** SARS-CoV-2 vRNA in cells transfected with siRNA targeting LASI (siLASI) compared to control siRNA (siCTRL) transfected cells and infected with 1 MOI of SARS-CoV-2. Relative expression of **(C.)** IRF3, **(D.)** DDX58, and **(E.)** MUC5AC mRNA following SARS-CoV-2 infection in siLASI-transfected cells

compared to siCTRL cells. (n=4/gp from 2 independent experiments; *p<0.05; **p<0.01; by Student's t-test). **(F.)** The micrographs of SARS-CoV-2 infected cells following siCTRL and siLASI transfection show MUC5AC (green) immunoreactivity and DAPI-stained nuclei (blue), scale - 5µ. **(G.)** Percentage of MUC5AC+ cells within each treatment group (n=10/gp; **p<0.001 by Student's t-test). **(H.)** MUC5AC mucin protein levels in the apical wash of CoV-2 infected cells and transfected with siLASI or siCTRL as determined by ELISA assay. (n=4/gp from 2 independent experiments; *p<0.05 by Student's t-test). Dr. D. Devadoss was the major contributor for this data. Original source (1).

Compared to siCTRL-transfected cells, siLASI-transfected cells exhibited a 7-fold reduction in *LASI* lncRNA expression (**Figure 35A**). Surprisingly, we also observed a marked >27-fold reduction in CoV-2 vRNA load in siLASI-transfected cells (**Figure 35B**). Furthermore, while *ICAM-1* (**Figure 36A**), *IL-6* (**Figure 36B**), *IFIH1* (**Figure 36C**), and *IFNB1* (**Figure 36D**) mRNA expressions were unaffected, mRNA levels of the antiviral interferon response gene, *IRF3*, were significantly reduced in siLASI-transfected cells (**Figure 35C**). In contrast, levels of *DDX58* mRNA were conversely induced compared to the siCTRL-transfected cells (**Figure 35D**). Among mucin genes, *MUC5AC* mRNA levels in siLASI-transfected cells showed a trend toward lower expression (**Figure 35E**) with no change in *MUC5B* mRNA levels (**Figure 36E**); however, *MUC2* (**Figure 36F**) and *MUC4* (**Figure 36G**) mRNAs were reduced following CoV-2 infection in siLASI-transfected cells compared to siCTRL-transfected cells. Notably, expressions of the *SPDEF* (**Figure 36H**) and the lncRNA *MALAT1* (**Figure 36I**) and *WAKMAR2* (**Figure 36J**) were not altered by siLASI treatment during CoV-2 infection. To further explore potential effects on mucin genes, we next immunoprobed for MUC5AC protein expression in siCTRL and siLASI transfected cells infected with CoV-2 at 48 hpi (**Figure 35F**). We found siLASI treatment resulted in a >2-fold reduction of MUC5AC+ cells,

where siCTRL-transfected cells had around 17.7% cells showing MUC5AC immunopositivity compared to 7.4% among siLASI-transfected cells (**Figure 35G**).

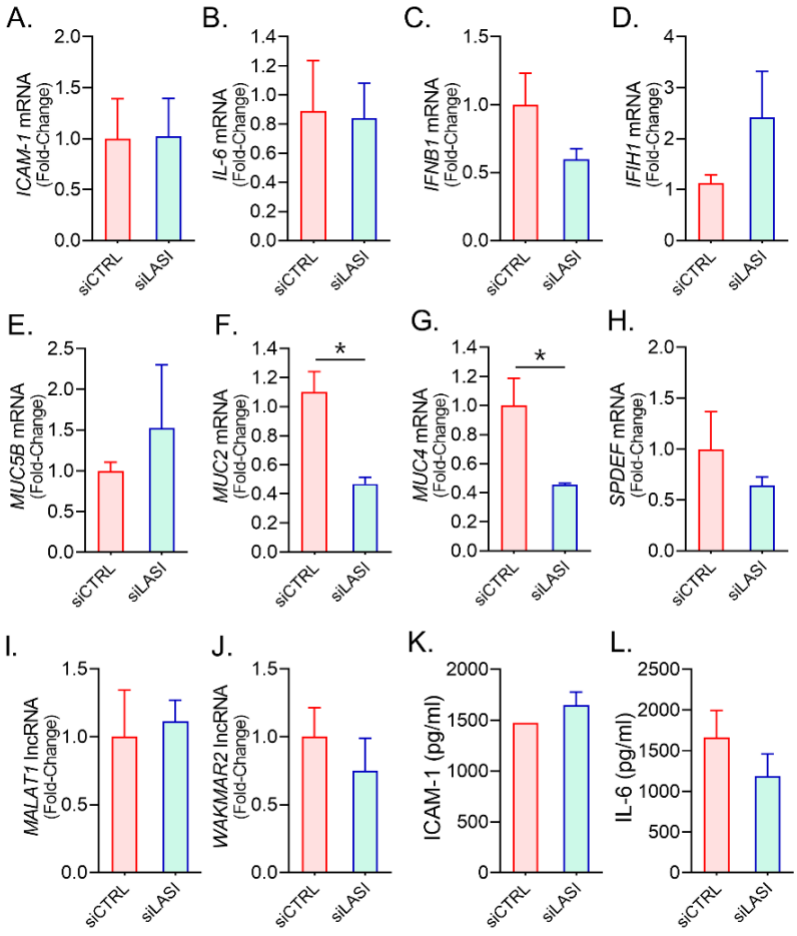

Figure 36. Blocking LASI lncRNA expression suppresses SARS-CoV-2 infection induced MUC2 and MUC4 mucin expression. Relative expression levels of inflammatory factors **(A.)** ICAM-1, **(B.)** IL-6; interferon responsive genes **(C.)** IFNB1, **(D.)** IFIH1; airway mucin **(E.)** MUC5B, **(F.)** MUC2, and **(G.)** MUC4; and **(H.)** SPDEF transcription factor mRNAs; and **(I.)** MALAT1, and **(J.)** WAKMAR2 lncRNAs following SARS-CoV-2 infection in siLASI-transfected cells compared to siCTRL cells. Protein levels of **(K.)** ICAM-1 and **(L.)** IL-6 in the basal culture media supernatant of siLASI or siCTRL transfected cells infected with CoV-2 as determined using specific ELISA assays. (n=4/gp from 2 independent experiments; *p<0.05 by Student's t-test). Dr. D. Devadoss was the major contributor for this data. Original source (1).

In agreement, MUC5AC-specific ELISA of apical washes from siCTRL-transfected cells averaged 121 ng/ml of MUC5AC content whereas siLASI-transfected cells averaged 47.5 ng/ml (**Figure 35H**), a more than 2-fold reduction. In contrast, we found ICAM-1 (**Figure 36K**) and IL-6 (**Figure 36L**) levels were not significantly changed in basal media supernatant following CoV-2 infection of siLASI-transfected cells as compared with siCTRL-transfected cells. Taken together, these data strongly suggest that *LASI* lncRNA represents an essential regulatory mediator in CoV-2 infection and the ensuing mucoinflammatory response of the respiratory airway epithelium.

VII. LASI lncRNA differentially modulates the host miRNAs associated with SARS-CoV-2 infection

LncRNAs also act as the molecular scaffold or sponge for miRNAs. Thus, they could indirectly modulate host cellular immune responses, for example, by miRNA mediated target mRNA-decay or by competing for the same miRNA binding region, like ceRNA. (248-251) In addition, host miRNAs can also directly bind to viral RNAs and/or modify the associated cell signaling mechanisms. So, to identify the miRNAs that *LASI* lncRNA may regulate, we performed a small RNA-sequencing of our 3D ALI model and analyzed for the miRNAs in SARS-CoV-2 infected cells that are siLASI-transfected compared to control cells. From the total of 721 miRNAs sequenced, there were 155 miRNAs that showed significant change. Further data mining revealed a total of 38 miRNAs differentially expressed in SARS-CoV-2 infection, of which seven miRNAs (miR-4488, let-7b-5p, miR-1301-3p, miR-181b-5p, miR-2110, miR-320b, and miR-744-5p) were expressed

over 2 log-fold higher while twenty-one miRNAs showed lower expression than uninfected cells including miR-23a-3p, miR-30d-5p, miR-200a-5p, miR-200b-3p, miR-1246. Interestingly, knocking down the *LASI* lncRNA reverted the expression levels of several of these miRNAs; for example, some of the miRNAs induced by CoV-2 infection were suppressed by silencing LASI lncRNA (**Figure 37A**) of which miR-4488, let-7b-5p, miR-584-5p, miR125-1-3p, and miR-181b-5p showed very high expression in siLASI-transfected and CoV-2 infected cells.

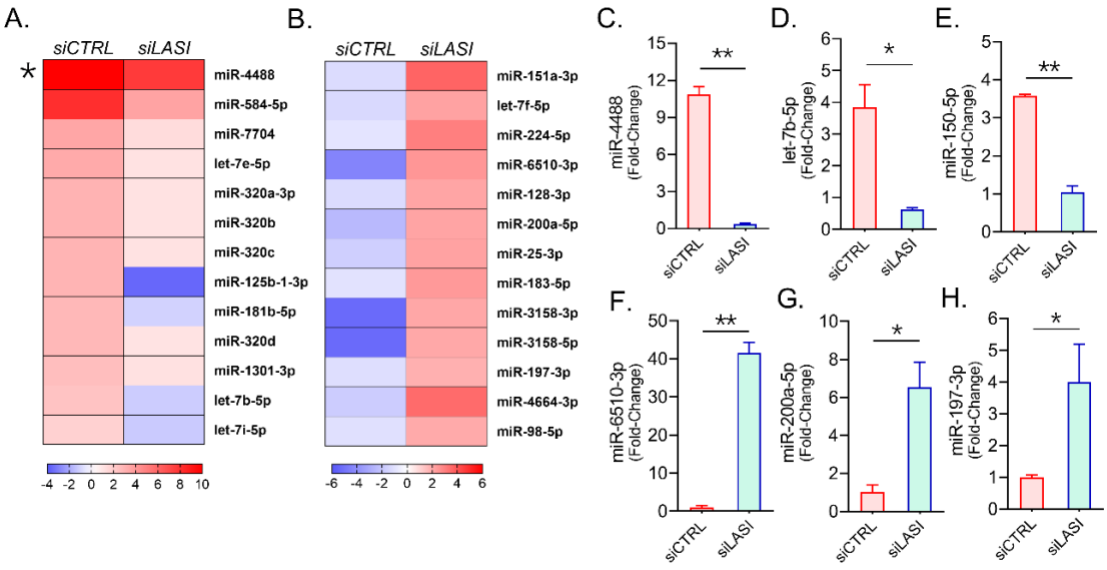

Figure 37. Airway epithelial miRNAs are modulated by SARS-CoV-2 infection and regulated by LASI lncRNA. Relative expression levels of miRNAs in siLASI-treated cells following 48 h SARS-CoV-2 infection compared to control infected cells as analyzed by small RNA-seq analysis. **(A.)** List of miRNAs upregulated by CoV-2 infection and suppressed in siLASI-treated cells (*miR-4488 was upregulated >200-fold in infected control cells). **(B.)** Expression levels of miRNAs that are downregulated by CoV-2 infection but induced in siLASI-treated cells. Relative quantitation of miRNAs: **(C.)** miR-4488, **(D.)** let-7b-5p, and **(E.)** miR-150-5p that were upregulated by SARS-CoV-2 infection in siCTRL cells but suppressed in siLASI-transfected cells. Relative expression of miRNAs: **(F.)** miR-6510-3p, **(G.)** miR-200a-5p, and **(H.)** miR-197-3p that were downregulated by SARS-CoV-2 infection in siCTRL cells but induced in siLASI-transfected cells. (*$p<0.05$; **$p<0.001$ by Student's t-test). Dr. D. Devadoss was the major contributor for this data. Original source (1).

At the same time there were miRNAs suppressed by CoV-2 infection that were highly induced in siLASI-transfected cells e.g., miR-151a-3p, miR-6510-3p, miR-200a-5p, miR-197-3p, and miR-4644-3p (**Figure 37B**). The changes in the expression levels of select miRNAs were confirmed by qPCR analysis of siCTRL and siLASI cells where levels of miR-4488 (**Figure 37C**), let-7b-5p (**Figure 37D**), miR-150-5p (**Figure 37E**), miR-6510-3p (**Figure 37F**), miR-200a-5p (**Figure 37G**), and miR-197-3p (**Figure 37H**) were confirmed to be reverted in siLASI-transfected cells compared to siCTRL-transfected cells. We also confirmed the expression levels of these lncRNA *LASI*-regulated miRNAs in nasal swab samples of our cohort and of these miRNAs (data not shown). Expression levels of let-7b-5p, miR-150-5p and miR-200a-5p showed a viral-load dependent increased expression. Taken together, these data suggest that let-7B-5p, miR-150-5p and miR-200a-5p may be important mediators of lncRNA LASI-mediated modulation of SARS-CoV-2-induced airway epithelial mucoinflammatory responses.

Chapter 4: Discussion

The pathogen-specific inflammatory response and subsequent successful resolution of inflammation and associated tissue remodeling in the upper respiratory tract determine the outcome of airborne infections. The SARS-CoV-2 infection continues to be a major healthcare problem. Many studies suggest that dysregulated inflammation and impaired ability to resolve inflammation and adjoining tissue remodeling are primary causes of increased morbidity and mortality in COVID-19. Airway mucoinflammatory response, being the primary host defense system, is severely altered by SARS-CoV-2 infection. Not much is known

about the immediate-early innate responses to SARS-CoV-2 infection. Thus, in this study, we focused on the effects of SARS-CoV-2 infection on airway mucus and inflammatory responses. We analyzed available RNA-seq data from COVID-19 patient nasal swab samples. We found that expressions of immunomodulatory lncRNAs, particularly *LASI* lncRNA, expressions were altered in infected patients with elevated expression of mucoinflammatory factors. In our independent cohort of COVID-19 patients, the nasal SARS-CoV-2 viral load directly correlated with mucoinflammatory responses where COVID-19 patients with high Hi-VL patients showed elevated expression of mucins and inflammatory factors compared to Lo-VL patients.

To understand the immediate-early response of AECs to SARS-CoV-2 infection, we examined a 3D human airway tissue model infected with a high MOI of SARS-CoV-2 isolate USA-WI1/2020 (B.1.1.7). We observed elevated secretory mucins and inflammatory factors expression as early as one-hour post-infection. Among the airway lncRNAs, we found *LASI* lncRNA expression strongly correlated with increased mucoinflammatory responses of the 3D airway tissue model.

Importantly, the roles of lncRNAs in the innate airway response to viral infection remain poorly understood. LncRNAs can interact with RNA, DNA/chromatin, and proteins, and form RNA-RNA, RNA-DNA (RNA-chromatin), and RNA-protein complexes, leading to gene expression regulation via multiple mechanisms, including modulation of transcription, mRNA stability, and translation. (166, 203) While little is known about specific lncRNA contributions to COVID-19 pathophysiology, several lncRNAs have now been suggested to

potentially interact with SARS-CoV-2. Using the experimentally determined secondary structure of HOTAIR lncRNA (252), a study recently predicted its interacting regions with Spike RNA. (220)

In contrast, our data suggest that *LASI* lncRNA may be a positive modulator of CoV-2 infection. Our computational analyses identified a putative interaction between *LASI* lncRNA and SARS-CoV-2 Spike RNA, suggesting that *LASI* may act as a molecular scaffold or sponge for viral RNA, potentially providing protection from degradation and/or other host factors. Regardless, we find inhibiting *LASI* lncRNA attenuates the SARS-CoV-2 viral load. Thus, targeting *LASI* may not only suppress the mucoinflammatory pathways but could also decrease the number of molecular scaffolds responsible for harboring the viral RNA and other components. Functional RNA-based therapeutics are currently being actively pursued as potential treatment strategies due to minimal off-target effects to a high-efficiency presentation (253), and lncRNA-targeted interventions can possibly mimic the mechanisms of many host immune response modulating RNAs. (208)

Acute inflammatory response to SARS-CoV-2 infection alters innate epithelial and vascular remodeling factors (254, 255) with distinct inflammatory signatures reported among COVID-19 patients with low versus higher viral load. (256) Notably, the localized expression and secretion of ICAM-1 and IL-6 by respiratory epithelial cells may regulate airway responses and mucosal tissue remodeling. (257) In previous immunohistological analyses, IL-6 and ICAM-1 expression were reportedly higher in the alveolar epithelium of COVID-19 patients compared to H1N1 influenza virus-infected patients or uninfected control subjects.

(258) We likewise find that ICAM-1 and IL-6 expressions are significantly higher in COVID-19 patients compared to controls, and patients with Hi-VL show increased expression of these inflammatory factors in our cohort.

Also of note, lncRNAs-mediated regulation of immune responses is potentially central to establishing airway mucosal immunity (167, 259, 260) and could be dysregulated in COVID-19 patients. Numerous lncRNAs have been experimentally characterized and were shown to affect the immune responses of AEC, exert epigenetic changes, and induce the premature aging of the lung epithelium. (167) However, among the lncRNAs analyzed, we found only *LASI* lncRNA expression to be consistently elevated in COVID-19 patients although there were significant downregulations of *NEAT1* and *MALAT1* lncRNAs (221); as recently confirmed in a separate computational analysis. (222) Further, we find that an acute effect of SARS-CoV-2 infection on airway mucin expression linked to *LASI* lncRNA expression could potentially hinder the effective mucociliary clearance of inhaled viral particles. We found that the expression of membrane-bound mucins was significantly upregulated during CoV-2 infection, and that depleting *LASI* lncRNA could suppress the CoV-2-induced expression of these mucin genes. Airway mucins trap inhaled viral particles in the lumens and direct them towards the oropharynx via mucociliary clearance mechanisms; therefore, any dysregulation of these processes leads to mucoinflammatory comorbidities and respiratory viral diseases. (26, 261) Excess mucus expression can lead to airway mucous obstruction due to mucin hyperexpression, hypersecretion, and goblet cell hyperplasia; and as reported here, SARS-CoV-2 alters these

mucoinflammatory responses in agreement with other seminal studies. (240, 262-264) If not treated, these conditions can cause a decline in lung function and significantly higher morbidity and mortality. That said, our findings strongly suggest that *LASI* lncRNA constitutes an important master mucin regulator.

In addition, blocking *LASI* lncRNA expression in the 3D airway model led to a suppressed expression of MUC5AC protein levels following CoV-2 infection, implicating a direct role of *LASI* in viral-induced mucoinflammatory response. However, unlike observed in the case of allergic reactions (2), there was no change in any of the mucin regulating transcription factor expression among CoV-2 infected cells, suggesting that *LASI* lncRNA may be engaging other regulatory pathways to induce airway mucin expression such as increasing the mucin mRNA stability and/or half-life to induce MUC5AC expression.

There are various other small ncRNAs called miRNAs that interact with lncRNAs and modulate the gene expression and functions. (166, 203) We have also identified several putative miRNA candidates that could assist *LASI* lncRNA in modulating the mucoinflammatory response genes that contribute to airway inflammation and mucin expression. Our targeted small RNA-seq data implicated many host miRNAs that could possibly mediate the *LASI* lncRNA-based modulation of SARS-CoV-2 infection and associated inflammation. For example, following CoV-2 infection a set of miRNAs including miR-4488, miR-584-5p, miR125-1-3p, miR-181b-5p and let-7b-5p were highly upregulated but blocking the *LASI* lncRNA resulted in their downregulation compared to controls. These miRNAs might be facilitating the CoV-2 infection in a *LASI*-dependent manner,

where *LASI* lncRNA may be acting as a molecular sponge or scaffold for these 'inflammatory' miRNAs. There is very limited information about the role of these miRNAs. A computational prediction analysis performed by Pierce *et al*., identified that miR-181-5p binds to the mRNAs of both TMPRSS2 and IFN-γ in human lung tissue. (265) Another RNA-seq data analysis from SARS-CoV-2 infected lung tissues identified that miRNA let-7b-5p might be involved in COVID-19-associated lung pathologies. (266, 267)

In contrast, specific miRNAs suppressed by CoV-2 infection were highly induced in siLASI-transfected cells, such as, miR-151a-3p, miR-6510-3p, miR-200a-5p, miR-25-3p, miR-3158-3p, miR-3158-5p, and miR-4644-3p. These miRNAs play an important role in regulating innate cellular responses and signaling pathways. (268, 269) This suggests that these miRNAs are an important component of the host immune response and are thus suppressed by CoV-2 infection in a mechanism dependent on *LASI* lncRNA levels. Based on the recent report on the interaction of miR-150-5p with CoV-2 nsp10 gene (270), we also found that CoV-2 infection modulates miR-150-5p expression in a *LASI*-dependent manner. It is noteworthy that nasal airway miR-150-5p expression was positively correlated with CoV-2 viral load in our cohort in contrast to the lower miR-150-5p levels reported in COVID-19 plasma samples. (270) Further investigations are needed to determine the role of miR-150-5p in systemic versus pulmonary inflammation by examining the levels of cellular and plasma miR-150-5p collected from same subjects. Thus, there is a large number of miRNAs that are directly impacted by *LASI* lncRNA and could be involved in CoV-2 infection and airway

inflammatory response. We also found that there are a number of miRNAs whose expression was not significantly impacted by *LASI* lncRNA levels, such as miR-1301-3p, which is known to interact with CoV-2 genes/RNAs (267, 271) and miR-320b, which interacts with viral NSP8 gene and is associated with transcription and replication of viral RNAs. (265)

There are several other limitations of this study. The lack of availability of a larger number of patient nasal swab samples from COVID-19 subjects may underscore the broader implications of the reported findings. The amount and quality of samples could have also been the contributing factor to the undiscernible and/or undetected levels of the genes analyzed that are expressed in low copy numbers such as genes regulating the antiviral and interferon response pathways. Further, our in-vitro studies primarily focused on the acute infection model, and we used high MOI of the original SARS-CoV-2 clinical isolate (B.1.1.7), and only the early time points were analyzed to understand the immediate-early changes in host innate response factors. The miRNAs identified to be responsible for *LASI* lncRNAs role in CoV-2 infection and associated inflammation need to be further validated by using state-of-the-art molecular techniques.

Due to the combined colossal efforts of the continuous global surveillance and the large-scale vaccination drives, COVID-19 has been mitigated to a manageable endemic threat. Nonetheless, with a more significant proportion of the population still infected, the undetected and asymptomatic SARS-CoV-2 infections and invading vaccine/natural antibodies in vaccinated or infected individuals are resulting in the emergence of variants of concerns or VOCs (272, 273) and thus,

continuous efforts are needed to better understand the host-pathogen interaction for these VOCs and to better prepare for any possible future viral outbreaks. The work presented here strongly suggests that lncRNAs constitute a significant component of our innate immunity potentially directly interacting with viral RNA and describing these interactions may significantly improve our understanding of host-factors involved in viral response. Specifically, we report that *LASI* lncRNA in airway epithelial cells is not only a putative scaffold for SARS-CoV-2 RNA but also modulates respiratory mucoinflammatory responses. Thus, modulating specific functional lncRNA expression may aptly equip the host with innate immunity to combat the COVID-19 infection and associated mucoinflammatory comorbidities.

Table 4. List of major contributors.

Figure #:	**Acknowledgement/Major contributors:**	**Reference:**
7,27,28, 29,30,31,33, 34,35,36,37	Dr. Dinesh Devadoss	(1, 2)
3	Dr. Christopher Long	(3)
6	Dr. Raymond Langley & Dr. Glen Borchert	(2)
26	Dr. Glen Borchert	(1)
32	Dr. Prem Chapagain & Mr. Michael Cioffi	(1)

Conclusions and Future Directions

In this report, the immunomodulatory lncRNA *LASI* has been identified in patients with or without disease. We have identified its role in mediating the CS-induced responses and COPD progression and found that it plays an important role in mediating viral infection. Of primary interest are the mechanisms by which lncRNA *LASI* is able to induce these changes. Firstly, analysis of *LASI* binding partners, and experimental confirmation of binding such as RNA pulldown, chromatin isolation by RNA purification (ChIRP), RNA antisense purification (RNA-RAP), luciferase reporter construct assays and other methodologies can be used to determine individual binding partners and elucidate the specific mechanisms of action and pathways that lncRNA *LASI* may be utilizing. We have identified miR-150-5p as a likely candidate for lncRNA-miRNA binding, however our RNA-sequencing data elucidates numerous additional miRNAs that are regulated by modulating the levels of lncRNA *LASI*. Whether there is direct interaction between *LASI* and miRNAs of interest needs to be further investigated. We were interested in the lncRNA-miRNA interactions however, it is likely that lncRNA *LASI* additionally binds to proteins, DNA, or chromatin. Interestingly, the role of miR-150-5p has not been investigated in COPD models. Both in vitro and in vivo investigation is necessary and could present miR-150-5p as a further notable and important regulatory element. Additionally, the effects of dual genetic editing of *LASI* lncRNA and miR-150-5p need to be investigated. Notably, the half-life of lncRNA *LASI* needs to be investigated as it may elucidate its importance. Furthermore, we have focused our studies downstream of *LASI* transcription,

however investigation of its upstream regulators needs investigation. The mechanism behind the induction of *LASI* by CS- or viral-mediated pathways needs to be investigated. It is likely that there is more than one pathway that initiates *LASI* transcription as it is upregulated by both viral infection as well as CS exposure. LncRNAs have only recently started to be investigated. There are many lncRNAs that need further investigation. Our preliminary results suggest that there are several lncRNA molecules that further warrant investigation and work in conjunction with *LASI* lncRNA. Lastly, the effect of CS exposure on the SARS-CoV-2 infection and associated inflammation has not been investigated and could offer exceptional insight into both the pathways inducing *LASI* lncRNA expression as well as potential therapeutic avenues. The direct binding proposed between *LASI* lncRNA and SARS-CoV-2 Spike protein warrants further investigation and experimental confirmation. Additionally, we have focused our studies on airway epithelium, however understanding the role of lncRNA *LASI* as well as miR-150-5p in other cell types and tissues may offer insight into other pathways and disease states. Further understanding regulatory lncRNAs such as *LASI* may offer exceptional opportunities to regulate the cellular responses across multiple pathways, and in the case of COPD, moderate the cellular responses in contrast to significantly knocking down individual elements involved, and avoiding unacceptable side effects. It further offers insight into novel regulatory pathways, and with the increased understanding and novel delivery methods available, targeting noncoding elements in therapeutic advances may offer treatment

opportunities for COPD, as well as many other diseases and debilitating conditions.

Appendix 1: Preclinical model efficacy testing of air purification filters in mitigating the airway responses to inhaled allergens

Appendix 1: Introduction

I. Animal model of allergic asthma

The efficacy of air filters was tested in an animal model of allergic asthma to pet dander allergens. A mouse model of allergic asthma was developed using cat dander (CDE) as an allergen. Adult mice were randomly assigned into four groups with 10 mice per group and were housed in separate custom-built state-of-the-art whole-body exposure chambers. Group 1 mice were used as negative controls (NC) which were kept in room air for the duration of experiment. Group 2 mice were exposed to aerosolized CDE with sham air-filters and served as a positive control (PC). Group 3 mice were exposed to CDE with the Test air-filter placed in the exposure chambers (TF group), whereas group 4 mice were also exposed to CDE along with a Control air filter (CF group). Inhalation exposures of aerosolized CDE allergen were conducted in separate exposure chambers for each condition. The goal was to obtain 60µg CDE protein per 2L of chamber air sample to achieve a pulmonary deposited dose equivalent to 20µg CDE per mouse per day. These deposited doses were achieved through modulation of the exposure duration and nebulizer suspension concentrations as standardized by Molekule Inc and there were comparable levels of CDE aerosol generated in each of the chambers throughout the six-weeks of study. Most importantly, the air sample analysis collected pre- and post- air-filtration shows that both Test filter and

Control filter were able to completely reduce the CDE allergen levels compared to the positive control chamber with sham air-filter.

Among the biological end-points, animals in the study weighed between 26 to 32 g. Animals in NC group gained around 8% of body weight during the study whereas the mice exposed to CDE aerosol failed to gain any weight with no significant difference of air-filtration use. Based on the lung function analysis, there was a significant increase in airway resistance in the allergen-exposed PC group with no air-filtration. Interestingly, use of air-filtration units both TF and CF rescued the mice lung function parameters that were indiscernible from the NC group. These data suggested that both TF and CF have functionally suppressed the CDE allergen levels. Next, the changes in CDE-induced airway cell infiltration were analyzed by collecting bronchoalveolar lavage (BAL) by specifically analyzing for eosinophil (Eos) recruitment. There was a significantly lower yield of total BAL cells with lower number of Eos observed in TF group than the CF group. There was a significant increase in blood plasma immunoglobulin E (IgE) and IL-13 cytokine levels in PC group that were attenuated in the TF and CF group. The BAL IgE levels were better attenuated in the TF group than the CF group in comparison with the PC group. There was no major difference in gross lung tissue histopathology in any of the groups in terms of cellularity around airways, blood vessels, or in parenchyma. However, the epithelium of conducting airways (bronchi) showed increased mucous metaplasia in PC mice and the TF and CF group showed attenuation of the mucous metaplasia as analyzed by histochemical

and immunological analyses. There was distinctive peribronchial eosinophilia in PC mice compared to NC mice and the TF significantly attenuated this increased eosinophil recruitment whereas CF group mice failed to show any change from the PC group. This pilot study thus suggests that chronic exposure to CDE aerosols induce airway hyperreactivity in a mouse model and the 'Test filter' is effective in controlling the CDE allergen levels and associated lung allergic responses than the 'control filter'.

Appendix 1: Methods

I. Animal quarantine, randomization, and study groups

Pathogen-free wild-type C57BL/6J mice were purchased from The Jackson Laboratory and were housed in cages with five mice per cage under specific pathogen-free conditions. All experiments were approved by the Institutional Animal Care and Use Committee and were conducted at FIU, a facility approved by the Association for the Assessment and Accreditation for Laboratory Animal Care International. Briefly, fifty C57BL/6 male mice of eighteen weeks age were purchased from Jackson Labs and upon arrival at animal care facility were quarantined for 10 days. Mice were then acclimatized to the exposure chambers for five days before the study. Mice were then individually weighed, randomized, and ear-tagged with numbers for identification. Mice were divided into four groups as shown in **Table 4**. Each group had two cages with five mice per cage. Briefly, Group 1 mice were placed in a chamber with the ‘sham air-filter’ (with no active filtration unit), to control for the noise, heat generated, and vibration levels and

were exposed to room air only. This group was referred to as Negative control (**NC**) group. Other three groups were exposed to aerosolized cat dander extract or CDE (Greer labs) on every other day for 6 weeks. Group 2 mice had a sham air-filter in their chamber and was referred to as positive control (**PC**) group. Group 3 mice had the 'Test air-filter' in their chamber and was referred to as Test Filter (**TF**) group. Group 4 mice had the 'Control air-filter' in their chamber and was referred to as Control Filter (**CF**) group.

Table 5. Summary of study groups with exposure conditions and the type of air-filters used.

Group	No. of Mice	Exposure/Challenge	Condition	I.D.
1	10 (5 x 2 cages)	Room Air	Sham Air Filter	Negative Control (**NC**)
2	10 (5 x 2 cages)	Cat Dander Extract	Sham Air Filter	Positive Control (**PC**)
3	10 (5 x 2 cages)	Cat Dander Extract	Test Air Filter	Test Filter (**TF**)
4	10 (5 x 2 cages)	Cat Dander Extract	Control Air Filter	Control Filter (**CF**)

II. Exposure chambers setup

A rodent whole body inhalation exposure chambers were configured and custom-built for each group to avoid cross-contamination and to efficiently manage the exposure schedule. Animals were exposed to aerosolized CDE generated following the standardized protocol. The study plan was to expose each group of mice in their own designated chambers with CDE aerosol allergen exposure housed in the same room (**Figure 38**). The NC group mice were exposed to room air with sham air filter in a separate room to avoid any cross contamination. All the

animals were housed together in a same facility throughout the study and the room temperature and humidity of all the chambers were monitored during the exposures.

Figure 38. Whole-body aerosol exposure chambers used in the study were housed in the FIU animal care facility.

III. CDE aerosolization and animal exposures

Mice in group 2, 3, & 4 were exposed to CDE aerosols for 1 hour per day, 3 days per week, for 6 weeks as outlined in Figure 2 in their designated chambers. Exposure concentrations of CDE protease Fel D1 was targeted at 20 µg/ms deposition i.e., 60 µg/2 L of chamber air sample. The aerosol samples were collected immediately after the aerosolization, and chamber airs were filtered using

the respective filters for one hour. Another chamber air sample chamber was collected after the air filtration.

IV. Body weights and daily observations

Each mouse on study was observed twice daily by animal care personnel for any clinical signs of abnormality, morbidity, or death. The observations were also conducted by the study personnel before and after exposures during chamber servicing and all observations were recorded. All mice will be weighed prior to randomization (not more than one week before their exposures are scheduled to begin), at least weekly, then at the time of necropsy. Clinical observations and weight data collected during each weighing session were reviewed by the Study Director and any errors or irregularities were brought to the attention of the Principal Investigator. Any moribund or dead animals found during the study were necropsied as soon as possible after being found (e.g., to determine the probable cause of death). At the end of the study, the lung function parameters were determined for five mice in each group. The remaining mice in each group were euthanized and blood plasma, bronchoalveolar lavage (BAL), and lung tissue samples were collected for further analysis.

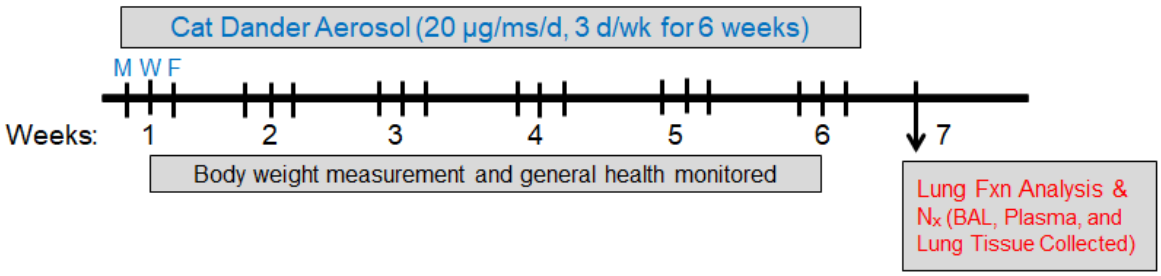

Figure 39. Schematic representation of the study schedule for animal model of allergic asthma.

V. Lung function analysis

Mice assigned for pulmonary function tests were anesthetized with ketamine/xylazine (80-100/5-10 mg/kg of K/X cocktail) via a single IP injection unless it was determined that the initial dose was insufficient, in which case more cocktail was given, and the pulmonary functions were tested by forced oscillation techniques (Buxco R/C system, DSI Int.). Lung functions were assessed following aerosolized methacholine (MCh) challenges to assess airway hyperresponsiveness (airway resistance and compliance). Anesthetized mice were intubated via a small superficial incision made in the ventral neck region above the trachea. After the lobes of the salivary gland were separated, a small incision was made in the trachea, and the trachea cannulated with a blunt-end 19-gauge needle hub. The cannula was secured by suture thread. Ventilation was performed through the cannula by positive pressure maneuvers on the R/C apparatus. Respiration rates were monitored and changes in rate indicated the need for supplementing the anesthesia (K/X cocktail i.p.). The supplemental doses of Ketamine were given at a dose of 100 mg/kg and the animal's respiration rate were monitored for a few minutes to determine if additional doses are needed. For

each mouse, baseline measurements of resistance and compliance were performed that consists of a slow stepwise or continuous (ramp) inflation to total lung capacity and deflation back to forced respiratory capacity, controlling for pressure. Immediately following, increasing doses of methacholine (0, 1, 3, 6, 12, 25, and 50 mg/ml) were delivered via aerosol and resistance and compliance were measured. Airway resistance and dynamic compliance for each Mch dose was calculated and the average ± SEM was plotted for all treatment group. Immediately following lung function determination, bronchoalveolar lavage was performed and blood plasma and lung tissues were harvested and stored for further analyses.

VI. Animal necropsy and tissue collection

For scheduled necropsies, mice were humanely euthanized using Euthasol solution (390 mg sodium pentobarbital/50 mg phenytoin sodium, Verbac AH Inc.) by intraperitoneal (IP) injection (200µg/g b. wt.). Euthanasia was confirmed by exsanguination followed by open chest necropsy. Blood plasma was collected, and animals were perfused using PBS and trachea were canulated for bronchoalveolar lavage (BAL) collection followed by lung and liver tissue collection.

VII. Plasma and lavage fluid analysis

Blood plasma was collected in EDTA-coated tubes following centrifugation and aliquots were stored for further analysis. BAL fluid and cells were collected, and aliquots were stored for further analysis. Plasma and BAL fluid were analyzed for IgE and T_H2 cytokine (e.g., IL-13) levels by specific ELISAs as per the

manufacturers' instructions. BAL cells were cytospun onto slides and stained for eosinophils by immunostaining.

VIII. Lung tissue analysis

Post-euthanasia and BAL collection the canulated trachea and lungs were either snap-frozen or were fixed in formalin for 2h while hanging under a constant pressure equivalent to 25cm. The formalin-fixed lungs were then for paraffin-embedding and lung tissue sections were prepared. Histochemical staining with H&E was carried out to assess the gross lung morphology. Serial sections were also stained with Alcian Blue (Richard-Allan Scientific) and AB/PAS to stain for mucin glycoproteins. The airway epithelial cell and mucous cell numbers per mm basal lamina (BL) were measured using the BZX700 All-in-one microscopy system (Keyence Inc., Japan). Another set of serial sections were used for airway mucin MUC5AC and eosinophil dual-immunostaining. In all cases, quantification and morphometry was carried out by a person unaware of slide identity.

The snap-frozen lung tissue aliquots were used for RNA isolation and gene expression analysis of select cytokines and inflammatory factors (*IL-6*, *IL-13*, and airway mucin *Muc5ac* and its master transcriptional regulator *Spdef* mRNA levels) using a real-time qRT-PCR analysis.

IX. Statistical analysis

Grouped results were expressed as means ± SEM and $p < 0.05$ was considered significant. Data were analyzed using GraphPad Prism Software

(GraphPad Software Inc.) using one-way analysis of variance (ANOVA) or a two-way ANOVA and with a post-hoc multiple comparison analysis. When significant effects were detected ($P < 0.05$), Fisher's least significant difference and student's t test was used to determine differences between groups.

Appendix 1: Results

I. Exposure conditions

Animals in all the chambers were exposed to similar environmental conditions as reflected by the average temperature and humidity recorded during the study as shown in **Table 5**. The average temperature in all of the chambers ranged between 20.32° C to 21.73° C with the humidity levels ranging from 49.92 to 56.69%.

Table 6. Average chamber temperatures and humidity percentages during the study period.

Chamber	Initial		End Temp (°C)		End Humidity (%)	
	Temp (°C)	Humidity (%)	Min	Max	Min	max
NC	21.36	55.38	21.12	21.73	53.08	56.92
PC	21.11	54.92	21.06	21.45	53.31	56.62
TF	20.37	55.54	20.32	21.02	51.62	56.69
CF	20.85	53.08	20.82	21.61	49.92	54.54

II. CDE aerosol concentrations

The analysis of the cat dander allergen protein Fel D1 in all of the chambers' air samples was performed by Indoor Technologies Inc. There were comparable levels of CDE aerosol generated in each of the chambers (PC, TF, and CF chambers) throughout the six-weeks of study with an average Fel D1 levels achieved at 60.05, 64.74, and 59.62 ng of Fel D1 (**Table 6**). Most importantly, the

air samples collected pre- and post- air-filtration shows that both the Test filter and the Control filter were able to completely suppress the Fel D1 levels in the each of the chambers compared to the positive control chamber with sham air-filter where there was still 50% of the initial Fel D1 aerosols was present in the air sample.

Table 7. Summary of total aerosol concentrations for FY14-089.

Time	PC Chamber		TF Chamber		CF Chamber	
(weeks)	Pre	Post	Pre	Post	Pre	Post
1	55.08	22.60	70.00	BDL	63.26	BDL
2	76.94	43.01	53.93	BDL	47.07	BDL
3	97.21	44.97	54.18	BDL	50.55	BDL
4	46.13	27.34	82.05	0.08	71.51	BDL
5	55.91	46.15	65.78	BDL	71.45	BDL
6	29.02	17.36	62.54	BDL	53.89	BDL
Mean	**60.05**	**33.57**	**64.74**	**0.08**	**59.62**	**BDL**
±SEM	9.77	5.16	4.33	BDL	4.35	BDL

*BDL- below detection limit

III. Mice body weights and daily observations

Animals in the study weighed between 26g and 32g in the beginning of the study with average body weight in each group around 30g. The changes in the body weights were calculated as the percentage of the initial body weight for each mouse and average change was plotted for each group (**Figure 40**). Animals in the room air gained around 8% of body weight during the study whereas the mice exposed to CDE aerosol failed to gain any weight with no significant difference among the PC, TF, and CF mice.

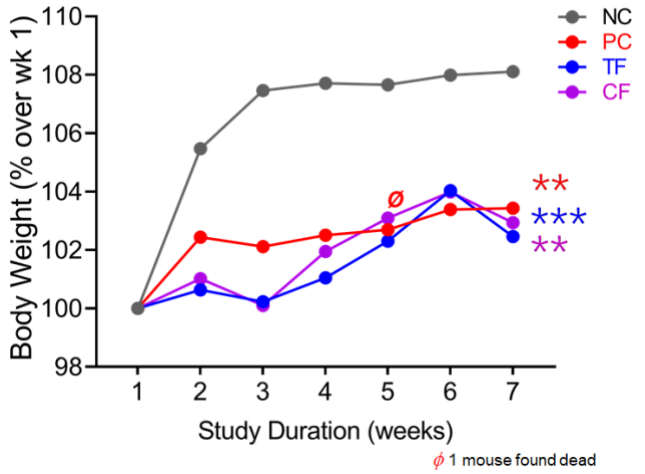

Figure 40. Average changes in the weekly body weights of mice in each group during the study.

IV. Lung function analyses

Five animals in each group were subjected to pulmonary function analysis to determine changes in airway hyperreactivity following methacholine (Mch) bronchoprovocation. There was significant increase in airway resistance in PC group of mice at 3 and 6 mg/ml of Mch challenges compared to the NC group (**Figure 41A and 41C**). Both the TF and CF mice airways were not sensitive to Mch challenges with changes in lung function parameters not distinctive from the NC group indicating that air-filtration by both TF and CF has functionally suppressed the CDE allergen levels. There were no significant changes observed in the dynamic compliance of mice airways for any of the groups tested (**Figure 41B and 41D**).

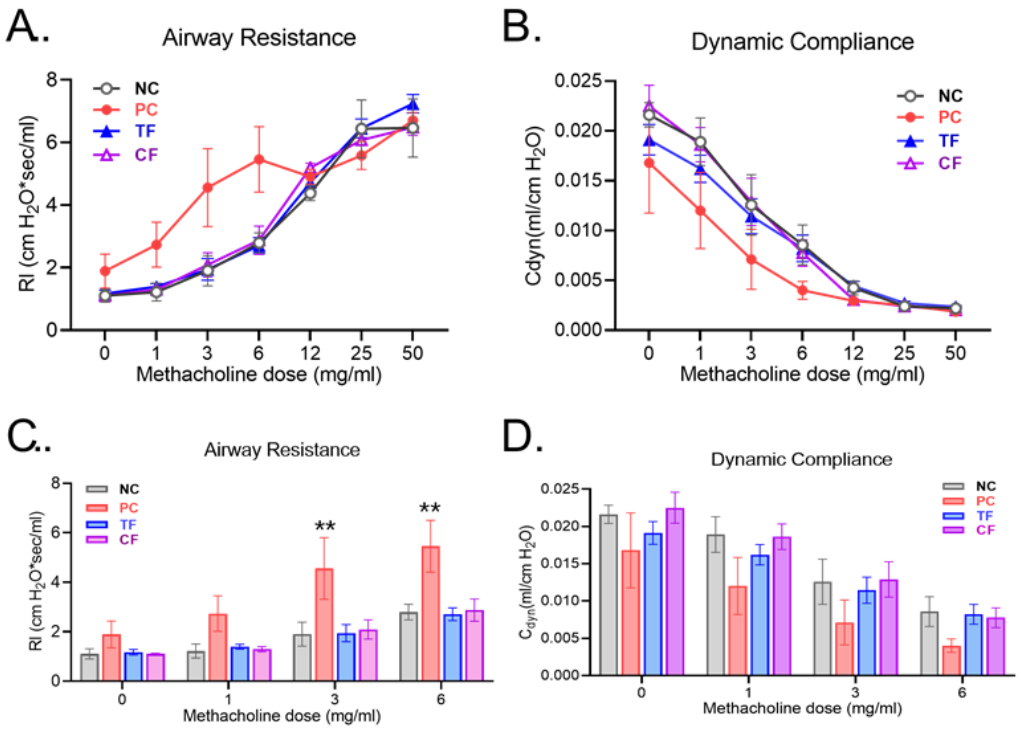

Figure 41. Changes in airway resistance (**A. and C.**) and dynamic compliance (**B. and D.**) of mice in each group following the increasing dose of methacholine aerosol challenges. Data shown as mean ± SEM for each datapoint; data analyzed by 2-way ANOVA; **p<0.01.

V. Lavage cells and airway eosinophilia

Among the BAL cells collected, there were on an average 3.53 x10^5 cells/ms in the NC group. The CDE allergen induce the cellularity in BAL by 4-fold yielding 12.05 x 10^5 cells/ms in PC group. There was significant attenuation of the BAL cell recruitment in TF animals with an average of 6.14 x 10^5 cells/ms (**Figure 42A**), whereas the CF mice only showed a trend toward lower BAL cell counts with an average of 9.44 x 10^5 cells/ms. Most of this cell infiltration was due to eosinophil recruitment as determined by immunostaining of BAL cytospins (**Figure 42B**) and quantification per mouse (**Figure 42C**) as well as eosinophils as a part of BAL cell

percentage (**Figure 42D**), wherein they accounted for around 32% of BAL cells in PC group with 3.96 x 10^5 Eos/mouse, and were significantly suppressed in the TF mice.

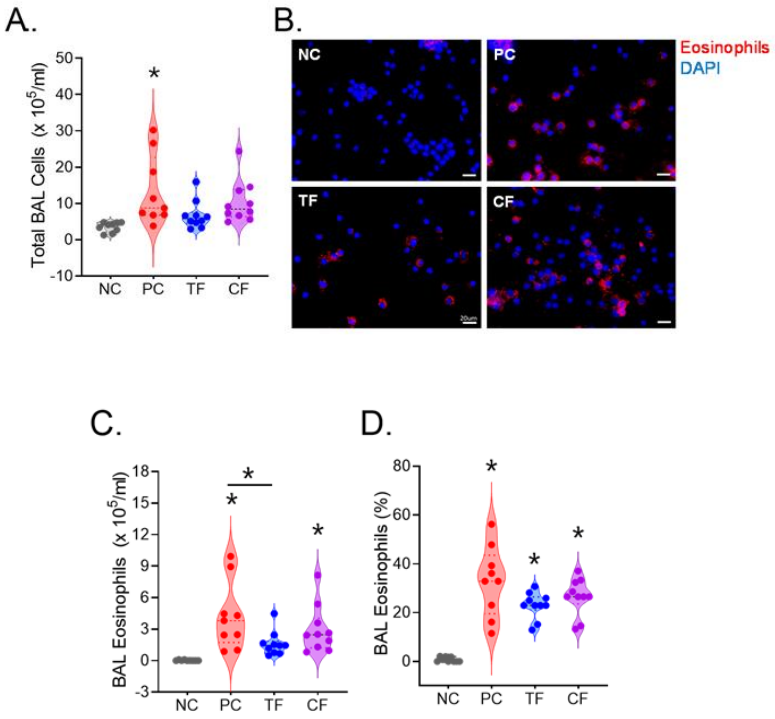

Figure 42. CDE aerosol induced airway eosinophilia is suppressed by Test filter use. **(A.)** Violin plot analysis of total BAL cells obtained from each group where each dot represents individual mouse per group. **(B.)** Representative micrographs showing immunostained eosinophils (shown in red) in BAL cytospins for each group with nuclei stained with DAPI (shown in blue), scale bar - 10µ. Quantitation of **(C.)** total eosinophils and **(D.)** eosinophil percentage per ms in each group. Data analyzed by ANOVA (n=10/gp except for PC, n=9); *p<0.05.

VI. Plasma and lavage IgE and IL-13 levels

Plasma and lavage fluid collected from each mouse were assessed for total IgE levels and IL-13 cytokine levels using respective ELISAs. There was a significant increase in plasma IgE levels that were attenuated in the TF and CF

group (**Figure 43A**). A similar significant suppression was observed in the plasma IL-13 levels of TF and CF groups that was induced in the PC group (**Figure 43B**). Analysis of BALF IgE levels also showed a similar trend where CF showed a better attenuation of CDE-induced IgE levels (**Figure 43C**) but there was no difference in the BALF IL-13 levels among the mice of all the groups analyzed (**Figure 43D**).

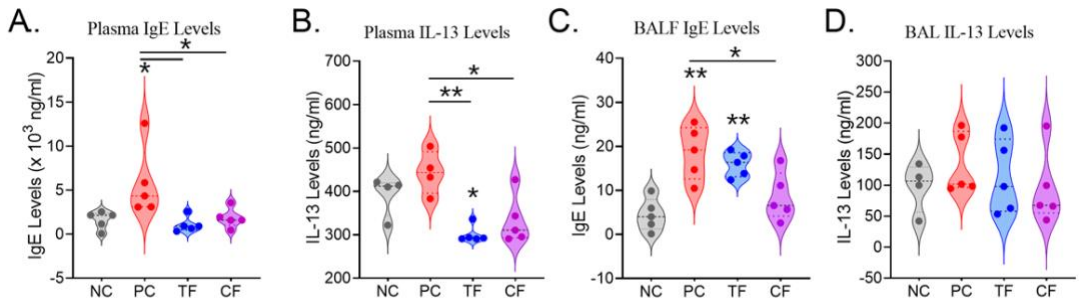

Figure 43. Quantitation of plasma **(A.)** IgE and **(B.)** IL-13, and BALF **(C.)** IgE and **(D.)** IL-13 levels in mice from each group as determined by ELISA. Data analyzed by ANOVA (n=5/gp); *p<0.05; **p<0.01.

VII. Inflammatory gene expression

Among the inflammatory genes analyzed there was not significant difference observed in the levels of *IL-6, IL-13, Muc5ac,* and *Spdef* mRNA levels in any of the mice groups (**Figure 44**).

VIII. Lung tissue histopathology

There was no significant difference in gross lung tissue histopathology in any of the groups in terms of cellularity around airways, blood vessels, or in parenchyma (**Figure 45A**). However, the axial airways showed increased mucous metaplasia in PC mice as shown in Figure 8B and the TF and CF group showed some attenuation of the mucous cell numbers per mm BL (**Figure 45B**).

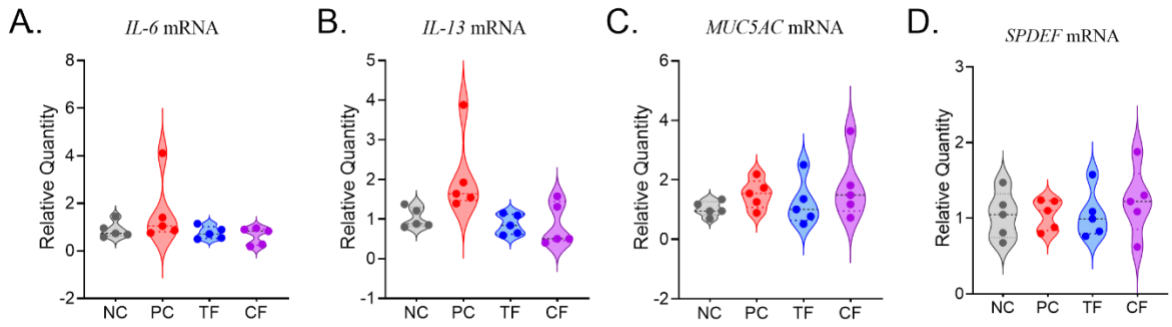

Figure 44. Relative quantities of IL-6, **(A.)** IL-13, **(B.)** MUC5AC, **(C.)** and SPDEF **(D.)** mRNA levels in NC, PC, TF, and CF mice lung tissues as analyzed by the real-time qRT-PCR analysis.

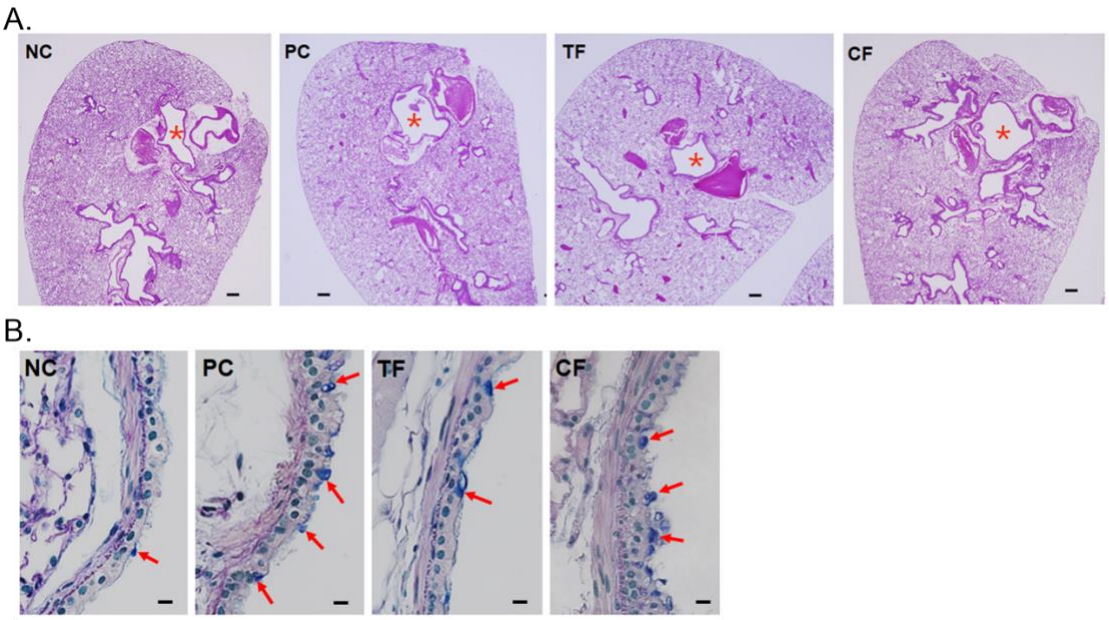

Figure 45. Representative micrographs of mouse lung tissue from each group showing gross morphology and airway mucous metaplasia. **(A.)** Low magnification images of whole lung section stained with H&E showing the bronchial airways (marked with a red asterisk), scale – 200 µM. **(B.)** A high magnification image of lung axial airways stained with AB/PAS showing the AB+ mucin glycoprotein marking the mucous/goblet cells (marked with red arrows), scale – 10 µM.

IX. Airway mucous metaplasia and peribronchial eosinophilia

The changes in mucous cell metaplasia were further confirmed by immunostaining of serial sections with antibody to Muc5ac that showed significant

attenuation in TF mice than the CF mice (**Figure 46A-46B**). The sections were also co-stained for eosinophils that marked a significant peribronchial eosinophilia in PC mice compared to NC mice and the TF significantly attenuated this increased eosinophil recruitment whereas CF group mice failed to show any change from the PC group (**Figure 46A and 46C**).

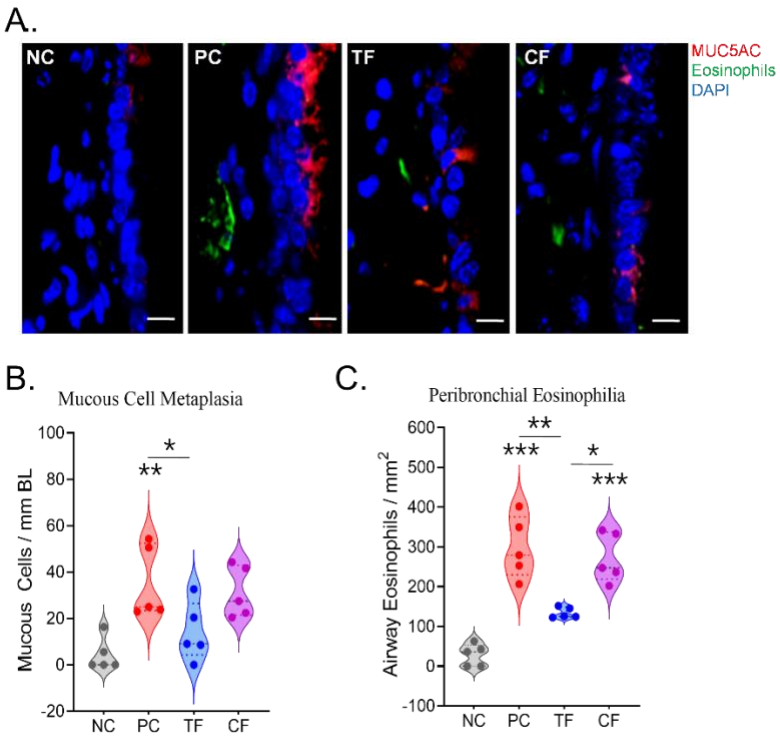

Figure 46. The airway mucous cell metaplasia and peribronchial eosinophilia caused by CDE aerosol exposure is mitigated by Test air-filter. **(A.)** Representative micrographs showing airway Muc5ac+ mucous/goblet cells (shown in red) and the eosinophils (shown in green) with nuclei stained with DAPI (shown in blue), scale bar - 10µ. Quantitation of **(B.)** mucous cells per mm of BL and **(C.)** Eosinophils per mm^2 area in each group of mice.

Appendix 2: E-Cigarette Aerosols such as Synthetic Cooling Agent WS-23 and Nicotine Differentially Modulate Airway Epithelial Cell Responses

Appendix 2: Introduction

I. Synthetic Cooling Agent WS-23 and Nicotine Modulation of Airway Epithelial Cell Responses

Recent studies have found that e-cigarette (e-cig)/electronic nicotine delivery systems (ENDS) use during smoking cessation led to both a reduced effectiveness in cessation and a higher relapse rate as compared to no product use. (274-278) Menthol usage in e-cigarettes, e-liquids, and other ENDS products is known to enhance the appeal of these products, particularly to young adult users, as it reduces the harshness and bitterness of the products. (279, 280) The U.S. Food and Drug Administration (FDA) recently banned flavorings other than menthol and tobacco in closed pod systems, dramatically increasing the use of menthol-containing e-cig/ENDS products. (281, 282) Reports have suggested that this change may have led to increased presence of menthol and cooling agents such as WS-23 in e-cig products which may ultimately exposure users to more harm. (283) Chemical analysis of various menthol-flavored e-cig products corroborated the presence of various harmful compounds (283-286). Despite efforts to curb the appeal of e-cigarettes, particularly to young adults, the use of menthol and "iced/cooling" flavors has only increased in popularity and has potentially contributed to the increased addictive properties of e-cigarettes. (286) Considering the recent outbreak of e-cigarette or vaping use-associated lung injury

(EVALI) the current rate of e-cig use may cause severe comorbid conditions among a larger population. (287) Among various cooling agents analyzed, the synthetic cooling agent WS-23 was reportedly used most prominently. (288) 2-isopropyl-N,2,3-trimethylbutyramide, commonly known as WS-23, was found to be present in most e-liquids marketed in the U.S. in quantities that may exceed consumer exposure safety standards. (288)

Although studies on the biological effects of WS-23 are lacking, a recent report found that there may be cytotoxicity induced by WS-23 exposure in vitro. (283) One study found that various flavoring products induced ROS generation and superoxide production in vitro in lung epithelial cell lines and monocytes. (289) Similarly, ROS generation and pro-inflammatory effects were observed to be induced by e-cig aerosol/vape exposure; these effects were further amplified by flavored e-cigs in periodontal fibroblasts. (290) Furthermore, e-cig use affected lung inflammatory responses, and importantly, the aerosols consisting of propylene glycol/vegetable glycerin (PG/VG) vehicle alone were found to induce a potent pro-inflammatory response and immune infiltration in BAL fluid (BALF). (291)

The respiratory AECs are pivotal to innate immune defense against inhaled toxicants/allergens, and the AEC responses to aerosolized e-cig components are crucial for orchestrating the lung immune responses. (68, 167) Any dysregulation in AEC-mediated responses can significantly impact the susceptibility to infection (292); a recent study has shown that e-cig use induces a reduction in AEC ciliary

beating frequency, as well as changes in cytokine and chemokine production. (293) Nevertheless, the impact of synthetic cooling agents such as WS-23 individually has not been investigated. With the continuously increasing usage of the WS-23 cooling agent, coupled with the increased usage of e-cigarettes, particularly in young adults, there is a need to assess the effects of WS-23 aerosols/vapes on both AECs and the innate immune response of airways.

Appendix 2: Materials and Methods

I. Human airway epithelial cell culture

Primary human AECs were seeded in clear TC-treated 6-well plates (Corning Costar®) using bronchial epithelial cell growth media (BEGM, Lonza, or UNC MLI Cell Culture Core), and e-cig aerosol treatments were started 24 hours after seeding. Alternatively, primary AECs were also grown in air-liquid interface (ALI) cultures as described previously (2) and cells were differentiated for a minimum of 21 days before treatments.

II. E-liquid reagents and e-cig aerosol/vape exposures

E-liquid synthetic cooling and flavoring agent WS-23 (CAS#51115-67-4, from FlavorJungle, Bellingham, WA) was used with or without Nicotine (Sigma-Aldrich, Inc.), and PG/VG (1:1, propylene glycol: vegetable glycerin) was used as a vehicle control. There were four treatment groups, where cells were treated with PG/VG, 3% WS-23 in PG/VG, 2.5% Nicotine in PG/VG, or 2.5% Nicotine + 3% WS-23 prepared in PG/VG. Human AECs were exposed to e-liquid aerosols using

the Buxco E-cigarette, Vapor, and Tobacco (EVT) exposure system (Data Sciences International, St. Paul, MN, USA) as described before (294). Briefly, cells were exposed to e-cig aerosols for 15 minutes per day with a puff topography of 2 puffs/minute (3 s/puff, 55 mL/puff). Smok® X-Priv mod kit was used for smoke delivery installed with Prince® V12 triple mesh coils with 90 watts coil wattage. After exposure, cells were incubated at 37°C and 5% CO_2 for another 24 hours and cells and media supernatant were harvested after 48 and 72 hours of exposure. Cell viability was assessed by the trypan blue exclusion method. Briefly, trypsinized cells were resuspended in phosphate-buffered saline (PBS), and samples were mixed 1:1 with 0.4% trypan blue solution (catalog no. 302643; Sigma-Aldrich), and live/dead cells were counted using TC20 automated cell counter (Bio-Rad Inc).

III. Inflammatory gene expression analysis by qRT-PCR

Total RNA extraction was performed using the RNeasy Mini kit (Qiagen) according to the manufacturer's instructions, and cDNAs were synthesized using the Applied Biosciences High-Capacity RNA-to-cDNA® Synthesis Kit (Thermo Fisher Scientific, Inc), per manufacturer's instructions. Expression levels of *ICAM-1* and *IL6* mRNAs were quantified using SYBR Green-based primers and the iTaq master mix (Bio-Rad Inc) in the Bio-Rad CFX Real-Time PCR detection system (Bio-Rad Inc). Relative quantification data were obtained using the delta-delta (ΔΔ)Ct method by normalizing to the respective *beta-actin* and/or *GAPDH* mRNA levels as described recently. (2)

IV. Secretory inflammatory factor analysis by ELISA

The protein levels of ICAM-1 and IL-6 were determined using human ELISA kits against ICAM-1 (LifeSpan Biosciences Inc., Seattle, WA) and IL-6 (BioLegend Inc., San Diego, CA), respectively, as per manufacturers' instructions.

V. Immunocytochemical staining and imaging analysis

For immunocytochemical staining, cells were fixed with 4% paraformaldehyde (PFA) and washed in 0.05% v Brij-35 in PBS (pH 7.4) and immunostained using antibodies to MUC5AC (Millipore Inc., Burlington, MA), CCSP (Santa Cruz Biotechnology, Santa Cruz, CA) and β-tubulin (Cell Signaling Tech., Danvers, MA) or isotype controls. Briefly, cells were blocked using a solution containing 3% BSA, 1% Gelatin, and 1% normal donkey serum with 0.1% Triton X-100 and 0.1% Saponin and were stained with antibodies. The immunolabelled cells were detected using respective secondary antibodies conjugated fluorescent dyes (Jackson ImmunoResearch Lab Inc., West Grove, PA) and mounted with 4',6-diamidino-2-phenylindole (DAPI) containing Fluormount-G™ (SouthernBiotech, Birmingham, AL) for nuclear staining. Immunofluorescent images were captured using the BZX700 Microscopy system (Keyence Corp., Japan) and analyzed using NIH Image J software.

VI. Statistical analysis

Data expressed as mean±SEM were analyzed using GraphPad Prism Software (GraphPad Software Inc.) using one-way analysis of variance (ANOVA) with and following Tukey's multiple comparison test. When significant main effects

were detected (p<0.05), student's t-test was used to determine differences between the groups. Studies were performed following three separate experiments.

Appendix 2: Results

I. Exposure to synthetic cooling agent WS-23 aerosols modulates airway epithelial cell viability

We first analyzed the effects of aerosolized 3% WS-23 on cell viability of AECs in submerged cultures at 48 and 72h of treatment. The viable cell counts showed no significant change in cell numbers among all the groups tested. However, the WS-23 aerosol-treated cells showed a trend toward reducing viable cell numbers (**Figure 47A**). Interestingly, at 72h of treatment, specifically in cells treated with 3% WS-23 or 2.5% nicotine aerosols, we observed a significant increase in viable cell numbers, but there was no synergistic effect observed in cells treated with WS-23+nicotine combination (**Figure 47B**). It is noteworthy that cells treated with PG/VG aerosols showed a marked reduction in cell numbers at 72h compared to 48h of treatment.

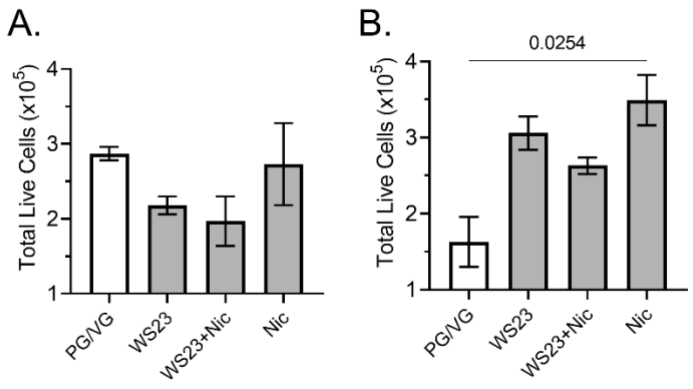

Figure 47. Synthetic flavoring agent WS-23 aerosols induce cell proliferation in AECs following 72 h of treatment. Live cell numbers following **(A.)** 48h, and **(B.)** 72h treatment with aerosolized PG/VG (50:50), PG/VG + 3% WS-23, PG/VG + 3% WS-23 + 2.5% nicotine, or PG/VG + 2.5% nicotine using Buxco EVT system. Data shown as mean ±SEM and analyzed by one-way ANOVA, n=2/gp. Original source (295).

II. PG/VG vehicle induces an inflammatory response in human AEC independent of nicotine and WS-23

As PG/VG has been shown to dysregulate AEC responses (296) we analyzed *IL-6* and *ICAM-1* mRNA levels upon exposure to PG/VG for 24h, 48h, and 72h. Interestingly, we observed a significant increase in both *IL-6* and *ICAM-1* mRNA at 48h of exposure, which was further potentiated at 72h of exposure time (**Figure 48A-48B**). These data suggest that PG/VG vehicle without added constituents can dysregulate the cellular responses, which may be further potentiated or inhibited by the addition of nicotine or WS-23.

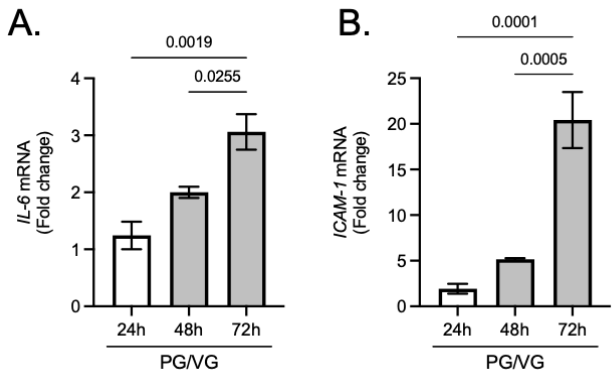

Figure 48. Propylene glycol (PG)/Vegetable glycerin (VG) induces increased IL-6 and ICAM-1 expression at 48h and 72h of exposure time. **(A.)** IL-6 and **(B.)** ICAM-1 mRNA levels upon 24h, 48h, and 72h of exposure to PG/VG vehicle. Data shown as mean±SEM and analyzed by one-way ANOVA, n=2/gp. Original source (295).

III. WS-23 aerosols alter innate inflammatory response kinetics of human AECs

We next analyzed the effects of WS-23 aerosols on AEC mRNA expression of inflammatory factors, *IL-6,* and *ICAM-1,* which are important modulators of AEC innate responses (2). At 48h of treatment, *IL-6* mRNA levels were significantly reduced by WS-23 or nicotine aerosol exposure, as the WS-23, WS-23+nicotine, and nicotine alone aerosol treated groups presented with 2.0-fold or higher reduction in *IL-6* mRNA levels, compared to PG/VG-treated controls (**Figure 49A**). In contrast, cells treated with WS-23 or nicotine aerosols showed a trend towards increased *ICAM-1* mRNA expression; however, WS-23+nicotine combined treatment induced a significant increase in *ICAM-1* expression (**Figure 49B**). Thus, *ICAM-1* mRNA levels were increased by WS-23 and nicotine treatments, and treatment with both WS-23 and nicotine in conjunction (WS-23+nicotine) further potentiated the increase in *ICAM-1* mRNA levels.

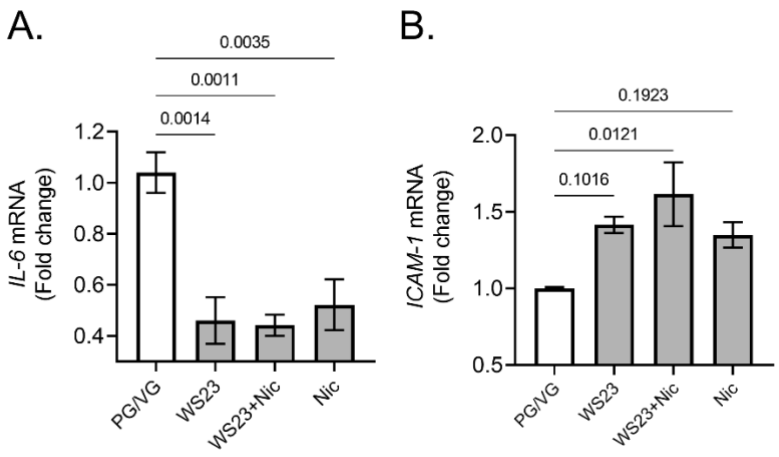

Figure 49. WS-23 flavored e-liquid aerosols suppress the expression of IL-6 and induce the expression of ICAM-1 following 48 h of treatment. Relative quantities of **(A.)** IL-6 and **(B.)** ICAM-1 mRNAs following 48 h exposure to aerosolized PG/VG, PG/VG + WS-23, PG/VG + WS-23 + nicotine, or PG/VG + nicotine. Data shown as mean±SEM and analyzed by one-way ANOVA, n=2/gp. Original source (295).

After 72h of treatment, we observed a similar trend in the expression levels of *IL-6* mRNA. Cells treated with WS-23, WS-23+nicotine, and nicotine alone aerosols presented with a 1.5-, 1.7-, and 2.0-fold decrease in *IL-6* mRNA levels, respectively, compared to PG/VG-treated controls after 72h of treatment (**Figure 50A**). Surprisingly, *ICAM-1* mRNA levels were markedly reduced, with WS-23, WS-23 + nicotine, and nicotine alone treatments causing a 1.8-, 1.75-, and 1.88-fold reduction in *ICAM-1* expression, respectively, when compared to the PG/VG-treated controls (**Figure 50B**).

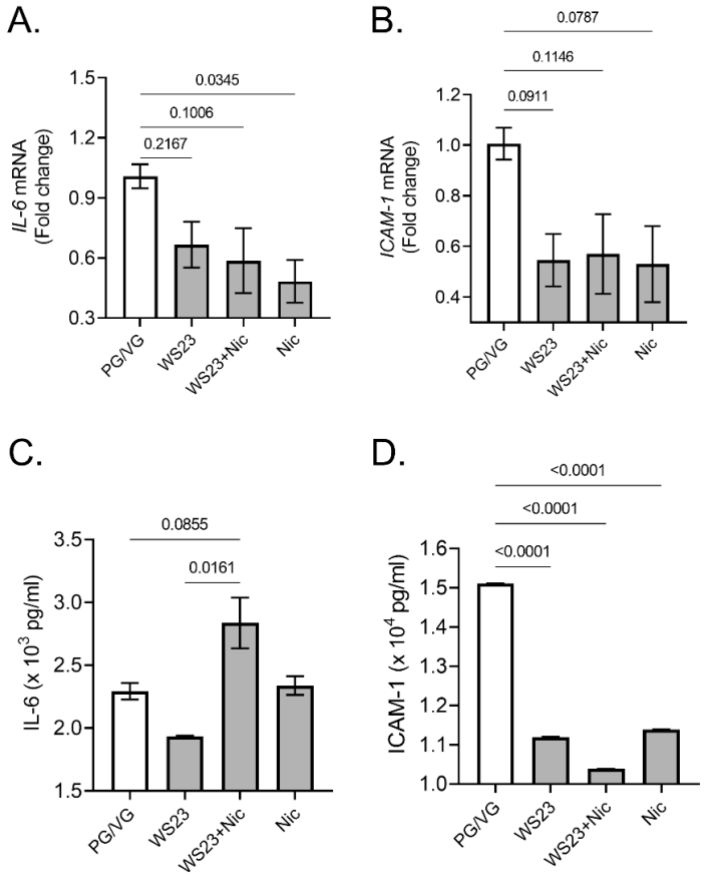

Figure 50. Aerosolized WS-23 exposure suppresses IL-6 and ICAM-1 expression and secretion in conjunction with nicotine aerosol exposure. Relative quantity of **(A.)** IL-6, and **(B.)** ICAM-1 mRNA levels following 72 h of exposure as evaluated by qRT-PCR. Secreted protein levels of **(C.)** IL-6, and **(D.)** ICAM-1 as evaluated in cell culture supernatants by specific ELISA assays after 72 h of aerosol exposure. Data shown as mean±SEM and analyzed by one-way ANOVA, n=2/gp. Original source (295).

We next corroborated these results by investigating the changes in protein levels of secretory IL-6 and ICAM-1 in culture media supernatants harvested at 72 h treatment. Interestingly, IL-6 secretory levels were on an average 2,292 pg/ml in PG/VG control culture media; and 1,932 pg/ml in WS-23; 2,835 pg/ml in WS-23+nicotine; and 2,338 pg/ml in nicotine treated groups (**Figure 50C**). There was

a significant reduction in ICAM-1 expression upon all three treatments. The PG/VG control treatment presented with 15,105 pg/ml of ICAM-1, whereas the WS-23, WS-23+nicotine, and nicotine alone treatments presented an average of 11,196, 10,381, and 11,388 pg/ml, respectively (**Figure 50D**). Thus, aerosolized synthetic cooling agent WS-23 alters the innate airway immune responses of human AECs.

IV. WS-23 aerosol exposure modulates the goblet cell differentiation in AECs

Next, we analyzed the effects of WS-23 aerosols on a differentiated AEC population cultured on an air-liquid interface. Groups of Transwells were treated with aerosolized PG/VG vehicle, WS-23, nicotine, and WS23+nicotine. After 72 h treatment, there were significant changes in MUC5AC+ mucous/goblet cells by both WS-23 or nicotine aerosol exposure (**Figure 51A**). The WS-23 and nicotine alone aerosol treated groups presented with increased goblet cells compared to PG/VG-treated controls, but there was no synergistic effect of WS-23+nicotine combination exposure (**Figure 51B**). In contrast, there was a reduction in CCSP+ secretory club cells in WS-23, WS-23+nicotine, or nicotine aerosols treated groups (**Figures 51C-51D**). Thus, WS-23 and nicotine aerosols modulate the airway secretory cell population by affecting the goblet cell hyperplasia, which could impact the respiratory physiology and needs further validation using in vivo exposure models.

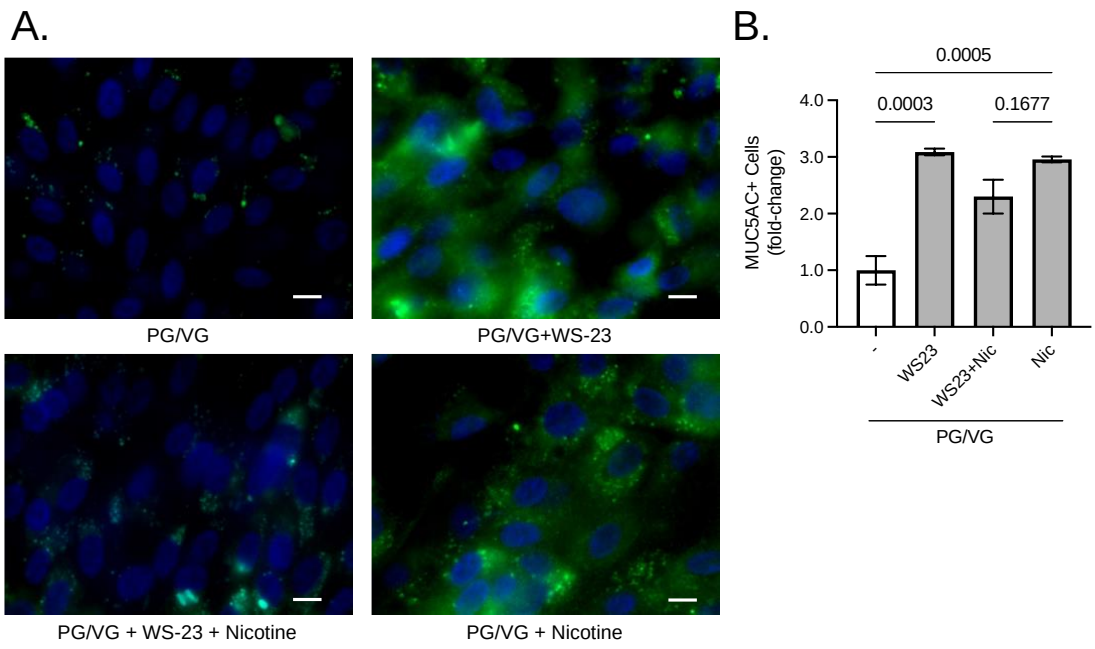

Figure 51. Aerosolized WS-23 exposure augments MUC5AC+ goblet cell hyperplasia and reduces the CCSP+ secretory club cell population in differentiated AECs. **(A.)** Representative micrographs showing MUC5AC immunopositivity (shown in green) in AECs treated with aerosolized PG/VG, PG/VG + WS-23, PG/VG + WS-23 + nicotine, or PG/VG + nicotine, and nuclei were stained by DAPI (shown in blue), scale – 5µm. **(B.)** Quantification of MUC5AC-positive (+) goblet cells in each treatment group. **(C.)** Representative micrographs showing CCSP immunopositivity (shown in red) in AECs treated with e-liquid aerosols. **(D.)** Quantification of CCSP-positive (+) cells in each group after 72h of aerosol exposure. Data shown as mean±SEM and analyzed by one-way ANOVA, n=2/gp. Original source (295).

Appendix 2: Discussion

The FDA considers flavoring and cooling agents safe when utilized as food additives; however, the risks associated with their inhalation, through vaping, are poorly defined. (297) Little is known about how e-cig constituents affect the respiratory tract, specifically when emerging evidence indicates that the acute effects of e-cig products use on the respiratory system need to be revisited. (296, 298-301) Furthermore, it has been reported that menthol, in concentrations found

in e-cig aerosols may disturb cell homeostasis and can trigger oxidative stress via the NF-κB pathway. (302) Induction of oxidative stress and chronic mitochondrial dysregulation is central in many pathologic conditions such as chronic inflammatory and aging-associated degenerative diseases. (205) Most importantly, alarmingly high toxic levels of synthetic cooling agents/coolants such as WS-3 or WS-23 carboxamides are used in the emerging e-cigs products. Still, the risk associated with their inhalation and safety regulations is understudied. These are not only found in mint/menthol-flavored products but also in the fruit-, candy-, and ice flavors, including the popular disposable pod- and mod-based products. Even without nicotine or flavoring agents, e-cig use can induce significant changes in the lung epithelium; one study found that chronic exposure to e-cig aerosols in a mouse model suppresses the innate immune response, particularly against viral infection. (296) Aerosolized e-liquid solvents exposure induces significant changes in the airway epithelium, with or without added flavoring elements. However, the results are highly variable. Contrasting changes in inflammatory factors expression were reported on a significant increase either in expression or with no change in the expression levels of IL-6 and CXCL-8. (293) This discrepancy could be mainly attributed to the exposure systems used for e-cig aerosols and the addition of nicotine or other flavoring chemicals. (293) There have been significant variations in study design, and the need for further investigation is dire. As newer ENDS emerge and regulations continue to change with evolving consumer preferences, it is crucial to understand the effects of prominently used flavoring compounds, like WS-23. Our results further indicate

that PG/VG dysregulates cellular responses with or without nicotine or flavoring agents. Notably, we found that those responses were inhibited by adding additional constituents such as WS-23 and nicotine.

In this study, we used a submerged culture model of primary AECs and exposed them to e-cig vapor using PG/VG as a vehicle-only control and compared the effects to those with PG/VG and WS-23, nicotine or WS-23 and nicotine exposure. Our results demonstrated that even at 48h after exposure, there is a significant reduction in the expression levels of IL-6, and concurrently, a trend of increased expression of ICAM-1, with a significant increase in ICAM-1 levels upon WS-23+nicotine treatment. These data further corroborate the observations that WS-23 may alter the innate immune responses of AEC. Suppressing the IL-6 levels may hinder the rapid AEC immune response to pathogen presence. (303) Alternatively, the increased levels of ICAM-1 suggest a differential effect on regulatory pathways. It has been reported that e-cig exposure without nicotine may induce a transient increase in secretory ICAM-1 levels; however, the effects of WS-23 on these pathways have not been thoroughly investigated. (304) Furthermore, at the 72-hour time point, we observed a significant reduction in the expression of *IL-6* mRNA levels, the expression of *ICAM-1* mRNA levels, and the secretory protein levels of ICAM-1. Research evaluating the effect of WS-23 on MUC5AC+ goblet cells and airway epithelial cells is lacking; however, it has been shown that WS-23 may induce MUC5AC expression in patients with chronic obstructive pulmonary disease (COPD) by binding to transient receptor potential cation

channel (TRMP)8, which is upregulated in COPD patients. (305, 306) Nicotine exposure has been well established as an inducer of mucin MUC5AC expression. (307, 308) Here, we report that WS-23 may be inducing a similar response independent of nicotine presence and may require further investigation into long-term effects.

Interestingly, it has been reported that nicotine can reduce the levels of CCSP by reducing the transcription factor FOXA2. (309, 310) However, research investigating the effect of WS-23 on CCSP expression is lacking. We found that exposure to both WS-23 and nicotine induced a trend of increased CCSP expression compared to PG/VG control; however, these results were not significant (data not shown). This may suggest that WS-23 induces an acute increase in secretory cells, and further investigation is required into the long-term changes that may be induced by WS-23 exposure, independent of nicotine.

Our data further corroborate the effects of both nicotine and WS-23 on AECs and suggest that flavoring agents may amplify or reduce the toxic effects of various e-cig components such as those induced by PG/VG vehicle and nicotine or nicotine salt additives. Notably, WS-23 and nicotine presence reduced the inflammatory responses that were strongly induced by PG/VG vehicle independently. These data collectively suggest that aerosolized synthetic cooling agent WS-23 alters the innate airway immune responses of human AECs and thus, potentially could increase the susceptibility to respiratory pathologies.

REFERENCES

1. Devadoss D, Acharya A, Manevski M, Houserova D, Cioffi MD, Pandey K, Nair M, Chapagain P, Mirsaeidi M, Borchert GM, Byrareddy SN, Chand HS. Immunomodulatory LncRNA on Antisense Strand of ICAM-1 Augments SARS-CoV-2 Infection-associated Airway Mucoinflammatory Phenotype. *iScience* 2022: 104685.

2. Devadoss D, Daly G, Manevski M, Houserova D, Hussain SS, Baumlin N, Salathe M, Borchert GM, Langley RJ, Chand HS. A long noncoding RNA antisense to ICAM-1 is involved in allergic asthma associated hyperreactive response of airway epithelial cells. *Mucosal Immunol* 2021; 14: 630-639.

3. Manevski M, Devadoss D, Long C, Singh SP, Nasser MW, Borchert GM, Nair MN, Rahman I, Sopori M, Chand HS. Increased Expression of LASI lncRNA Regulates the Cigarette Smoke and COPD Associated Airway Inflammation and Mucous Cell Hyperplasia. *Frontiers in Immunology* 2022; 13.

4. Disease GIfCOL. Global strategy for the diagnosis, management, and prevention of chronic obstructive pulmonary disease 2022 report. Available from: file:///Users/manevskim_home/Downloads/GOLD-REPORT-2022-v1.1-22Nov2021_WMV.pdf.

5. (WHO) WHO. Global Health Estimates. 2019.

6. Pauwels RA, Buist AS, Calverley PM, Jenkins CR, Hurd SS. Global strategy for the diagnosis, management, and prevention of chronic obstructive pulmonary disease. NHLBI/WHO Global Initiative for Chronic Obstructive Lung Disease (GOLD) Workshop summary. *Am J Respir Crit Care Med* 2001; 163: 1256-1276.

7. Global, regional, and national incidence, prevalence, and years lived with disability for 354 diseases and injuries for 195 countries and territories, 1990-2017: a systematic analysis for the Global Burden of Disease Study 2017. *Lancet* 2018; 392: 1789-1858.

8. Adeloye D, Chua S, Lee C, Basquill C, Papana A, Theodoratou E, Nair H, Gasevic D, Sridhar D, Campbell H, Chan KY, Sheikh A, Rudan I, Global Health Epidemiology Reference G. Global and regional estimates of COPD prevalence: Systematic review and meta-analysis. *J Glob Health* 2015; 5: 020415-020415.

9. Adeloye D, Chua S, Lee C, Basquill C, Papana A, Theodoratou E, Nair H, Gasevic D, Sridhar D, Campbell H, Chan KY, Sheikh A, Rudan I. Global

and regional estimates of COPD prevalence: Systematic review and meta-analysis. *J Glob Health* 2015; 5: 020415.

10. Gershon AS, Warner L, Cascagnette P, Victor JC, To T. Lifetime risk of developing chronic obstructive pulmonary disease: a longitudinal population study. *Lancet* 2011; 378: 991-996.

11. Lamprecht B, Soriano JB, Studnicka M, Kaiser B, Vanfleteren LE, Gnatiuc L, Burney P, Miravitlles M, García-Rio F, Akbari K, Ancochea J, Menezes AM, Perez-Padilla R, Montes de Oca M, Torres-Duque CA, Caballero A, González-García M, Buist S. Determinants of underdiagnosis of COPD in national and international surveys. *Chest* 2015; 148: 971-985.

12. Martinez FJ, Mannino D, Leidy NK, Malley KG, Bacci ED, Barr RG, Bowler RP, Han MK, Houfek JF, Make B, Meldrum CA, Rennard S, Thomashow B, Walsh J, Yawn BP. A New Approach for Identifying Patients with Undiagnosed Chronic Obstructive Pulmonary Disease. *Am J Respir Crit Care Med* 2017; 195: 748-756.

13. Disease GIfCOL. Global strategy for the diagnosis, management, and prevention of chronic obstructive pulmonary disease (2020 report). 2020.

14. Vogelmeier CF, Román-Rodríguez M, Singh D, Han MK, Rodríguez-Roisin R, Ferguson GT. Goals of COPD treatment: Focus on symptoms and exacerbations. *Respir Med* 2020; 166: 105938.

15. Wang S. Spatial patterns and social-economic influential factors of population aging: A global assessment from 1990 to 2010. *Soc Sci Med* 2020; 253: 112963.

16. Wong AWM, Gan WQ, Burns J, Sin DD, van Eeden SF. Acute exacerbation of chronic obstructive pulmonary disease: influence of social factors in determining length of hospital stay and readmission rates. *Can Respir J* 2008; 15: 361-364.

17. Saha SP, Bhalla DK, Whayne TF, Jr., Gairola C. Cigarette smoke and adverse health effects: An overview of research trends and future needs. *Int J Angiol* 2007; 16: 77-83.

18. Rabe KF, Watz H. Chronic obstructive pulmonary disease. *Lancet* 2017; 389: 1931-1940.

19. Lortet-Tieulent J, Soerjomataram I, López-Campos JL, Ancochea J, Coebergh JW, Soriano JB. International trends in COPD mortality, 1995-2017. *Eur Respir J* 2019; 54.

20. Lindberg A, Lindberg L, Sawalha S, Nilsson U, Stridsman C, Lundbäck B, Backman H. Large underreporting of COPD as cause of death-results from a population-based cohort study. *Respir Med* 2021; 186: 106518.

21. Mucha L, Stephenson J, Morandi N, Dirani R. Meta-analysis of disease risk associated with smoking, by gender and intensity of smoking. *Gend Med* 2006; 3: 279-291.

22. Kim V, Criner GJ. Chronic bronchitis and chronic obstructive pulmonary disease. *Am J Respir Crit Care Med* 2013; 187: 228-237.

23. Button B, Anderson WH, Boucher RC. Mucus Hyperconcentration as a Unifying Aspect of the Chronic Bronchitic Phenotype. *Ann Am Thorac Soc* 2016; 13 Suppl 2: S156-162.

24. Zhou-Suckow Z, Duerr J, Hagner M, Agrawal R, Mall MA. Airway mucus, inflammation and remodeling: emerging links in the pathogenesis of chronic lung diseases. *Cell Tissue Res* 2017; 367: 537-550.

25. Ridley C, Thornton DJ. Mucins: the frontline defence of the lung. *Biochem Soc Trans* 2018; 46: 1099-1106.

26. Ma J, Rubin BK, Voynow JA. Mucins, Mucus, and Goblet Cells. *Chest* 2018; 154: 169-176.

27. Mall MA, Danahay H, Boucher RC. Emerging Concepts and Therapies for Mucoobstructive Lung Disease. *Ann Am Thorac Soc* 2018; 15: S216-s226.

28. Sears MR, Greene JM, Willan AR, Wiecek EM, Taylor DR, Flannery EM, Cowan JO, Herbison GP, Silva PA, Poulton R. A longitudinal, population-based, cohort study of childhood asthma followed to adulthood. *N Engl J Med* 2003; 349: 1414-1422.

29. Aghapour M, Raee P, Moghaddam SJ, Hiemstra PS, Heijink IH. Airway Epithelial Barrier Dysfunction in Chronic Obstructive Pulmonary Disease: Role of Cigarette Smoke Exposure. *Am J Respir Cell Mol Biol* 2018; 58: 157-169.

30. Hewitt RJ, Lloyd CM. Regulation of immune responses by the airway epithelial cell landscape. *Nat Rev Immunol* 2021; 21: 347-362.

31. Fahy JV, Dickey BF. Airway mucus function and dysfunction. *N Engl J Med* 2010; 363: 2233-2247.

32. Gao W, Li L, Wang Y, Zhang S, Adcock IM, Barnes PJ, Huang M, Yao X. Bronchial epithelial cells: The key effector cells in the pathogenesis of chronic obstructive pulmonary disease? *Respirology* 2015; 20: 722-729.

33. Deprez M, Zaragosi LE, Truchi M, Becavin C, Ruiz García S, Arguel MJ, Plaisant M, Magnone V, Lebrigand K, Abelanet S, Brau F, Paquet A, Pe'er D, Marquette CH, Leroy S, Barbry P. A Single-Cell Atlas of the Human Healthy Airways. *Am J Respir Crit Care Med* 2020; 202: 1636-1645.

34. Schneider C, O'Leary CE, Locksley RM. Regulation of immune responses by tuft cells. *Nat Rev Immunol* 2019; 19: 584-593.

35. Goldfarbmuren KC, Jackson ND, Sajuthi SP, Dyjack N, Li KS, Rios CL, Plender EG, Montgomery MT, Everman JL, Bratcher PE, Vladar EK, Seibold MA. Dissecting the cellular specificity of smoking effects and reconstructing lineages in the human airway epithelium. *Nat Commun* 2020; 11: 2485.

36. Montoro DT, Haber AL, Biton M, Vinarsky V, Lin B, Birket SE, Yuan F, Chen S, Leung HM, Villoria J, Rogel N, Burgin G, Tsankov AM, Waghray A, Slyper M, Waldman J, Nguyen L, Dionne D, Rozenblatt-Rosen O, Tata PR, Mou H, Shivaraju M, Bihler H, Mense M, Tearney GJ, Rowe SM, Engelhardt JF, Regev A, Rajagopal J. A revised airway epithelial hierarchy includes CFTR-expressing ionocytes. *Nature* 2018; 560: 319-324.

37. Basil MC, Cardenas-Diaz FL, Kathiriya JJ, Morley MP, Carl J, Brumwell AN, Katzen J, Slovik KJ, Babu A, Zhou S, Kremp MM, McCauley KB, Li S, Planer JD, Hussain SS, Liu X, Windmueller R, Ying Y, Stewart KM, Oyster M, Christie JD, Diamond JM, Engelhardt JF, Cantu E, Rowe SM, Kotton DN, Chapman HA, Morrisey EE. Human distal airways contain a multipotent secretory cell that can regenerate alveoli. *Nature* 2022; 604: 120-126.

38. Shaykhiev R. Emerging biology of persistent mucous cell hyperplasia in COPD. *Thorax* 2019; 74: 4-6.

39. Ghosh B, Nishida K, Chandrala L, Mahmud S, Thapa S, Swaby C, Chen S, Khosla AA, Katz J, Sidhaye VK. Epithelial plasticity in COPD results in cellular unjamming due to an increase in polymerized actin. *J Cell Sci* 2022; 135.

40. Carolan BJ, Hughes G, Morrow J, Hersh CP, O'Neal WK, Rennard S, Pillai SG, Belloni P, Cockayne DA, Comellas AP, Han M, Zemans RL, Kechris K, Bowler RP. The association of plasma biomarkers with computed tomography-assessed emphysema phenotypes. *Respir Res* 2014; 15: 127.

41. Nishida K, Brune KA, Putcha N, Mandke P, O'Neal WK, Shade D, Srivastava V, Wang M, Lam H, An SS, Drummond MB, Hansel NN, Robinson DN, Sidhaye VK. Cigarette smoke disrupts monolayer integrity by altering epithelial cell-cell adhesion and cortical tension. *Am J Physiol Lung Cell Mol Physiol* 2017; 313: L581-l591.

42. Rogers DF. Physiology of airway mucus secretion and pathophysiology of hypersecretion. *Respir Care* 2007; 52: 1134-1146; discussion 1146-1139.

43. Richmond BW, Brucker RM, Han W, Du RH, Zhang Y, Cheng DS, Gleaves L, Abdolrasulnia R, Polosukhina D, Clark PE, Bordenstein SR, Blackwell TS, Polosukhin VV. Airway bacteria drive a progressive COPD-like phenotype in mice with polymeric immunoglobulin receptor deficiency. *Nat Commun* 2016; 7: 11240.

44. Rose MC, Voynow JA. Respiratory tract mucin genes and mucin glycoproteins in health and disease. *Physiol Rev* 2006; 86: 245-278.

45. Imberty A, Varrot A. Microbial recognition of human cell surface glycoconjugates. *Curr Opin Struct Biol* 2008; 18: 567-576.

46. Kelsen SG. The Unfolded Protein Response in Chronic Obstructive Pulmonary Disease. *Ann Am Thorac Soc* 2016; 13 Suppl 2: S138-S145.

47. Biondi-Zoccai G, Sciarretta S, Bullen C, Nocella C, Violi F, Loffredo L, Pignatelli P, Perri L, Peruzzi M, Marullo AGM, De Falco E, Chimenti I, Cammisotto V, Valenti V, Coluzzi F, Cavarretta E, Carrizzo A, Prati F, Carnevale R, Frati G. Acute Effects of Heat-Not-Burn, Electronic Vaping, and Traditional Tobacco Combustion Cigarettes: The Sapienza University of Rome-Vascular Assessment of Proatherosclerotic Effects of Smoking (SUR - VAPES) 2 Randomized Trial. *J Am Heart Assoc* 2019; 8: e010455.

48. Bahl V, Weng NJ, Schick SF, Sleiman M, Whitehead J, Ibarra A, Talbot P. Cytotoxicity of Thirdhand Smoke and Identification of Acrolein as a Volatile Thirdhand Smoke Chemical That Inhibits Cell Proliferation. *Toxicol Sci* 2016; 150: 234-246.

49. Li X, Yang H, Sun H, Lu R, Zhang C, Gao N, Meng Q, Wu S, Wang S, Aschner M, Wu J, Tang B, Gu A, Kay SA, Chen R. Taurine ameliorates particulate matter-induced emphysema by switching on mitochondrial NADH dehydrogenase genes. *Proc Natl Acad Sci U S A* 2017; 114: E9655-e9664.

50. Bonser LR, Erle DJ. Airway Mucus and Asthma: The Role of MUC5AC and MUC5B. *J Clin Med* 2017; 6.

51. Saco TV, Breitzig MT, Lockey RF, Kolliputi N. Epigenetics of Mucus Hypersecretion in Chronic Respiratory Diseases. *Am J Respir Cell Mol Biol* 2018; 58: 299-309.

52. Anagnostis A, Neofytou E, Soulitzis N, Kampas D, Drositis I, Dermitzaki D, Tzanakis N, Schiza S, Siafakas NM, Tzortzaki EG. Molecular profiling of EGFR family in chronic obstructive pulmonary disease: correlation with airway obstruction. *Eur J Clin Invest* 2013; 43: 1299-1306.

53. Rodrigues SdO, Cunha CMCd, Soares GMV, Silva PL, Silva AR, Gonçalves-de-Albuquerque CF. Mechanisms, Pathophysiology and Currently Proposed Treatments of Chronic Obstructive Pulmonary Disease. *Pharmaceuticals (Basel)* 2021; 14: 979.

54. Feldman MB, Wood M, Lapey A, Mou H. SMAD Signaling Restricts Mucous Cell Differentiation in Human Airway Epithelium. *Am J Respir Cell Mol Biol* 2019; 61: 322-331.

55. Takeyama K, Jung B, Shim JJ, Burgel PR, Dao-Pick T, Ueki IF, Protin U, Kroschel P, Nadel JA. Activation of epidermal growth factor receptors is responsible for mucin synthesis induced by cigarette smoke. *Am J Physiol Lung Cell Mol Physiol* 2001; 280: L165-172.

56. Kettle R, Simmons J, Schindler F, Jones P, Dicker T, Dubois G, Giddings J, Van Heeke G, Jones CE. Regulation of neuregulin 1beta1-induced MUC5AC and MUC5B expression in human airway epithelium. *Am J Respir Cell Mol Biol* 2010; 42: 472-481.

57. Mall MA, Harkema JR, Trojanek JB, Treis D, Livraghi A, Schubert S, Zhou Z, Kreda SM, Tilley SL, Hudson EJ, O'Neal WK, Boucher RC. Development of chronic bronchitis and emphysema in beta-epithelial Na+ channel-overexpressing mice. *Am J Respir Crit Care Med* 2008; 177: 730-742.

58. Fritzsching B, Zhou-Suckow Z, Trojanek JB, Schubert SC, Schatterny J, Hirtz S, Agrawal R, Muley T, Kahn N, Sticht C, Gunkel N, Welte T, Randell SH, Länger F, Schnabel P, Herth FJF, Mall MA. Hypoxic epithelial necrosis triggers neutrophilic inflammation via IL-1 receptor signaling in cystic fibrosis lung disease. *American journal of respiratory and critical care medicine* 2015; 191: 902-913.

59. Cloonan SM, Choi AM. Mitochondria in lung disease. *J Clin Invest* 2016; 126: 809-820.

60. Dela Cruz CS, Kang MJ. Mitochondrial dysfunction and damage associated molecular patterns (DAMPs) in chronic inflammatory diseases. *Mitochondrion* 2018; 41: 37-44.

61. Lerner CA, Sundar IK, Rahman I. Mitochondrial redox system, dynamics, and dysfunction in lung inflammaging and COPD. *Int J Biochem Cell Biol* 2016; 81: 294-306.

62. Nunnari J, Suomalainen A. Mitochondria: in sickness and in health. *Cell* 2012; 148: 1145-1159.

63. Chen ACH, Burr L, McGuckin MA. Oxidative and endoplasmic reticulum stress in respiratory disease. *Clin Transl Immunology* 2018; 7: e1019-e1019.

64. Dufey E, Sepúlveda D, Rojas-Rivera D, Hetz C. Cellular mechanisms of endoplasmic reticulum stress signaling in health and disease. 1. An overview. *Am J Physiol Cell Physiol* 2014; 307: C582-594.

65. Filadi R, Theurey P, Pizzo P. The endoplasmic reticulum-mitochondria coupling in health and disease: Molecules, functions and significance. *Cell Calcium* 2017; 62: 1-15.

66. Marchi S, Bittremieux M, Missiroli S, Morganti C, Patergnani S, Sbano L, Rimessi A, Kerkhofs M, Parys JB, Bultynck G, Giorgi C, Pinton P. Endoplasmic Reticulum-Mitochondria Communication Through Ca(2+) Signaling: The Importance of Mitochondria-Associated Membranes (MAMs). *Adv Exp Med Biol* 2017; 997: 49-67.

67. Oakes SA, Papa FR. The role of endoplasmic reticulum stress in human pathology. *Annu Rev Pathol* 2015; 10: 173-194.

68. Manevski M, Muthumalage T, Devadoss D, Sundar IK, Wang Q, Singh KP, Unwalla HJ, Chand HS, Rahman I. Cellular stress responses and dysfunctional Mitochondrial-cellular senescence, and therapeutics in chronic respiratory diseases. *Redox Biol* 2020; 33: 101443.

69. Kenche H, Baty CJ, Vedagiri K, Shapiro SD, Blumental-Perry A. Cigarette smoking affects oxidative protein folding in endoplasmic reticulum by modifying protein disulfide isomerase. *Faseb j* 2013; 27: 965-977.

70. Somborac-Bacura A, van der Toorn M, Franciosi L, Slebos DJ, Zanic-Grubisic T, Bischoff R, van Oosterhout AJ. Cigarette smoke induces endoplasmic reticulum stress response and proteasomal dysfunction in human alveolar epithelial cells. *Exp Physiol* 2013; 98: 316-325.

71. Geraghty P, Baumlin N, Salathe MA, Foronjy RF, D'Armiento JM. Glutathione Peroxidase-1 Suppresses the Unfolded Protein Response upon Cigarette Smoke Exposure. *Mediators Inflamm* 2016; 2016: 9461289.

72. Geraghty P, Wallace A, D'Armiento JM. Induction of the unfolded protein response by cigarette smoke is primarily an activating transcription factor 4-C/EBP homologous protein mediated process. *Int J Chron Obstruct Pulmon Dis* 2011; 6: 309-319.

73. Kelsen SG, Duan X, Ji R, Perez O, Liu C, Merali S. Cigarette smoke induces an unfolded protein response in the human lung: a proteomic approach. *Am J Respir Cell Mol Biol* 2008; 38: 541-550.

74. Aksoy MO, Kim V, Cornwell WD, Rogers TJ, Kosmider B, Bahmed K, Barrero C, Merali S, Shetty N, Kelsen SG. Secretion of the endoplasmic reticulum stress protein, GRP78, into the BALF is increased in cigarette smokers. *Respir Res* 2017; 18: 78.

75. Kenche H, Ye ZW, Vedagiri K, Richards DM, Gao XH, Tew KD, Townsend DM, Blumental-Perry A. Adverse Outcomes Associated with Cigarette Smoke Radicals Related to Damage to Protein-disulfide Isomerase. *J Biol Chem* 2016; 291: 4763-4778.

76. van Rijt SH, Keller IE, John G, Kohse K, Yildirim A, Eickelberg O, Meiners S. Acute cigarette smoke exposure impairs proteasome function in the lung. *Am J Physiol Lung Cell Mol Physiol* 2012; 303: L814-823.

77. Wang Y, Wu ZZ, Wang W. Inhibition of endoplasmic reticulum stress alleviates cigarette smoke-induced airway inflammation and emphysema. *Oncotarget* 2017; 8: 77685-77695.

78. Flodby P, Li C, Liu Y, Wang H, Marconett CN, Laird-Offringa IA, Minoo P, Lee AS, Zhou B. The 78-kD Glucose-Regulated Protein Regulates Endoplasmic Reticulum Homeostasis and Distal Epithelial Cell Survival during Lung Development. *Am J Respir Cell Mol Biol* 2016; 55: 135-149.

79. Pobre KFR, Poet GJ, Hendershot LM. The endoplasmic reticulum (ER) chaperone BiP is a master regulator of ER functions: Getting by with a little help from ERdj friends. *J Biol Chem* 2019; 294: 2098-2108.

80. Wang M, Wey S, Zhang Y, Ye R, Lee AS. Role of the unfolded protein response regulator GRP78/BiP in development, cancer, and neurological disorders. *Antioxid Redox Signal* 2009; 11: 2307-2316.

81. Merali S, Barrero CA, Bowler RP, Chen DE, Criner G, Braverman A, Litwin S, Yeung A, Kelsen SG. Analysis of the plasma proteome in COPD: Novel low abundance proteins reflect the severity of lung remodeling. *Copd* 2014; 11: 177-189.

82. Ayaub EA, Kolb PS, Mohammed-Ali Z, Tat V, Murphy J, Bellaye PS, Shimbori C, Boivin FJ, Lai R, Lynn EG, Lhoták Š, Bridgewater D, Kolb MR, Inman MD, Dickhout JG, Austin RC, Ask K. GRP78 and CHOP modulate macrophage apoptosis and the development of bleomycin-induced pulmonary fibrosis. *J Pathol* 2016; 239: 411-425.

83. He CH, Gong P, Hu B, Stewart D, Choi ME, Choi AM, Alam J. Identification of activating transcription factor 4 (ATF4) as an Nrf2-interacting protein. Implication for heme oxygenase-1 gene regulation. *J Biol Chem* 2001; 276: 20858-20865.

84. Hikichi M, Mizumura K, Maruoka S, Gon Y. Pathogenesis of chronic obstructive pulmonary disease (COPD) induced by cigarette smoke. *J Thorac Dis* 2019; 11: S2129-S2140.

85. Kasai S, Yamazaki H, Tanji K, Engler MJ, Matsumiya T, Itoh K. Role of the ISR-ATF4 pathway and its cross talk with Nrf2 in mitochondrial quality control. *J Clin Biochem Nutr* 2019; 64: 1-12.

86. Marciniak SJ, Yun CY, Oyadomari S, Novoa I, Zhang Y, Jungreis R, Nagata K, Harding HP, Ron D. CHOP induces death by promoting protein synthesis and oxidation in the stressed endoplasmic reticulum. *Genes Dev* 2004; 18: 3066-3077.

87. Hollien J, Lin JH, Li H, Stevens N, Walter P, Weissman JS. Regulated Ire1-dependent decay of messenger RNAs in mammalian cells. *J Cell Biol* 2009; 186: 323-331.

88. Milisav I, Šuput D, Ribarič S. Unfolded Protein Response and Macroautophagy in Alzheimer's, Parkinson's and Prion Diseases. *Molecules* 2015; 20: 22718-22756.

89. Pepe AE, Xiao Q, Zampetaki A, Zhang Z, Kobayashi A, Hu Y, Xu Q. Crucial role of nrf3 in smooth muscle cell differentiation from stem cells. *Circ Res* 2010; 106: 870-879.

90. Cai Y, Deng Y, Horenkamp F, Reinisch KM, Burd CG. Sac1-Vps74 structure reveals a mechanism to terminate phosphoinositide signaling in the Golgi apparatus. *The Journal of cell biology* 2014; 206: 485-491.

91. Shanmugasundaram K, Nayak BK, Friedrichs WE, Kaushik D, Rodriguez R, Block K. NOX4 functions as a mitochondrial energetic sensor coupling cancer metabolic reprogramming to drug resistance. *Nature Communications* 2017; 8: 997.

92. Yu KN, Kim HJ, Kim S, Dawaadamdin O, Lee AY, Hong SH, Chang SH, Choi SJ, Shim SM, Lee K, Cho MH. Cigarette Smoking Condensate Disrupts Endoplasmic Reticulum-Golgi Network Homeostasis Through GOLPH3 Expression in Normal Lung Epithelial Cells. *Nicotine Tob Res* 2016; 18: 1877-1885.

93. Cai Y, Deng Y, Horenkamp F, Reinisch KM, Burd CG. Sac1-Vps74 structure reveals a mechanism to terminate phosphoinositide signaling in the Golgi apparatus. *J Cell Biol* 2014; 206: 485-491.

94. De Boer WI. Cytokines and therapy in COPD: a promising combination? *Chest* 2002; 121: 209s-218s.

95. Monteagudo M, Barrecheguren M, Solntseva I, Dhalwani N, Booth A, Nuñez A, Lambrelli D, Miravitlles M. Clinical characteristics and factors associated with triple therapy use in newly diagnosed patients with COPD. *NPJ Prim Care Respir Med* 2021; 31: 16.

96. Barnes PJ. Future Advances in COPD Therapy. *Respiration* 2001; 68: 441-448.

97. Glassberg MK, Csete I, Simonet E, Elliot SJ. Stem Cell Therapy for COPD: Hope and Exploitation. *Chest* 2021; 160: 1271-1281.

98. Gangemi S, Tonacci A. AntagomiRs: A novel therapeutic strategy for challenging COVID-19 cytokine storm. *Cytokine Growth Factor Rev* 2021; 58: 111-113.

99. Bernhagen J. A new cytokine target for chronic obstructive pulmonary disease? *EBioMedicine* 2021; 69: 103479.

100. Han MK, Agusti A, Celli BR, Criner GJ, Halpin DMG, Roche N, Papi A, Stockley RA, Wedzicha J, Vogelmeier CF. From GOLD 0 to Pre-COPD. *Am J Respir Crit Care Med* 2021; 203: 414-423.

101. Singh SP, Devadoss D, Manevski M, Sheybani A, Ivanciuc T, Exil V, Agarwal H, Raizada V, Garofalo RP, Chand HS, Sopori ML. Gestational Exposure to Cigarette Smoke Suppresses the Gasotransmitter H(2)S Biogenesis and the Effects Are Transmitted Transgenerationally. *Front Immunol* 2020; 11: 1628.

102. Chand HS, Mebratu YA, Kuehl PJ, Tesfaigzi Y. Blocking Bcl-2 resolves IL-13-mediated mucous cell hyperplasia in a Bik-dependent manner. *J Allergy Clin Immunol* 2017.

103. Mirza S, Clay RD, Koslow MA, Scanlon PD. COPD Guidelines: A Review of the 2018 GOLD Report. *Mayo Clin Proc* 2018; 93: 1488-1502.

104. Baginski TK, Dabbagh K, Satjawatcharaphong C, Swinney DC. Cigarette smoke synergistically enhances respiratory mucin induction by proinflammatory stimuli. *Am J Respir Cell Mol Biol* 2006; 35: 165-174.

105. Caramori G, Casolari P, Di Gregorio C, Saetta M, Baraldo S, Boschetto P, Ito K, Fabbri LM, Barnes PJ, Adcock IM, Cavallesco G, Chung KF, Papi A. MUC5AC expression is increased in bronchial submucosal glands of stable COPD patients. *Histopathology* 2009; 55: 321-331.

106. Kesimer M, Ford AA, Ceppe A, Radicioni G, Cao R, Davis CW, Doerschuk CM, Alexis NE, Anderson WH, Henderson AG, Barr RG, Bleecker ER, Christenson SA, Cooper CB, Han MK, Hansel NN, Hastie AT, Hoffman EA, Kanner RE, Martinez F, Paine R, 3rd, Woodruff PG, O'Neal WK, Boucher RC. Airway Mucin Concentration as a Marker of Chronic Bronchitis. *N Engl J Med* 2017; 377: 911-922.

107. Okuda K, Chen G, Subramani DB, Wolf M, Gilmore RC, Kato T, Radicioni G, Kesimer M, Chua M, Dang H, Livraghi-Butrico A, Ehre C, Doerschuk CM, Randell SH, Matsui H, Nagase T, O'Neal WK, Boucher RC. Localization of Secretory Mucins MUC5AC and MUC5B in Normal/Healthy Human Airways. *Am J Respir Crit Care Med* 2019; 199: 715-727.

108. Radicioni G, Ceppe A, Ford AA, Alexis NE, Barr RG, Bleecker ER, Christenson SA, Cooper CB, Han MK, Hansel NN, Hastie AT, Hoffman EA, Kanner RE, Martinez FJ, Ozkan E, Paine R, 3rd, Woodruff PG, O'Neal WK, Boucher RC, Kesimer M. Airway mucin MUC5AC and MUC5B concentrations and the initiation and progression of chronic obstructive pulmonary disease: an analysis of the SPIROMICS cohort. *Lancet Respir Med* 2021.

109. Chen LL. Ling-Ling Chen: Linking Long Noncoding RNA Processing and Function to RNA Biology. *Trends Biochem Sci* 2016; 41: 733-734.

110. Zong D, Liu X, Li J, Ouyang R, Chen P. The role of cigarette smoke-induced epigenetic alterations in inflammation. *Epigenetics Chromatin* 2019; 12: 65.

111. Soares do Amaral N, Cruz E Melo N, de Melo Maia B, Malagoli Rocha R. Noncoding RNA Profiles in Tobacco- and Alcohol-Associated Diseases. *Genes (Basel)* 2016; 8: 6.

112. Wu Y, Liu X, Zhou Q, Huang C, Meng X, Xu F, Li J. Silent information regulator 1 (SIRT1) ameliorates liver fibrosis via promoting activated stellate cell apoptosis and reversion. *Toxicol Appl Pharmacol* 2015; 289: 163-176.

113. Marchese FP, Raimondi I, Huarte M. The multidimensional mechanisms of long noncoding RNA function. *Genome biology* 2017; 18: 206.

114. Feng Z, Qi S, Zhang Y, Qi Z, Yan L, Zhou J, He F, Li Q, Yang Y, Chen Q, Xiao S, Li Q, Chen Y, Zhang Y. Ly6G+ neutrophil-derived miR-223 inhibits the NLRP3 inflammasome in mitochondrial DAMP-induced acute lung injury. *Cell Death Dis* 2017; 8: e3170.

115. Iyer SS, He Q, Janczy JR, Elliott EI, Zhong Z, Olivier AK, Sadler JJ, Knepper-Adrian V, Han R, Qiao L, Eisenbarth SC, Nauseef WM, Cassel SL, Sutterwala FS. Mitochondrial cardiolipin is required for Nlrp3 inflammasome activation. *Immunity* 2013; 39: 311-323.

116. Mao C, Zhang J, Lin S, Jing L, Xiang J, Wang M, Wang B, Xu P, Liu W, Song X, Lv C. MiRNA-30a inhibits AECs-II apoptosis by blocking mitochondrial fission dependent on Drp-1. *Journal of cellular and molecular medicine* 2014; 18: 2404-2416.

117. Song R, Walentek P, Sponer N, Klimke A, Lee JS, Dixon G, Harland R, Wan Y, Lishko P, Lize M, Kessel M, He L. miR-34/449 miRNAs are required for motile ciliogenesis by repressing cp110. *Nature* 2014; 510: 115-120.

118. Vohwinkel CU, Lecuona E, Sun H, Sommer N, Vadász I, Chandel NS, Sznajder JI. Elevated CO(2) levels cause mitochondrial dysfunction and impair cell proliferation. *J Biol Chem* 2011; 286: 37067-37076.

119. Lizé M, Herr C, Klimke A, Bals R, Dobbelstein M. MicroRNA-449a levels increase by several orders of magnitude during mucociliary differentiation of airway epithelia. *Cell Cycle* 2010; 9: 4579-4583.

120. Tasena H, Faiz A, Timens W, Noordhoek J, Hylkema MN, Gosens R, Hiemstra PS, Spira A, Postma DS, Tew GW, Grimbaldeston MA, van den Berge M, Heijink IH, Brandsma CA. microRNA-mRNA regulatory networks underlying chronic mucus hypersecretion in COPD. *Eur Respir J* 2018; 52.

121. Pandit KV, Corcoran D, Yousef H, Yarlagadda M, Tzouvelekis A, Gibson KF, Konishi K, Yousem SA, Singh M, Handley D, Richards T, Selman M, Watkins SC, Pardo A, Ben-Yehudah A, Bouros D, Eickelberg O, Ray P, Benos PV, Kaminski N. Inhibition and role of let-7d in idiopathic pulmonary fibrosis. *Am J Respir Crit Care Med* 2010; 182: 220-229.

122. Liu G, Friggeri A, Yang Y, Milosevic J, Ding Q, Thannickal VJ, Kaminski N, Abraham E. miR-21 mediates fibrogenic activation of pulmonary fibroblasts and lung fibrosis. *J Exp Med* 2010; 207: 1589-1597.

123. Dutta RK, Chinnapaiyan S, Rasmussen L, Raju SV, Unwalla HJ. A Neutralizing Aptamer to TGFBR2 and miR-145 Antagonism Rescue Cigarette Smoke- and TGF-β-Mediated CFTR Expression. *Mol Ther* 2019; 27: 442-455.

124. Dong Y, Yoshitomi T, Hu JF, Cui J. Long noncoding RNAs coordinate functions between mitochondria and the nucleus. *Epigenetics Chromatin* 2017; 10: 41.

125. Kim KM, Noh JH, Abdelmohsen K, Gorospe M. Mitochondrial noncoding RNA transport. *BMB Rep* 2017; 50: 164-174.

126. Van Pottelberge GR, Mestdagh P, Bracke KR, Thas O, van Durme YM, Joos GF, Vandesompele J, Brusselle GG. MicroRNA expression in induced sputum of smokers and patients with chronic obstructive pulmonary disease. *Am J Respir Crit Care Med* 2011; 183: 898-906.

127. Chen F, Wu W, Millman A, Craft JF, Chen E, Patel N, Boucher JL, Urban JF, Jr., Kim CC, Gause WC. Neutrophils prime a long-lived effector macrophage phenotype that mediates accelerated helminth expulsion. *Nat Immunol*; 15: 938-946.

128. Segal LN, Martinez FJ. Chronic obstructive pulmonary disease subpopulations and phenotyping. *J Allergy Clin Immunol* 2018; 141: 1961-1971.

129. Li X, Zheng M, Pu J, Zhou Y, Hong W, Fu X, Peng Y, Zhou W, Pan H, Li B, Ran P. Identification of abnormally expressed lncRNAs induced by PM2.5 in human bronchial epithelial cells. *Bioscience reports* 2018; 38.

130. Yuan S, Liu Q, Hu Z, Zhou Z, Wang G, Li C, Xie W, Meng G, Xiang Y, Wu N, Wu L, Yu Z, Bai L, Li Y. Long non-coding RNA MUC5B-AS1 promotes metastasis through mutually regulating MUC5B expression in lung adenocarcinoma. *Cell Death Dis* 2018; 9: 450.

131. Bi H, Zhou J, Wu D, Gao W, Li L, Yu L, Liu F, Huang M, Adcock IM, Barnes PJ, Yao X. Microarray analysis of long non-coding RNAs in COPD lung tissue. *Inflamm Res* 2015; 64: 119-126.

132. Qu X, Dang X, Wang W, Li Y, Xu D, Shang D, Chang Y. Long Noncoding RNAs and mRNA Regulation in Peripheral Blood Mononuclear Cells of Patients with Chronic Obstructive Pulmonary Disease. *Mediators of inflammation* 2018; 2018: 7501851.

133. Parker MM, Chase RP, Lamb A, Reyes A, Saferali A, Yun JH, Himes BE, Silverman EK, Hersh CP, Castaldi PJ. RNA sequencing identifies novel

non-coding RNA and exon-specific effects associated with cigarette smoking. *BMC medical genomics* 2017; 10: 58.

134. Qian Y, Mao ZD, Shi YJ, Liu ZG, Cao Q, Zhang Q. Comprehensive Analysis of miRNA-mRNA-lncRNA Networks in Non-Smoking and Smoking Patients with Chronic Obstructive Pulmonary Disease. *Cellular physiology and biochemistry : international journal of experimental cellular physiology, biochemistry, and pharmacology* 2018; 50: 1140-1153.

135. Bai Y, Nie S, Jiang G, Zhou Y, Zhou M, Zhao Y, Li S, Wang F, Lv Q, Huang Y, Yang Q, Li Q, Li Y, Xia Y, Liu Y, Liu J, Qian J, Li B, Wu G, Wu Y, Wang B, Cheng X, Yang Y, Ke T, Li H, Ren X, Ma X, Liao Y, Xu C, Tu X, Wang QK. Regulation of CARD8 expression by ANRIL and association of CARD8 single nucleotide polymorphism rs2043211 (p.C10X) with ischemic stroke. *Stroke* 2014; 45: 383-388.

136. Zhao JJ, Hao S, Wang LL, Hu CY, Zhang S, Guo LJ, Zhang G, Gao B, Jiang Y, Tian WG, Luo DL. Long non-coding RNA ANRIL promotes the invasion and metastasis of thyroid cancer cells through TGF-beta/Smad signaling pathway. *Oncotarget* 2016; 7: 57903-57918.

137. Ge J, Geng S, Jiang H. Long noncoding RNAs antisense noncoding RNA in the INK4 locus (ANRIL) correlates with lower acute exacerbation risk, decreased inflammatory cytokines, and mild GOLD stage in patients with chronic obstructive pulmonary disease. *Journal of clinical laboratory analysis* 2019; 33: e22678.

138. Zhang H, Sun D, Li D, Zheng Z, Xu J, Liang X, Zhang C, Wang S, Wang J, Lu W. Long non-coding RNA expression patterns in lung tissues of chronic cigarette smoke induced COPD mouse model. *Scientific reports* 2018; 8: 7609.

139. Min T, Bodas M, Mazur S, Vij N. Critical role of proteostasis-imbalance in pathogenesis of COPD and severe emphysema. *Journal of molecular medicine* 2011; 89: 577-593.

140. Wang H, Chen L, Li D, Zeng N, Wu Y, Wang T, Shen Y, Xu D, Wen F. Microarray analysis of lung long non-coding RNAs in cigarette smoke-exposed mouse model. *Oncotarget* 2017; 8: 115647-115656.

141. Wang G, Xu Z, Wang R, Al-Hijji M, Salit J, Strulovici-Barel Y, Tilley AE, Mezey JG, Crystal RG. Genes associated with MUC5AC expression in small airway epithelium of human smokers and non-smokers. *BMC medical genomics* 2012; 5: 21.

142. Hicks A, Kourteva G, Hilton H, Li H, Lin TA, Liao W, Li Y, Wei X, March T, Benson J, Renzetti LM. Cellular and molecular characterization of ozone-induced pulmonary inflammation in the Cynomolgus monkey. *Inflammation* 2010; 33: 144-156.

143. Gu C, Li Y, Liu J, Ying X, Liu Y, Yan J, Chen C, Zhou H, Cao L, Ma Y. LncRNAmediated SIRT1/FoxO3a and SIRT1/p53 signaling pathways regulate type II alveolar epithelial cell senescence in patients with chronic obstructive pulmonary disease. *Mol Med Rep* 2017; 15: 3129-3134.

144. Tang W, Shen Z, Guo J, Sun S. Screening of long non-coding RNA and TUG1 inhibits proliferation with TGF-beta induction in patients with COPD. *International journal of chronic obstructive pulmonary disease* 2016; 11: 2951-2964.

145. Liu SJ, Horlbeck MA, Cho SW, Birk HS, Malatesta M, He D, Attenello FJ, Villalta JE, Cho MY, Chen Y, Mandegar MA, Olvera MP, Gilbert LA, Conklin BR, Chang HY, Weissman JS, Lim DA. CRISPRi-based genome-scale identification of functional long noncoding RNA loci in human cells. *Science* 2017; 355.

146. Chung S, Baumlin N, Dennis JS, Moore R, Salathe SF, Whitney PL, Sabater J, Abraham WM, Kim MD, Salathe M. Electronic Cigarette Vapor with Nicotine Causes Airway Mucociliary Dysfunction Preferentially via TRPA1 Receptors. *Am J Respir Crit Care Med* 2019; 200: 1134-1145.

147. Sailland J, Grosche A, Baumlin N, Dennis JS, Schmid A, Krick S, Salathe M. Role of Smad3 and p38 Signalling in Cigarette Smoke-induced CFTR and BK dysfunction in Primary Human Bronchial Airway Epithelial Cells. *Sci Rep* 2017; 7: 10506.

148. Sweeney TE, Azad TD, Donato M, Haynes WA, Perumal TM, Henao R, Bermejo-Martin JF, Almansa R, Tamayo E, Howrylak JA, Choi A, Parnell GP, Tang B, Nichols M, Woods CW, Ginsburg GS, Kingsmore SF, Omberg L, Mangravite LM, Wong HR, Tsalik EL, Langley RJ, Khatri P. Unsupervised Analysis of Transcriptomics in Bacterial Sepsis Across Multiple Datasets Reveals Three Robust Clusters. *Crit Care Med* 2018; 46: 915-925.

149. Tsalik EL, Willig LK, Rice BJ, van Velkinburgh JC, Mohney RP, McDunn JE, Dinwiddie DL, Miller NA, Mayer ES, Glickman SW, Jaehne AK, Glew RH, Sopori ML, Otero RM, Harrod KS, Cairns CB, Fowler VG, Rivers EP, Woods CW, Kingsmore SF, Langley RJ. Renal systems biology of patients with systemic inflammatory response syndrome. *Kidney Int* 2015; 88: 804-814.

150. Tsalik EL, Langley RJ, Dinwiddie DL, Miller NA, Yoo B, van Velkinburgh JC, Smith LD, Thiffault I, Jaehne AK, Valente AM, Henao R, Yuan X, Glickman SW, Rice BJ, McClain MT, Carin L, Corey GR, Ginsburg GS, Cairns CB, Otero RM, Fowler VG, Jr., Rivers EP, Woods CW, Kingsmore SF. An integrated transcriptome and expressed variant analysis of sepsis survival and death. *Genome Med* 2014; 6: 111.

151. Chand HS, Mebratu YA, Kuehl PJ, Tesfaigzi Y. Blocking Bcl-2 resolves IL-13-mediated mucous cell hyperplasia in a Bik-dependent manner. *J Allergy Clin Immunol* 2017; 140: 1456-1459.e1459.

152. Lumsden AL, Ma Y, Ashander LM, Stempel AJ, Keating DJ, Smith JR, Appukuttan B. ICAM-1-related long non-coding RNA: promoter analysis and expression in human retinal endothelial cells. *BMC Res Notes* 2018; 11: 285.

153. Janson C, Ludviksdottir D, Gunnbjornsdottir M, Bjornsson EH, Hakansson L, Venge P, group BH-s. Circulating adhesion molecules in allergic and non-allergic asthma. *Respir Med* 2005; 99: 45-51.

154. Edgar R, Domrachev M, Lash AE. Gene Expression Omnibus: NCBI gene expression and hybridization array data repository. *Nucleic Acids Res* 2002; 30: 207-210.

155. Chand HS, Mebratu YA, Montera M, Tesfaigzi Y. T cells suppress memory-dependent rapid mucous cell metaplasia in mouse airways. *Respir Res* 2016; 17: 132.

156. Kirjavainen PV, Karvonen AM, Adams RI, Taubel M, Roponen M, Tuoresmaki P, Loss G, Jayaprakash B, Depner M, Ege MJ, Renz H, Pfefferle PI, Schaub B, Lauener R, Hyvarinen A, Knight R, Heederik DJJ, von Mutius E, Pekkanen J. Farm-like indoor microbiota in non-farm homes protects children from asthma development. *Nat Med* 2019; 25: 1089-1095.

157. Stein MM, Hrusch CL, Gozdz J, Igartua C, Pivniouk V, Murray SE, Ledford JG, Marques Dos Santos M, Anderson RL, Metwali N, Neilson JW, Maier RM, Gilbert JA, Holbreich M, Thorne PS, Martinez FD, von Mutius E, Vercelli D, Ober C, Sperling AI. Innate Immunity and Asthma Risk in Amish and Hutterite Farm Children. *N Engl J Med* 2016; 375: 411-421.

158. Schuijs MJ, Willart MA, Vergote K, Gras D, Deswarte K, Ege MJ, Madeira FB, Beyaert R, van Loo G, Bracher F, von Mutius E, Chanez P, Lambrecht BN, Hammad H. Farm dust and endotoxin protect against allergy through A20 induction in lung epithelial cells. *Science* 2015; 349: 1106-1110.

159. Netea MG, Joosten LAB. Trained Immunity and Local Innate Immune Memory in the Lung. *Cell* 2018; 175: 1463-1465.

160. Zheng M, Hong W, Gao M, Yi E, Zhang J, Hao B, Liang C, Li X, Li C, Ye X, Liao B, He F, Zhou Y, Li B, Ran P. Long Noncoding RNA COPDA1 Promotes Airway Smooth Muscle Cell Proliferation in Chronic Obstructive Pulmonary Disease. *Am J Respir Cell Mol Biol* 2019; 61: 584-596.

161. Li Z, Zhang Q, Wu Y, Hu F, Gu L, Chen T, Wang W. lncRNA Malat1 modulates the maturation process, cytokine secretion and apoptosis in airway epithelial cell-conditioned dendritic cells. *Exp Ther Med* 2018; 16: 3951-3958.

162. Zhu YJ, Mao D, Gao W, Hu H. Peripheral whole blood lncRNA expression analysis in patients with eosinophilic asthma. *Medicine (Baltimore)* 2018; 97: e9817.

163. Zhu Y, Mao D, Gao W, Han G, Hu H. Analysis of lncRNA Expression in Patients With Eosinophilic and Neutrophilic Asthma Focusing on LNC_000127. *Front Genet* 2019; 10: 141.

164. Lin J, Feng X, Zhang J, Tong Z. Long noncoding RNA TUG1 promotes airway smooth muscle cells proliferation and migration via sponging miR-590-5p/FGF1 in asthma. *Am J Transl Res* 2019; 11: 3159-3166.

165. Fan M, Xu J, Xiao Q, Chen F, Han X. Long non-coding RNA TCF7 contributes to the growth and migration of airway smooth muscle cells in asthma through targeting TIMMDC1/Akt axis. *Biochem Biophys Res Commun* 2019; 508: 749-755.

166. Yao RW, Wang Y, Chen LL. Cellular functions of long noncoding RNAs. *Nat Cell Biol* 2019; 21: 542-551.

167. Devadoss D, Long C, Langley RJ, Manevski M, Nair M, Campos MA, Borchert G, Rahman I, Chand HS. Long Noncoding Transcriptome in Chronic Obstructive Pulmonary Disease. *Am J Respir Cell Mol Biol* 2019; 61: 678-688.

168. Cabili MN, Dunagin MC, McClanahan PD, Biaesch A, Padovan-Merhar O, Regev A, Rinn JL, Raj A. Localization and abundance analysis of human lncRNAs at single-cell and single-molecule resolution. *Genome Biol* 2015; 16: 20.

169. Fernandes JCR, Acuna SM, Aoki JI, Floeter-Winter LM, Muxel SM. Long Non-Coding RNAs in the Regulation of Gene Expression: Physiology and Disease. *Noncoding RNA* 2019; 5.

170. Long Y, Wang X, Youmans DT, Cech TR. How do lncRNAs regulate transcription? *Sci Adv* 2017; 3: eaao2110.

171. Mitchell PD, O'Byrne PM. Epithelial-Derived Cytokines in Asthma. *Chest* 2017; 151: 1338-1344.

172. Khair OA, Devalia JL, Abdelaziz MM, Sapsford RJ, Davies RJ. Effect of erythromycin on Haemophilus influenzae endotoxin-induced release of IL-6, IL-8 and sICAM-1 by cultured human bronchial epithelial cells. *Eur Respir J* 1995; 8: 1451-1457.

173. Jevnikar Z, Ostling J, Ax E, Calven J, Thorn K, Israelsson E, Oberg L, Singhania A, Lau LCK, Wilson SJ, Ward JA, Chauhan A, Sousa AR, De Meulder B, Loza MJ, Baribaud F, Sterk PJ, Chung KF, Sun K, Guo Y, Adcock IM, Payne D, Dahlen B, Chanez P, Shaw DE, Krug N, Hohlfeld JM, Sandstrom T, Djukanovic R, James A, Hinks TSC, Howarth PH, Vaarala O, van Geest M, Olsson H, Unbiased Biomarkers in Prediction of Respiratory Disease Outcomes study g. Epithelial IL-6 trans-signaling defines a new asthma phenotype with increased airway inflammation. *J Allergy Clin Immunol* 2019; 143: 577-590.

174. Hadjicharalambous MR, Roux BT, Feghali-Bostwick CA, Murray LA, Clarke DL, Lindsay MA. Long Non-coding RNAs Are Central Regulators of the IL-1beta-Induced Inflammatory Response in Normal and Idiopathic Pulmonary Lung Fibroblasts. *Front Immunol* 2018; 9: 2906.

175. Perry MM, Tsitsiou E, Austin PJ, Lindsay MA, Gibeon DS, Adcock IM, Chung KF. Role of non-coding RNAs in maintaining primary airway smooth muscle cells. *Respir Res* 2014; 15: 58.

176. Austin PJ, Tsitsiou E, Boardman C, Jones SW, Lindsay MA, Adcock IM, Chung KF, Perry MM. Transcriptional profiling identifies the long noncoding RNA plasmacytoma variant translocation (PVT1) as a novel regulator of the asthmatic phenotype in human airway smooth muscle. *J Allergy Clin Immunol* 2017; 139: 780-789.

177. Qian X, Shi S, Zhang G. Long non-coding RNA antisense non-coding RNA in the INK4 locus expression correlates with increased disease risk, severity, and inflammation of allergic rhinitis. *Medicine (Baltimore)* 2019; 98: e15247.

178. Sundar IK, Rahman I. Gene expression profiling of epigenetic chromatin modification enzymes and histone marks by cigarette smoke: implications for COPD and lung cancer. *Am J Physiol Lung Cell Mol Physiol* 2016; 311: L1245-l1258.

179. Schmitz SU, Grote P, Herrmann BG. Mechanisms of long noncoding RNA function in development and disease. *Cell Mol Life Sci* 2016; 73: 2491-2509.

180. Faiz A, Steiling K, Roffel MP, Postma DS, Spira A, Lenburg ME, Borggrewe M, Eijgenraam TR, Jonker MR, Koppelman GH, Pouwels SD, Liu G, Alekseyev YO, Lam S, Hiemstra PS, Sterk PJ, Timens W, Brandsma CA, Heijink IH, van den Berge M. Effect of long-term corticosteroid treatment on microRNA and gene-expression profiles in COPD. *Eur Respir J* 2019; 53.

181. Hu TJ, Huang HB, Shen HB, Chen W, Yang ZH. Role of long non-coding RNA MALAT1 in chronic obstructive pulmonary disease. *Exp Ther Med* 2020; 20: 2691-2697.

182. Chand HS, Vazquez-Guillamet R, Royer C, Rudolph K, Mishra N, Singh SP, Hussain SS, Barrett E, Callen S, Byrareddy SN, Guillamet MCV, Abukhalaf J, Sheybani A, Exil V, Raizada V, Agarwal H, Nair M, Villinger F, Buch S, Sopori M. Cigarette smoke and HIV synergistically affect lung pathology in cynomolgus macaques. *J Clin Invest* 2018; 128: 5428-5433.

183. Guo W, Liu S, Cheng Y, Lu L, Shi J, Xu G, Li N, Cheng K, Wu M, Cheng S, Liu S. ICAM-1-Related Noncoding RNA in Cancer Stem Cells Maintains ICAM-1 Expression in Hepatocellular Carcinoma. *Clin Cancer Res* 2016; 22: 2041-2050.

184. Ming X, Duan W, Yi W. Long non-coding RNA NEAT1 predicts elevated chronic obstructive pulmonary disease (COPD) susceptibility and acute exacerbation risk, and correlates with higher disease severity, inflammation, and lower miR-193a in COPD patients. *Int J Clin Exp Pathol* 2019; 12: 2837-2848.

185. Hu T-J, Huang H-B, Shen H-B, Chen W, Yang Z-H. Role of long non-coding RNA MALAT1 in chronic obstructive pulmonary disease. *Experimental and therapeutic medicine* 2020; 20: 2691-2697.

186. Herter EK, Li D, Toma MA, Vij M, Li X, Visscher D, Wang A, Chu T, Sommar P, Blomqvist L, Berglund D, Ståhle M, Wikstrom JD, Xu Landén N. WAKMAR2, a Long Noncoding RNA Downregulated in Human Chronic Wounds, Modulates Keratinocyte Motility and Production of Inflammatory Chemokines. *J Invest Dermatol* 2019; 139: 1373-1384.

187. Petit A, Knabe L, Khelloufi K, Jory M, Gras D, Cabon Y, Begg M, Richard S, Massiera G, Chanez P, Vachier I, Bourdin A. Bronchial Epithelial Calcium Metabolism Impairment in Smokers and Chronic Obstructive Pulmonary

Disease. Decreased ORAI3 Signaling. *Am J Respir Cell Mol Biol* 2019; 61: 501-511.

188. Guo-Parke H, Linden D, Mousnier A, Scott IC, Killick H, Borthwick LA, Fisher AJ, Weldon S, Taggart CC, Kidney JC. Altered Differentiation and Inflammation Profiles Contribute to Enhanced Innate Responses in Severe COPD Epithelium to Rhinovirus Infection. *Front Med (Lausanne)* 2022; 9: 741989.

189. Hussain SS, George S, Singh S, Jayant R, Hu CA, Sopori M, Chand HS. A Small Molecule BH3-mimetic Suppresses Cigarette Smoke-Induced Mucous Expression in Airway Epithelial Cells. *Sci Rep* 2018; 8: 13796.

190. Chinnapaiyan S, Dutta RK, Devadoss D, Chand HS, Rahman I, Unwalla HJ. Role of Non-Coding RNAs in Lung Circadian Clock Related Diseases. *Int J Mol Sci* 2020; 21.

191. Eisner MD, Anthonisen N, Coultas D, Kuenzli N, Perez-Padilla R, Postma D, Romieu I, Silverman EK, Balmes JR. An official American Thoracic Society public policy statement: Novel risk factors and the global burden of chronic obstructive pulmonary disease. *Am J Respir Crit Care Med* 2010; 182: 693-718.

192. Christenson SA, van den Berge M, Faiz A, Inkamp K, Bhakta N, Bonser LR, Zlock LT, Barjaktarevic IZ, Barr RG, Bleecker ER, Boucher RC, Bowler RP, Comellas AP, Curtis JL, Han MK, Hansel NN, Hiemstra PS, Kaner RJ, Krishnanm JA, Martinez FJ, O'Neal WK, Paine R, 3rd, Timens W, Wells JM, Spira A, Erle DJ, Woodruff PG. An airway epithelial IL-17A response signature identifies a steroid-unresponsive COPD patient subgroup. *J Clin Invest* 2019; 129: 169-181.

193. Decramer M, Janssens W, Miravitlles M. Chronic obstructive pulmonary disease. *Lancet* 2012; 379: 1341-1351.

194. Nyunoya T, Mebratu Y, Contreras A, Delgado M, Chand HS, Tesfaigzi Y. Molecular processes that drive cigarette smoke-induced epithelial cell fate of the lung. *Am J Respir Cell Mol Biol* 2014; 50: 471-482.

195. Walter RE, Wilk JB, Larson MG, Vasan RS, Keaney JF, Jr., Lipinska I, O'Connor GT, Benjamin EJ. Systemic inflammation and COPD: the Framingham Heart Study. *Chest* 2008; 133: 19-25.

196. Fanucchi S, Fok ET, Dalla E, Shibayama Y, Börner K, Chang EY, Stoychev S, Imakaev M, Grimm D, Wang KC, Li G, Sung WK, Mhlanga MM. Immune genes are primed for robust transcription by proximal long

noncoding RNAs located in nuclear compartments. *Nat Genet* 2019; 51: 138-150.

197. Rao W, Wang S, Duleba M, Niroula S, Goller K, Xie J, Mahalingam R, Neupane R, Liew AA, Vincent M, Okuda K, O'Neal WK, Boucher RC, Dickey BF, Wechsler ME, Ibrahim O, Engelhardt JF, Mertens TCJ, Wang W, Jyothula SSK, Crum CP, Karmouty-Quintana H, Parekh KR, Metersky ML, McKeon FD, Xian W. Regenerative Metaplastic Clones in COPD Lung Drive Inflammation and Fibrosis. *Cell* 2020; 181: 848-864.e818.

198. Gindele JA, Kiechle T, Benediktus K, Birk G, Brendel M, Heinemann F, Wohnhaas CT, LeBlanc M, Zhang H, Strulovici-Barel Y, Crystal RG, Thomas MJ, Stierstorfer B, Quast K, Schymeinsky J. Intermittent exposure to whole cigarette smoke alters the differentiation of primary small airway epithelial cells in the air-liquid interface culture. *Sci Rep* 2020; 10: 6257.

199. Bodas M, Moore AR, Subramaniyan B, Georgescu C, Wren JD, Freeman WM, Brown BR, Metcalf JP, Walters MS. Cigarette Smoke Activates NOTCH3 to Promote Goblet Cell Differentiation in Human Airway Epithelial Cells. *Am J Respir Cell Mol Biol* 2021; 64: 426-440.

200. Gu W, Yuan Y, Wang L, Yang H, Li S, Tang Z, Li Q. Long non-coding RNA TUG1 promotes airway remodelling by suppressing the miR-145-5p/DUSP6 axis in cigarette smoke-induced COPD. *J Cell Mol Med* 2019; 23: 7200-7209.

201. Mei J, Zhang Y, Lu S, Wang J. Long non-coding RNA NNT-AS1 regulates proliferation, apoptosis, inflammation and airway remodeling of chronic obstructive pulmonary disease via targeting miR-582-5p/FBXO11 axis. *Biomed Pharmacother* 2020; 129: 110326.

202. Yi E, Zhang J, Zheng M, Zhang Y, Liang C, Hao B, Hong W, Lin B, Pu J, Lin Z, Huang P, Li B, Zhou Y, Ran P. Long noncoding RNA IL6-AS1 is highly expressed in chronic obstructive pulmonary disease and is associated with interleukin 6 by targeting miR-149-5p and early B-cell factor 1. *Clin Transl Med* 2021; 11: e479.

203. Statello L, Guo CJ, Chen LL, Huarte M. Gene regulation by long non-coding RNAs and its biological functions. *Nat Rev Mol Cell Biol* 2021; 22: 96-118.

204. Caobi A, Dutta RK, Garbinski LD, Esteban-Lopez M, Ceyhan Y, Andre M, Manevski M, Ojha CR, Lapierre J, Tiwari S, Parira T, El-Hage N. The Impact of CRISPR-Cas9 on Age-related Disorders: From Pathology to Therapy. *Aging Dis* 2020; 11: 895-915.

205. Manevski M, Devadoss D, Castro R, Delatorre L, Yndart A, Jayant RD, Nair M, Chand HS. Development and Challenges of Nanotherapeutic Formulations for Targeting Mitochondrial Cell Death Pathways in Lung and Brain Degenerative Diseases. *Crit Rev Biomed Eng* 2020; 48: 137-152.

206. Rogers DF, Barnes PJ. Treatment of airway mucus hypersecretion. *Ann Med* 2006; 38: 116-125.

207. Cerveri I, Brusasco V. Revisited role for mucus hypersecretion in the pathogenesis of COPD. *Eur Respir Rev* 2010; 19: 109-112.

208. Winkle M, El-Daly SM, Fabbri M, Calin GA. Noncoding RNA therapeutics - challenges and potential solutions. *Nat Rev Drug Discov* 2021; 20: 629-651.

209. Vitale J, Mumoli N, Clerici P, De Paschale M, Evangelista I, Cei M, Mazzone A. Assessment of SARS-CoV-2 Reinfection 1 Year After Primary Infection in a Population in Lombardy, Italy. *JAMA Intern Med* 2021; 181: 1407-1408.

210. Fageeh H, Alshehri A, Fageeh H, Bizzoca ME, Lo Muzio L, Quadri MFA. Re-infection of SARS-CoV-2: A case in a young dental healthcare worker. *J Infect Public Health* 2021; 14: 685-688.

211. Kannan SR, Spratt AN, Sharma K, Chand HS, Byrareddy SN, Singh K. Omicron SARS-CoV-2 variant: Unique features and their impact on pre-existing antibodies. *J Autoimmun* 2021.

212. Hoffmann M, Kleine-Weber H, Schroeder S, Kruger N, Herrler T, Erichsen S, Schiergens TS, Herrler G, Wu NH, Nitsche A, Muller MA, Drosten C, Pohlmann S. SARS-CoV-2 Cell Entry Depends on ACE2 and TMPRSS2 and Is Blocked by a Clinically Proven Protease Inhibitor. *Cell* 2020; 181: 271-280 e278.

213. Hou YJ, Okuda K, Edwards CE, Martinez DR, Asakura T, Dinnon KH, 3rd, Kato T, Lee RE, Yount BL, Mascenik TM, Chen G, Olivier KN, Ghio A, Tse LV, Leist SR, Gralinski LE, Schafer A, Dang H, Gilmore R, Nakano S, Sun L, Fulcher ML, Livraghi-Butrico A, Nicely NI, Cameron M, Cameron C, Kelvin DJ, de Silva A, Margolis DM, Markmann A, Bartelt L, Zumwalt R, Martinez FJ, Salvatore SP, Borczuk A, Tata PR, Sontake V, Kimple A, Jaspers I, O'Neal WK, Randell SH, Boucher RC, Baric RS. SARS-CoV-2 Reverse Genetics Reveals a Variable Infection Gradient in the Respiratory Tract. *Cell* 2020; 182: 429-446 e414.

214. Olwenyi OA, Dyavar SR, Acharya A, Podany AT, Fletcher CV, Ng CL, Reid SP, Byrareddy SN. Immuno-epidemiology and pathophysiology of coronavirus disease 2019 (COVID-19). *J Mol Med (Berl)* 2020; 98: 1369-1383.

215. Rothan HA, Byrareddy SN. The epidemiology and pathogenesis of coronavirus disease (COVID-19) outbreak. *J Autoimmun* 2020; 109: 102433.

216. Ravindra NG, Alfajaro MM, Gasque V, Huston NC, Wan H, Szigeti-Buck K, Yasumoto Y, Greaney AM, Habet V, Chow RD, Chen JS, Wei J, Filler RB, Wang B, Wang G, Niklason LE, Montgomery RR, Eisenbarth SC, Chen S, Williams A, Iwasaki A, Horvath TL, Foxman EF, Pierce RW, Pyle AM, van Dijk D, Wilen CB. Single-cell longitudinal analysis of SARS-CoV-2 infection in human airway epithelium identifies target cells, alterations in gene expression, and cell state changes. *PLoS Biol* 2021; 19: e3001143.

217. He X, Lau EHY, Wu P, Deng X, Wang J, Hao X, Lau YC, Wong JY, Guan Y, Tan X, Mo X, Chen Y, Liao B, Chen W, Hu F, Zhang Q, Zhong M, Wu Y, Zhao L, Zhang F, Cowling BJ, Li F, Leung GM. Temporal dynamics in viral shedding and transmissibility of COVID-19. *Nat Med* 2020; 26: 672-675.

218. Hewitt RJ, Lloyd CM. Regulation of immune responses by the airway epithelial cell landscape. *Nat Rev Immunol* 2021.

219. Turjya RR, Khan MA, Mir Md Khademul Islam AB. Perversely expressed long noncoding RNAs can alter host response and viral proliferation in SARS-CoV-2 infection. *Future Virol* 2020; 15: 577-593.

220. Natarelli L, Parca L, Mazza T, Weber C, Virgili F, Fratantonio D. MicroRNAs and Long Non-Coding RNAs as Potential Candidates to Target Specific Motifs of SARS-CoV-2. *Noncoding RNA* 2021; 7.

221. Blanco-Melo D, Nilsson-Payant BE, Liu WC, Uhl S, Hoagland D, Moller R, Jordan TX, Oishi K, Panis M, Sachs D, Wang TT, Schwartz RE, Lim JK, Albrecht RA, tenOever BR. Imbalanced Host Response to SARS-CoV-2 Drives Development of COVID-19. *Cell* 2020; 181: 1036-1045 e1039.

222. Vishnubalaji R, Shaath H, Alajez NM. Protein Coding and Long Noncoding RNA (lncRNA) Transcriptional Landscape in SARS-CoV-2 Infected Bronchial Epithelial Cells Highlight a Role for Interferon and Inflammatory Response. *Genes (Basel)* 2020; 11.

223. Mukherjee S, Banerjee B, Karasik D, Frenkel-Morgenstern M. mRNA-lncRNA Co-Expression Network Analysis Reveals the Role of lncRNAs in

Immune Dysfunction during Severe SARS-CoV-2 Infection. *Viruses* 2021; 13.

224. Cheng J, Zhou X, Feng W, Jia M, Zhang X, An T, Luan M, Pan Y, Zhang S, Zhou Z, Wen L, Sun Y, Zhou C. Risk stratification by long non-coding RNAs profiling in COVID-19 patients. *J Cell Mol Med* 2021; 25: 4753-4764.

225. Morenikeji OB, Bernard K, Strutton E, Wallace M, Thomas BN. Evolutionarily Conserved Long Non-coding RNA Regulates Gene Expression in Cytokine Storm During COVID-19. *Front Bioeng Biotechnol* 2020; 8: 582953.

226. Meydan C, Madrer N, Soreq H. The Neat Dance of COVID-19: NEAT1, DANCR, and Co-Modulated Cholinergic RNAs Link to Inflammation. *Front Immunol* 2020; 11: 590870.

227. Cheemarla NR, Watkins TA, Mihaylova VT, Wang B, Zhao D, Wang G, Landry ML, Foxman EF. Dynamic innate immune response determines susceptibility to SARS-CoV-2 infection and early replication kinetics. *J Exp Med* 2021; 218.

228. Acharya A, Pandey K, Thurman M, Klug E, Trivedi J, Sharma K, Lorson CL, Singh K, Byrareddy SN. Discovery and evaluation of entry inhibitors for SARS-CoV-2 and its emerging variants. *J Virol* 2021: JVI0143721.

229. Abdelmoaty MM, Yeapuri P, Machhi J, Olson KE, Shahjin F, Kumar V, Zhou Y, Liang J, Pandey K, Acharya A, Byrareddy SN, Mosley RL, Gendelman HE. Defining the Innate Immune Responses for SARS-CoV-2-Human Macrophage Interactions. *Front Immunol* 2021; 12: 741502.

230. Mann M, Wright PR, Backofen R. IntaRNA 2.0: enhanced and customizable prediction of RNA-RNA interactions. *Nucleic Acids Res* 2017; 45: W435-W439.

231. Antczak M, Popenda M, Zok T, Sarzynska J, Ratajczak T, Tomczyk K, Adamiak RW, Szachniuk M. New functionality of RNAComposer: an application to shape the axis of miR160 precursor structure. *Acta Biochim Pol* 2016; 63: 737-744.

232. Gruber AR, Bernhart SH, Lorenz R. The ViennaRNA web services. *Methods Mol Biol* 2015; 1269: 307-326.

233. Lee J, Cheng X, Swails JM, Yeom MS, Eastman PK, Lemkul JA, Wei S, Buckner J, Jeong JC, Qi Y, Jo S, Pande VS, Case DA, Brooks CL, 3rd, MacKerell AD, Jr., Klauda JB, Im W. CHARMM-GUI Input Generator for

NAMD, GROMACS, AMBER, OpenMM, and CHARMM/OpenMM Simulations Using the CHARMM36 Additive Force Field. *J Chem Theory Comput* 2016; 12: 405-413.

234. Phillips JC, Hardy DJ, Maia JDC, Stone JE, Ribeiro JV, Bernardi RC, Buch R, Fiorin G, Henin J, Jiang W, McGreevy R, Melo MCR, Radak BK, Skeel RD, Singharoy A, Wang Y, Roux B, Aksimentiev A, Luthey-Schulten Z, Kale LV, Schulten K, Chipot C, Tajkhorshid E. Scalable molecular dynamics on CPU and GPU architectures with NAMD. *J Chem Phys* 2020; 153: 044130.

235. Baral P, Bhattarai N, Hossen ML, Stebliankin V, Gerstman BS, Narasimhan G, Chapagain PP. Mutation-induced changes in the receptor-binding interface of the SARS-CoV-2 Delta variant B.1.617.2 and implications for immune evasion. *Biochem Biophys Res Commun* 2021; 574: 14-19.

236. Humphrey W, Dalke A, Schulten K. VMD: visual molecular dynamics. *J Mol Graph* 1996; 14: 33-38, 27-38.

237. Camacho C, Coulouris G, Avagyan V, Ma N, Papadopoulos J, Bealer K, Madden TL. BLAST+: architecture and applications. *BMC Bioinformatics* 2009; 10: 421.

238. Babicki S, Arndt D, Marcu A, Liang Y, Grant JR, Maciejewski A, Wishart DS. Heatmapper: web-enabled heat mapping for all. *Nucleic Acids Res* 2016; 44: W147-153.

239. Weitnauer M, Mijosek V, Dalpke AH. Control of local immunity by airway epithelial cells. *Mucosal Immunol* 2016; 9: 287-298.

240. Lu W, Liu X, Wang T, Liu F, Zhu A, Lin Y, Luo J, Ye F, He J, Zhao J, Li Y, Zhong N. Elevated MUC1 and MUC5AC mucin protein levels in airway mucus of critical ill COVID-19 patients. *J Med Virol* 2021; 93: 582-584.

241. Li G, Fan Y, Lai Y, Han T, Li Z, Zhou P, Pan P, Wang W, Hu D, Liu X, Zhang Q, Wu J. Coronavirus infections and immune responses. *J Med Virol* 2020; 92: 424-432.

242. Maltezou HC, Raftopoulos V, Vorou R, Papadima K, Mellou K, Spanakis N, Kossyvakis A, Gioula G, Exindari M, Froukala E, Martinez-Gonzalez B, Panayiotakopoulos G, Papa A, Mentis A, Tsakris A. Association Between Upper Respiratory Tract Viral Load, Comorbidities, Disease Severity, and Outcome of Patients With SARS-CoV-2 Infection. *J Infect Dis* 2021; 223: 1132-1138.

243. Cui H, Banerjee S, Guo S, Xie N, Ge J, Jiang D, Zornig M, Thannickal VJ, Liu G. Long noncoding RNA Malat1 regulates differential activation of macrophages and response to lung injury. *JCI Insight* 2019; 4.

244. Lee S, Kim T, Lee E, Lee C, Kim H, Rhee H, Park SY, Son HJ, Yu S, Park JW, Choo EJ, Park S, Loeb M, Kim TH. Clinical Course and Molecular Viral Shedding Among Asymptomatic and Symptomatic Patients With SARS-CoV-2 Infection in a Community Treatment Center in the Republic of Korea. *JAMA Intern Med* 2020; 180: 1447-1452.

245. Fajnzylber J, Regan J, Coxen K, Corry H, Wong C, Rosenthal A, Worrall D, Giguel F, Piechocka-Trocha A, Atyeo C, Fischinger S, Chan A, Flaherty KT, Hall K, Dougan M, Ryan ET, Gillespie E, Chishti R, Li Y, Jilg N, Hanidziar D, Baron RM, Baden L, Tsibris AM, Armstrong KA, Kuritzkes DR, Alter G, Walker BD, Yu X, Li JZ, Massachusetts Consortium for Pathogen R. SARS-CoV-2 viral load is associated with increased disease severity and mortality. *Nat Commun* 2020; 11: 5493.

246. Fliesser E, Birnhuber A, Marsh LM, Gschwandtner E, Klepetko W, Olschewski H, Kwapiszewska G. Dysbalance of ACE2 levels - a possible cause for severe COVID-19 outcome in COPD. *J Pathol Clin Res* 2021.

247. Matusiak M, Schurch CM. Expression of SARS-CoV-2 entry receptors in the respiratory tract of healthy individuals, smokers and asthmatics. *Respir Res* 2020; 21: 252.

248. Zhang X, Zhou Y, Chen S, Li W, Chen W, Gu W. LncRNA MACC1-AS1 sponges multiple miRNAs and RNA-binding protein PTBP1. *Oncogenesis* 2019; 8: 73.

249. Abu-Izneid T, AlHajri N, Ibrahim AM, Javed MN, Salem KM, Pottoo FH, Kamal MA. Micro-RNAs in the regulation of immune response against SARS CoV-2 and other viral infections. *J Adv Res* 2021; 30: 133-145.

250. Siniscalchi C, Di Palo A, Russo A, Potenza N. Human MicroRNAs Interacting With SARS-CoV-2 RNA Sequences: Computational Analysis and Experimental Target Validation. *Front Genet* 2021; 12: 678994.

251. Yousefi H, Poursheikhani A, Bahmanpour Z, Vatanmakanian M, Taheri M, Mashouri L, Alahari SK. SARS-CoV infection crosstalk with human host cell noncoding-RNA machinery: An in-silico approach. *Biomed Pharmacother* 2020; 130: 110548.

252. Somarowthu S, Legiewicz M, Chillon I, Marcia M, Liu F, Pyle AM. HOTAIR forms an intricate and modular secondary structure. *Mol Cell* 2015; 58: 353-361.

253. Civenni G. Targeting Promoter-Associated Noncoding RNA In Vivo. *Methods Mol Biol* 2017; 1543: 259-270.

254. Smith N, Goncalves P, Charbit B, Grzelak L, Beretta M, Planchais C, Bruel T, Rouilly V, Bondet V, Hadjadj J, Yatim N, Pere H, Merkling SH, Ghozlane A, Kerneis S, Rieux-Laucat F, Terrier B, Schwartz O, Mouquet H, Duffy D, Di Santo JP. Distinct systemic and mucosal immune responses during acute SARS-CoV-2 infection. *Nat Immunol* 2021; 22: 1428-1439.

255. Froberg J, Diavatopoulos DA. Mucosal immunity to severe acute respiratory syndrome coronavirus 2 infection. *Curr Opin Infect Dis* 2021; 34: 181-186.

256. Cervia C, Nilsson J, Zurbuchen Y, Valaperti A, Schreiner J, Wolfensberger A, Raeber ME, Adamo S, Weigang S, Emmenegger M, Hasler S, Bosshard PP, De Cecco E, Bachli E, Rudiger A, Stussi-Helbling M, Huber LC, Zinkernagel AS, Schaer DJ, Aguzzi A, Kochs G, Held U, Probst-Muller E, Rampini SK, Boyman O. Systemic and mucosal antibody responses specific to SARS-CoV-2 during mild versus severe COVID-19. *J Allergy Clin Immunol* 2021; 147: 545-557 e549.

257. Manevski M, Muthumalage T, Devadoss D, Sundar IK, Wang Q, Singh KP, Unwalla HJ, Chand HS, Rahman I. Cellular stress responses and dysfunctional Mitochondrial-cellular senescence, and therapeutics in chronic respiratory diseases. *Redox Biol* 2020: 101443.

258. Malaquias MAS, Gadotti AC, Motta-Junior JDS, Martins APC, Azevedo MLV, Benevides APK, Cezar-Neto P, Panini do Carmo LA, Zeni RC, Raboni SM, Fonseca AS, Machado-Souza C, Moreno-Amaral AN, de Noronha L. The role of the lectin pathway of the complement system in SARS-CoV-2 lung injury. *Transl Res* 2021; 231: 55-63.

259. Ouyang J, Hu J, Chen JL. lncRNAs regulate the innate immune response to viral infection. *Wiley Interdiscip Rev RNA* 2016; 7: 129-143.

260. Agirre X, Meydan C, Jiang Y, Garate L, Doane AS, Li Z, Verma A, Paiva B, Martin-Subero JI, Elemento O, Mason CE, Prosper F, Melnick A. Long non-coding RNAs discriminate the stages and gene regulatory states of human humoral immune response. *Nat Commun* 2019; 10: 821.

261. Holtzman MJ, Byers DE, Brett JA, Patel AC, Agapov E, Jin X, Wu K. Linking acute infection to chronic lung disease. The role of IL-33-expressing epithelial progenitor cells. *Ann Am Thorac Soc* 2014; 11 Suppl 5: S287-291.

262. Yin W, Cao W, Zhou G, Wang L, Sun J, Zhu A, Wang Z, Zhou Y, Liu X, Li Y, Zhong N, Zhao J, Liu L, Ran P. Analysis of pathological changes in the epithelium in COVID-19 patient airways. *ERJ Open Res* 2021; 7.

263. Desai N, Neyaz A, Szabolcs A, Shih AR, Chen JH, Thapar V, Nieman LT, Solovyov A, Mehta A, Lieb DJ, Kulkarni AS, Jaicks C, Xu KH, Raabe MJ, Pinto CJ, Juric D, Chebib I, Colvin RB, Kim AY, Monroe R, Warren SE, Danaher P, Reeves JW, Gong J, Rueckert EH, Greenbaum BD, Hacohen N, Lagana SM, Rivera MN, Sholl LM, Stone JR, Ting DT, Deshpande V. Temporal and spatial heterogeneity of host response to SARS-CoV-2 pulmonary infection. *Nat Commun* 2020; 11: 6319.

264. Smet A, Breugelmans T, Michiels J, Lamote K, Arras W, De Man JG, Heyndrickx L, Hauner A, Huizing M, Malhotra-Kumar S, Lammens M, Hotterbeekx A, Kumar-Singh S, Verstraeten A, Loeys B, Verhoeven V, Jacobs R, Dams K, Coenen S, Arien KK, Jorens PG, De Winter BY. A dynamic mucin mRNA signature associates with COVID-19 disease presentation and severity. *JCI Insight* 2021; 6.

265. Pierce JB, Simion V, Icli B, Perez-Cremades D, Cheng HS, Feinberg MW. Computational Analysis of Targeting SARS-CoV-2, Viral Entry Proteins ACE2 and TMPRSS2, and Interferon Genes by Host MicroRNAs. *Genes (Basel)* 2020; 11.

266. Jafarinejad-Farsangi S, Jazi MM, Rostamzadeh F, Hadizadeh M. High affinity of host human microRNAs to SARS-CoV-2 genome: An in silico analysis. *Noncoding RNA Res* 2020; 5: 222-231.

267. Chow JT, Salmena L. Prediction and Analysis of SARS-CoV-2-Targeting MicroRNA in Human Lung Epithelium. *Genes (Basel)* 2020; 11.

268. Hosseini Rad Sm A, McLellan AD. Implications of SARS-CoV-2 Mutations for Genomic RNA Structure and Host microRNA Targeting. *Int J Mol Sci* 2020; 21.

269. Banaganapalli B, Al-Rayes N, Awan ZA, Alsulaimany FA, Alamri AS, Elango R, Malik MZ, Shaik NA. Multilevel systems biology analysis of lung transcriptomics data identifies key miRNAs and potential miRNA target genes for SARS-CoV-2 infection. *Comput Biol Med* 2021; 135: 104570.

270. Akula SM, Bolin P, Cook PP. Cellular miR-150-5p may have a crucial role to play in the biology of SARS-CoV-2 infection by regulating nsp10 gene. *RNA Biol* 2022; 19: 1-11.

271. Sacar Demirci MD, Adan A. Computational analysis of microRNA-mediated interactions in SARS-CoV-2 infection. *PeerJ* 2020; 8: e9369.

272. Kannan SR, Spratt AN, Cohen AR, Naqvi SH, Chand HS, Quinn TP, Lorson CL, Byrareddy SN, Singh K. Evolutionary analysis of the Delta and Delta Plus variants of the SARS-CoV-2 viruses. *J Autoimmun* 2021; 124: 102715.

273. Spratt AN, Kannan SR, Woods LT, Weisman GA, Quinn TP, Lorson CL, Sonnerborg A, Byrareddy SN, Singh K. Evolution, correlation, structural impact and dynamics of emerging SARS-CoV-2 variants. *Comput Struct Biotechnol J* 2021; 19: 3799-3809.

274. Kalkhoran S, Glantz SA. E-cigarettes and smoking cessation in real-world and clinical settings: a systematic review and meta-analysis. *Lancet Respir Med* 2016; 4: 116-128.

275. Baenziger ON, Ford L, Yazidjoglou A, Joshy G, Banks E. E-cigarette use and combustible tobacco cigarette smoking uptake among non-smokers, including relapse in former smokers: umbrella review, systematic review and meta-analysis. *BMJ Open* 2021; 11: e045603.

276. Pierce JP, Chen R, Kealey S, Leas EC, White MM, Stone MD, McMenamin SB, Trinidad DR, Strong DR, Benmarhnia T, Messer K. Incidence of Cigarette Smoking Relapse Among Individuals Who Switched to e-Cigarettes or Other Tobacco Products. *JAMA Netw Open* 2021; 4: e2128810.

277. Wang RJ, Bhadriraju S, Glantz SA. E-Cigarette Use and Adult Cigarette Smoking Cessation: A Meta-Analysis. *Am J Public Health* 2021; 111: 230-246.

278. Chen R, Pierce JP, Leas EC, Benmarhnia T, Strong DR, White MM, Stone M, Trinidad DR, McMenamin SB, Messer K. Effectiveness of e-cigarettes as aids for smoking cessation: evidence from the PATH Study cohort, 2017-2019. *Tob Control* 2022.

279. Gaiha SM, Lempert LK, McKelvey K, Halpern-Felsher B. E-cigarette devices, brands, and flavors attract youth: Informing FDA's policies and priorities to close critical gaps. *Addict Behav* 2022; 126: 107179.

280. FDA. Menthol and Other Flavors in Tobacco Products. . *FDA* 2021.

281. FDA. FDA fnalizes enforcement policy on unauthorized favored cartridge-based e-cigarettes that appeal to children, including fruit and mint. *FDA* 2020.

282. Wang TW, Neff LJ, Park-Lee E, Ren C, Cullen KA, King BA. E-cigarette Use Among Middle and High School Students - United States, 2020. *MMWR Morb Mortal Wkly Rep* 2020; 69: 1310-1312.

283. Omaiye EE, Luo W, McWhirter KJ, Pankow JF, Talbot P. Flavour chemicals, synthetic coolants and pulegone in popular mint-flavoured and menthol-flavoured e-cigarettes. *Tob Control* 2021.

284. Jabba SV, Jordt SE. Risk Analysis for the Carcinogen Pulegone in Mint- and Menthol-Flavored e-Cigarettes and Smokeless Tobacco Products. *JAMA Intern Med* 2019; 179: 1721-1723.

285. Gerloff J, Sundar IK, Freter R, Sekera ER, Friedman AE, Robinson R, Pagano T, Rahman I. Inflammatory Response and Barrier Dysfunction by Different e-Cigarette Flavoring Chemicals Identified by Gas Chromatography-Mass Spectrometry in e-Liquids and e-Vapors on Human Lung Epithelial Cells and Fibroblasts. *Appl In Vitro Toxicol* 2017; 3: 28-40.

286. Kaur G, Gaurav A, Lamb T, Perkins M, Muthumalage T, Rahman I. Current Perspectives on Characteristics, Compositions, and Toxicological Effects of E-Cigarettes Containing Tobacco and Menthol/Mint Flavors. *Front Physiol* 2020; 11: 613948.

287. Chand HS, Muthumalage T, Maziak W, Rahman I. Pulmonary Toxicity and the Pathophysiology of Electronic Cigarette, or Vaping Product, Use Associated Lung Injury. *Front Pharmacol* 2019; 10: 1619.

288. Jabba SV, Erythropel HC, Torres DG, Delgado LA, Woodrow JG, Anastas PT, Zimmerman JB, Jordt SE. Synthetic Cooling Agents in US-marketed E-cigarette Refill Liquids and Popular Disposable Ecigarettes: Chemical Analysis and Risk Assessment. *Nicotine Tob Res* 2022.

289. Muthumalage T, Lamb T, Friedman MR, Rahman I. E-cigarette flavored pods induce inflammation, epithelial barrier dysfunction, and DNA damage in lung epithelial cells and monocytes. *Sci Rep* 2019; 9: 19035.

290. Sundar IK, Javed F, Romanos GE, Rahman I. E-cigarettes and flavorings induce inflammatory and pro-senescence responses in oral epithelial cells and periodontal fibroblasts. *Oncotarget* 2016; 7: 77196-77204.

291. Wang Q, Sundar IK, Li D, Lucas JH, Muthumalage T, McDonough SR, Rahman I. E-cigarette-induced pulmonary inflammation and dysregulated repair are mediated by nAChR α7 receptor: role of nAChR α7 in SARS-CoV-2 Covid-19 ACE2 receptor regulation. *Respir Res* 2020; 21: 154.

292. Devadoss D, Acharya A, Manevski M, Pandey K, Borchert GM, Nair M, Mirsaeidi M, Byrareddy SN, Chand HS. Distinct Mucoinflammatory Phenotype and the Immunomodulatory Long Noncoding Transcripts Associated with SARS-CoV-2 Airway Infection. *medRxiv* 2021.

293. Jasper AE, Sapey E, Thickett DR, Scott A. Understanding potential mechanisms of harm: the drivers of electronic cigarette-induced changes in alveolar macrophages, neutrophils, and lung epithelial cells. *Am J Physiol Lung Cell Mol Physiol* 2021; 321: L336-l348.

294. Yogeswaran S, Rahman I. Differences in Acellular Reactive Oxygen Species (ROS) Generation by E-Cigarettes Containing Synthetic Nicotine and Tobacco-Derived Nicotine. *Toxics* 2022; 10.

295. Manevski M, Devadoss D, Yogeswaran S, Rahman I, Chand HS. E-Cigarette Synthetic Cooling Agent WS-23 and Nicotine Aerosols Differentially Modulate Airway Epithelial Cell Responses. *bioRxiv* 2022: 2022.2006.2020.496868.

296. Madison MC, Landers CT, Gu BH, Chang CY, Tung HY, You R, Hong MJ, Baghaei N, Song LZ, Porter P, Putluri N, Salas R, Gilbert BE, Levental I, Campen MJ, Corry DB, Kheradmand F. Electronic cigarettes disrupt lung lipid homeostasis and innate immunity independent of nicotine. *J Clin Invest* 2019; 129: 4290-4304.

297. Hallagan J. The Safety Assessment and Regulatory Authority to Use Flavors – Focus on E-Cigarettes. 2015.

298. Viswam D, Trotter S, Burge PS, Walters GI. Respiratory failure caused by lipoid pneumonia from vaping e-cigarettes. *BMJ Case Rep* 2018; 2018.

299. Khan MS, Khateeb F, Akhtar J, Khan Z, Lal A, Kholodovych V, Hammersley J. Organizing pneumonia related to electronic cigarette use: A case report and review of literature. *Clin Respir J* 2018; 12: 1295-1299.

300. Sommerfeld CG, Weiner DJ, Nowalk A, Larkin A. Hypersensitivity Pneumonitis and Acute Respiratory Distress Syndrome From E-Cigarette Use. *Pediatrics* 2018; 141.

301. Layden JE, Ghinai I, Pray I, Kimball A, Layer M, Tenforde M, Navon L, Hoots B, Salvatore PP, Elderbrook M, Haupt T, Kanne J, Patel MT, Saathoff-Huber L, King BA, Schier JG, Mikosz CA, Meiman J. Pulmonary Illness Related to E-Cigarette Use in Illinois and Wisconsin - Preliminary Report. *N Engl J Med* 2019.

302. Nair V, Tran M, Behar RZ, Zhai S, Cui X, Phandthong R, Wang Y, Pan S, Luo W, Pankow JF, Volz DC, Talbot P. Menthol in electronic cigarettes: A contributor to respiratory disease? *Toxicol Appl Pharmacol* 2020; 407: 115238.

303. Jones SA, Jenkins BJ. Recent insights into targeting the IL-6 cytokine family in inflammatory diseases and cancer. *Nat Rev Immunol* 2018; 18: 773-789.

304. Chatterjee S, Tao J-Q, Johncola A, Guo W, Caporale A, Langham MC, Wehrli FW. Acute exposure to e-cigarettes causes inflammation and pulmonary endothelial oxidative stress in nonsmoking, healthy young subjects. *American journal of physiology Lung cellular and molecular physiology* 2019; 317: L155-L166.

305. Li Y, Jia YC, Cui K, Li N, Zheng ZY, Wang YZ, Yuan XB. Essential role of TRPC channels in the guidance of nerve growth cones by brain-derived neurotrophic factor. *Nature* 2005; 434: 894-898.

306. Kaneko Y, Szallasi A. Transient receptor potential (TRP) channels: a clinical perspective. *Br J Pharmacol* 2014; 171: 2474-2507.

307. Escobar YH, Morrison CB, Chen Y, Hickman E, Love CA, Rebuli ME, Surratt JD, Ehre C, Jaspers I. Differential responses to e-cig generated aerosols from humectants and different forms of nicotine in epithelial cells from nonsmokers and smokers. *Am J Physiol Lung Cell Mol Physiol* 2021; 320: L1064-l1073.

308. Haswell LE, Smart D, Jaunky T, Baxter A, Santopietro S, Meredith S, Camacho OM, Breheny D, Thorne D, Gaca MD. The development of an in vitro 3D model of goblet cell hyperplasia using MUC5AC expression and repeated whole aerosol exposures. *Toxicol Lett* 2021; 347: 45-57.

309. Warren R, O'Reilly MA. An Elusive Fox that Suppresses Scgb1a1 in Asthma Has Been Found. *Am J Respir Cell Mol Biol* 2019; 60: 615-617.

310. Zhu L, An L, Ran D, Lizarraga R, Bondy C, Zhou X, Harper RW, Liao SY, Chen Y. The Club Cell Marker SCGB1A1 Downstream of FOXA2 is Reduced in Asthma. *Am J Respir Cell Mol Biol* 2019; 60: 695-704.

VITA

MARKO MANEVSKI

EDUCATION

- Candidate for Doctor of Philosophy in Biomedical Sciences – Hebert Wertheim College of Medicine, Florida International University, Miami, FL - 2022
- Bachelor of Science in Biology – Union College, Schenectady, NY - *2018*.

PUBLICATIONS AND PRESENTATIONS

1. Manevski M, Devadoss D, Long C, Singh S, Nasser MW, Borchert GM, Nair M, Rahman I, Sopori M, Chand HS. Increased Expression of LASI LncRNA Regulates the Cigarette Smoke and COPD Associated Airway Inflammation and Mucous Cell Hyperplasia. *Front Immunol*. 13. DOI: 10.3389/fimmu.2022.803362. PMID: 35774797.
2. Manevski M, Muthumalage T, Devadoss D, Sundar IK, Wang Q, Singh KP, Unwalla HJ, Chand HS, Rahman I. Cellular stress responses and dysfunctional Mitochondrial-cellular senescence, and therapeutics in chronic respiratory diseases. *Redox Biol*. 2020 Jun;33:101443. DOI: 10.1016/j.redox.2020.101443. PMID: 32037306.
3. Devadoss D, Acharya A, Manevski M, Pandey K, Borchert GM, Nair M, Mirsaeidi M, Byrareddy SN, Chand HS. Immunomodulatory LncRNA on Antisense Strand of ICAM-1 Augments the SARS-CoV-2 Infection Associated Airway Mucoinflammatory Phenotype. *iScience*. In press.
4. Devadoss D, Dali G, Manevski M, Houserova D, Hussain SS, Baumlin N, Salathe M, Borchert GM, Langley RJ, Chand HS. A long noncoding RNA antisense to ICAM-1 is involved in allergic asthma associated hyperreactive response of airway epithelial cells. *Mucosal Immunol*. 2021 May;14(3):630-639. DOI: 10.1038/s41385-020-00352-9. PMID: 33122732.
5. Devadoss D, Singh SP, Acharya A, Do KC, Periyasamy P, Manevski M, Mishra N, Tellez CS, Ramakrishnan S, Belinsky SA, Byrareddy SN, Buch S, Chand HS, Sopori M. HIV-1 Productively Infects and Integrates in Bronchial Epithelial Cells. *Front Cell Infect Microbiol*. 2021 Feb 4;10:612360. DOI: 10.3389/fcimb.2020.612360. PMID: 33614527.
6. Manevski M, Devadoss D, Castro R, Delatorre L, Yndart A, Jayant RD, Nair M, Chand HS. Development and Challenges of Nanotherapeutic Formulations for Targeting Mitochondrial Cell Death Pathways in Lung and

Brain Degenerative Diseases. *Crit Rev Biomed Eng*. 2020;48(3):137-152. DOI: 10.1615/CritRevBiomedEng.2020034546. PMID: 33389892.

7. Singh SP, Devadoss D, Manevski M, Sheybani A, Ivanciuc T, Exil V, Agarwal H, Raizada V, Garofalo RP, Chand HS, Sopori ML. Gestational Exposure to Cigarette Smoke Suppresses the Gasotransmitter H2S Biogenesis and the Effects Are Transmitted Transgenerationally. *Front Immunol*. 2020 Jul 28;11:1628. DOI: 10.3389/fimmu.2020.01628. PMID: 32849552.
8. Devadoss D, Long C, Langley RJ, Manevski M, Nair M, Campos MA, Borchert G, Rahman I, Chand HS. Long Noncoding Transcriptome in Chronic Obstructive Pulmonary Disease. *Am J Respir Cell Mol Biol*. 2019; Dec;61(6):678-688. PMID: 31486667.
9. Esteban-Lopez M, Perry MD, Garbinski LD, Manevski M, Andre M, Ceyhan Y, Caobi A, Paul P, Seng Lau L, Ramelow J, El-Hage N. Health Effects and Known Pathology Associated with Electronic Nicotine Delivery Systems. *Toxicol Rep*. 2022. DOI: 10.1016/j.toxrep.2022.06.006.
10. Manevski M, Devadoss D, Yogeswaran S, Rahman I, Chand HS. E-Cigarette Synthetic Cooling Agent WS-23 and Nicotine Aerosols Differentially Modulate Airway Epithelial Cell Responses. *bioRxiv* 2022: 2022.2006.2020.496868.
11. Presenting Author, Poster
    - *Title*: Cigarette Smoke Exposure Increases the Airway Epithelial Cell Susceptibility to HIV-1 Infection Mediated by ICAM-1 and Long Noncoding RNAs (*May 2022*).
    - *Conference*: American Thoracic Society (ATS) 2022 International Conference.
12. Invited Speaker
    - *Title:* Long Noncoding RNAs and their Emerging Role in Innate Immune Modulation and Chronic Lung Disease (*Feb. 2022*)
    - *Session:* Research in Progress Series, Herbert Wertheim College of Medicine
13. Presenting Author, Poster
    - *Title:* Increased Expression of LASI LncRNA Regulates the Cigarette Smoke and COPD Associated Airway Inflammation and Mucus Dysregulation (*Mar. 2022*).
    - *Conference*: Society of Toxicology (SOT) Annual Meeting 2022.